MODELING AND SIMULATION OF VAN FOR SIDE IMPACT SENSING TESTS

Chin-Hsu Lin
General Motors R&D Center
USA
Paper Number 07-0060

ABSTRACT

An extensive study on using non-linear finite element analyses to aid in calibrating a thorax or roof rail curtain airbag sensing system is presented. Modeling techniques and lessons learned from previously investigated frontal sensing finite element analyses were adopted in this side impact study. Modeling techniques that can be applied to the side impact simulations were identified and incorporated in a chosen van model. The van model was then used to simulate a set of no-deployment and deployment side impact calibration events. The simulation results were compared with available test data and side impact sensing algorithms were used to determine the airbag deployment time from the simulations. Airbag deployment times from the simulations are comparable to the test and it is strongly suggested from this study that a high fidelity vehicle model with a FEA-compatible sensing algorithm can greatly improve sensing simulation capability for side impacts.

INTRODUCTION

The use of math-based tools has reduced the need for hardware prototyping and testing, which in turn reduces a vehicle's development time and cost. However, there are still many tasks in the vehicle development process that math-based tools cannot do well. Of these, the task of calibrating a side airbag sensing system is a major task that has not been addressed. To obtain the required acceleration signals for sensing calibration, expensive prototype vehicles have been routinely crashed for vehicle development. A math-based side sensing calibration capability could significantly reduce prototyping and testing costs, as well as shorten the vehicle development time.

There have been a few papers published for the frontal sensing impact simulations [1,2,3,4,5] but none for the side impact sensing impact simulation. The major difference between the frontal impact and the side impact is that the latter generally requires a much earlier airbag deployment time, which, in turn, demands an even higher degree of model fidelity to ensure timely deployment. In these frontal sensing studies, the necessary modeling techniques to achieve high fidelity FEA models for simulating a suite of frontal sensing impact events have been documented. In this paper, study of the FEA-compatible sensing impact tests is extended to side impact sensing tests. The modeling techniques identified in previous studies are employed, if applicable, onto the side impact model and other necessary and unique side sensing impact modeling techniques are identified and studied so a high fidelity FEA-compatible side sensing impact vehicle model can be built to replace some of the tests and speed up the vehicle development process.

A van, shown in Figure 1, is selected for study in this paper. The following seven van vehicle side impact tests are available for correlation study: Side NCAP(New Car Assessment Program), FMVSS214 MDB (Moving Deformable Barrier) impact, IIHS (Insurance Institute for Highway Safety) side impact, front and rear door pole impacts, EEVC (European Enhanced Vehicle-safety Committee) barrier impact, and MDB no-deployment impact. The van side impact calibration crash matrix is shown in Table 1. Non destructive immunity tests, such as door slam, shopping cart/bicycle hits, etc., are not studied in this paper since they can be conducted more efficiently and economically in the test laboratories.

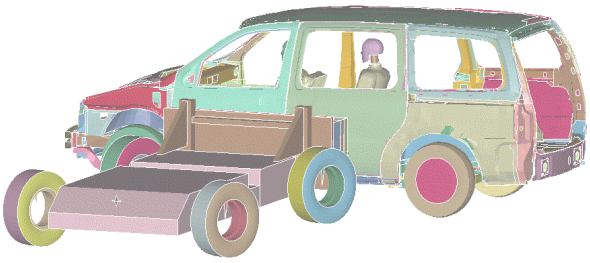

Figure 1. The van vehicle model.

Table 1.
Sensing calibration test matrix.

Tests
IIHS
Side NCAP
FMVSS214
Front Door Pole
Rear Door Pole
EEVC
MDB No-Deployment

MODELING TECHNIQUES CRUCIAL FOR CRASH TEST SIMULATIONS

Finite element simulations have been conducted routinely in the past decade to evaluate and improve crash and safety designs for specific high-speed impact conditions or regulations. Knowledge of fundamental modeling techniques had been

accumulated for building a quality finite element model. These fundamental modeling techniques are:

- Reduce element size to about 10 mm in the crush zone to capture correct buckling modes
- Avoid initial penetration between parts
- Use joints, instead of rigid connection, to represent the door hinge and latch/striker system
- Use mass scaling option with caution
- Space the welding locations close to physical model and minimize the weld length
- Include gravitational force

All the analyses are completed using LS-DYNA version 960.1488[6]. The number of parts, elements and nodes of the model are summarized in Table 2. In what follows, we document the crucial modeling techniques, beyond what have been stated above, that are required for building a high fidelity side impact model for sensing calibration purpose.

Table 2.
Total number of parts, elements and nodes of the van FE model.

	Van FE Model
No. of Parts	246
No. of Nodes	232,959
No. of Shell Elements	227,223
No. of Solid Elements	829
No. of Beam Elements	28

Crucial Sensing Modeling Techniques For Side and Frontal Vehicles

Accelerometers -

Physical accelerometers measure the acceleration and deceleration in a fixed local frame, which translate and rotate with the component that the accelerometers are mounted on. Hence, the "ELEMENT_SEATBELT_ACCELEROMETER" card in LS-DYNA is used in our model to monitor the acceleration change in such a local coordinate frame. The FEA velocity curves shown in this paper are obtained by integrating the acceleration, filtered through SAE 180 class.

Six side impact sensor locations, the front door beam, BSIS (B-Pillar Side Impact Sensor), rear door beam, C-pillar at beltline, CSIS (C-Pillar Side Impact Sensor), and the SDM (Sensing Diagnostic Module) on the floor under the passenger's seat, shown in Figure 2, are used in this study for correlating crash pulses with available tests.

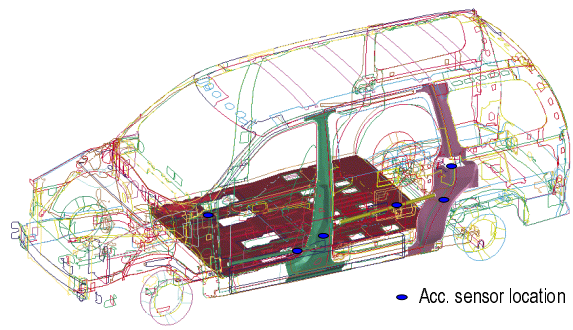

Figure 2. Monitored sensor locations: front door beam, BSIS, rear door beam, CSIS, C-pillar at beltline, and the SDM on the floor under the passenger's seat.

Strain Rate Effect

The strain rate effect of the materials was previously identified as the most crucial factor that must be incorporated in a frontal impact model to simulate a set of frontal impacts, high-speed deploy and low-speed no-deploy events [2,3,5,7]. In this side impact sensing study, the engineering properties of the metallic materials in the van FE model are updated to include strain rate sensitive material. A quasi-static stress-strain curve is substituted to study the results of the velocity changes in a high-speed FMVSS214 test and a low-speed MDB no-deployment impact test. The simulation setup for the FMVSS214 impact is shown in Figure 3. The differences of the velocity at the BSIS between the two simulations, shown in Figure 4, are insignificant before the side bags' required deployment time while the SDM velocity curve of the simulation using a quasi-static stress-strain curve exhibits a slightly softer response since softer material properties are used. For the lower speed MDB no-deployment impact, the differences of the simulations are less noticeable, as shown in Figure 5, with the quasi-static stress-strain material model showing a slightly softer response. The differences are not as significant as documented for the frontal impacts.

In the frontal impacts, the rails and cradle are loaded axially, and these major energy absorbing components can yield different crush modes when not employing the strain rate effect. This results in significant velocity deviation. The B-Pillar and the door beams, designed mainly for side impact protection, are designed to resist the bending force during the side impacts, and these components will not have dramatic differences in deformations if the material properties are modeled using a single quasi-static stress-strain curve; hence the deviation in the velocity curves is not as pronounced as the frontal impact events. However, significant differences might exist for vehicles, say, with a cross car beam design.

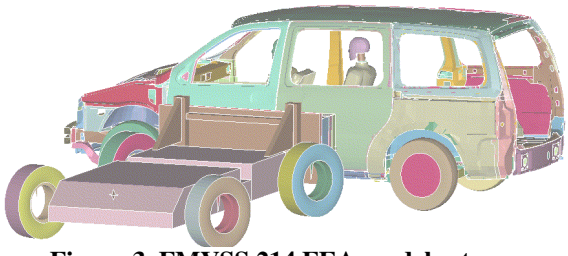

Figure 3. FMVSS 214 FEA model setup.

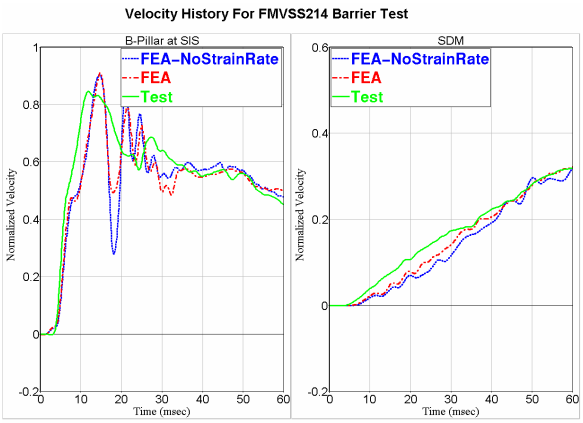

Figure 4. Comparing the FEA velocity curves with and without strain rate effect for FMVSS214 impact test.

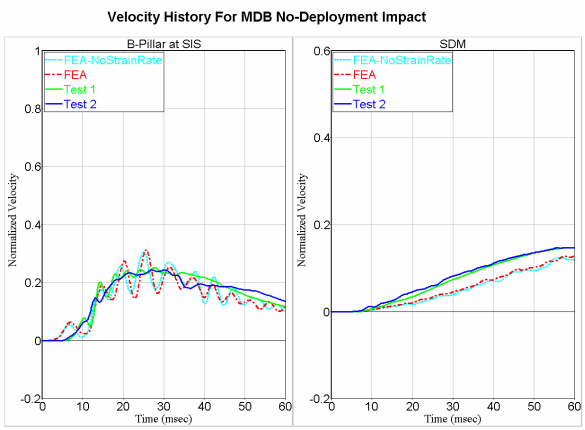

Figure 5. Comparing the FEA velocity curves with and without strain rate effect for MDB no-deployment impact test.

Segment-Based Contact

A full vehicle crash analysis involves interaction between all free surfaces, which includes contact at corners and edges. Correlation with the tests might be degraded significantly if the contacts are not defined properly. In one of the previous validation study [8], it was found that the velocity pulse correlation was improved by using the segment-based contact option in LS-DYNA. In this side impact study, however, the use of this option did not yield significant differences, as shown in Figure 6. To avoid any unrealized or unforeseen contact issues, it is still strongly recommended that the segment-based contact search parameter be considered when defining the contacts.

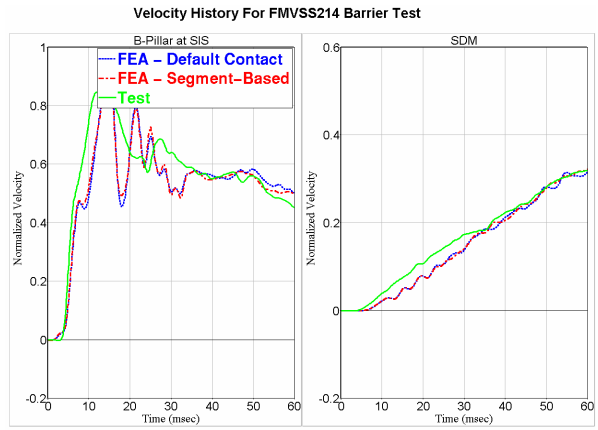

Figure 6. Comparing the FEA velocity curves with and without segment-based contact option for FMVSS214 impact test simulation.

Shell Element Type 16 and Type 2

Many shell element formulations are available to the users in LS-DYNA while formulation types 16 and 2 are the most commonly used. Use of the element formulation type 16 [6] significantly improves the overall SDM velocity correlation, depicted in Figure 7. The shell element formulation type 16, a fully integrated shell element, costs about 2.8 times more CPU-time than the default Belytschko-Tsay (BT) element (shell formulation type 2 in LS-DYNA). However, the BT shell element is very sensitive to element warping. Using the shell formulation type 2 tends to make a vehicle model softer, and the velocity response at the SDM showed this trend while the response at the BSIS did not.

For the lower speed MDB no-deployment impact, it has less effect on the SDM velocity, shown in Figure 8. It is observed that the velocity at the BSIS is less wavy when the shell formulation type 2 is used. When the shell formulation type 2 is used, accuracy of the analysis can be improved by turning on the warping stiffness control and updating the shell normal direction based on the nodal rotation available in the *CONTROL_SHELL card and using the stiffness form hourglass formulation. Use of those parameters for shell type 2 did not bring the SDM velocity of FMVSS 214 simulation closer to the test and match the result of shell type 16 as expected, shown in Figures 7 and 8.

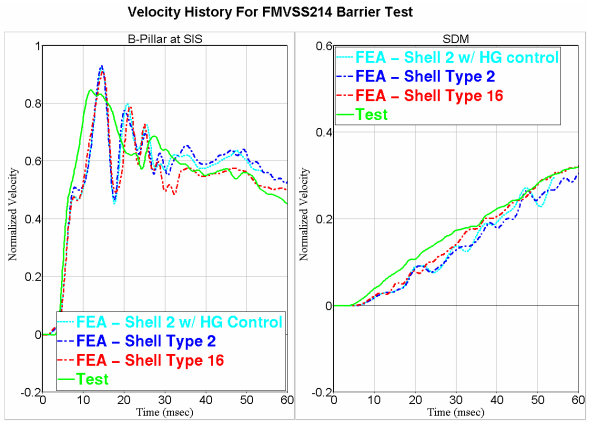

Figure 7. Comparing the FEA velocity curves with different shell element formulations, type 2 and type 16, for FMVSS214 impact.

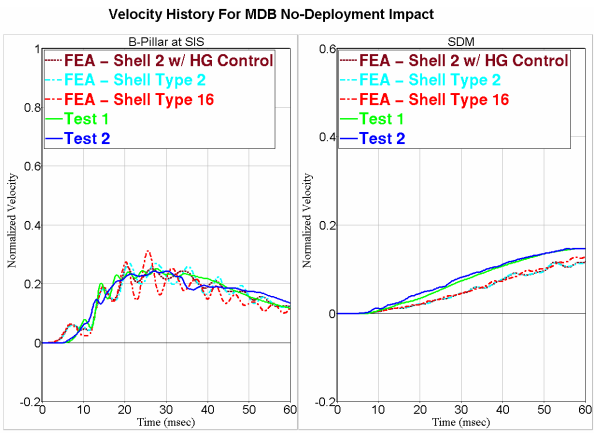

Figure 8. Comparing the FEA velocity curves with different shell element formulations, type 2 and type 16, for MDB no-deployment impact.

Crucial Modeling Techniques For side impact vehicles ONLY

Modeling of Door Striker

In simulating the FMVSS214 quasi-static test, the inclusion of a detailed modeling of door striker and latch system can improve the correlation of the resistance force. The improvement is from the small relative displacement between the striker and the latch system. In our dynamic crash study, this system is modeled as a joint to allow the realistic relative displacement and rotation between the door and B-Pillar. When the joint is replaced by a rigid connection, it does not result in significant difference in the overall SDM response as shown in Figure 9 and it shows a slightly stiffer response in the BSIS at airbag deployment time.

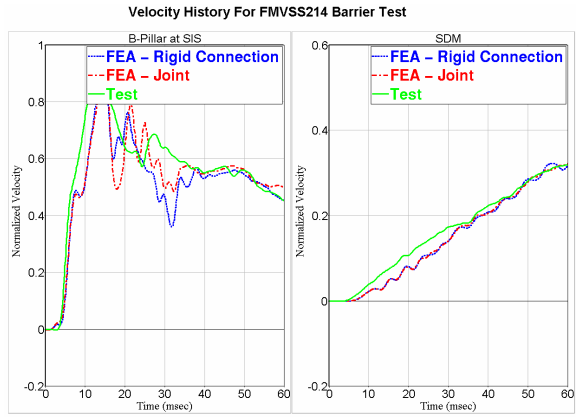

Figure 9. Comparing the FEA velocity curves for the modeling of striker and hinge system for FMVSS214 impact.

Friction Coefficient Between Barrier and Vehicle

The friction coefficient between the moving deformable barrier and the vehicle in the crash test is also studied so that a proper coefficient can be established. The friction coefficient values of 0.0, 0.2, and 0.4 are used to study their effects on the SDM velocity. As a higher friction coefficient is used, the vehicle has a slightly stiffer response at the SDM, i.e., greater velocity change, shown in Figure 10, while the response change at the BSIS is less noticeable. It is concluded from this study that a friction coefficient of 0.2 can achieve better correlation.

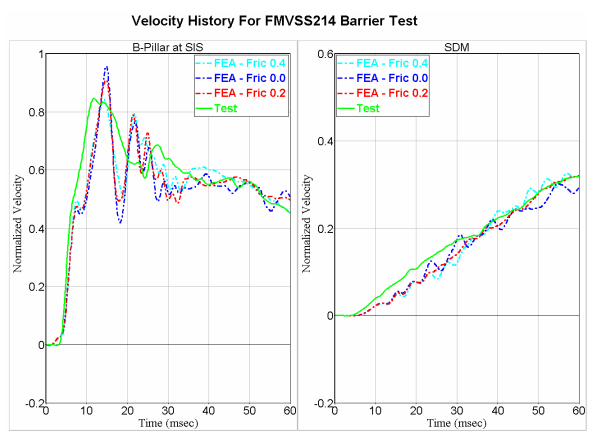

Figure 10. Different friction coefficients between the barrier and the vehicle for FMVSS 214 simulation.

SIMULATION RESULTS

Comparison Between the Tests and Simulations

Using the enhanced model by employing the modeling techniques described above, we simulated seven side crash tests listed in Table 1 using a consistent vehicle model. FEA accelerations at the target locations are first extracted from the simulations and then integrated

to obtain the velocity histories. The complete velocity time histories for the seven side impact tests are shown in the Appendix. For the Side-NCAP and EEVC impact conditions, only the velocity curves at the SDM and BSIS for the tests are shown for comparisons, since there is no data available for the other locations.

In this section, the IIHS side impact simulation results are selected to compare with the test. Deformation of the vehicle model after the impact is shown in Figure 11. Correlations of the velocity history at selected locations are shown in Figure 12. The front door beam sensor signal was prematurely terminated before 3 msec into this test. Comparing the velocity change at the BSIS, shown in Figure 12, between the simulation and the test, good agreement was observed upto 7 msec into the crash event. Efforts were focused on improving the velocity at the BSIS, and it indeed results in a good correlation. For the rear door beam and C-pillar sensors, FEA velocity curves show a 2 ~3 msec earlier rise than the test, but they do have similar velocity characteristics. The velocity curve at SDM for the IIHS impact simulation is lagging behind the test, which indicates that the FEA model has a softer overall response than that of the vehicle. Among all the simulated impacts events, MDB no-deployment impact, FMVSS214, EEVC, and front door side pole impacts have good SDM velocity correlation with the available tests, while the Side-NCAP, IIHS, and rear door side pole impacts show softer response, as shown in the Appendix.

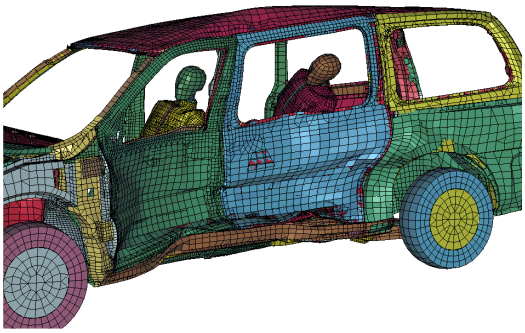

Figure 11. FEA model after the IIHS impact test.

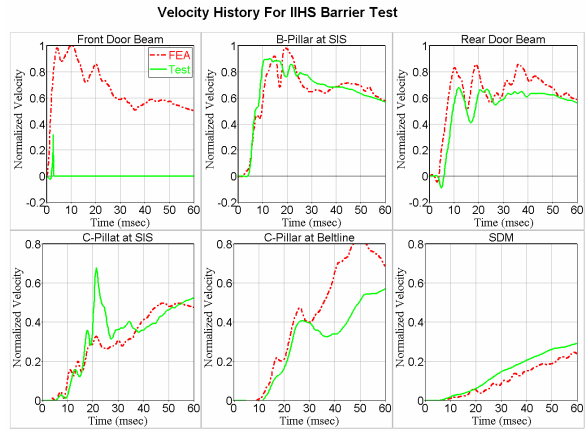

Figure 12. Velocity histories for IIHS side impact at the targeted locations for both simulation and test.

FEA-COMPATIBLE PARAMETERS

One of the objectives of this study is to identify what output parameters from finite element analysis generally correlate well with test data. These parameters are termed the FEA-compatible parameters, which are ideally suited for crash sensing algorithms if crash simulations will be used in place of crash tests for sensing algorithm calibration.

Figures 13 and 14 depict the correlations between the simulated and the measured accelerations of the FMVSS214 vehicle test at the BSIS and SDM. The acceleration data shown in the two figures is filtered through a different SAE filtering class, class 60 and class 180. Acceleration correlations before the first 7 msec at the two locations are fair, and the acceleration data can potentially be used for safing purpose, if the required airbag deployment time for FMVSS 214 is within 7 msec. The entire histories of the FEA accelerations, however, do not correlate well with the test.

Velocity, shown in Figure 15, at both SDM and BSIS shows reasonable agreement with the test, and the displacements, plotted in Figure 16, shows good agreement. It is clearly indicated from the figures that the acceleration is not a FEA-compatible measure. A similar trend is observed from other types of crash events. Complete velocity pulses for other impact tests and sensor locations are shown in the Appendix.

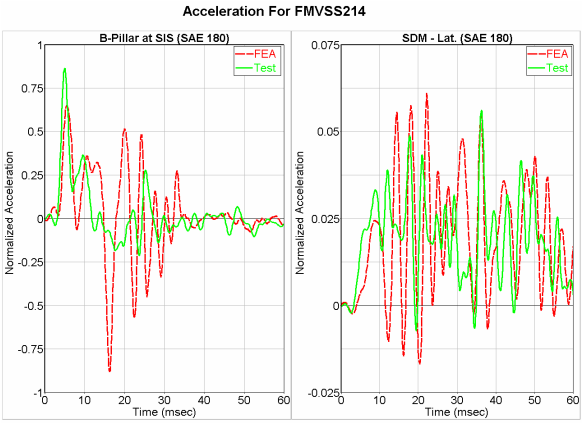

Figure 13. Acceleration histories, filter with SAE 180, for FMVSS214 side impact at the BSIS and SDM.

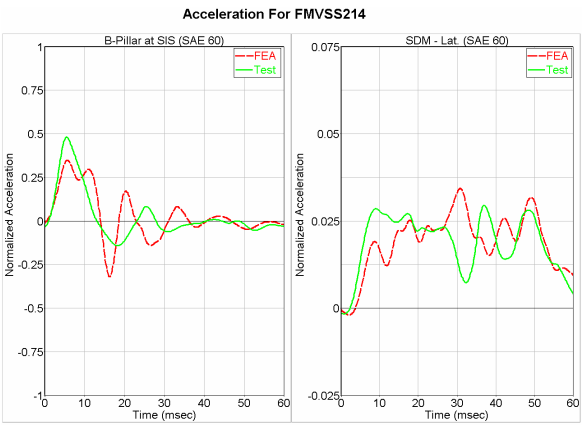

Figure 14. Acceleration histories, filter with SAE 60, for FMVSS214 side impact at the BSIS and SDM.

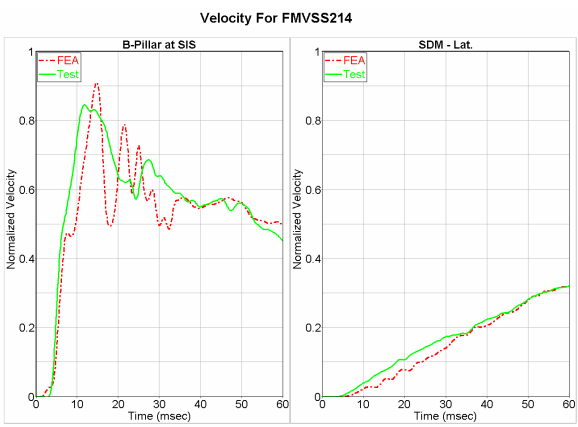

Figure 15. Velocity histories for FMVSS214 side impact at the BSIS and SDM.

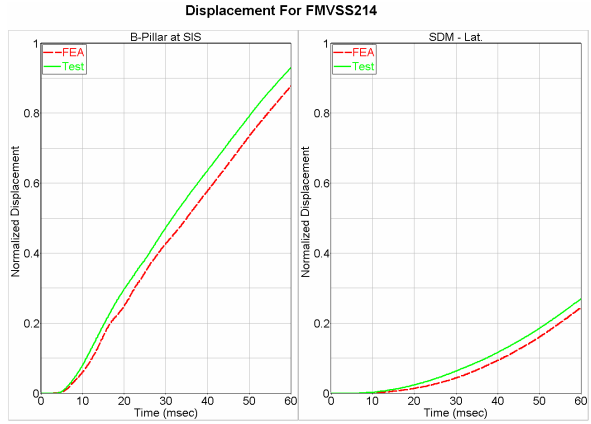

Figure 16. Displacement histories for FMVSS214 side impact at the BSIS and SDM.

We summarized our observations on the FEA compatibility of each measurement in Table 3. Those parameters rated as "fair" or "good" are ideally suited for building FEA-compatible crash sensing algorithms.

Table 3.
FEA compatibility.

Parameters	FEA-Compatibility
Jerk at SDM and Satellite Sensors	Poor
Acceleration at SDM (Entire Duration)	Poor
Acceleration at Satellite Sensors (Entire Duration)	Poor
Acceleration at SDM (Before Airbag Deployment)	Fair
Acceleration at Satellite Sensors (Before Airbag Deployment)	Fair
Velocity at SDM	Fair
Velocity at Front Sensors	Fair
Displacement at SDM	Good
Displacement at Front Sensors	Good

FEA PERFORMANCE USING EXISTING ALGORITHM AND CALIBRATION

Simulations inherently have a higher frequency content than the tests. An example of these accelerations and their frequency content at the front door beam for front door side pole impact is plotted in Figure 17. Satellite sensor signals received by SDM are also constrained by the sensor resolution and frequency of the communication. These constraints result in different clipped signals between the tests and the simulations. The filtered acceleration magnitude of the un-clipped FEA acceleration, shown in Figure 18, is higher than the test, while the magnitude of the clipped FEA data is smaller. This signal clipping and

filtering may produce different sensing performances between the test and the simulation, even though the FEA velocity correlates well with the test.

Acceleration signals from the tests were first calibrated to meet the airbag deployment target times using the test data. Algorithms were then used to determine the airbag deployment times of the simulations without changing the existing algorithms and the thresholds. It was observed from this exercise that the FEA side sensing system performance was comparable with the tests and the development of a FEA-compatible side impact sensing algorithm becomes more favorable for side impacts sensing system.

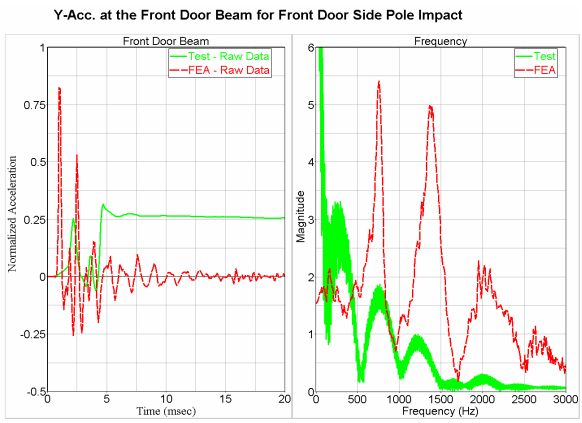

Figure 17. Test and FEA accelerations and frequency contents at the front door beam for the front door side pole impact.

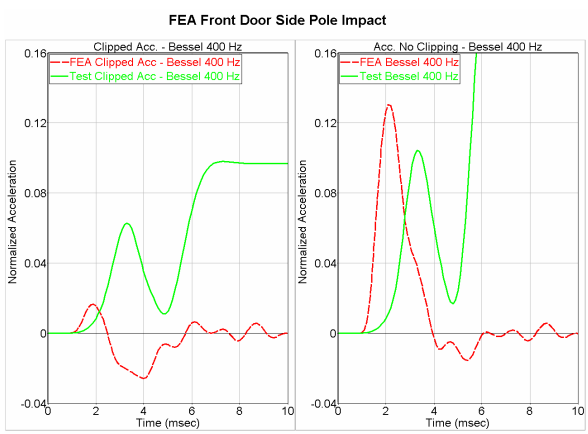

Figure 18. Test and FEA front door beam accelerations of the original and the clipped signals filtered through 4-Pole Bessel filter for the front door side pole impact.

SUMMARY

We identified and applied the critical modeling techniques and guidelines for building a high fidelity side impact finite element model for the van vehicle that could be used to simulate a suite of side impact tests for crash sensing calibration purposes. Using this enhanced model, we simulated seven different side crash events. Acceleration signals from the tests along with corresponding simulation results were calibrated to determine the side airbag deployment times without changing the existing sensing algorithms calibrated based on the tests. It was observed that the FEA side sensing system performance was comparable with the tests.

From the velocity correlations and calibration results, it is strongly suggested that the acceleration data and the calculated vehicle velocity and displacement at both satellite sensors and SDM can be subsequently used in the development of a FEA-compatible sensing algorithm.

REFERENCES

[1] Lin, Chin-Hsu and Wang, J.T., “Modeling and Simulation of Body-On-Frame Vehicles For Frontal Impact Sensing Tests”, ASME International Mechanical Engineering Congress & Exposition, Chicago, Nov. 4-10, 2006

[2] Lin, Chin-Hsu, Neal, Mark O., Wang, J.T., “Modeling And Simulations of Frontal Impact Crash Sensing Tests”, June, 2002. ASME International Mechanical Engineering Congress & Exposition, New Orleans, Lousiana, Nov. 17-22, 2002.

[3] Lin, Chin-Hsu, Neal, Mark O., and Wang, J.T., “A Case Study of FEA-Based Crash Sensing System Calibration", International Journal of Vehicle Design, 2002, vol. 29, pp.269-287

[4] Chou, C.C., Le, J., Chen, P., and Bauch, D., “Development of CAE Simulated Crash Pulses for Airbag Sensor Algorithm/Calibration in Frontal Impacts,” 17th International Technical Conference on the Enhanced safety of Vehicles, Amsterdam, June 4-7, 2001.

[5] Lin, Chin-Hsu, Neal, Mark O., and Wang, J.T., “Can Finite Element Models be Used to aid in Calibrating a Crash Sensing System”, ASME 2000 International Design Engineering Technical Conference.

[6] Livermore Software Technology Corporation, LS-DYNA Keyword User’s Manual, Version 960.

[7] Mahadevan, Kumar, Liang, Pau, and Fekete, Jim, “Effect of Strain Rate in Full Vehicle Frontal Crash Analysis,” SAE Technical Paper Series 2000-01-0625, March 6-9, 2000.

[8] Hasselman, T. K., Yap, K. C, Lin, C-H. and Cafeo, J., “A Case Study in Model Improvement For Vehicle Crashworthiness Simulation,” The 23st Int’l Modal Analysis Conf. (IMAC) 2005.

APPENDIX

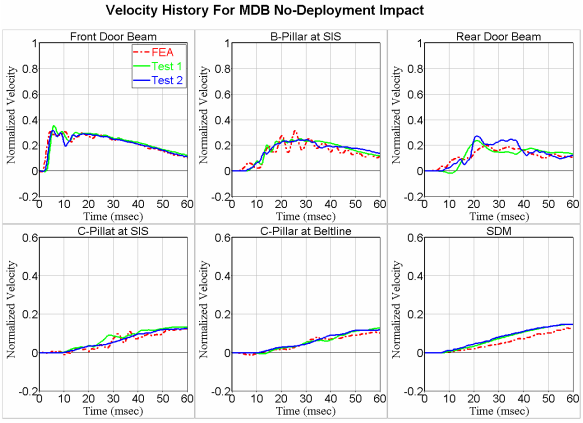

Figure A1. Velocity histories for the MDB no-deployment impact.

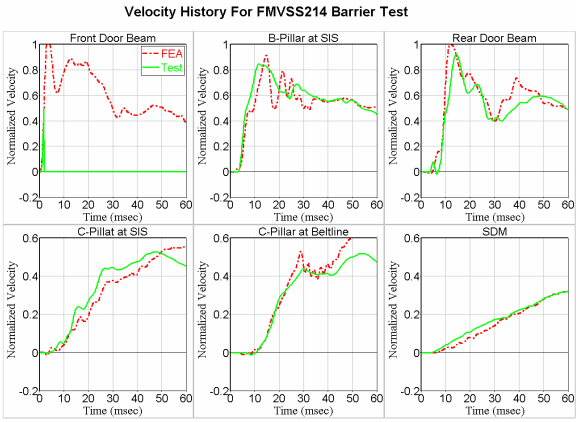

Figure A2. Velocity histories for the FMVSS214 impact.

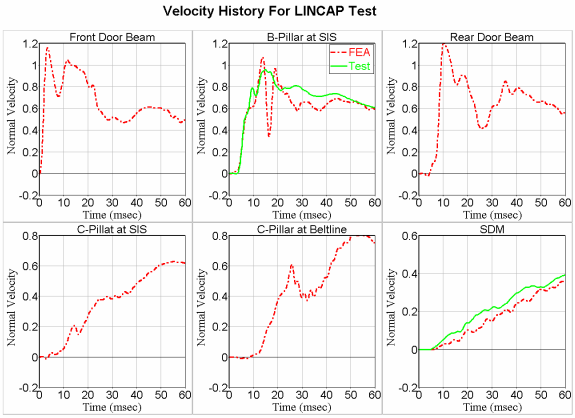

Figure A3. Velocity histories for the Side NCAP impact.

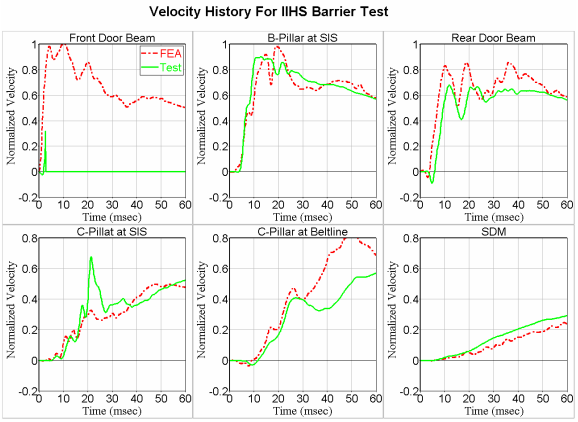

Figure A4. Velocity histories for the IIHS impact.

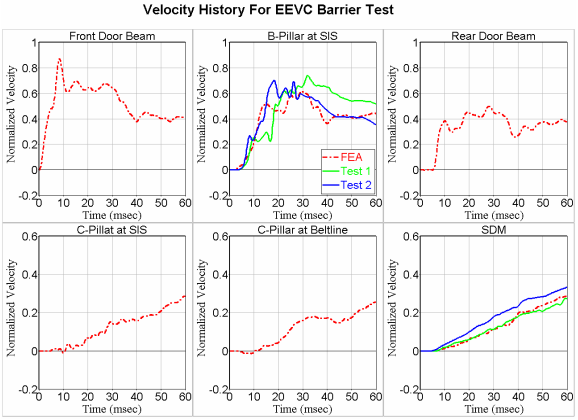

Figure A5. Velocity histories for the EEVC impact.

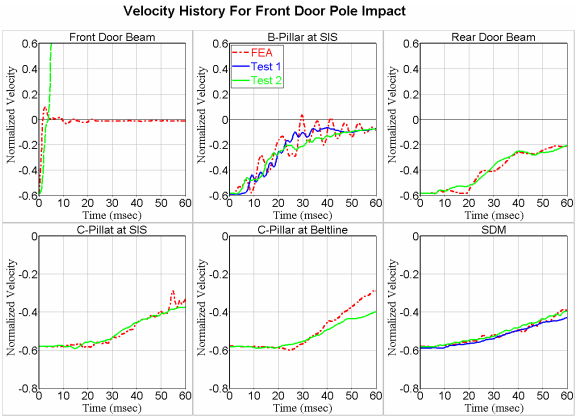

Figure A6. Velocity histories for the front door pole impact.

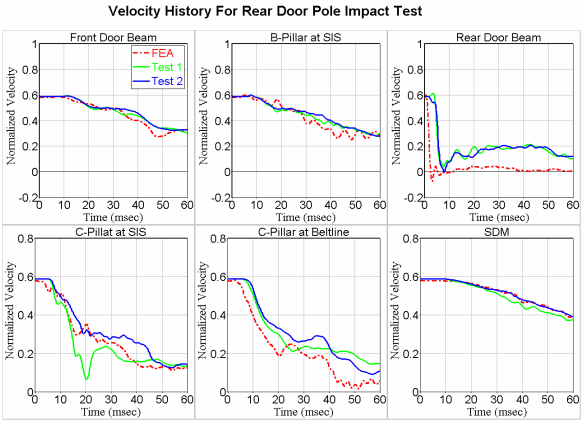

Figure A7. Velocity histories for the rear door pole impact.

INJURY OPTIMIZATION OF THE FRONTAL CRASH SUPPLEMENTAL RESTRAINT SYSTEM (SRS) DEPLOYMENT MATRIX

Ryan A. Miller
Brian T. Allen
Honda R&D Americas, Inc.
United States of America
Paper No. 07-0073

ABSTRACT

With the introduction of the FMVSS 208 upgrade for U.S. frontal crash safety, many new requirements were added. In order to meet these new requirements, manufacturers had to develop new methodologies for sensing, controlling, and deploying airbags. The standard achievement method is to use dual stage airbags with two firing thresholds.

The objective of this research was to improve three key areas of the standard method:

1) Prevent risk of inadvertent high output deployment for small occupants.
2) Improve occupant injury by achieving the ideal deployment mode
3) Reduce the complexity of the system to increase robustness.

In order to achieve these goals, it was proposed that a single ideal deployment mode could be developed by performing a parametric study where Time to Fire (TTF) and the delay between firing the first and second stage were varied independently for the driver and passenger Anthropomorphic Test Devices (ATDs). This was done for AM50% and AF5% ATDs in a front 40 km/h unbelted test mode. Once the 'ideal' TTF/delay was determined, the test speed was increased to 48 km/h and 56 km/h respectively for both belted and unbelted occupants.
The research showed that for the driver, an early TTF (10-15 ms) with a 20-30 ms delay provided the best combination of restraint for the AM50% ATD. This also allowed for good injury results in the AF5% low risk deployment mode. For the passenger, an early TTF (10-15 ms), with a longer delay (130 ms) showed the best combination of injury results. This allowed for successful Out of Position (OOP) deployments as well as good frontal crash results. It was also discovered during this research that there are some key interior lay out items that must be maintained in order to use this type of deployment strategy.

INTRODUCTION

Prior to the FMVSS 208 upgrade, most vehicles used a single stage inflator with a simple on/off firing threshold.

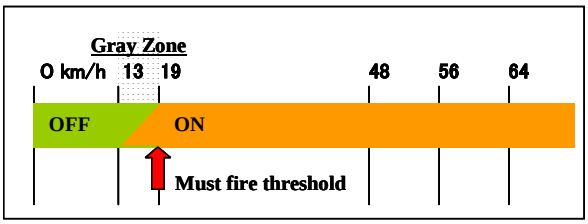

Figure 1: Pre FMVSS208 upgrade firing strategy

In this case the airbag would be guaranteed not to fire below 13 km/h, and guaranteed to fire above 19 km/h. A gray zone is created between these speeds were either condition may occur, which is shown in Figure 1. This airbag firing strategy was designed to protect for the regulation matrix shown Figure 2.

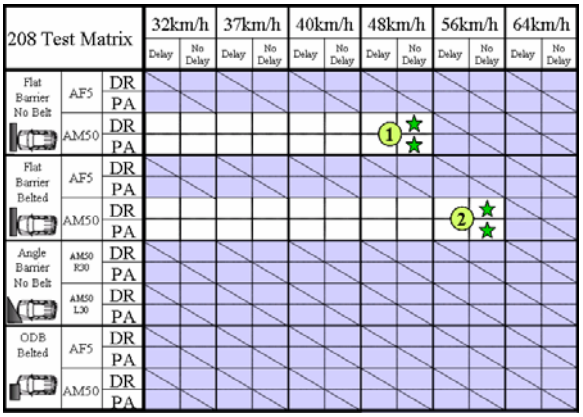

Figure 2: Pre FMVSS208 upgrade regulation matrix

In an effort to increase protection for children and smaller stature adults, the U.S. government upgraded FMVSS208 to include Low Risk Deployments (LRD) for AF5% drivers and the OOP deployments for CRABI, C3Y, and C6Y children. Increased frontal crash regulations were also added to the FMVSS 208 upgrade [1-FMVSS]. The updated frontal crash regulation matrix is shown in Figure 3.

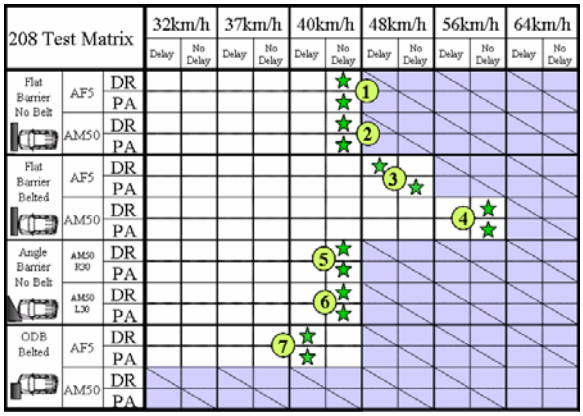

Figure 3: New FMVSS208 upgrade regulation matrix

This change in regulation necessitated a new approach involving dual stage airbags coupled with a redesigned SRS firing map to control them. Manufacturers needed a way to fire the airbags in a 'soft' deployment for AF5% and OOP children, which meant a delay prior to the second stage being fired, but also be able to fire both stages at the same time for AM50% occupants in more severe crash modes. This resulted in the SRS map shown in Figure 4.

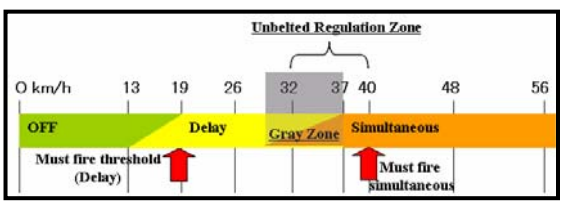

Figure 4: New FMVSS208 upgrade SRS firing map

The OOP portion of the regulation is written so that the firing time for the OOP occupant will be the same as the firing time that occurs when an AF5% occupant is placed in the passenger seat and the vehicle impacts a flat barrier at 26 km/h. Ensuring that a delay fire occurs at 26 km/h results in a gray zone between the belted and unbelted regulation zones where a vehicle could fire in either delay or simultaneous mode. To guarantee the regulation, the test matrix shown in Figure 5 is required. As can be seen, this gray zone requires four additional test modes.

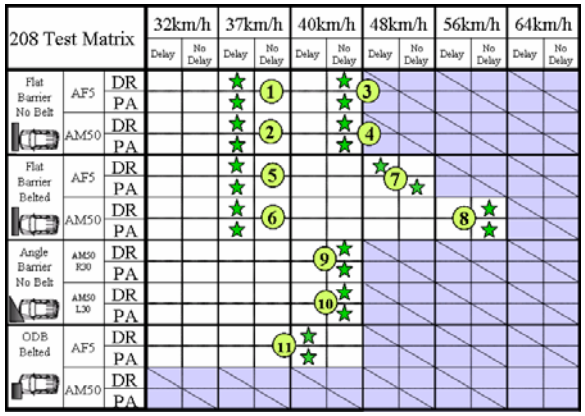

Figure 5: New FMVSS208 upgrade test matrix

METHODS

Crash Simulator System and Test Devices

This parametric study was done using AM50% HYBRID III test devices positioned according to the FMVSS 208 regulation [1-FMVSS]. The ATDs were seated in a sled buck which was built by cutting a full vehicle body in front of the A-pillar and just behind the B-pillar. Full instrument panel, steering system, pedals, and seats were applied to the sled buck, shown in Figure 6.

Figure 6: Crash simulator test buck

The crash simulator, shown in Figure 7, is a hydraulically controlled G-pulse matching device. This device includes full linear acceleration control as well as vehicle pitch control, which is shown in Figure 7.

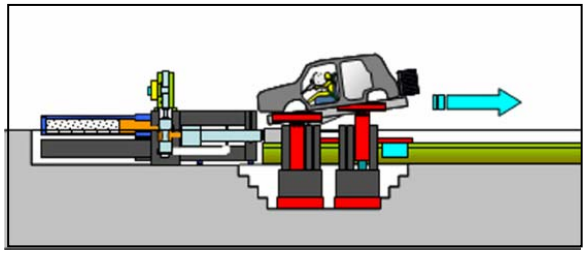

Figure 7: Crash simulator

A vehicle deceleration pulse is taken from a full CBU frontal impact then applied to the crash simulator software. The software interpolates the pulse and recreates it on the sled buck with a high degree of accuracy. An example comparison of crash simulator and crash barrier Floor G is shown in Figure 8.

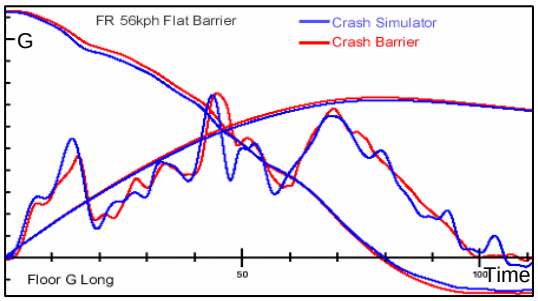

Figure 8: Crash simulator G-pulse vs. actual full vehicle frontal impact G-pulse

This accuracy and repeatability is ideal for this type of parametric study where the change in one variable can be assessed.

Test Matrix and Injury Metrics Assessed

Although all FMVSS 208 injury metrics were recorded, HIC, Chest G, Chest Deflection, and Neck Injury (NIJ) were the primary focus for comparison. Since the goal of the study was to determine the ideal TTF and delay for the airbag, the following test matrix in Figure 9 was used.

40 km/h	AM50%	No Belt	10ms	30ms
40 km/h	AM50%	No Belt	20ms	40ms
40 km/h	AM50%	No Belt	30ms	50ms
40 km/h	AM50%	No Belt	10ms	30ms
40 km/h	AM50%	No Belt	10ms	40ms
40 km/h	AM50%	No Belt	10ms	50ms
40 km/h	AM50%	No Belt	10ms	60ms

Figure 9: Initial testing matrix

Real World Injury Assessment

In addition to the primary goals of this study, it was deemed important to confirm that the ideal firing case for the AM50% dummy at the regulated velocity of 40 km/h would not cause a negative effect on unbelted occupants at speeds above the regulation. An additional test matrix was proposed to assess this possibility by comparing the traditional TTF/delay vs. the proposed 'ideal' TTF/delay.

				Driver	Passenger
40 km/h	AM50%	No Belt	10ms	40ms	140ms
56 km/h	AM50%	No Belt	10ms	40ms	140ms
40 km/h	AM50%	No Belt	10ms	15ms	
56 km/h	AM50%	No Belt	10ms	15ms	

Figure 10: Additional testing matrix

RESULTS / DISCUSSION

Once the initial test matrix was run, the resulting injury data was collected and graphed. The data was normalized as a percentage of target injury. 100% injury represents 80% of the FMVSS 208 regulation values.

Unbelted Driver Injury Comparison with Variable Second Stage Airbag Delay

The first comparison was done on the Driver. In this test series, the TTF was maintained at 10 ms and the second stage firing was varied from 20-60 ms. The critical injury parameters in this mode were Chest G,

Chest Deflection, and NIJ. These were compared with the standard TTF/delay of 10/15 ms.

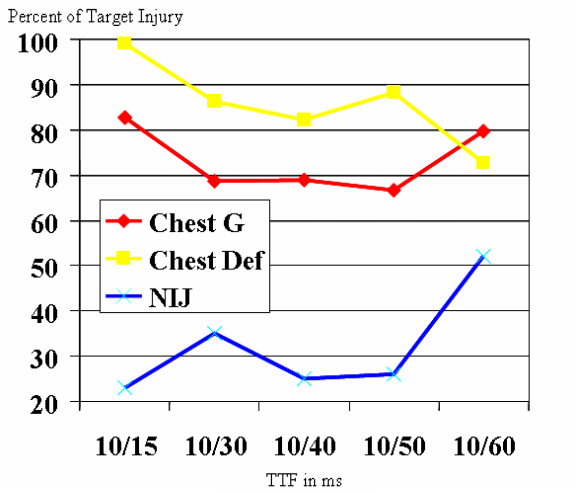

Figure 11: Unbelted Driver Injury for Variable Delay

In this case, the 'ideal' delay timing was from 30-40 ms. It became apparent that for the driver in the unbelted mode, the maximum amount of airbag restraint was preferable. This was accomplished by firing the airbag early (10 ms) to get it into position, than increase the bag pressure with the second stage fire just before the unbelted occupant made contact. The delay limit was 50 ms. At this point the second stage was pressurizing the bag while it was contacting the occupant. This caused the bag to get under the chin and increase the neck tension and extension.

Figure 12: 50ms Delay Causing Increasing Neck Injury

Although the neck injury was below the max target injury level, this mode was deemed to be unacceptable.

Unbelted Driver Injury Comparison With Variable Time to Fire

The second portion of the test matrix was to identify the 'ideal' initial fire time.

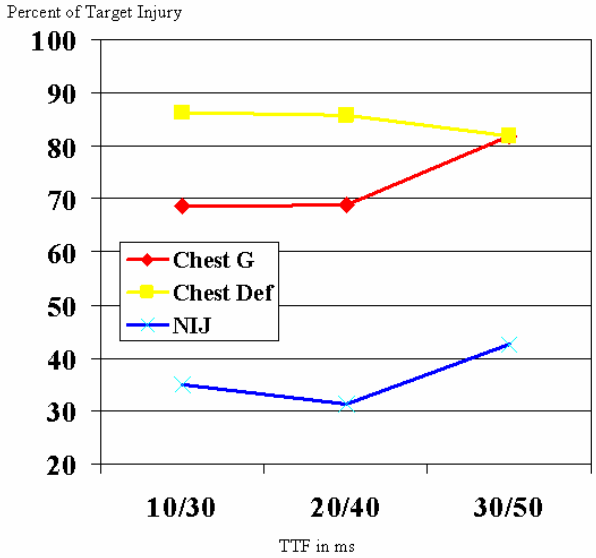

Figure 13: Unbelted Driver Injury for Delayed TTF

Based on the test results, it was determined that a fire time between 10-20 ms was preferable. At 30 ms, the airbag was not able to get into position on time and occupant injury began to increase.

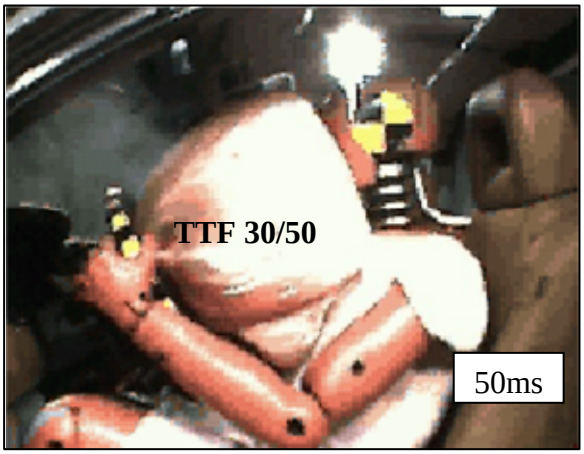

Figure 14: Airbag getting into position late with a 30ms TTF

Unbelted Passenger Injury Comparison With Variable Second Stage Airbag Delay

The passenger test matrix includes delays from 5ms to 140 ms. The long delay of 140 ms is considered a disposal stage and occurs after peak occupant injury. As can be seen in Figure 14, the increase in delay has only minimal impact on the occupant injury.

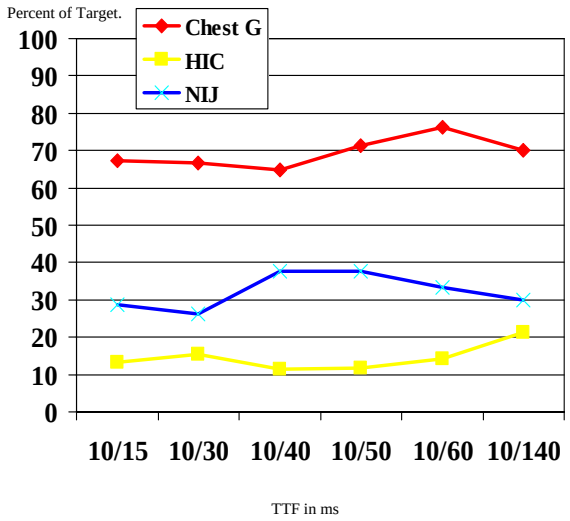

Figure 15: Comparison of delay timing on passenger injury

It is important to note that the passenger side occupant's pelvis must be restrained sufficiently to allow the head to arc into the airbag without contacting the windshield. This causes the occupant to use a much greater portion of the airbag allowing it to be softer [2-Miller].

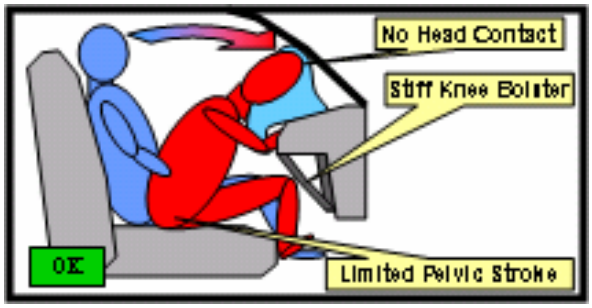

Figure 16 Illustration of head arcing with no windshield contact

Unbelted Passenger Injury Comparison with Variable TTF

The passenger side TTF was varied from 10 to 40 ms and judged according to mode and restraint performance. Again, an early deployment (10-20 ms) was preferable. By 40 ms, the airbag was unable to get into position on time.

Figure 17: Occupant is contacting the airbag before it is in position.

This late deployment reduces restraint and allows the airbag to get under the chin resulting in high neck moments.

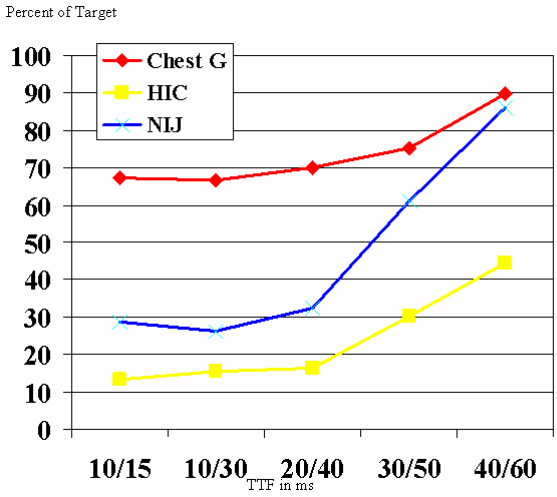

Figure 18: Passenger injury comparison with variable TTF

The final step for this study was to investigate the TTF/delay effect on AM50% occupants in a high

speed (56 km/h) unbelted condition. The injury was then compared to a typical TTF/delay.

Although all injury was compared, head and Chest Gs for the driver are shown below for comparison.

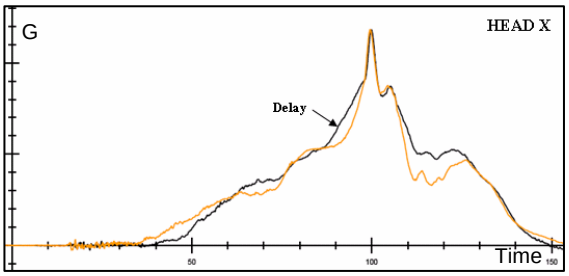

Figure 19: Driver head injury comparison

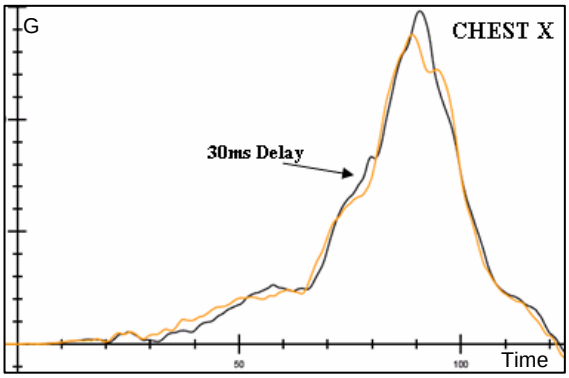

Figure 20: Driver chest injury comparison

Although the injury levels are high, as would be expected in a high speed unbelted crash, there is no significant difference in injury between the standard mode and the new proposed mode. This holds true for the passenger results which have slightly lower injury values with the new longer delay mode.

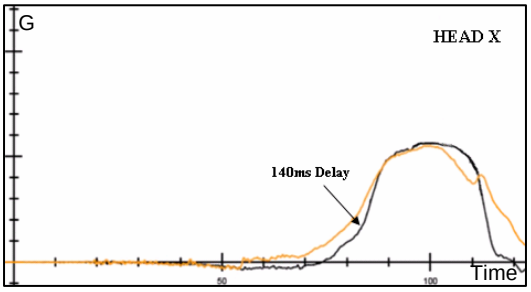

Figure 21: Passenger head injury comparison

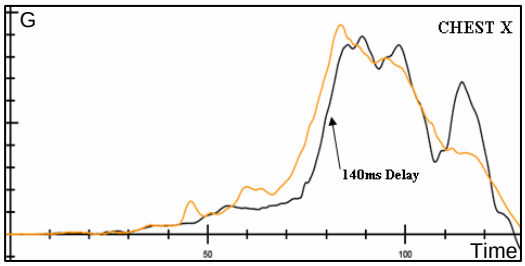

Figure 22: Passenger chest injury comparison

CONCLUSIONS

Although this was a relatively straightforward study, the conclusions are very significant. By creating an ideal TTF/delay time for the driver and passenger, the sensing system only needs to fire in one mode. This removes the gray zone from the SRS map [3-Miller].

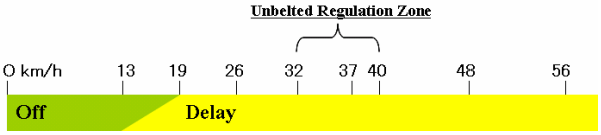

Figure 23: SRS map with only one firing mode

Since there is no longer a gray zone, crash verification no longer needs to be done for those speeds in the zone.

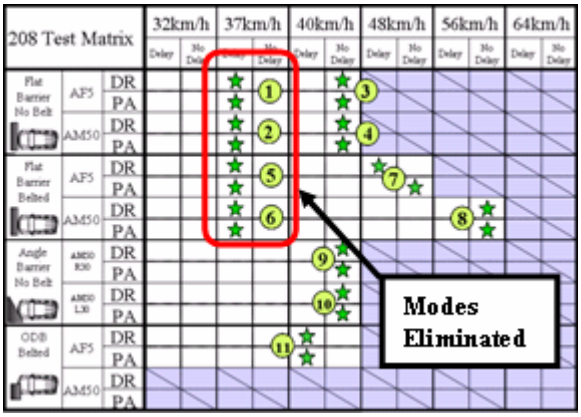

Figure 24: Verification test matrix with gray zone eliminated

This creates a more robust system with less chance for unintended deployment modes. This also opens up the future possibility of using a different firing mode to help protect occupants, like AM95% size occupants, that are currently not covered by regulation.

Due to the significant softening of the passenger airbag deployment (130 ms delay) further benefits can be realized for in-position as well as out of position small stature occupants and children.

Following the conclusion of this research, a full series of FMVSS 208 test were run using complete body units (CBU) with the 'ideal' TTF/delay SRS map. The results are summarized in Figure 25 below.

Mode	Results
FR40 km/h Flat Barrier AM50% No Belt	**OK**
FR40 km/h Flat Barrier AF5% No Belt	**OK**
FR48 km/h Flat Barrier AM50% Belted	**OK**
FR48 km/h Flat Barrier AF5% Belted	**OK**
FR40 km/h Right Angle AM50% No Belt	**OK**
FR40 km/h Left Angle AM50% No Belt	**OK**
FR40 km/h ODB AF5% Belted	**OK**
Low Risk Deployment AF5% Pos 1	**OK**
Low Risk Deployment AF5% Pos 2	**OK**
Out of Position C6Y Pos 1	**OK**
Out of Position C6Y Pos 2	**OK**

Figure 25: CBU confirmation test matrix

REFERENCES

[1] Code of Federal Regulations., US DOT, Office of the Federal Register National Archives and Records Administration. Washington, D.C.: 2004

[2] Miller, United States Patent Application, 2006/0174689, Published August 10, 2006

[3] Miller et al, United States Patent Application, 2006/0175807, Published August 10, 2006

DEVELOPMENT OF PROPOSED CRASH TEST PROCEDURES FOR AMBULANCE VEHICLES

Nadine Levick
Objective Safety LLC
USA
Raphael Grzebieta
Monash University
Australia
Paper Number 07-0074

ABSTRACT

Ambulance vehicles are a unique passenger environment with complex crashworthiness and occupant protection issues, eg. occupants in various orientations, unique human factors aspects and an array of aftermarket interior modifications. In the USA, ambulance vehicle occupant protection, crashworthiness and safety testing lags 30 years behind current general automotive safety technology. This paper proposes crash test procedures and outlines some of the challenges faced for such vehicles based on manufacturer and consumer conducted pre-modification crash tests and previous ambulance sled and full scale crash tests.

A typical ambulance vehicle from one of the largest fleets globally, was addressed. Based on manufacturer specifications, crash test data for the vehicle, inspections and other published data regarding ambulance vehicle crashes, sled and crash testing were considered – an approach to an impact testing procedure is outlined and developed by a multidisciplinary team.

Assessment and development focused on vehicle crashworthiness performance and real world human factors aspects of aftermarket interior modifications. Frontal and side impact crashworthiness testing profiles for this vehicle were determined and developed inline with parameters outlined in ASA 4535 (ambulance restraint systems standard) and the CEN 1789 standard. The testing profiles include a recumbent occupant, rear and forward facing seated occupants, 50th and 95th percentile ATDs, including side impact ATDs for seating positions exposed to side impacts.

The authors propose that ambulance vehicle safety testing and design should be driven by accepted automotive safety practice. In a setting of high crash rates, a complex occupant and emergency care environment, and the absence of prescribed dynamic crashworthiness test procedures for ambulances - the proposed test procedures in this paper provide a first approach to describe the approach to the technical development of comprehensive crash testing profiles in this setting. Such profiles for this environment will ensure that system safety can be ascertained and optimized for these vehicles, and support safety enhancements and occupant protection for ambulance vehicle development.

INTRODUCTION

Emergency Medical Service (EMS) vehicles, ambulances, are relatively familiar vehicles to the community in general. They are perceived as 'life savers' racing through the streets to provide emergency medical care to the public. It is the vehicle that comes to rescue crash victims on roads and highways. However, what are the safety issues that pertain to this important public service and public safety vehicle? How safe are these vehicles and to what standards are they designed and tested?

EMS is a relatively new industry, an industry that has an unusual history of beginnings within the mortician industry. The first modern ambulances were hearses, usually a Cadillac, a vehicle in which an occupant could be transported in the recumbent position. Over the past 30 years, the sophistication of the medical care possible to provide in the EMS environment has advanced dramatically, with EMS providers over that short time becoming highly skilled and expertly trained emergency health care professionals – with use of high tech medications and equipment. However, the vehicle occupant safety issues pertaining to the delivery of EMS care have not kept pace with the advancement of the medical emergency care provided. Nor has EMS vehicle safety kept pace with the developments in automotive safety. This is possibly due to the ambulance graduating from the Cadillac to a combined chassis with a mounted box, somehow outside of the purview of both automotive safety and also occupational safety and health arenas.

Compounding this also is that ambulance vehicles in many parts of the world are a very diverse fleet: vans, light and heavy trucks and freightliners. Despite the large strides the general automotive industry has made in the last 30 years in passenger vehicles occupant protection and passive and active safety, this expertise has not yet translated substantively to the safety of ambulance vehicles particularly in the USA.

There are few safety standards and no crashworthiness safety test procedures and guidelines that pertain to ambulance vehicles in the USA and very limited safety testing requirements in Europe established in 1999 (CEN1789). Australia has had the ambulance restraint standard ASA 4535 in place since 1999 (AS/NZS 4535:1999), and it is the most stringent to date globally. Thus ascertaining the safety of EMS transport vehicles (and products in that environment) remained limited largely to expert opinion and peer evaluation in a piecemeal fashion until 1999 in Australia and 2000 in Europe, and still remain so in USA.

EMS in the USA has been generally demonstrated recently to be a dangerous profession, and vehicles crashes have been shown to be the most likely cause of a work related fatality in EMS (Maguire 2002). The most dangerous part of the ambulance vehicle has been demonstrated in both biomechanical and epidemiological studies to be the rear patient compartment (Becker 2003, Levick 2000-2001), which currently is a part of the ambulance vehicle that is largely exempt from the USA Federal Motor Vehicle Safety Standards (FMVSS 49CFR).

There is approximately one ambulance crash fatality per week in the USA, and a number of serious injuries for each fatality, with over 4,000 reportable crashes per year (Becker 2003). Unfortunately in the USA, no national reporting system or database exists specifically for identifying ambulance crash related injuries and their nature. Hence, specific details as to which injuries occurred and what specifically were the mechanisms which caused them are scarce, and there is not yet a national system for this data capture. What we do know is that ambulances have high crash fatality rates per mile, well above those of passenger vehicles, or even when compared to similar sized vehicles (Ray 2005) and also when compared to buses and trucks (FMCSA). There are numerous reports of serious injury occurring from loose equipment becoming projectiles, and occupants being ejected from vehicles - all issue that can be addressed with a combination of restraint standards for occupants and equipment – and practice policies mandating the use of such restraint systems.

There has been a limited number of peer reviewed automotive safety engineering testing conducted for the EMS environment in Sweden (Turbell 1980), Australia (Best 1993, Levick 1998), and the USA (Levick 2000-2001). That which has been conducted has clearly identified some predictable and largely preventable hazards, particularly pertaining to intersection crashes and the hazards of the rear patient compartment, demonstrating the benefit of use of existing restraints for occupants, the importance of over the shoulder harnesses for the recumbent patient and firmly securing all equipment (Best 1993, Levick 1998-2001). These studies also identify hostile and hazardous interior surfaces of the rear compartment, as well as a need for head protection. Many fatal and injurious ambulance crashes occur at intersections, failure to come to a complete stop has been identified as an extremely high risk practice, Lack of use of seatbelts by EMS personnel is cited frequently in the literature as a predominant cause for the high injury and fatality rates for occupants in EMS crashes (Becker 2003). The hazards resulting from the failure to secure equipment in the patient compartment, which has also been found to cause serious injury in the event of a collision has also been documented. This is supported by the engineering data from ambulance safety research involving crash tests (Levick 2001), as well as insurance and litigation records. With ambulance crashes being identified in the USA as the highest cause of patient adverse event mortality and serious morbidity (Wang 2007)

Existing Ambulance Standards

Prior to 1999 there were no dynamic safety performance standards for ambulances globally. The first nationally approved safety performance standard was the Australian ASA 4535, in 1999 that required dynamic impact testing of the components in the ambulance vehicle, and the use of a 50th percentile and a 95th percentile, anthropomorphic crash test dummy (ATD) with a 24 G impact test forward and rear and 10 G laterally.

The CEN followed, implemented in 2000 in Europe, requiring safety performance testing to 10 G forward, rear, laterally and vertically, being a much reduced severity level. There is a 2006 revised draft currently under review.

Both the ASA and CEN are mandated and not voluntary.

The very recently developed USA American National Standards Institute/American Society of Safety Engineers Z15.1 Fleet Safety Standard (ASSE/ANSI 2006) is possibly the only nationally approved fleet safety standard that is now applicable to the safety management of EMS vehicle fleets in the USA. It requires that the vehicles be crashworthy and safe – yet, in the USA there are no crashworthiness standards for these vehicles. The GSA KKK ambulance vehicle specification guideline, currently version E and soon to be updated to version F – is a purchase specification and not a safety performance standard (GSA KKK), and does not provide for guidelines for any dynamic crash testing – rather simply static tests. Moreover it has no automotive safety crashworthiness impact performance requirements. It does make reference to the Federal Motor Vehicle Safety Standards – however in the USA ambulances have a specific exemption from that standard (FMVSS). Also the GSA KKK is a voluntary specification and compliance is not mandated. It is likely that the implementation of the new ASSE/ANSI standard will enhance the data collected regarding EMS vehicle safety, and hopefully provide more emphasis on EMS vehicle safety generally and assist in bringing EMS vehicle safety more inline with state of the art automotive safety practices.

Study focus vehicle selection

Much of Europe, Scandinavia, Asia and Australasia currently use fleets of automotive industry designed and manufactured vans with specialized aftermarket additional retrofits to adapt them to the ambulance market. There is decreasing presence of the chassis with aftermarket box outside of the USA.

There are some interesting challenges pertaining to ambulance vehicle crashworthiness. Asides from the fact that the CEN standard is a less severe impact testing profile than the ASA standard, both are standards which only require deceleration/acceleration sled testing. In other words these are tests of stability and safety performance of the retrofit under acceleration/deceleration conditions – in contrast to structural crashworthiness testing of the whole vehicle with impact, barrier or full vehicle deforming and intrusion crash tests.

This is an important aspect of the safety and safety testing of these vehicles. Vehicles manufactured by the automotive industry are complete vehicles subjected to sophisticated structural and automotive crashworthiness design, testing and oversight prior to their retrofit. Furthermore, any ambulance retrofits built into structurally modified vehicles or the chassis/box design, may well not share safety performance of ambulance vehicles with retrofits built into an intact automotive industry manufactured vehicle, where there are no structural modifications. In the case of the chassis /box type of ambulance – in the USA there has been no formal sophisticated automotive industry dynamic or impact structural and automotive crashworthiness impact design, testing and oversight in the manufacture of the rear passenger compartment box asides from the research conducted by the authors (Levick 2000-2001), and one project conducted in Canada, for which comprehensive findings are still pending. In the USA there is currently no requirement or parameters by which to dynamically crash test the rear compartment box or the chassis/box combination.

Thus the ambulance retrofit into a complete intact automotive industry designed and manufactured vehicle such as a van, is in a vehicle which has already a high degree of structural crashworthiness design and testing at the outset by the original automotive manufacturer – so a basic deceleration/acceleration sled test is more a test of the safety performance of the retrofit modifications, and rather than a test for the safety of the vehicle as a whole. Albeit that there does exist some useful indication of general vehicle safety and crashworthiness performance with acceleration/deceleration dynamic testing. Thus the testing of the performance of the retrofit and equipment mounts are somewhat of an additional issue beyond the whole vehicle's crashworthiness including intrusion and vehicle structural deformation and crashworthiness for a vehicle that has already been subjected to this type of testing. However it is understood that the retrofit may perform differently to some degree in a setting of vehicle deformation and intrusion. In the setting of the chassis/box design – these rear occupant compartments are not produced by the automotive safety engineering and manufacturing industry and are not required to be dynamically safety tested in the USA by automotive industry manufacturers. Thus if the only dynamic impact testing these aftermarket chassis/ box combination vehicles are subjected to would be a deceleration/acceleration test – this is a test that does not involve any automotive structural deformation crashworthiness testing but is simply the deceleration test of the retrofit. Thus the safety of the chassis/box construction under true impact, deformation and intrusion conditions cannot be effectively demonstrated with the existing ambulance testing standards, either CEN or ASA. Although the ASA and CEN may give some indication of the

performance of the retrofit under deceleration conditions – it does not address the combined vehicle and retrofit performance structurally under impact crashworthiness conditions in the real world setting of a crash – where intrusion occurs.

For these reasons additionally, the vehicle selected here for this paper was the automotive industry manufactured intact structurally unmodified van and not the combined box and chassis vehicle, and also not a van that has undergone any structural after market modification. For those vehicles the research team suggests that this form of testing is suboptimal.

Approach to Crash Test Profiles

Configuration of ambulance vehicles to reflect real world practice and within realistic parameters of anthropometric test devices (ATDs) for each test procedure are key aspects of safety testing of ambulances. Ambulances differ from other passenger vehicles in that the occupants are oriented in a range of seating and lying positions and the medics are trying to perform clinical and emergency care during transport. Although in only less than 5% of transports is it life threatening care. Additionally there is often heavy equipment in close proximity to occupants, such as oxygen cylinders and cardiac monitors.

Despite the comparatively small market of the ambulance retrofit industry when compared to the general automotive market – it is important that testing requirements and standards be designed to address real world risks and hazards for the occupants of these vehicles. In the general automotive industry – crashworthiness testing is driven strongly by real world injury data, with the design and ongoing development of the New Car Assessment Program (NCAP) testing (EuroNCAP, USA and Australian NCAP). However, real world injury data on ambulance occupants for each vehicle and retrofit type is at best limited, if available at all. Also, the ambulance environment is an unusual environment where occupant protection is impacted by both realms of vehicle and interior design and also practice policy. Policies such as seat belt use, equipment required to be carried on the vehicles and procedures that are required to be performed all have bearing on what design and testing is appropriate. This makes the design of testing procedures very complex – Additionally, given the expense of testing for this small niche market, it is important that the testing procedures are not redundant – ie. requiring protection in a part of the vehicle that has no injury hazards described. For example, if it were that the occupants were to be seated and belted at all times in a moving vehicle then the focus of interior design and testing may differ if this was not the case. Challenges faced by the ambulance retrofit industry in Europe are two fold: one that any testing required be testing that improves safety and outcome, and two that the 'standard writing' process is voluntary - and participation is not reimbursed and thus that active input from the retrofit manufacturers is likely to be minimal due to the expense of participation in the process. Hence there are concerns from the retrofit manufacturers regarding the concept of safety testing standards in the absence of real world injury data and also the practical challenges for their input to be included.

Recent epidemiologic data describes frontal impact, right side impact and rollover as the most frequent mechanisms that occur with serious morbidity and mortality in the USA – often the result of intersection crashes.

An additional challenge is that in most USA ambulances, the right hand side of the vehicle is fitted with a 'squad bench' – a structure that has minimal if any automotive safety features. And this is a structure which has been described in previous military vehicle crash testing to be a hazardous mode of occupant transport in a forward traveling vehicle (Richardson et al 1999, Zou et al 1999).

Also as per the ASA 4345 standard occupant seating in the ambulance vehicle is required to include 50th - 95th percentile male ATD. The seating position options include rear facing captains chair, one to three occupants on the right sided 'squad bench' seated sideways facing toward the left wall over the vehicle - and a recumbent patient (See Fig 1). Some USA ambulances also have a seated occupant in a small seat (the CPR seat) in the middle of the cabinetry on the left wall of the ambulance. Although most USA ambulances are configured with a squad bench – and some the CPR seat, the new proposed KKK – F purchase specifications do not mandate a squad bench. Thus a testing profile should consider the possibility for a similar occupant layout as in the European and Australian ambulance vehicles. Neither the testing profiles for the European ambulance vehicles, nor the testing profiles for the Australian ambulance vehicles specify a side impact ATD for the occupants seated in seating positions vulnerable to a side impact crash.

So there are fundamentally three issues that appear to have bearing on the real world applicability of existing testing profiles of ambulance vehicles: one is the difference between acceleration/deceleration

testing of the retro fit separately from full crash and deformation testing of the full vehicle with the retrofit in place, the second is the use of a side impact ATD for occupants in involved in a crash scenario where they would be seated sideways, and thirdly the limitation of real world injury and crash data for guiding design and testing profiles. These three issues are also confounded to some degree by the impact of practice policies on the potential for specific risks and hazards – as well as the broad spectrum of ambulance vehicle configurations in the USA, and that currently that those designs are strongly being driven by end users who have no formal background in automotive safety.

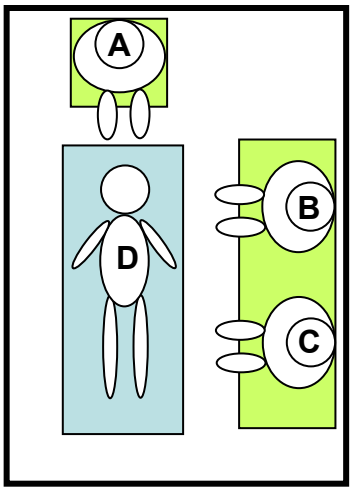

Figure 1. Seating positions as per. As per current USA ambulance layout – Test Plan 1

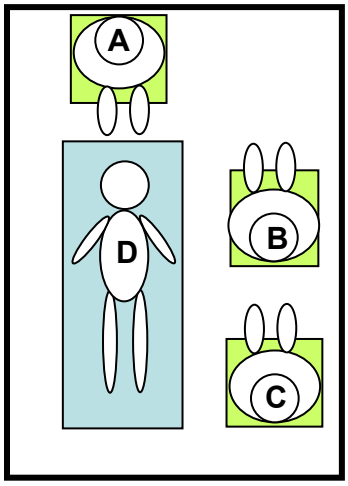

Figure 2. Seating positions as per anticipated USA ambulance layout post KKK F release, with only forward and rear facing seats – Test Plan 2

Test procedure

As stated above, given that the chassis/box style vehicle is not crash tested as a unit prior to retrofit it is felt that the testing profile of this vehicle would not be included within the constraints of this paper and that the profiles discussed here will be restricted to application in the setting of an automotive industry built structurally intact van with an ambulance retrofit that does not interfere with the original vehicle structure. The chassis/box combination would require more extensive and detailed testing, including full vehicle testing to ascertain the crashworthiness of the structure as a whole and to be deemed safe for occupants than this profile provides.

Also there is no specific ATD for a recumbent patient – so a standard 50th percentile ATD such as a Hybrid III with articulating legs, is suggested in this testing for the recumbent occupant, although the existing standards suggest that a simple mass object could replace the recumbent occupant. Given that the effectiveness of the recumbent occupant restraint system has been demonstrated to be a potential injury hazard – this opportunity to evaluate that system should be considered. For each test where seated occupants are subjected to a side impact force – a side impact ATD should be used to demonstrate more accurately what the hazards are for that occupant and the restraint of that occupant. Ascertaining which sized ATD should be in which seating position is challenging as there is no population data to describe the real world situation.

The test procedure described here attempts to address testing that reflects the safety of real world practice and under real world conditions.

For frontal and rear collision, from the limited crash data that exists – it appears that USA ambulances are most frequently involved in frontal high speed and rear lower speed impacts. As such a test procedure as outlined in the ASA for frontal impact of 24 G and a rear impact of 10 G as specified in the CEN could also be considered appropriate. The nature of the ATDs for each position, should reflect real world practice, and the 50th and 95th percentile ATDs as described in the ASA standards address the size spectrum of ambulance occupants. The restraint configuration used should be the restraint configuration to be implemented in the on road vehicle – and restraint of medics, patient, and other occupants, key equipment such as oxygen tanks, sharps containers and cardiac monitors as well as medication bags and communications equipment should be addressed.

There is much discussion in the literature regarding the optimal restraint configuration for a side facing occupant in a forward moving vehicle. Ideally the floor plan for Test Plan 2 provides more optimal occupant protection for all occupants in a frontal or rear crash, and likely also a side impact when compared to Test Plan 1's layout.

It is unfortunate that the side of the vehicle that is most frequently struck in a side impact, is the right side of the vehicle (due primarily to the driver being on the left). It is also the side of the vehicle that has the most seated occupants. However as there are other issues that come into play regarding the access to the vehicle and the safety of that with respect to road traffic this is likely to be a feature of the ongoing design of ambulance vehicles in the USA. An important aspect to consider in the testing is for the correct type of ATD to be in the positions that coincide with the location of occupants in the real world setting.

The following are possible test procedures that could be applied in this environment. They are based on current ASA and CEN documented and mandated test requirements. However the authors note that there are no injury criteria (NHTSA) associated with these published requirements, never the less these procedures could act as a first step to bring the USA up to current world practice. Even though the authors believe these procedures as described, are deficient.

Frontal

In the longitudinal direction with a 50th percentile ATD in forward or rearward seating positions A, B, C, D. When the test rig (sled) is subject to a velocity change of not less than 49 km/h in the forward direction, a deceleration of between 24g and 34g shall be achieved within 30 milliseconds. The deceleration shall remain within the range of 24g to 34g for not less than 20 milliseconds, deceleration values outside this range that occur for period of not greater than 1 millisecond may be disregarded.

In the longitudinal direction with a 95th percentile ATD in forward or rearward seating positions A, B, C, D. When the test rig (sled) is subject to a velocity change of not less than 49 km/h in the forward direction, a deceleration of between 18.2g and 26g shall be achieved within 30 milliseconds. The deceleration shall remain within the range of 18.2g to 26g for not less than 20 milliseconds, deceleration values outside this range that occur for period of not greater than 1 millisecond may be disregarded.

Rear

In the longitudinal direction with a 50th percentile ATD in forward or rearward seating positions A, B, C, D. When the test rig (sled) is subject to a velocity change of not less than 32 km/h in the rear direction, a deceleration of between 12g and 22g shall be achieved within 30 milliseconds. The deceleration shall remain within the range of 10g to 17g for not less than 20 milliseconds, but deceleration values outside this range that occur for periods of not greater than 1 millisecond may be disregarded.

For the 95th percentile ATD, when the test rig (sled) is subject to a velocity change of not less than 32 km/h in the rear direction, a deceleration of between 9g and 19g shall be achieved within 30 milliseconds. The deceleration shall remain within the range of 10g to 17g for not less than 20 milliseconds, but deceleration values outside this range that occur for periods of not greater than 1 millisecond may be disregarded.

Right Side Impact

For the squad bench layout Test Plan 1, the 50th and 95th percentile manikins could be utilized for this test in that seating position. However, for the Test Plan 2 layout, in the side impact test – the side impact ATD should be utilized.

For the 50th percentile ATD, when the test rig (sled) is subject to a velocity change of not less than 32 km/h in the lateral direction, a deceleration of between 12g and 22g shall be achieved within 30 milliseconds. The deceleration shall remain within the range of 10g to 17g for not less than 20 milliseconds, but deceleration values outside this range that occur for periods of not greater than 1 millisecond may be disregarded.

For the 95th percentile ATD, when the test rig (sled) is subject to a velocity change of not less than 32 km/h in the lateral direction, a deceleration of between 9g and 19g shall be achieved within 30 milliseconds. The deceleration shall remain within the range of 10g to 17g for not less than 20 milliseconds, but deceleration values outside this range that occur for periods of not greater than 1 millisecond may be disregarded.

Vertical

This test is to provide for safety performance in the setting of an aspect of a rollover situation. Clearly this is not a rollover simulation – but a proxy for the performance of the ambulance retrofit in this orientation for impact. Ideally a roll over test would provide far more comprehensive and valuable information, however this may not be realistic to achieve in the real world setting of this particular industry at present. The ASA 4535 does not include a vertical component. Nevertheless, given the nature of ambulance crashes – it is felt by the authors that this test should be included in this test profile. For a 50th percentile ATD, when the test rig (sled) is subject to a velocity change of not less than 32 km/h in the vertical direction, a deceleration of between 12g and 22g shall be achieved within 30 milliseconds. The deceleration shall remain within the range of 10g to 17g for not less than 20 milliseconds, but deceleration values outside this range that occur for periods of not greater than 1 millisecond may be disregarded.

For the 95th percentile ATD, when the test rig (sled) is subject to a velocity change of not less than 32 km/h in the vertical direction, a deceleration of between 9g and 19g shall be achieved within 30 milliseconds. The deceleration shall remain within the range of 10g to 17g for not less than 20 milliseconds, but deceleration values outside this range that occur for periods of not greater than 1 millisecond may be disregarded.

CONCEPTUAL DISCUSSION

This paper presents a basic and initial step in addressing the automotive safety testing and safety performance standards for ambulance vehicles in the USA. The testing parameters put forward in this paper have been modeled on the existing two accepted and ratified ambulance safety performance testing standards, ASA 4535 and CEN 1789, thus these are recommendations that are within the currently available ASA and CEN standards. Whilst the authors would like to see changes in the USA ambulance safety and crashworthiness practice and standards incorporating these suggested requirements as outlined in this paper - It is clear that what has been suggested here is but a first step. These requirements are in no way regarded as adequate from an automotive safety engineering perspective. True vehicle performance and crashworthiness safety standards should include comprehensive real world crash data, full vehicle crash test data, include formal injury data and address known injury criteria, and embrace active involvement of the automotive safety engineering industry as is accepted practice in the field of automotive safety engineering.

Regarding specific aspects of the USA ambulance vehicle interior retrofit, an issue that is of major concern is that the practice of use of a side facing 'squad bench' – a structure constructed devoid of automotive safety principles (Richardson et al 1999, Zou et al 1999) – This issue should be addressed in the USA in a similar fashion as Europe and Australia - ie. discontinued – there is no supporting medical evidence for its need, and extensive automotive safety evidence that it is a dangerous occupant practice- both in the setting of frontal and side impacts, as well as of limited ergonomic function. Additionally, in the setting of side impacts, even with the use of automotive designed seating forward or rear facing - the issue of side impact protection is of concern. A potential solution to this is to design a seat for this environment that integrates some side impact head and upper body protection.

Importantly there is no reference to any injury criteria, for example, the HIC or chest decelerations (NHTSA) - this is of great concern particularly given two data points. One being that ambulance vehicles in the USA have a specific exemption from FMVSS CFR 49 517 (for head impact protection) and secondly that it has been documented that serious head injury is associated with greater than 60% of rear occupant fatalities.

Furthermore, it is the opinion of the authors that for ambulance vehicles which are <u>not</u> retrofits of intact and structurally unmodified automotive industry complete vehicles (structurally intact vans) – such as the chassis and box design or also retrofits of vans that involve any structural modifications that may affect crashworthiness performance, that standards such as the CEN and the ASA are inadequate for demonstrating the occupant safety of such combination or structurally modified vehicles. In such circumstances, with structurally modified vehicles or combination vehicles, demonstration of occupant safety and crashworthiness would require full vehicle crash testing – simple deceleration/acceleration testing of an intact vehicle shell may not provide meaningful results – particularly at 10G - as deformation of the structure of the shell via intrusion is not able to be modeled in a simple deceleration/acceleration test. There is much evidence from real world crash ambulance crashes, even relatively low speed intersection collisions or collisions involving fixed objects that there are serious occupant hazards and failures of occupant

protection of the chassis and box type of ambulance design, particularly for the rear compartment occupants. It remains an irony that the occupant protection for the rear compartment of vehicles carrying laundry and packages is no different from a dynamic impact crashworthiness perspective than for these chassis box combination ambulance vehicles carrying our emergency providers, patients and next of kin in the USA.

CONCLUSIONS

Emergency medical service transport is occurring in a setting where its own vehicle safety has been identified as less than optimal in the USA. Ambulance vehicle design and safety testing should be driven by accepted automotive safety and engineering practice. In a setting of high crash rates, a complex occupant and emergency care environment, and the absence of prescribed dynamic crashworthiness test procedures for ambulances - the proposed test procedures in this paper provide a first approach to describe the technical development of comprehensive crash testing profiles in this setting in the USA. Ambulance vehicles that are not intact automotive industry manufactured vehicles, or are structurally modified cannot be demonstrated to be safe for occupants in the rear compartment in the absence of full vehicle dynamic impact testing to demonstrate intrusion. Additionally, use of design features such as a non automotive designed side facing squad bench should be avoided given the challenges in addressing both occupant safety and the provision of patient care with this orientation. Such profiles as outlined in this paper for the ambulance environment could ensure that vehicle design and vehicle system safety can be ascertained and optimized, and also support safety enhancements for ongoing ambulance vehicle development.

REFERENCES

ANSI/ASSE Z15.1-2006 American Standard: Safe Practices for Motor Vehicle Operations, American National Standards Institute (ANSI)/American Society of Safety Engineers (ASSE) Accredited Standards Committee, **Z-15**, March 2006 http://www.asse.org

Becker LR, Zaloshnja E, Levick N, Miller TR, Relative risk of injury and death in ambulances and other emergency vehicles, Accident Analysis and Prevention **35**, 2003, 941–948

Best GH, Zivkovic G, Ryan GA, Development of an effective ambulance patient restraint, Society of Automotive Engineering Australasia Journal, Vol. **53**, No. 1, p. 17 (4pp) 1993

Eppinger R, Sun E, Bandak F, Haffner M, Khaewpong N, Maltese M
National Highway Traffic Safety Administration National Transportation Biomechanics Research Center (NTBRC), Kuppa S, Nguyen T, Takhounts E, Tannous R, Zhang A, Conrad Technologies, Inc. Saul R, National Highway Traffic Safety (NHTSA) Administration Vehicle Research & Test Center (VRTC), Development of Improved Injury Criteria for the Assessment of Advanced Automotive Restraint Systems – II, Table ES-6, page ES-11, NHTSA 1999

European Ambulance Restraint Systems Standards CEN, European Committee for Standardization, EN **1789**:1999, 2002

Federal Motor Vehicle Carrier Safety Administration (FMCSA) – Safety and Security Databases, http://www.fmcsa.dot.gov/safety-security/safety-security.htm

Joint Standards Australia/Standards New Zealand Committee ME/48 on Restraint Systems in Vehicles, Standards for Ambulance Restraint Systems, Joint Standards Australia/Standards New Zealand ASN/ZS **4535**:1999

General Services Administration, Federal Ambulance Specification KKK-A- **1822E**, Automotive Commodity Center, Federal Supply Service. 2002

Levick NR, Grabowski JG, Becker L, Better A, Tsai A, Li G, Injury hazards in pediatric ambulance transport, Pediatric Research **47 (4):** 113A-113A 662 Part 2 Suppl. S, Apr 2000

Levick NR, Li G, Yannaccone J, Development of a dynamic testing procedure to assess crashworthiness of the rear patient compartment of ambulance vehicles, Enhanced Safety of Vehicles, Technical paper series Paper # **454**, May 2001 http://www-nrd.nhtsa.dot.gov/pdf/nrd-01/esv/esv17/proceed/00053.pdf

Levick NR, Donnelly BR, Blatt A, Gillespie G, Schultze M, Ambulance crashworthiness and occupant dynamics in vehicle-to-vehicle crash tests: Preliminary report, Enhanced Safety of Vehicles, Technical paper series Paper # **452**, May 2001 http://www-nrd.nhtsa.dot.gov/pdf/nrd-01/esv/esv17/proceed/00012.pdf

Levick NR, Li G, Yannaccone J, Biomechanics of the patient compartment of ambulance vehicles under crash conditions: testing countermeasures to mitigate injury, Society of Automotive Engineering, Technical paper **2001-01-1173**, March 2001

Levick NR, Schelew WB, Blatt A, Gillespie G, Li G, Occupant Injury Hazards in Ambulance Transport, Findings from Full Vehicle Crash Testing, Academic Emergency Medicine Volume **8**, Number 5 527, 2001

Levick NR, Hazard Analysis and Vehicle Safety Issues for Emergency Medical Service Vehicles: Where is the State of the Art? American Society of Safety Engineers, PDC Proceedings, No. **732**, June 2006
http://www.objectivesafety.net/LevickIEA2006.pdf

Levick NR, Winston F, Aitken S, Freemantle R, Marshall F, Smith G. "Development and Application of a Dynamic Testing Procedure for Ambulance Pediatric Restraint Systems", Society of Automotive Engineering Australasia March/April 1998;**58**:2:45-51

Levick NR, Hazard Analysis and Vehicle Safety Issues for Emergency Medical Service Vehicles: Where is the State of the Art? American Society of Safety Engineers, PDC Proceedings, No. **732**, June 2006
http://www.objectivesafety.net/LevickIEA2006.pdf

Maguire BJ., Hunting KL., Smith GS., Levick NR., Occupational Fatalities in Emergency Medical Services: A Hidden Crisis. Annals of Emergency Medicine, **40**: 625-32; 2002.

National Highway Traffic Safety Administration (NHTSA), Head Impact Protection exemption, Federal Motor Vehicle Safety Standards (FMVSS), Dept Transportation, 49 CFR, Parts 571, 572 and 589, Docket No. **92-28**, Notice 7, RIN No. 2127-AB85

Ray A, Kupas D, Comparison Of Crashes Involving Ambulances With Those Of Similar Sized Vehicles – Pre-hospital and Emergency Care, Dec 2005;**9**:412-415

Richardson S.A., Grzebieta R. H. and R. Zou, Development of a Side Facing Seat and Seat Belt System for the Australian Army Perentie 4 x 4, Int. J. of Crash.,Vol. **4** No. 3, pp. 239 – 259, 1999.

Turbell T, Barriarkollision med ambulans, VTI Meddelande, National Road Traffic Research Institute, Fack – S- 58101 Linkoping, **206**:1980, ISSN 0347-6049

Wang H, RJ. Fairbanks, MN Shah, DM Yealy Tort Claims from Adverse Events in Emergency Medical Services, Pre-Hospital and Emergency Care, **11**: 1 January 2007, pages 94 - 136

Zou R., Richardson S., Grzebieta R.H., (1999) Occupant protection in Side Facing Seats, Proc. 1999 Australian MADYMO users meeting, AVEA Engineering, Melbourne, Australia.

PREGNANT OCCUPANT INJURY RISK USING COMPUTER SIMULATIONS WITH NCAP VEHICLE CRASH TEST DATA

Sarah J. Manoogian
Stefan M. Duma
Virginia Tech – Wake Forest Center for Injury Biomechanics
United States
David M. Moorcroft
Federal Aviation Administration
Civil Aerospace Medical Institute
Paper Number 07-0168

ABSTRACT

Automobile crashes are the largest single cause of death for pregnant females and the leading cause of traumatic fetal injury mortality in the United States. A previously validated MADYMO computer model of a 30-week pregnant occupant was used in this study to investigate the pregnant occupant response in a New Car Assessment Program (NCAP) frontal barrier motor vehicle crash. The effect of the restraints, all tests had a 3 point seatbelt and an airbag, and the vehicle performance in the crash are incorporated by applying the measured pelvic acceleration in the front seat passenger dummy to the pregnant occupant model. Included in the study are nine vehicle models that represent the compact, medium, and sport utility vehicle classes during the years 1996 to 2006 for a total of 26 NCAP tests with corresponding simulations. Uterine strain from the computational model, a good predictive measure of the risk of fetal injury due to placental abruption, indicates the average risk of adverse fetal outcome associated with these NCAP tests is 85 ± 13% with a minimum risk of 55% and a maximum risk of 100%. NCAP star rating correlates with the risk of adverse fetal outcome (p=0.001) with 3 stars having an average risk of 99 ± 3% (n=3), 4 stars having an average risk of 89 ± 11% (n=14), and 5 stars having an average risk of 75 ± 13% (n=9). However, even the best NCAP rating, 5 stars, is still indicative of a high risk of fetal injury. This high risk is consistent with published pregnant occupant case studies that have an equivalent change in velocity of slightly more than 56.3 kph (35 mph). Although this study is limited to computational modeling, it suggests more research in protecting the pregnant occupant is needed.

INTRODUCTION

Automobile crashes are the largest cause of death for pregnant females (Attico, 1986) and the leading cause of traumatic fetal injury mortality in the United States (US) (Weiss, 2002). Each year in the US, 160 pregnant women are killed in motor-vehicle crashes and an additional 800 to 3200 fetuses are killed when the mother survives (Klinich, 1999a, 1999b). The best way to protect the fetus is to protect the mother considering that maternal death has a near 100% fetal loss rate (Pearlman, 1990b). If the mother survives, protection of the fetus may best be accomplished by preventing placental abruption. Placental abruption, which is the premature separation of the placenta from the uterus, has been shown to account for 50% to 70% of fetal losses in motor vehicle crashes (Pearlman, 1990a). Information gathered from crash investigations shows that placental abruption can occur without other, more severe injuries, such as uterine rupture or direct fetal injury. However, when these more severe injuries do occur they are often accompanied by placental abruption (Rupp, 2001).

Since real world crash data is limited and cadaver studies are not feasible, a previously validated Mathematical Dynamic Modeler (MADYMO) computer model of a 30-week pregnant occupant has been a useful tool in researching risk of adverse fetal outcome for motor vehicle crashes involving a pregnant occupant (Moorcroft, 2003a). Adverse fetal outcome is defined as placental abruption, uterine laceration, direct fetal injury, premature delivery due to the crash, and fetal loss (Klinich, 1999b). Previous studies have utilized the pregnant occupant computational model to assess the risk of fetal loss based on occupant position, belt placement, impact direction, and advanced restraint systems (Moorcroft, 2004; Duma, 2006). Data for dynamic failure testing of maternal tissues are available for the uterus and placenta (Manoogian, 2007a, 2007b). Currently, the only alternative pregnant surrogate is a 30-week gestation 5th percentile female crash test dummy called the Maternal Anthropomorphic Measurement Apparatus version 2B (MAMA-2B) (Rupp, 2001). Validation tests have related the peak pressure of the

simulated uterus in the MAMA-2B with real world fetal loss risk data. The pregnant surrogate has been used in further analysis to determine the risk of fetal loss for different restraint conditions in a frontal impact. However, the crash test dummy is limited in its ability to model several crash scenarios in a timely and cost effective manner. For this study, the validated computational model was selected.

One type of vehicle safety rating is reported based on the National Highway Traffic Safety Administration (NHTSA) New Car Assessment Program (NCAP). The NCAP tests include front, side, and rollover star ratings. The large available data set from these tests proved a valuable resource of occupant response to the same impact condition for several vehicle models. In an analysis of data from the National Automobile Sampling System Crashworthiness Data System (NASS CDS), it was found that 53% of pregnant occupant motor vehicle crashes are frontal impacts (Duma, 2006). Therefore, data from NCAP frontal barrier impacts are chosen for this study. The purpose of this study is to use the pregnant occupant model to assess the risk of adverse fetal outcome in a NCAP frontal barrier motor vehicle crash.

METHODS

VT Pregnant Model

A previously validated MADYMO computer model of a 30-week pregnant occupant has been created to investigate pregnant occupant biomechanics in motor vehicle crashes. The details of model development and validation are available in Moorcroft, et al. (2003a, 2003b, 2003c), but are briefly summarized here. In order to create the model of the pregnant occupant, the finite element model of a pregnant uterus was inserted into the abdomen of a multibody human model. The finite element model anthropometry was designed to represent an occupant in her 30th week of gestation based on data from Klinich (1999a) for the second-generation pregnant dummy. The abdomen consists of the uterus, placenta, and amniotic fluid. A fetus was not included because the injury mechanism that predominantly contributes to fetal loss is placental abruption, as described by Rupp (2001). The human model is a 5th percentile female (1.52 m tall, 50 kg) and the weight of the pregnant occupant model is 61.2 kg (135 lbs). This multibody human model provides biofidelic response of an occupant in a motor vehicle crash, while reducing the computational time compared to a more complex full finite element human model.

Four techniques were used to validate the pregnant model. First, a global biofidelity response was evaluated by using a seatbelt to compress dynamically the pregnant abdomen (Moorcroft, 2003b). The force versus compression results were within the published corridors from scaled cadaver tests (Hardy, 2001). Second, a similar validation procedure was performed with a 2.54 cm diameter rigid bar (48 kg) at an impact speed of 6 m/s and these results were also consistent with previous data (Rupp, 2001; Hardy, 2001). The third technique involved validating the model against real-world crashes in order to investigate the model's ability to predict injury. Using fatal crashes involving pregnant occupants, the model showed strong correlation ($R^2 = 0.85$) between peak strain at the utero-placental interface (UPI) as measured in the model compared to risk of fetal demise as reported in the real-world crashes over a range of impact velocities and restraint conditions (Klinich, 1999b). The forth method compared the physiological failure strain from placental tissue tests to the failure strain measured in the model. Rupp presented a summary of pregnant uterine and placental tests which suggest approximately a 60% failure strain for the UPI (Rupp, 2001). This is in agreement with the model's prediction of 80% risk of fetal loss at a 60% strain in the UPI (Moorcroft, 2003). In summary, the global, injury, and tissue level validation techniques all indicate the model is good at predicting injurious events for the pregnant occupant.

The model calculates the risk of adverse fetal outcome, or fetal loss, on the basis of statistical analyses of case report data performed by Klinich, et al. (1999b). A two variable linear regression of the entire data shows that the uterine strain from the computational model is a good predictive measure of the risk of fetal injury due to placental abruption ($R^2 = 0.85$). The regression shows that uterine strain increases linearly to tissue failure as the risk approaches 100%.

NCAP Frontal Barrier Test

NHTSA uses NCAP to rate vehicles based on their safety performance. The NCAP frontal test is a standardized test to crash a vehicle with an initial velocity of 56.3 kph (35 mph) into a fixed barrier with the full width of the front of the vehicle. This yields an equivalent change in velocity of 59.5-64.4 kph (37-40 mph) when the vehicle rebounds. During this test, the driver and front seat passenger of the vehicle are 50th percentile Hybrid III male crash test dummies. Although there are several instrumentation devices on board the vehicle and the dummies, only

head and chest acceleration measurements are used for the injury criteria which determine the NCAP star rating. The highest NCAP rating is five stars and indicates a 10% or less chance of a serious injury. The lowest NCAP star rating, one star, is associated with 46% or greater chance of serious injury. The NHTSA definition of a serious injury is one requiring immediate hospitalization and may be life threatening.

In order to use the data from the NCAP test in the pregnant occupant model, a few methodological assumptions were made. First, since the data collected is for the 50th percentile male, it was assumed that the 50th percentile male response was similar to what the 5th percentile female would experience in the motor vehicle crash. Second, it was assumed that the effect of the vehicle structure and restraints on the passenger kinematics is incorporated in the pelvic acceleration response. Moreover, only the linear acceleration of the pelvis was known, so the simulation assumes there was negligible pelvic rotation. Because there is no method to validate the interaction with the restraints and vehicle interior, the only cause of uterine strain in the simulations was due to inertial loading from pelvic acceleration. As a result, this study used the three linear acceleration components of the pelvis as inputs to the simulations. These limitations are discussed further in the discussion.

Simulations

The MADYMO simulations in this study modeled a total of twenty-six NCAP tests from the years 1996 to 2006. Three vehicle models were selected from each of the three vehicle classes: passenger car compact (PC/C), passenger car medium (PC/Me), and sport utility vehicle (SUV). All of the tests chosen had a three point seatbelt and at least a front airbag for the passenger. Previous research shows the pregnant occupant is the driver in 75% of pregnant occupant related motor vehicle crashes (Duma, 2006). However, the pregnant occupant in the driver seat also has more interaction with the vehicle interior in a motor vehicle crash (Moorcroft, 2004). Because the goal of this study is only modeling the inertial loading and not the contact loading to the abdomen, the simplified case of the pregnant occupant passenger was chosen. Data were collected from the front seat passenger pelvis accelerometer in each of the NCAP tests evaluated.

The MADYMO pregnant occupant model was locked in a standard sitting position as measured by Klinich et al. for the small female group at 30-weeks gestation (Klinich, 1999a). By locking the occupant's joints, she moved as a rigid body in inertial space. Internally the uterus, placenta, and amniotic fluid were allowed to translate and rotate in the abdomen (Figure 1). Since no vehicle interior or restraints were added to the model, only the inertial response of the uterus is measured without external contact forces or compression due to thoracic movement. The pelvic linear acceleration data extracted from the NCAP tests was filtered to CFC600 per SAE J211. Applying the x, y, and z components of the pelvic acceleration pulse to the model for 0.125 seconds provided a simulation of the inertial effect pelvic acceleration would have on a pregnant abdomen. As a result, the uterus strained and rotated from the inertial loading. Since the assumed injury mechanism is placental abruption, the simulations output uterine strain at the fundus of the uterus for the duration of the impact. The peak von mises uterine strain corresponds to a risk of fetal demise using the linear relationship from the previous validation of this model. It is anticipated that this loading presents a best case scenario for the pregnant occupant in an NCAP style crash given no abdominal intrusion from the steering wheel or belt.

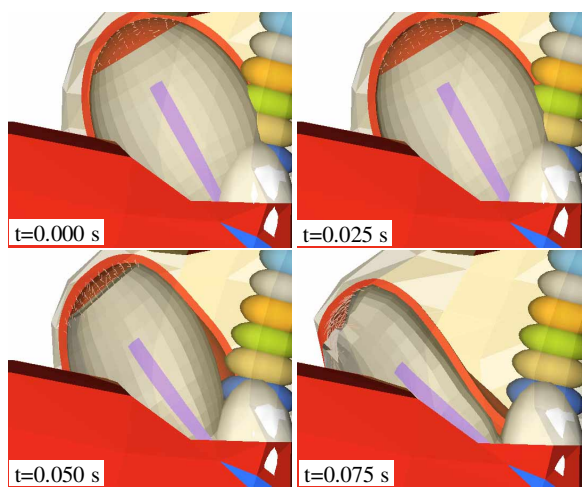

Figure 1: The simulation emulates the response of the uterus from pelvic acceleration due to a motor vehicle crash.

RESULTS

The results for this study include the risk of fetal loss for 26 different NCAP frontal barrier tests (Table 1). The average risk associated with these tests is 85 ± 13% with a minimum risk of 55% and a maximum risk of 100%. This information provides insight into how the vehicle type and pelvis acceleration determine the inertial loading of a 30-week pregnant uterus in a motor vehicle crash.

Table 1: A total of 26 simulations included nine vehicles in three vehicle size groups.

Vehicle Type	Model Year	NCAP Star Rating	Peak Pelvis X Acceleration (g)	Risk of Adverse Fetal Outcome (%)
PC/C 1	1996	5	49.4	87
	1999	4	48.5	74
	2006	5	44.0	55
PC/C 2	1998	4	55.6	82
	2003	5	42.4	77
	2005	5	46.3	97
PC/C 3	2000	4	73.0	100
	2002	4	92.8	100
PC/Me 1	1998	4	53.1	77
	2000	4	51.5	72
	2003	5	46.5	65
PC/Me 2	1996	4	42.2	88
	2000	5	59.6	75
	2004	5	39.3	72
PC/Me 3	1997	4	53.1	93
	2000	5	51.9	67
	2004	4	79.7	78
SUV 1	1998	3	74.2	100
	2001	4	84.3	100
	2004	5	59.7	80
SUV 2	1998	4	66.8	99
	2002	3	80.1	100
	2005	4	69.6	100
SUV 3	1996	3	66.4	95
	2001	4	67.5	100
	2004	4	58.1	83

Vehicle Type

When the risk of adverse fetal outcome is considered for each vehicle type, the medium size passenger car group had the lowest risk associated to it with an average of 76 ± 9%. The sport utility vehicle group had the highest average risk of 95±8%. The passenger compact car group was in between these two with an average risk of 84 ± 16%. The former group had the largest standard deviation with the minimum risk being 55% and the maximum risk being 100%. The only statistically significant difference was between the medium passenger car and the sport utility vehicle groups (Figure 2). Within each vehicle group, the risk was evaluated for a vehicle model as the model year progressed. In the 17 comparisons made between the same model car and an increase in model year, the risk of injury did not always decrease over time (Figure 3). The peak uterine strain increased in five of these cases with the associated risk either increasing or remaining the same at 100% (Figure 4). The remaining 12 cases showed a decrease in uterine strain and risk with an increase in model year. Because some vehicles had poor performance in recent years, there is not a significant trend associated with an increase in model year.

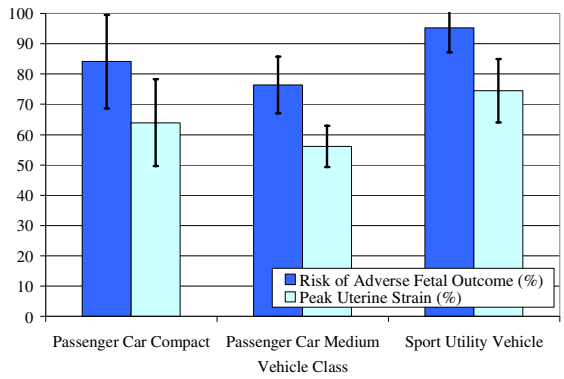

Figure 2: The medium passenger car class had a significantly lower risk associated with it than the sport utility vehicle class (p<0.001).

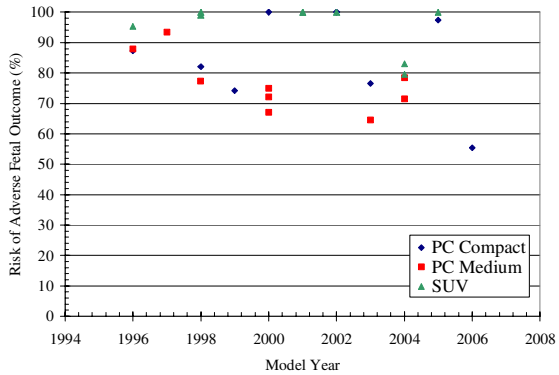

Figure 3: The risk of fetal loss versus vehicle model year indicates a decrease in risk for the medium passenger car class.

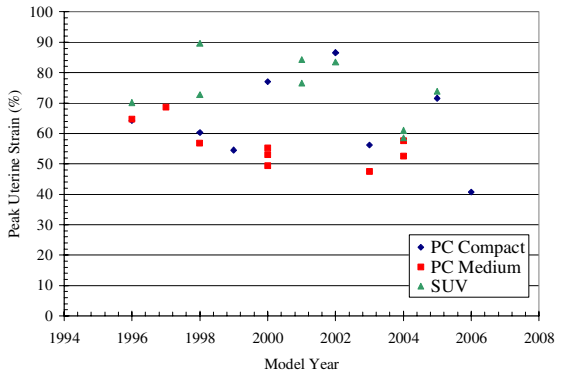

Figure 4: Peak uterine strain decreases in 12 of the 15 vehicle model year comparisons in this study.

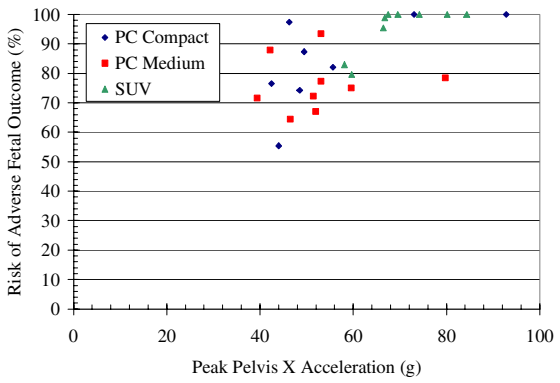

Figure 5: Overall, the SUV class had higher peak accelerations which correspond to higher risks of fetal demise.

Peak Pelvic Acceleration

The risk of placental abruption and peak pelvic acceleration in the x direction had a statistically significant relationship ($p<0.001$). The peak pelvic x acceleration is used rather than the resultant pelvic acceleration because in the frontal crash this value is dominant. Due to inertial loading only, 7 out of 8 vehicles with a peak pelvic acceleration above 67 g had a 100% risk of fetal loss (Figure 5). The relationship between peak pelvic acceleration and peak uterine strain is also shown, although a strain of above 74% corresponds to a 100% risk of fetal demise (Figure 6). Since all of these vehicles experience approximately the same change in velocity, the acceleration curves differ mainly in their peak acceleration and duration. This difference is seen best between the acceleration pulses that resulted in the least and greatest uterine strain (Figure 7). The acceleration curve with a peak pelvis x acceleration of 74.2 g maintains above a 5 g load for 0.0493 seconds and corresponds to the highest value of peak uterine strain, 90%. However, the acceleration curve with the lowest resulting peak uterine strain of 41% holds an acceleration above 5 g for 0.0889 seconds with a peak of 44.0 g. The longer duration, lower peak g acceleration curve results in a lower peak uterine strain and an analogous reduction in risk of fetal loss for the pregnant occupant.

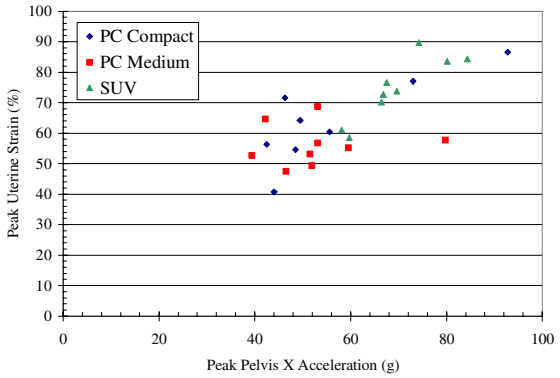

Figure 6: The linear relationship between peak pelvis x acceleration and peak uterine strain is significant but not strongly correlated due to differences in the acceleration profiles.

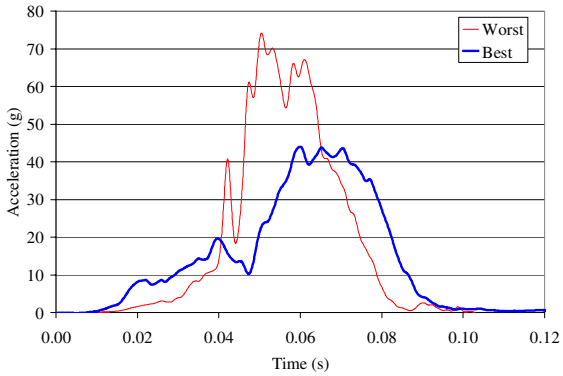

Figure 7: The acceleration pulses that resulted in the least and greatest uterine strain are plotted for comparison.

Although there was an increase in risk with an increase in pelvic acceleration, it was not strongly correlated. Some vehicles had similar peak pelvis x acceleration values and very different associated peak uterine strains. A closer evaluation of the acceleration profiles and their matching strain outputs addresses the weak correlation. When the pelvic acceleration and uterine strain profiles are plotted together, a time delay between the input and the response is present for the inertial loading. Due to the delay, a rapid change in pelvic acceleration does not have time to load the uterus. For example, an acceleration curve which has a peak duration of less than 5 milliseconds does not have a parallel large peak in the uterine strain (Figure 8). On the other hand, a curve with a steady increasing acceleration causes a similar steady increase in uterine strain (Figure 9). Therefore, two acceleration profiles with similar peak values can have different fetal injury risks associated with them.

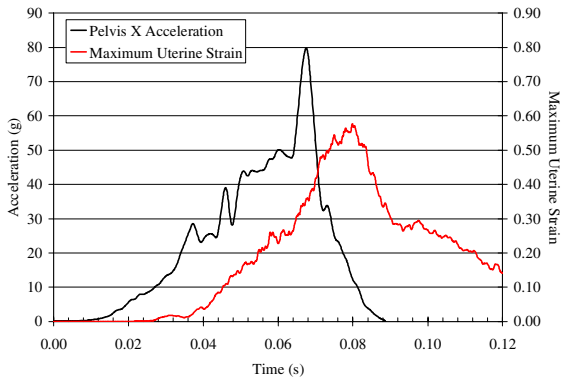

Figure 8: The large peak in the pelvis x acceleration does not have an equivalent large peak in the uterine strain measure.

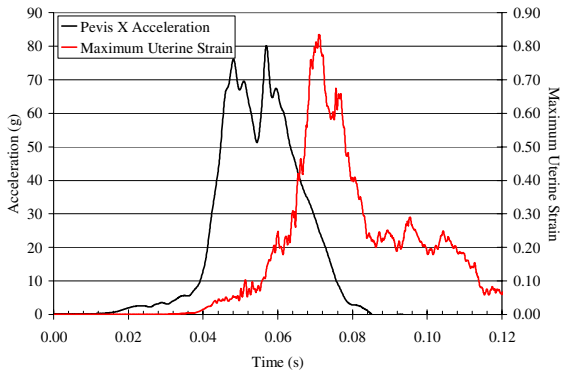

Figure 9: The steady increase in pelvis x acceleration has a corresponding increase in the peak uterine strain.

NCAP Score

The NCAP star rating for each vehicle indicates the risk of injury for the occupant based on head and chest criteria. The NCAP data used in this study was the pelvic acceleration. It was found that with an increase in the frontal NCAP star rating there was a decrease in peak pelvic acceleration for the x direction. The five star rating corresponds to a 48.8±7.2 g peak pelvic acceleration for the tests evaluated in this study. This value increased to 73.6±6.9 g for a low rating of three stars. Additionally, it was found that the star rating had a statistically significant relationship to the risk of fetal loss ($p=0.001$). The NCAP tests with 3 stars have an average risk of 99 ± 3% (n=3), 4 stars have an average risk of 89 ± 11% (n=14), and 5 stars have an average risk of 75 ± 13% (n=9) (Figure 10). These three groups are statistically different from each other and show that risk of adverse fetal outcome from placental abruption increases to almost 100% in a vehicle that passes the NCAP frontal barrier test with 3 stars. While the best NCAP rating of 5 stars indicates less than 10% risk of injury to the front passenger, it corresponds to a 75% risk of injury to the fetus.

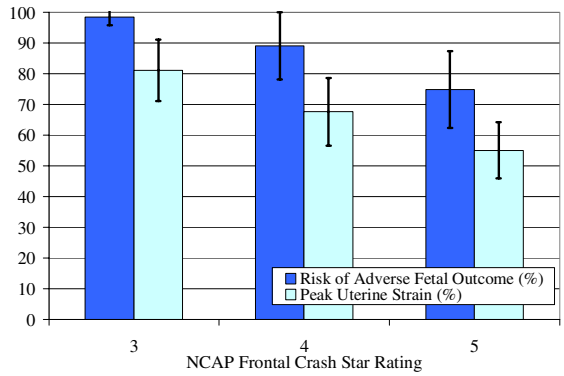

Figure 10: The best NCAP rating of 5 stars is indicative of a 75% risk of fetal loss in a 56.3 kph frontal barrier crash.

DISCUSSION

Real world pregnant occupant motor vehicle crash data and pregnant crash dummy data confirms the results from this study. In an analysis of case data for pregnant occupants, the estimated risk of fetal loss for a crash severity of 56.3 kph (35 mph) is 93% when the occupant has the proper restraint (Klinich, 1999b) (Figure 11). This risk is the minimum value associated with an NCAP test since the actual change in velocity with the rebound is generally 59.5-64.4 kph (37-40 mph). A crash severity of 64.4 kph (40 mph) is associated with 97% risk of fetal loss. Previous research using the pregnant crash test dummy MAMA-2B evaluated the uterine pressure during a sled impact with a 52.6 kph (32.7 mph) change in velocity. The result of this impact with the dummy as the passenger and wearing a 3 point belt was a risk of adverse fetal outcome equal to 87.5%. The average risk calculated in the current study for the inertial loading condition during a front impact is 85 ± 13%. All three of these methods of evaluating the pregnant occupant with the proper restraint indicate a high risk of fetal loss for a crash severity equivalent to that of an NCAP test.

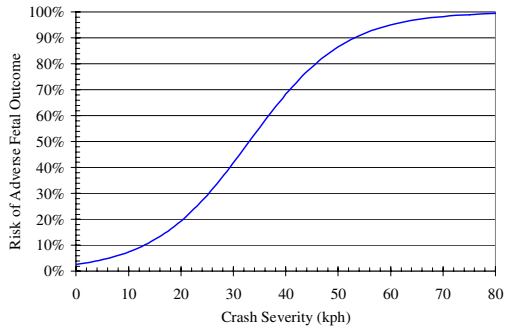

Figure 11: Risk of adverse fetal outcome as a function of crash severity for the properly restrained pregnant occupant indicates a 92% risk with a 56.3 kph impact (Klinich, 1999b).

Limitations of this study arise from the information available from a frontal NCAP barrier test. A pregnant surrogate is not used in the NCAP frontal barrier test so it is assumed that the kinematic response of the 50th percentile male is similar to that of a 30-week gestation 5th percentile female. Anthropometric differences would cause variations in the loading by the restraint system and ultimately the kinematics of the dummy. Since this cannot be accounted for, it is assumed that the pelvis of the small female has the same acceleration profile as that of the large male. As a result of a smaller mass and equivalent acceleration, a lesser force would be required by the restraints to stop the pelvis.

The data is not adequate to recreate the full body kinematics such as torso rotation and contact loading from the restraints or vehicle interior that contribute to uterine strain. Therefore, the model predicts the fetal outcome for an ideal loading scenario of a pregnant occupant in a 56.3 kph (35 mph) frontal impact. The assumption of a 3-point seatbelt positioned correctly minimizes the risk because placing the seatbelt too high on the abdomen can increase the risk of fetal loss by contributing unfavorably to uterine compression (Moorcroft, 2004). Additionally, using the shoulder belt and airbag decreases the risk of injury (Klinich, 1999b). These simulations do not consider contact loads from the seatbelt and vehicle interior to the abdomen since they could not be validated. Contact loads can increase the risk of fetal complications because of abdominal compression. Early research on the pregnant occupant indicated that bending of the torso also increased uterine pressure (King, 1971). These effects are not modeled since the body is locked in a seated position.

Moreover, this model does not predict the additional complications for the fetus due to maternal injury. A 3 star NCAP rating for the front passenger indicates a 21% to 35% risk of serious injury to the mother. Serious injury to the mother further increases risk of adverse outcome to the fetus. Because the model simulations are evaluating an ideal scenario, the associated risk is expected to be greater in a real world crash for a 56.3 kph (35 mph) impact. Overall, the attachment of the placenta is very delicate, and the data from this study and previous studies indicate that prevention of placental abruption with such a severe impact may not be plausible.

CONCLUSIONS

Using a validated pregnant occupant computer model, this study assessed the risk of fetal loss for the pregnant front seat passenger in 26 different NCAP frontal barrier tests. Nine vehicles were selected that ranged 10 model years and three vehicle weight classes. The results from this study show that in an ideal loading condition the average risk of adverse fetal outcome is 85% due to inertial loading only. Moreover, all vehicle models for all years showed a greater than 50% risk of fetal loss. When compared to previous research, the results from this study are confirmed. Although this study is limited to computational modeling, it suggests even with the best case restraint system scenario the risk of fetal death is highly probable in severe crashes like those that the NCAP standard emulates.

REFERENCES

Attico, N.B., Smith III, R.J., Fitzpatrick, M.B. 1986. "Automobile safety restraints for pregnant women and children." Journal of Reproductive Medicine, 31, No. 3: 187-92.

Duma, S.M., Moorcroft, D.M., Gabler, H.C. 2006. "Analysis of Pregnant Occupant Crash Exposure and the Potential Effectiveness of Four-Point Seatbelts in Far Side Crashes." Annual Proceedings of the Association for the Advancement of Automotive Medicine, 50: 177-188.

Hardy, W.N., Schneider, L.W., Rouhana, S.W. 2001. "Abdominal impact response to rigid-bar, seatbelt, and airbag loading." Stapp Car Crash Journal, 45: 1-32.

King, A.I., Eppinger, R.H., Crosby, W.M., Stout, C. 1971. "Effects lap belt three-point restraints pregnant baboons subjected deceleration." Stapp Car Crash Journal, 15: 68-83.

Klinich, K.D., Schneider, L.W., Eby, B., Rupp, J., Pearlman, M.D. 1999a. "Seated anthropometry during pregnancy." UMTRI-99-16.

Klinich, K.D., Schneider, L.W., Moore, J.L., Pearlman, M.D. 1999b. "Investigations of crashes involving pregnant occupants." UMTRI-99-29.

Manoogian, S.J., McNally, C., Calloway, B.R., Duma, S.M., Mertz, H.L. 2007a. "Utilizing Cryogenic Grips for Dynamic Tension Testing of Human Placenta Tissue." Biomedical Sciences Instrumentation, 43.

Manoogian, S.J., McNally, C., Calloway, B.R., Duma, S.M. 2007b. "Methodology for Dynamic Biaxial Tension Testing of Pregnant Uterine Tissue." Biomedical Sciences Instrumentation, 43.

Moorcroft, D.M., Duma, S.M., Stitzel, J.D., Duma, G.G. 2003a. "Computational Model of the Pregnant Occupant: Predicting the Risk of Injury in Automobile Crashes." American Journal of Obstetrics and Gynecology, 189, No. 2: 540-544.

Moorcroft, D.M., Duma, S.M., Stitzel, J.D., Duma, G.G. 2003b. "A finite element and multi-body model of the pregnant occupant for the analysis of restraint effectiveness." SAE Technical Paper. 2003-01-0157.

Moorcroft, D.M., Stitzel, J.D., Duma, S.M., Duma, G.G. 2003c. "The Effects of Uterine Ligaments on the Fetal Injury Risk in Frontal Automobile Crashes." Journal of Automobile Engineering, 217, Part D: 1049-1055.

Moorcroft, D.M., Duma, S.M., Stitzel, J.D., Duma, G.G. 2004. "The effect of pregnant occupant position and belt placement on the risk of fetal injury." SAE Technical Paper. 2004-01-0324.

Pearlman, M.D., Tintinalli, J.E., Lorenz, R.P. 1990a. "A prospective controlled study of outcome after trauma during pregnancy." American Journal of Obstetrics and Gynecology 162: 1502-1510.

Pearlman, M.D., Tintinalli, J.E., Lorenz, R.P. 1990b. "Blunt trauma during pregnancy." New England Journal of Medicine, 323, No. 23: 1690-1613.

Rupp, J.D., Klinich, K.D., Moss, S., Zhou, J., Pearlman, M.D., Schneider, L.W. 2001. "Development and testing of a prototype pregnant abdomen for the small-female Hybrid III ATD." Stapp Car Crash Journal, 45: 61-78.

Weiss, H.B., Strotmeyer, S. 2002. "Characteristics of pregnant women in motor vehicle crashes." Injury Prevention, 8, No.3: 207-214.

THE MECHANISM OF BELT INDUCED CHEST DEFLECTION: ANALYSIS AND POSSIBILITIES FOR REDUCTION.

Burkhard Eickhoff
Harald Zellmer
Autoliv B.V. & Co. KG, Elmshorn, Germany
Erik Forster
Autoliv B.V. & Co. KG, Dachau, Germany

Paper Number 07-0202

ABSTRACT

A precondition for a good rating in Euro-NCAP frontal impact is a low value for chest deflection. To achieve this, detailed knowledge of the mechanism of chest deflection is needed. Consequently, the objectives of this study were a detailed analysis of the belt induced chest deflection and a finding of solutions to reduce it.

Theoretical investigations as well as simulation (software Madymo 6.1) were used to study the mechanism of chest deflection. The simulation environment represented a typical middle class vehicle. A special simulation dummy which allowed a detailed analysis of the internal and external forces acting on the thorax was used. Finally, sled tests were carried out in order to confirm the theoretical and numerical results.

For the environment investigated, the belt force turned out to be the dominant factor for chest deflection. In fact, the value for chest deflection showed a good correlation to the arithmetic mean of the shoulder belt force (FB3) and the force of the inner diagonal belt (FB4). While FB3 is commonly limited by a load limiter in the retractor, FB4 is strongly influenced by the forces in the lap portion of the belt. These forces are usually 1kN to 2kN larger than the level of load limitation. Preventing the belt slippage through the buckle tongue proved to substantially reduce FB4. Along with this chest deflection in tests with Euro-NCAP deceleration pulse was reduced.

A prototype of a locking tongue was developed and sled tests were carried out in different vehicle environments. It was shown that depending on belt geometry a reduction in chest deflection of 10-25% could be achieved.

1. INTRODUCTION

During the past years load limiting of safety belts has become standard in vehicles on front seats. The reason of the implementation of load limiters was to reduce the force at the shoulder belt to a pre-defined level and achieve an optimal usage of the space available in the passenger compartment during retention /1/. The benefit of load limiting is evident and can be seen as well in real life, cp. fig.1.

Due to the importance of chest deflection in real life and testing (Euro-NCAP, e.g.), effects which influence chest deflection were analyzed. As a result of this, the correlation between shoulder belt load and chest deflection is commonly accepted /1/ /2/ /3/ /4/ /5/.

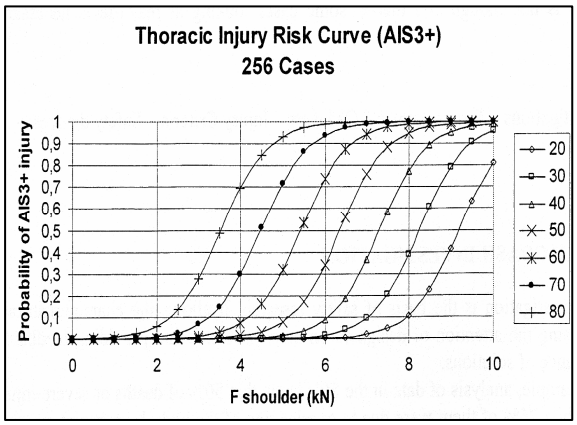

Figure 1. Probability of severe thoracic injuries (AIS3 or more severe) depending on the shoulder belt force and the occupant's age /2/.

In fact, previous studies discuss the interaction between shoulder belt load and chest deflection. Other belt parameters, which might influence chest deflection, are not matter of previous investigations.

As a result of these considerations, belt induced chest deflection has to be analysed in detail to find other belt parameters which effect on chest deflection.

2. BELT INDUCED CHEST DEFLECTION

Belt induced chest deflection is caused by the resultant force on the sternum. This force depends on

- the geometry of the belt system
- the magnitude of the forces FB3 (shoulder belt) and FB4 (diagonal inner belt), cp. figure 2.

Figure 2. Location of belt force sensors.

2.1 Belt Load

In a typical frontal crash with a standard belt system which includes a constant load limiter the belt load FB3 has an almost constant level. In contrast to this an increasing in belt load FB4 and FB6 (belt force at the anchor plate) is noticeable, cp. figure 3. The increase in belt force FB4 is caused by higher forces in the lap belt compared to the diagonal belt.
As the resultant force on the thorax depends on the magnitude of both forces FB3 and FB4, it is also increasing.

As a result of these considerations, the belt force FB4 should be also limited respectively reduced to decrease belt induced chest deflection.

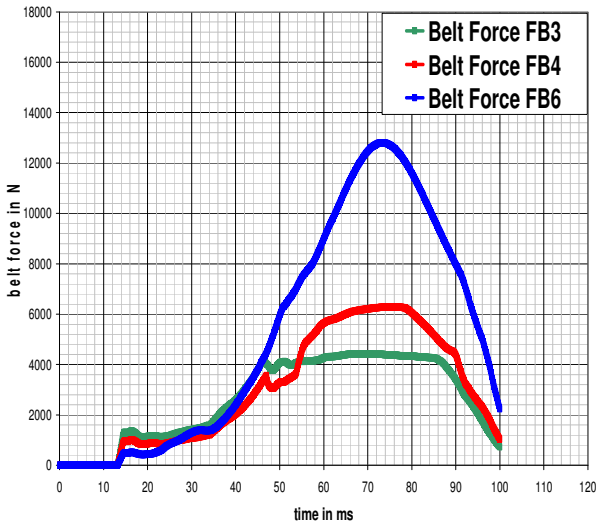

Figure 3. Exemplary curve progression of belt forces versus time with a constant load limiter. The belt force FB3 has a constant level, an increasing in belt forces FB4 and FB6 is noticeable.

2.2 Geometry effects

Assuming a constant load in the webbing, the resultant force of the belt on the thorax depends on the direction of the belt forces FB3 and FB4. During forward displacement, the load on the thorax increases due to the change of the direction of the belt forces, cp. figure 4.

Furthermore, during forward displacement of the dummy with rotation, the load on the clavicle increases and consequently the load on the sternum decreases.

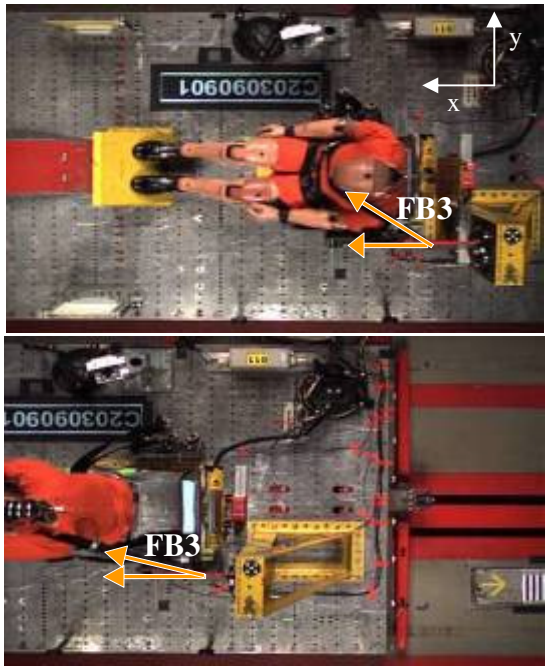

Figure 4. Belt force vector of the shoulder part increases in x-direction due to forward displacement which leads to an increase in the resultant force on thorax.

3. METHODS

3.1 Environment used for testing and simulation

In addition to theoretical considerations sled-tests and MADYMO simulations were done in an environment which represents a typical middle class vehicle on the driver side.

For the calculation a MADYMO 6.1 model was used. Following properties have to be mentioned:

- the original steering column was replaced by a fixed one
- a special software dummy called Force Balanced Dummy was used

Compared to the standard simulation dummy the Force Balanced Dummy can record and evaluate internal forces (like shear forces between parts of the body), airbag, seatbelt and seat forces on the dummy segments separately. It is comparable with the simulation dummy, which is known as E-Dummy /6/.

Concerning the set-up of the dynamic tests following conditions characterise the environment:

- serial seat
- serial driver airbag
- rigid steering column
- no IP (no knee contact)
- belt system with load limiter and retractor pretensioning
- Dummy Hybrid III 50th percentile
- US - / Euro-NCAP pulse

3.2 Reduction of the belt force FB4

As a result of the considerations in chapter 2.1, the reduction of belt load FB4 has to be realised in simulation and test environment.

One way to reduce the belt force FB4 is to prevent slippage from the diagonal belt into the lap belt. Slippage from lap into the diagonal belt is

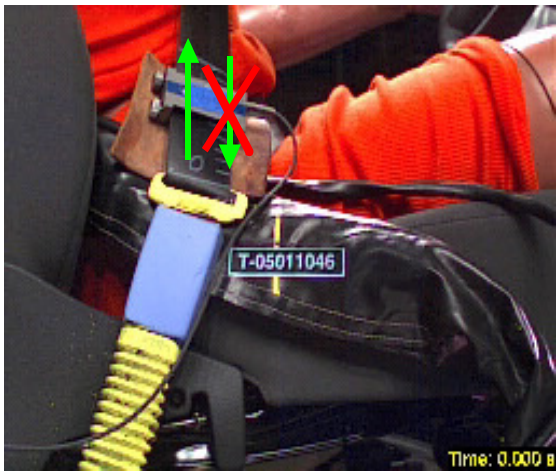

Figure 5. Principle of a tongue, which prevents slippage from diagonal in the lap portion.

possible (in order to enable webbing slippage through the tongue during retractor pretensioning). The opposite direction of webbing slippage, from the diagonal to the lap portion, is prevented, see figure 5. The expected effect is a reduction in belt force FB4 (diagonal inner) and an increase in the force on pelvis due to higher forces in the lap belt. Furthermore, the change of the load path should lead to higher shear forces between pelvis and thorax, cp. figure 6.

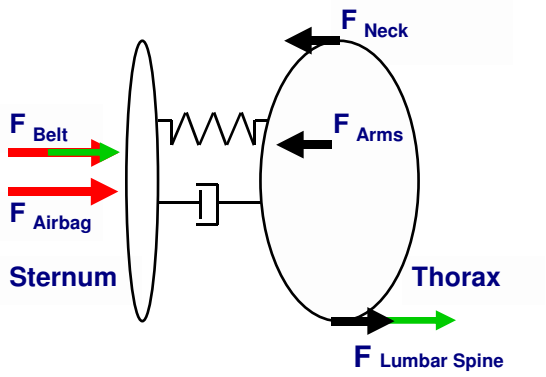

Figure 6. Change of the load path: Reduction of the resultant belt load on the thorax, increasing in shear force F Lumbar Spine.

4. SIMULATION AND TEST RESULTS

4.1 Simulation Results

In order to demonstrate the effect, simulations were done in the described environment. Figure 7 points out the forces on the thorax with a standard belt system, and a tongue, which prevents slippage in one direction (hereafter referred to as locking tongue).

As expected a reduction in the belt force on the thorax and an increase in the shear forces between thorax and pelvis can be observed in the simulation environment by using the locking tongue. The change of the load path is evident.

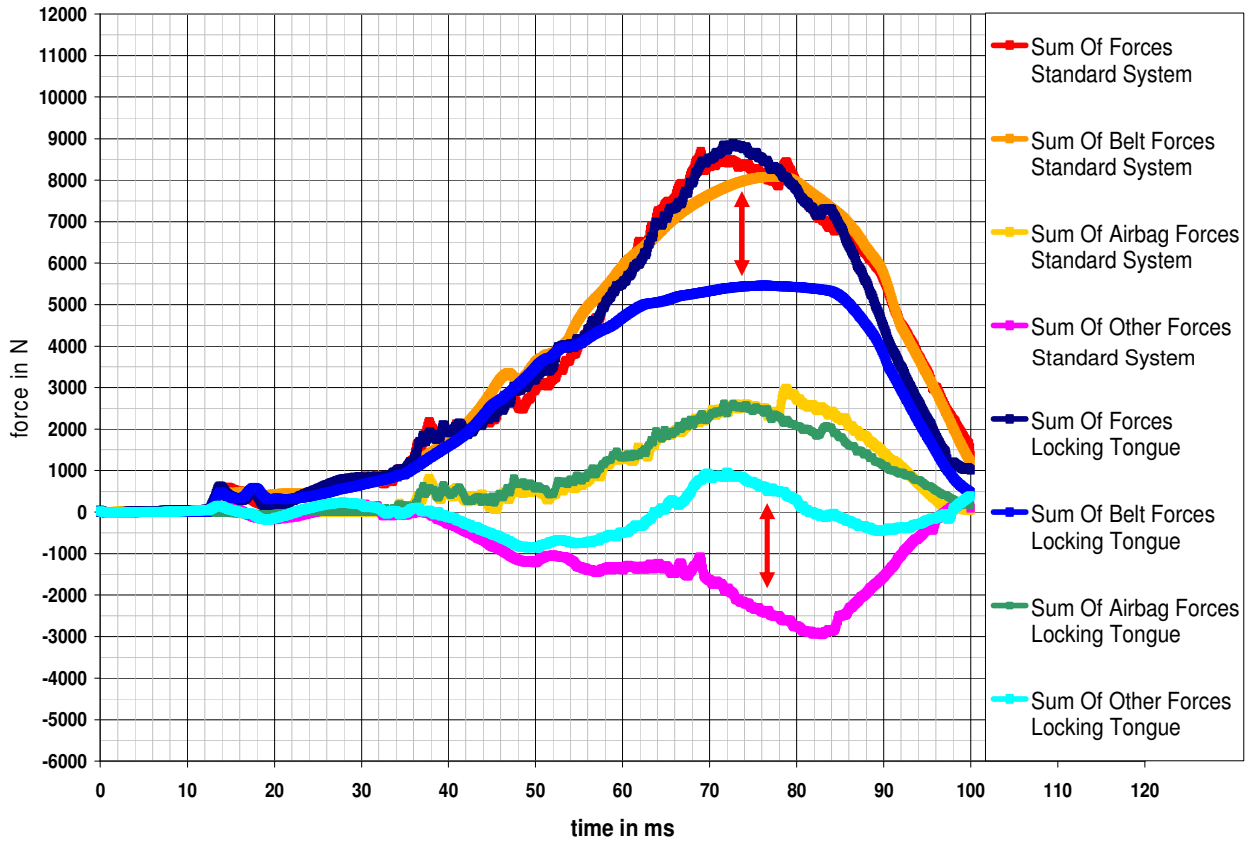

Figure 7. Forces on the thorax with a standard belt system and a tongue, which prevents slippage in one direction. A reduction of the resultant belt load on the thorax and a increasing in the shear forces can be noticed.

The effect on injury criteria and the dummy forward displacement is given in table 1.

	Chest deflection in mm	Chest acceleration 3ms in g	Pelvis forward displacement in mm
Standard Tongue	39	51,4	233
Locking Tongue	32	52,8	229

Table 1. Simulation results with HIII 50% and Euro-NCAP pulse. The reduction in chest deflection is evident.

As a result, a reduction in chest deflection of 7mm (18%) with a usage of the locking tongue is noticeable. Furthermore a not relevant increasing in chest acceleration can be established. Finally, the forward displacement of the dummy decreases marginally compared to the standard belt system.

In addition to this two relevant influences on the effect should be mentioned.
In table 2 the difference between HIII 50% and HIII 5% is demonstrated, calculated with an US-NCAP pulse (56km/h, 0°). As we can see, the effect depends on the occupant's mass. A higher mass leads to enlarge the effect.

	HIII 50%	HIII 5%
Percentile benefit concerning chest deflection by using a locking tongue	33%	13,5%

Table 2. Benefit concerning chest deflection with different dummies, calculated with US-NCAP pulse. A higher reduction in chest deflection with the 50% dummy compared to the 5% dummy can be noticed.

As a second influence the stiffness of the pulse has to be mentioned. Stiffer pulses lead to amplify the effect, cp. table 3.

	35 km/h crash velocity	45 km/h crash velocity	56km/h crash velocity
Percentile benefit concerning chest deflection by using a locking tongue	11%	28%	33%

Table 3. Benefit concerning chest deflection with different pulses. Stiffer pulses lead to amplify of the effect.

As described in chapter 2.2, geometry effects lead to different loading of the thorax. Under the condition of constant belt loads FB3 (shoulder) and FB4 (diagonal inner), realised with a locked tongue,

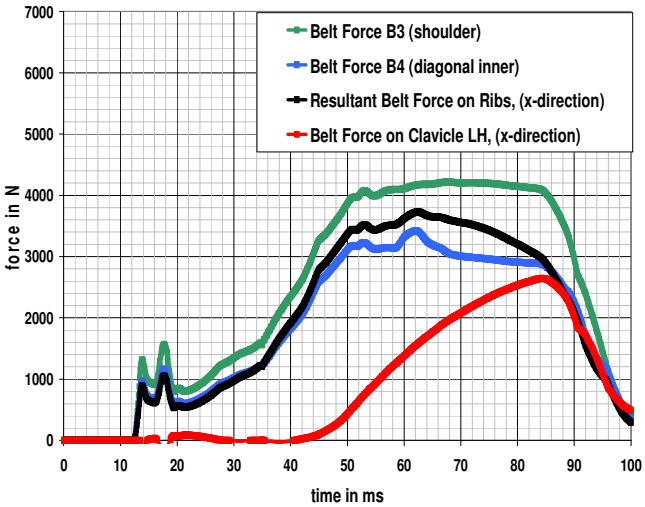

Figure 8. Almost constant belt loads FB3 and FB4. The result of the belt loading is an almost constant load on ribs and an increasing in load on clavicle.

chest deflection shows an almost constant behaviour in the environment investigated. Furthermore an increasing in load on the clavicle was noticeable, cp. figure 8.

Summarised: An increasing in the resultant force on the thorax is calculated, see figure 7. The resultant force itself is the sum of the load on the sternum (which has an almost constant curve progression) and the load on the clavicle (which increases), cp. fig. 8.

4.2 Test Results

To verify the simulation results and to measure the benefit concerning chest deflection, sled-tests were performed in the described environment, cp. chapter 3.1.

The following figures will describe the results of this comparison with a standard belt system (conventional tongue) and a system, which includes a locking tongue. The locking mechanism of the tested tongue is equivalent to the mentioned principle in chapter 3.2.

Due to the importance of chest deflection in Euro-NCAP tests, a Euro-NCAP pulse was used.

In figure 9 the belt force FB3 of both systems are shown. As expected, the curves are comparable.

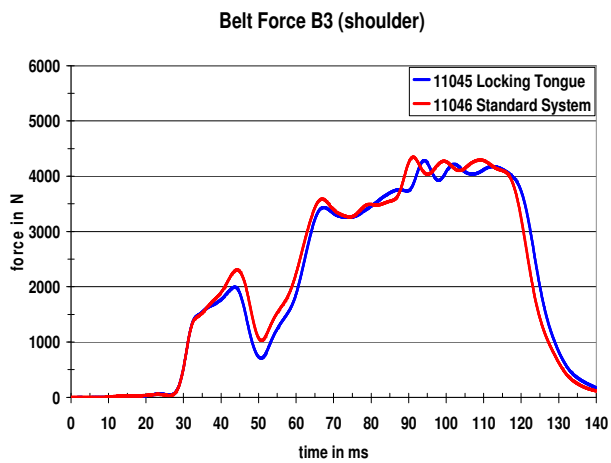

Figure 9. Shoulder belt force FB3 versus time.

In contrast to this, a difference in belt force FB4 (diagonal inner) is noticeable. After 78ms the belt force increase with the standard system and achieve a level of about 6 kN, the system with locked tongue has a maximum value of about 4 kN belt force. Consequently, the system with the locked tongue reduces the belt force of about 2 kN compared with the reference system, cp. figure 10.

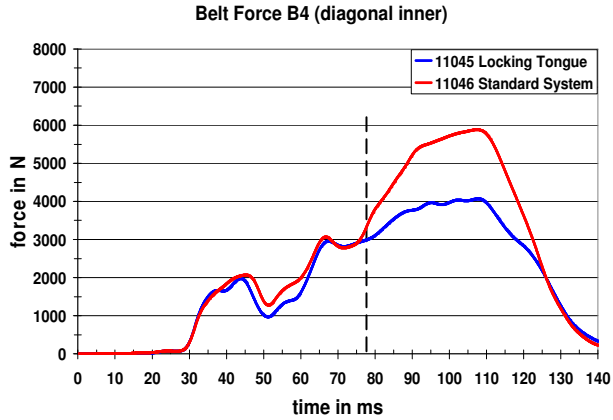

Figure 10. Belt force FB4 (diagonal inner) versus time. A reduction of belt load with the locked tongue of about 2 kN is noticeable.

As described in chapter 3.2, the change of the load path with a locked tongue leads to higher belt forces on the pelvis lap compared with a standard tongue. An increasing in belt force FB6 (anchor plate) of about 1.5 kN can be noticed (fig. 11).

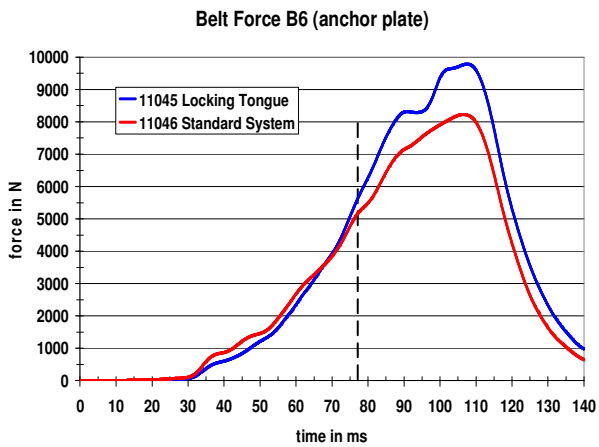

Figure 11. Belt force FB6 (anchor plate) versus time. An increasing belt force with the locking tongue can be observed.

After about 78 ms the differences in the chest deflection between the locked tongue and the reference tongue are noticeable, cp. figure 12.

In fact, the maximum value of chest deflection could be reduced at about 8mm and 25%, respectively.

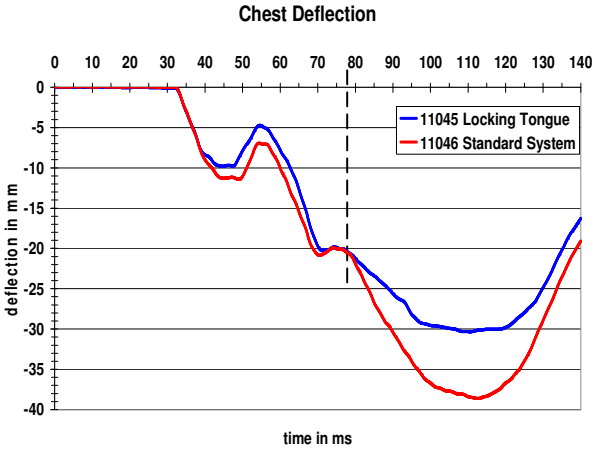

Figure 12. Reduction in the chest deflection with a locked tongue.

The following figures show the influence of the effect on chest and pelvis acceleration.
The resultant chest acceleration with both tongues is comparable, cp. figure 13.

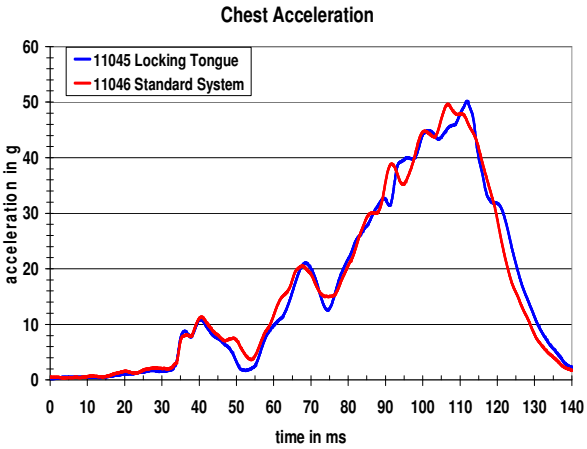

Figure 13. Resultant chest acceleration with comparable curve progressions.

Concerning pelvis acceleration the measured data show an increase in the maximum value of about 3.5g, see figure 14.

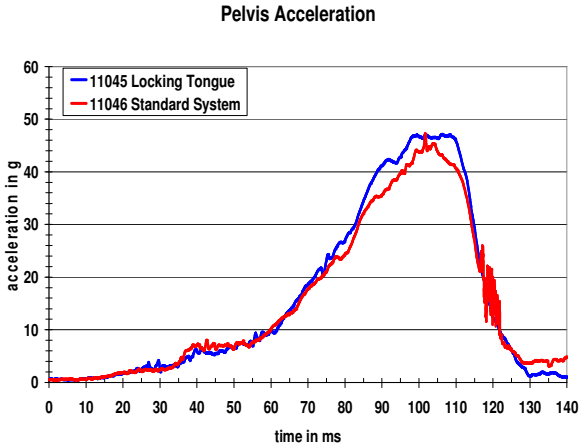

Figure 14. Resultant pelvis acceleration versus time. A small increasing in acceleration with the locked tongue can be noticed.

5. DISCUSSION

As shown in theoretical consideration, simulation and sled-test results, belt induced chest deflection depends on belt force shoulder FB3 and diagonal inner FB4 and the belt geometry.

Due to the usual limitation of the shoulder belt force FB3 by the retractor the belt load diagonal inner FB4 was the focus of the investigation.
Chest deflection is directly influenced by this belt force. A benefit of 18% concerning deflection in simulation with a reduced belt force diagonal inner was achieved, cp. table 1.
In sled tests comparable magnitude of reduction in chest deflection could be achieved, cp. figure 10 (belt forces) and fig. 12 (chest deflection).

The maximum value of the belt force FB4 depends on pelvis retention. Components (e.g. knee bag, pelvis restraint cushion, double pretensioning /1/), which lead to higher pelvis retention, will reduce the belt load in the lap portion of the belt. As a result of this the belt force diagonal inner FB4 also decreases. As an example, the benefit concerning chest deflection by using a knee – airbag is, among others, the result of this effect.

Concerning the injury values chest- and pelvis acceleration, simulation and testing lead to minor different results. Both show an increasing in pelvis acceleration. In contrast to this simulation results show a small increasing in chest acceleration, too, which wasn't measured in testing, cp. fig. 13.
In terms of the usage in Euro-NCAP with the focus on chest deflection, the calculated / measured

increasing in dummy acceleration values seems to be not relevant.

Concerning the geometry two important effects have to be mentioned: An increasing in the resultant force on the thorax and a reduction of load on the ribs by increasing in load on the clavicle. In the environment investigated, these effects are compensating each other, cp. fig. 8. The dimension of each effect depends on the vehicle environment, of course. On the one hand, they are affected by buckle and pillar loop geometry in respect of the dummy position. On the other hand, the reduction of belt load on the ribs by loading the clavicle depends on the dummy rotation during the load limiting phases. More rotation of the dummy or occupant leads to more load on the clavicle and less on the ribs.

In Euro-NCAP knee impact is also an important point of interest. A system with a locked buckle tongue, which prevents belt slippage from diagonal into the lap portion, will lead to less pelvis displacement. As a result of this, femur forces (induced by knee impact) can be potentially reduced. In the environment investigated, no knee contact was defined. So, the evidence about the dimension of this effect can't be given and should be investigated.
However, the positive effect on femur forces seems to be smaller compared with double pretensioning systems.

Closing, the utilization of a system with a locking tongue has to be discussed. To reduce chest deflection with a reduction of the belt force FB4 following boundary conditions have to be analysed:

- Belt slippages with a standard buckle tongue.
  The slippage shows the dimension of the pelvis retention. If no slippage is noticeable, an implementation of a locking tongue won't affect the chest deflection positively.

- Airbag influence
  Chest deflection is a function of loads from belt and airbag on the sternum. The magnitude of loading on the sternum by airbags varies. In some cases the airbag becomes possibly the dominant factor for chest deflection. As a result of this, the locking tongue would not reduce the maximum of chest deflection.

To analyse this, however, further investigations are needed.

6. CONCLUSIONS

Chest deflection is induced by airbag and belt loads on the thorax. Concerning the belt induced load on the thorax, both belt loads FB3 (shoulder) and FB4 (diagonal inner) influences chest deflection. The belt load FB3 is mainly influenced by the load limiter of the retractor, FB4 by the belt load in the lap portion.

In current belt systems the force in the lap portion of the belt is much higher compared with belt force of the shoulder. The result of this is an increase in belt forces of the lower diagonal portion. As a result of this, chest deflection also increases.

The dimension of the difference in belt loads between the lap portion of the belt and the diagonal portion depends on the pelvis retention. Furthermore, pelvis retention is responsible for the dummy kinematics – and, as well known, dummy rotation is beneficial for the deflection values.

One solution to reduce the belt force FB4 is preventing the slippage through the buckle during load limiting. In the environment investigated, tests with a modified tongue reduced the deflection of about 25%.

7. REFERENCES

/1/ H. Zellmer, C. Kahler, B. Eickhoff: Optimized Pretensioning of the Belt System: A Rating Criterion and the Benefit in Consumer Tests. ESV Conference 2005.

/2/ X. Trosseille: Accident Investigation and Biomechancial Research: A Joint Approach for Road User Protection. IRCOBI Conference 2000.

/3/ A. Petitjean, M. Lebarbe, P. Potier, X. Trosseille, J.-P. Lassau: Laboratory Reconstructions of Real World Frontal Crash Configurations using the Hybrid III and THOR Dummies and PMHS, Stapp Crash Journal Vol. 46, 2002

/4/ R. W. Kent, J. R. Crandall, R. W. Rudd, D. Lessly: Load Distribution-Specific Viscoelatic Characterization of the Hybrid III Chest, SAE 2002-01-0024

/5/ N. Yoganandan, D. Skrade, F. Pintar, J. Reinartz, A. Sances, Jr.: Thoracic Deformation Contours in a Frontal Impact. Hybrid III: The first Human-Like Crash Test Dummy, SAE PT 44, 1994

/6/ T. Grandfils, K. Ikels: Improvement of Occupant
Restraint Systems using Enhanced Hybrid III:
Dummy Models in MADYMO-3D
3rd European MADYMO Users' Meeting
Stuttgart, September 14, 2001

EFFECTIVENESS OF SEATBELT FOR REAR SEAT OCCUPANTS IN FRONTAL CRASHES

Koji Mizuno
Nagoya University
Takahiro Ikari and Kenich Tomita
National Agency for Automobile Safety and Victim's Aid
Yasuhiro Matsui
National Traffic Safety and Environment Laboratory
Japan
Paper Number 07-0224

ABSTRACT

Recently, the general public in Japan is attaching increasing importance to the wearing of seatbelts by rear seat occupants. Some projects have been launched to have more rear seat occupants wear seatbelts in Japan. The National Agency for Automobile Safety and Victim's Aid (NASVA), for example, conducted a research project to evaluate the effectiveness of wearing a seatbelt based on crash tests. Full-width rigid barrier tests were conducted using Hybrid III AF05 and 3YO dummies in belted or unbelted conditions in the rear seat. This paper summarizes the analyses of crash tests in this project.

For the belted AF05 and 3YO in the rear seat, the injury criteria were relatively low since contact with the car interior was prevented by a seatbelt, though the chest deflection of AF05 was large by the shoulder belt. However, when the AF05 was not belted, the knees and the head made contact with the seatback of the front seat and the head of the front seat dummy, respectively. The injury criteria were extremely high and exceeded the injury assessment reference values (IARVs). Due to this impact by the AF05, the injury criteria of the driver dummy became high. The unbelted Hybrid III 3YO was thrown around inside the passenger compartment, making contact at several locations. It was demonstrated that a seatbelt is useful for preventing hard contact with the vehicle interior. However, some challenges remain, one of which is that the loading by the conventional seatbelt is too large for the Hybrid III AF05 chest.

INTRODUCTION

In general, the percentage of rear seat occupants wearing seatbelts is small compared to that of front seat occupants. For example, according to the investigation by the Japan Automobile Federation (JAF) in 2005, the percentage of front seat occupants wearing seatbelts was 92.4%, against a mere 8.1% in rear seat occupants in Japan [1]. Because of these low percentages as well as the wide age distribution of occupants in the rear seat, the target population is limited, which makes it rather difficult to conduct a statistical analysis to investigate injuries to the rear seat occupants.

Many accident analyses have demonstrated the effectiveness of wearing a seatbelt for injury risks to occupants in rear seat. Morgan [2] reported that the reduction of fatalities is 32% based on the Fatality Analysis Reporting System (FARS) in the US. In the UK, Cueradan [4] reported 41% for the reduction of MAIS 1+ injuries using the Co-operative Crash Injury Study (CCIS). Shimamura [3] estimated the effect of seatbelt for rear seat occupants by applying logit model to the national accident data in Japan (1995-2000). If the unbelted rear seat occupants changed to belted, the number of fatalities of rear seat occupants would decrease by 45%.

Some features are observed in injury body regions for rear seat occupants. According to the accident analyses by Cuerdan [4], the frequency of chest injuries by shoulder belt is largest in the belted occupants in the rear seat. He also reported the frequencies are high in head and lower extremity injuries due to contact with the front seatback in addition to whiplash injuries. In unbelted rear seat occupants, the frequency of head injuries was largest, and the injury sources were front seats, head restraints and external objects.

Parenteau and Viano [5] also examined the injury risks to occupants over age 13 who were in rear seats and involved in frontal impacts using the US accident data (NASS-CDC 1991-1998, FARS

1988-1996). For occupants with a 3-point seatbelt in the rear seat, the frequency of chest injury was largest. For unbelted occupants, injuries to various body regions such as upper extremities, head and upper extremities occurred frequently. Based on these results, they concluded that a seatbelt force limiter and energy absorption of the front seatback and of the vehicle interior would be effective for the protection of rear seat occupants.

The influences of the behavior of the rear seat occupants on the injury risks in front seat occupants were investigated. Using the national accident data in Japan, Ichikawa et al. [6] showed that the injury risks to front occupants were five times higher when there were occupants in the rear seat. Broughton [7] also examined the increasing injury risks to front seat occupants based on the UK accident data, and found that the injury risks increased by 1.79 times for driver and by 1.73 times for front passenger when there were rear seat occupants. Based on the logit model by Shimamura [3], the number of driver and front passenger fatalities would decrease by 25% and 28%, respectively.

Using in-depth accident data of ITARDA (Institute for Traffic Accident Research and Data Analysis), Shimamura [8] also examined 123 rear-seat unbelted occupants. He classified the behavior of unbelted 101 rear seat occupants whose contact location was identified, into three categories. First is the case where the rear seat occupants are stopped by the seatback of the front seat (82 cases). Second is when the rear seat occupants are thrown over the front seat (6 cases). And third is when the rear seat occupants are moved through either side of the front seats (13 cases). There were several accidents in which the front seat occupants sustained injuries to the chest and abdomen since the rear seat passengers impacted the front seatback and the front seat occupants were compressed by the deformation of the front seatback.

At present, the adult occupants are not positioned in the rear seat in the frontal crash test regulation. For the rear seat, there are no airbags, and many vehicles have only conventional seatbelts without a pretensioner or force limiter. Accordingly, the injury risk to rear seat occupants is likely to be higher than to front seat occupants. Recently, the injury risk to rear occupants has probably been increasing because the vehicle acceleration is inclined to be high due to the stiff passenger compartment.

The National Highway Traffic Safety Administration (NHTSA) has a research program focusing on rear seat occupant safety [9]. In the research, the Hybrid III AM50 (adult male 50th percentile) and AF05 (adult female 5th percentile) dummies in the rear seat showed larger injury criteria than those in the front seat, especially for HIC15, neck (tension and Nij) and chest deflection. Transport Canada also has a research project dealing with rear seat safety [10]. The Hybrid III AF05, 6YO (year-old) and 3YO were tested, and the Hybrid III AF05 in the rear seat was likely to have a large chest deflection, and depending on the location of seatbelt anchor, the lap belt could intrude into the abdomen.

The seatbelt design method for rear seat occupant safety has been analyzed. Zellmer et al. [11] examined the behavior and injury risk of rear seat occupants based on Hybrid III AM50 test and MADYMO analysis. It was shown that a seatbelt pretensioner and force limiter were effective for reduction of chest loadings, and they proposed that a 6-kN force limiter be used to reduce both chest loadings and head excursion. Kawaguchi et al. [12] tried an optimized design for various size occupants in the rear seat. They concluded that to reduce the injury criteria of various size dummies, a seatbelt force limiter of 3.5 kN and belt outlet of 0-200 mm retractor were useful.

In May 2006, the Council of Transport Policy Council, Road Traffic Working Group in Japan published a report for the future road traffic safety underscoring the need for measures to encourage the use of safety devices among car users in order to reduce the number of traffic fatalities. The use of seatbelts by rear seat occupants is one of the important issues to be tackled, even though widely recognized. The National Agency for Automotive Safety & Victims' Aid (NASVA) conducted a research project for rear seat occupant safety. This paper summarizes the results of crash tests in this NASVA research project to demonstrate the effectiveness of seatbelts for the safety of rear seat occupants.

METHOD

Test Conditions

The effect of a seatbelt in a rear seat was investigated based on crash tests using a crash dummy seated in a rear seat with and without seatbelt. Figure 1 shows the test condition. Two tests (test 1 and 2) were carried out. Full-width rigid barrier tests were conducted at 55 km/h in the same condition as the JNCAP (Japan New Car Assessment Program) test. In a full-width rigid barrier test, since the vehicle acceleration is high and the dummy loading is great, this test is suitable for the evaluation of a restraint system. A compact wagon (curb mass 1220 kg, engine displacement 1498 cc) was used in the test. Three-point seat belts were installed in the rear seat. In both tests, in the rear seat, the Hybrid III AF05 was seated behind the driver seat, and the Hybrid III 3YO dummy behind the front passenger seat. The Hybrid III AF50 was seated in the driver and front passenger seats.

In test 1, the Hybrid AF05 wore a three-point seat belt, and the Hybrid 3YO was restrained in the forward-facing child restraint system (CRS) in the rear seat. In test 2, the Hybrid III AF05 did not wear a seat belt. The Hybrid III 3YO was seated on the CRS without a CRS harness strap restraint, though the CRS was fixed on the rear seat with a seatbelt. Figure 2 shows the seating posture of dummies in the rear seat. In both tests, the Hybrid III AM50 was seated in the driver and passenger seat while wearing a seatbelt. To examine the influence of the rear seat occupants on the injury risk to the front seat occupants, injury criteria of the driver dummy were compared to those in the JNCAP full-width rigid barrier test without rear seat occupants.

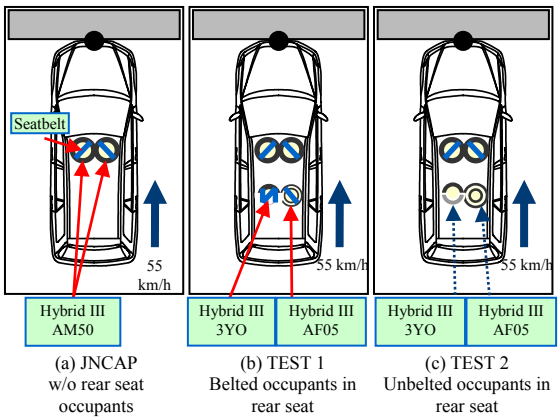

Figure 1. Test conditions.

Figure 2. Rear seat dummies in test 1 and 2.

Injury Criteria

Injury criteria of dummies in the rear and front seats were examined. Injury assessment reference values (IARVs) from FMVSS 208, ECE R94 and the literature by Mertz [13] were used. The IARV of chest deflection depends on the loading configuration on the chest. For the unbelted Hybrid III AF05 and 3YO dummies, the IARV of the chest deflection by the distributed load were used from FMVSS 208. The IARV of the distributed load was also used for the Hybrid III 3YO in the CRS because the load on the Hybrid III 3YO chest is likely to be distributed in the 5-point harness CRS. The IARV of chest deflection in the concentrated load due to the shoulder belt was applied from the ECE R94 to the belted AM50 dummy, and the IARV in the literature [13] was applied to the belted AF05 dummy.

The probability of injury was also calculated based on the injury criteria of the crash dummy. Basically, injury risk curves were adopted from those used in the JNCAP to calculate scores. The injury risk curve of the head was from Mertz et al. [13], and that of the chest and the femur was according to Viano and Arepally [14]. For unbelted occupants, the risk curve of the chest injury due to the distributed load was from Mertz et al. [13]. To calculate the probability of injury for AF05 and 3YO from that of AM50, their scale factors indicated by Mertz et al. [13] were used.

RESULTS

Car Deformation and Acceleration

Figure 3 presents photos of the deformed cars after crash. The passenger compartment was intact, and the intrusion was small. The acceleration-time histories are shown in Figure 4. Since the vehicle deceleration in JNCAP, test 1 and test 2 were similar, the inertial loads applied to the occupants are likely to be similar in the three tests.

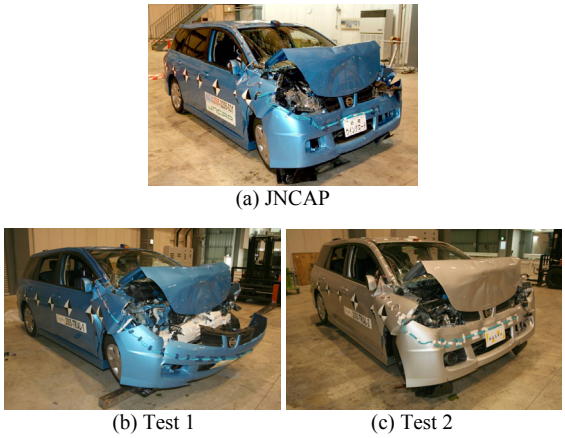

(a) JNCAP

(b) Test 1 (c) Test 2

Figure 3. Car deformation.

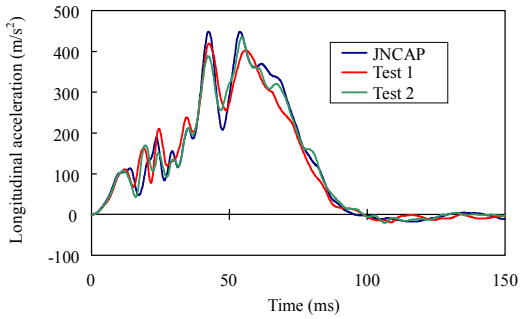

Figure 4. Car acceleration-time histories.

Occupant Kinematics

<u>Test 1 (belted rear seat occupants)</u>

The behavior of belted-in occupants is restrained during impact. Figures 5 and 6 present the behavior and readings for the dummies in the rear seat. Under the restraint of the seatbelt, the torso and neck of both dummies flexed. The chest acceleration of the AF05 has a maximum value at 65 ms, although no contact of the dummy with the car interior was observed from a high-speed video. The head accelerations and excursions of both dummies are maximal at 88 ms and at 102 ms, respectively. The chin made contact with the sternum (105 ms), which led to high head acceleration, especially for 3YO. In the rebound phase, both dummies moved backward in the initial seated position (1000 ms). Since the Hybrid III AF05 was restrained by the seatbelt, the head contacted neither the vehicle interior nor the front seat dummies. The Hybrid III 3YO in the CRS also did not make contact with the car interior, except for the contact between the feet and the seatback. Judging from the kinematics of the lower extremities, the impact force is probably small.

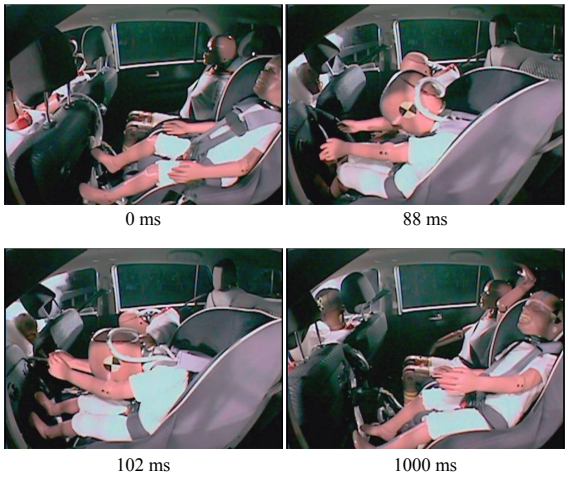

0 ms 88 ms

102 ms 1000 ms

Figure 5. Kinematics of belted dummies in rear seat (test 1).

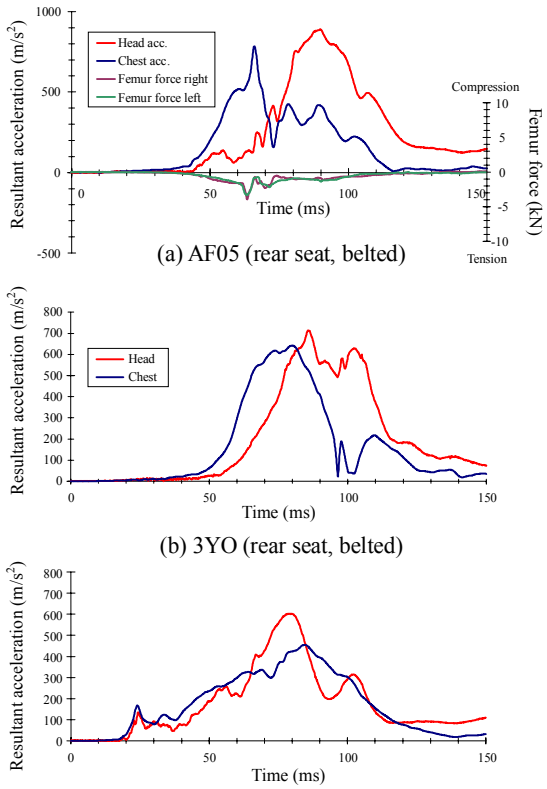

(a) AF05 (rear seat, belted)

(b) 3YO (rear seat, belted)

(c) AM50 (driver, belted)

Figure 6. Dummy readings in test 1.

Test 2 (unbelted rear seat occupants)

Because the rear seat occupants were not restrained, the moved forward under impact. Occupant movement was decelerated by impact with several locations in the car interior until the occupant moved with the same velocity as the car. Figures 7 and 8 show the unbelted occupant kinematics in the rear seat. Figure 9 plots the acceleration of the dummies.

The Hybrid III AF05 dummy moved forward in the initial seated posture. Its knees made contact with the front seatback (70 ms), and the femur force and pelvis acceleration were maximal (86 ms). The upper body started to rotate around the knee in the forward direction (100 ms), then was thrown over the front seat. The chest made contact with the seatback, and the face of the Hybrid III AF05 hit the pole of the head restraint at 47 km/h (120 ms). The Hybrid III AF05 also hit the occipital region of the driver dummy head at 36 km/h (122 ms). The Hybrid III AF05 continued to rotate forward, and the back region and the head hit the roof and the windshield, respectively (192 ms).

The unbelted Hybrid III 3YO also moved forward in the initial seated posture, and the foot soles and knees made contact with the seatback of the front passenger seat at 60 ms and 86 ms, respectively. Then the upper body rotated and was thrown over the front seat. The head traveling velocity was about 44 km/h based on the video analysis. The head hit the roof header at 135 ms, and the back region hit the roof at 170 ms. Its head struck the windshield, and finally dropped on top of the instrument panel at 200 ms.

Figure 7. Kinematics of unbelted Hybrid III AF05 in rear seat (test 2).

Figure 8. Kinematics of unbelted Hybrid III 3YO in rear seat (test 2).

For the driver dummy, there are peaks in the chest acceleration (90 ms) due to the impact by the rear seat Hybrid III AF05. Energy absorption of the airbag was almost finalized at 125 ms. However, the driver head was impacted from the rear by the face of the rear seat Hybrid III AF05, after which the driver head was thrown against the steering wheel (Figure 7).

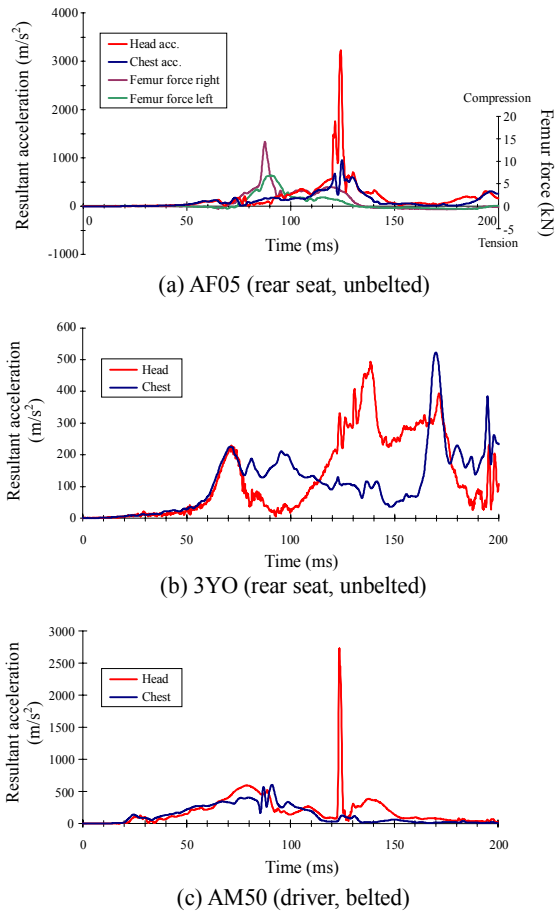

Figure 9. Dummy readings in test 2.

Injury Criteria

Injury criteria of dummies in the rear seat and in the front seat are shown in Tables 1 and 2, respectively. Based on these criteria, the ratio of injury criteria to the IARVs and the probability of injury are shown in Figures 10 and 11.

When the Hybrid III AF05 was belted in the rear seat, the head and chest injury criteria were relatively larger than the IARVs. For the unbelted AF05, the HIC15 and the femur forces were extremely high. Based on the injury criteria, the probability of head injury is 95% for AIS 4+ and that of femur fracture is 99.8%. Thus, serious injuries are very likely to occur.

For the belted Hybrid III 3YO, the injury criteria of head and chest were less than IARVs. The HIC15 and chest deflection of the unbelted Hybrid III 3YO were far less than IARVs. The chest acceleration (3 ms clip) took a maximum value of 470 m/s^2 when the back region of the Hybrid III 3YO made contact with the roof (see Figure 9), though this value was also less than the 539 m/s^2 prescribed in the FMVSS 208.

The injury criteria of the driver dummies in the JNCAP and in the test 1 are similar, which indicates that the belted rear-seat occupants have little influence on the injury criteria of the dummies in the front seat. When the Hybrid III AF05 in the rear seat was not belted, the HIC15 of the driver dummy exceeded the IARV due to impact by the AF05 head. In this case, the chest of the driver dummy was compressed, and chest deflection of the driver dummy was also larger than in other tests, because the front seatback was struck by the impact of the rear-seat Hybrid III AF05.

Table 1. Injury criteria (rear seat dummies)

	Rear seat AF05		Rear seat 3YO	
	Belted (Test 1)	Unbelted (Test 2)	Belted (Test 1)	Unbelted (Test 2)
HIC15[(1)]	972 (700*)	2403 (700*)	466 (570*)	138 (570*)
Chest deflection (mm)	49.5 (41**)	1.0 (52*)	25.2 (34*)	6.6 (34*)
Femur force right (kN)	0.1 (6.8*)	14.3 (6.8*)	NA	NA
Femur force left (kN)	0.2 (6.8*)	6.8 (6.8*)	NA	NA

Parentheses show injury reference values from * FMVSS 208 and **Mertz et al. [13].

Table 2. Injury criteria (driver dummy)

	Belted driver dummy (AM50)		
Rear seat dummy	No dummy (JNCAP)	Belted AF05 (Test 1)	Unbelted AF05 (Test 2)
HIC15	358 (700*)	344 (700*)	1218 (700*)
Chest deflection (mm)	27.2 (50**)	25.8 (50**)	29.2 (50**)
Femur force right (kN)	0.3 (10.0*)	0.4 (10.0*)	0.4 (10.0*)
Femur force left (kN)	1.8 (10.0*)	1.7 (10.0*)	1.6 (10.0*)

Parentheses show injury reference values from *FMVSS 208 and **ECE R94.

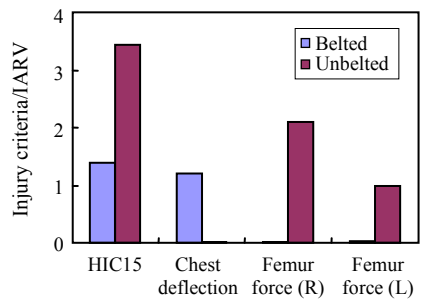

(a) Rear AF05

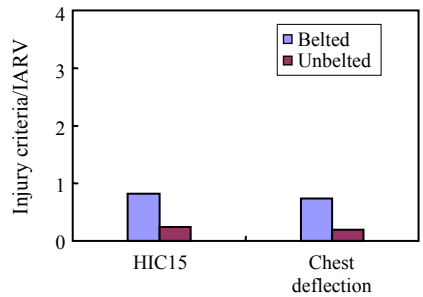

(b) Rear 3YO

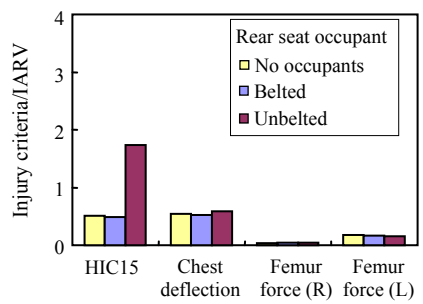

(c) Driver AM50

Figure 10. Ratio of injury criteria to IARVs.

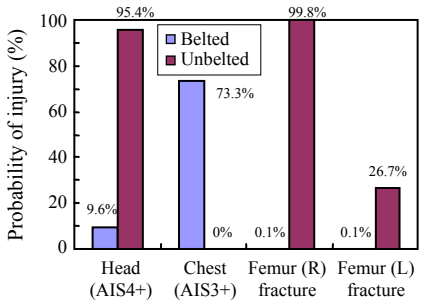

(a) Rear AF05

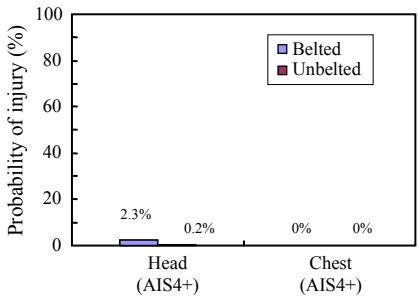

(b) Rear 3YO

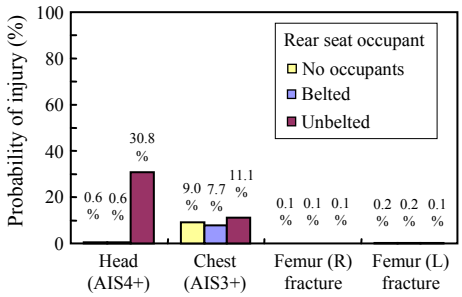

(c) Driver AM50

Figure 11. Probability of injury calculated based on IARVs.

DISCUSSION

In test 2, the unbelted Hybrid III AF05 and 3YO in the rear seat were thrown over the front seat. The Ministry of Land, Infrastructure and Transport, Japan conducted a full-width rigid barrier test with two unrestrained Hybrid III AM50 dummies in the rear seat [15]. In the test, the Hybrid III AM50 in the rear seat collided against the seatback of the front seat and rebounded into the rear seat. JAF also conducted offset frontal impact tests with the Hybrid III AF05 and 3YO in the rear seat under conditions similar to those used in test 1 and 2. The Hybrid III 3YO moved in between the driver seat and the front passenger seat. Based on the in-depth accident analysis by Shimamura [3], 81% of the unbelted rear-seat occupants were stopped by the front seat, and 19% were thrown over the front seat. In this accident data, many low velocity accidents were probably included, which made for the high frequency with which rear seat occupants returned to their original position after collision. Therefore, the behavior of the unbelted rear-seat dummy varies with its body size, impact velocity and impact force direction. Depending on the collision situation, an unbelted occupant can even be ejected from the passenger compartment.

The HIC15 and chest deflection of the belted Hybrid III AF05 exceeded the IARVs, though there were no significant contacts between the dummy and the car interior. It is not clear whether the HIC15 can be applied to assess the head injury to rear seat occupants when there is no hard head contact. The chest acceleration of belted Hybrid III AF05 was also high in the initial phase before flexion of torso occurred (see Figure 6), though the force path for this high acceleration is not clear. Even though the injury criteria were relatively high for the belted AF05, the safety effectiveness of the seatbelt for the rear occupant injury risk is clear. The injury criteria of unbelted AF05 in the rear seat were extremely high due to contact with several locations in light of the uncontrolled behavior.

The unbelted Hybrid III 3YO was thrown around inside the passenger compartment, and gradually decelerated by impact with several locations. Surprisingly, all measured injury criteria were less than IARVs. However, it is difficult to say that the injury risks of the unbelted Hybrid III 3YO were small based on this test since various body regions of the Hybrid III 3YO made contact with the interior of the car, and the injury risks were difficult to determine.

It was demonstrated that the injury to the front seat occupant could be affected by the unbelted occupants in the rear seat. Under the rear occupant impact into the seatback of the front seat, the chest acceleration and chest deflection of the front seat occupant can become large. It is not clear that such great injury criteria really reflect injury risks to front seat occupants from the rear impact because of the

Hybrid III limitation. However, accident analysis has demonstrated that the injury risks to front occupants increase when there are unbelted rear-seat occupants [3,6,7,8].

The kinematics and injury criteria of the dummy in the rear seat were probably affected by various factors such as car acceleration, initial posture, and the size and properties of dummies. Further investigation of the safety of the rear-seat occupants is warranted taking into account the various sizes of rear seat occupants.

CONCLUSIONS

The Hybrid III AF05 and 3YO dummies were seated in the rear seat in the belted or unbelted condition, and full-width rigid barrier tests were carried out at 55 km/h. The conclusions may be summarized as follows:

1. The injury risk was low for the belted AF05 in the rear seat because the contact with the car interior was prevented by the seatbelt, though the chest deflection was large by the shoulder belt. When the AF05 was not belted, risks of head injury and femur fracture were particularly high due to contact with several locations in the car interior.
2. When the Hybrid III 3YO was restrained by the CRS, the only contact with the car interior was between the feet and front seatback. The unbelted Hybrid III 3YO was thrown over the front seat, making contact with the front seat, roof and instrument panel.
3. When the Hybrid III AF05 in the rear seat was belted in, the AF05 did not affect the driver dummy behavior. However, the unbelted AF05 made contact with the rear seatback and the driver head, which could result in severe injuries to the head and chest of the driver dummy.

REFERENCES

[1] http://www/jaf.or.jp

[2] Morgan, C., “Effectiveness of lap/shoulder belts in the back outboard seating position”, NHTSA Technical Report, DOT HS 808 945, 1999.

[3] Shimamura, M., Yamazaki M., Fujita G., “Method to evaluate the effect of safety belt use by rear seat passengers on the injury severity of front seat occupants”, Accident Analysis and Prevention, Volume 37, Issue 1, pp. 5-17, 2005.

[4] Cuerdan, R.W., Scott, A.W., Hassen, A.M., Mackay, M., “The injury experience of adult rear seat car passengers”, IRCOBI, 1997.

[5] Parenteau, C., Viano, D.C., “Field data analysis of rear occupant injuries. Part I: adults and teenagers”, SAE Paper 2003-01-0153, 2003.

[6] Ichikawa, M., Nakahara, S., Wakai, S., “Mortality of front-seat occupants attributable to unbelted rear-seat passengers in car crashes”, Lancet 359, 43–44, 2002.

[7] Broughton, J., “The actual threat posed by unrestrained rear seat car passengers”, Accident analysis and prevention, Vol. 36, pp.627-629, 2004.

[8] Shimamura, M., Ohashi, H., Yamazaki, M., Okamura, K., “In-depth study of front seat occupants in accidents in relation to seat belt use of rear seat passengers”, 1st Conference for ESAR, 2004.

[9] Kuppa, S., Saunders, J., Fessahaie, O., “Rear seat occupant protection in frontal crashes”, 19th ESV, 05-0212, 2005.

[10] Tylko, S., Dalmotas, D., “Protection of rear seat occupants in frontal crashes”, 19th ESV, Paper No. 05-258, 2005.

[11] Zellmer, H., Luhrs, S., Bruggenrmann, K., “Optimized restraint systems for rear seat passengers”, 16th ESV, Paper No. 98-S1-W23, 1998.

[12] Kawaguchi, K., Kaneko, N., Iwamoto, T., Fukushima, M., Abe, A., Ogawa, S., “Optimized restraint systems for various-sized rear seat occupants in frontal crash”, SAE Paper 2003-01-1230.

[13] Mertz, H., Irwin, A., Prasad, P., “Biomechanical and scaling bases for frontal and side impact injury assessment reference values”, 47th Stapp Car Crash Conference, 2003-22-0009, 2003.

[14] Viano, D.C., Arepally, S., “Assessing the safety performance of occupant restraint systems”, SAE Paper 902328.

[15] Arai, Y., Kiuchi, N., “The influence of unbelted rear occupants on injuries to front occupants”, JARI Research Journal, Vol. 27, No.1, 2005 (in Japanese).

The Crash Problem for Advanced Restraints

Ana Maria Eigen
Sarah A. Bentil
David L. Smith

National Highway Traffic Safety Administration
United States of America
Paper Number 07-0234

ABSTRACT

In response to evolving sensor and occupant retention technologies, the National Highway Traffic Safety Administration (NHTSA) will soon begin cooperative research to develop test procedures for advanced occupant restraints. It is believed that these restraints will be real-time adaptive to a variety of crash types and severities, as well as address such problems as improving belt effectiveness in front-front crashes to higher than the current 50% fatality reduction level and possibly making the belts and air bags better suited for rollover and offset crashes. The research will address: identification of potential improvements in current restraints, identification of minimum performance and objective testing, as well as performance metrics, and calculation of benefits inherent in such improvements. To complete these tasks, the identification of a target crash population, estimations of the effectiveness of advanced restraints from test and evaluation, and benefits calculation based upon the target population and the effectiveness estimates is necessary. This paper serves as an initial analysis of the advanced restraint system target population.

The Crashworthiness Data System (CDS) of the National Automotive Sampling System (NASS) was chosen for the initial work owing to its complete crash, vehicle, occupant, and injury reporting in the U.S. In addition, in order to maintain a focus on recent vehicle designs and performance, the most recent eight years of data were used for an occupant population that contains only belted drivers and passengers. By analyzing this population, attention was focused on the current performance of restraints in order to identify opportunities for restraint improvement. Restrained occupants with Maximum Abbreviated Injury Scale (MAIS) groupings of 3+ (serious injuries and higher) were quantified. Disaggregations of the primary direction of force, impact area, and injury types, among others, were computed across all crash types in order to develop an understanding of the requirements for advanced restraint prototype designs.

INTRODUCTION

NHTSA is interested in developing research on objective performance tests for advanced integrated safety systems and is now focusing attention on two projects in this area: crash imminent automatic braking, and advanced restraints. The first of these projects assumes the current state of the art in restraint technology and seeks to leverage crash avoidance sensor technology to make restraints perform better, while the second is focused more on using the sensors to accomplish real-time adaptation in the restraints. Although these projects are not directly linked, the advanced restraints project will use many data techniques identified in the imminent braking project, which include using data set queries of the NASS CDS data to build and study target crash scenarios. These scenarios will then be used to identify opportunities for intervention and corresponding benefits. This paper reports on the initial steps of this effort, determining the crash target population for advanced restraints.

The advanced restraints data analysis project is deemed a continuation of the work started in support of the imminent braking project. As basis for that effort, a 36 crash typology was developed using the General Estimates System (GES) of the NASS (Najm and Smith, 2007). The NASS GES is a sample of police-reported crashes occurring on public roadways in the United States and, with weighting factors for the samples, provides overall crash frequency data.

In the previous work, the 36 GES crash types were ranked according to frequency, economic cost, and occupant functional years lost. However, a large portion of these crashes were damage only crashes, which are of little interest in developing advanced restraints. For this reason, a new approach was sought to characterize pre-crash and crash scenarios that could form a basis for the injury reduction benefits analysis.

Table 1 (tables and figures are presented at the end of the paper) shows an initial taxonomy of crash

configurations disaggregated by vehicle or object contact. Note that the object type struck for frontal impacts may be either a wide or narrow object and it is important to distinguish these. Frontal, left side, and right side are for planar crash events. The rollover event has been disaggregated by initiation type and does not rely on vehicle damage.

Advanced restraint systems could incorporate sensors such as vision and radar that provide data in the crash timeline before the vehicle-vehicle contact occurs. In this way the system could see, anticipate, and provide the best protection to the occupants. This action likely follows a crash avoidance segment where driver braking, roadway geometry, vehicle characteristics, and vehicle handling are critical. However, in the case of advanced restraints, although interest exists in the vehicle characteristics, issues of handling become more obscure owing to the foregone notion that a crash will occur and the restraint should mitigate rather than avoid the crash. For this reason, NASS CDS was consulted to build the scenarios summarized in Table 1. NASS CDS is a sample of tow-away crashes with injuries occurring on public roadways in the United States. Variables and attributes describe more complete occupant demography than that seen in GES, as well as a listing of injuries by body region, type, severity, and location on the given body region, as well as injury source.

The approach taken in this initial effort was to develop and evaluate the problem definition by first determining the most common and the most harmful crashes for belted occupants and then to present these results in scenarios detailing the sequence of events. This paper presents the initial data analysis effort that could lead to advanced restraint scenario creation. Such scenarios will eventually be used as the basis for countermeasure development, testing, and, finally, benefits analysis.

METHODOLOGY

The creation of initial scenarios was approached in two ways that were merged for a final result. A top-down approach was used on the CDS data to step-wise disaggregrate the belted driver data into crash types to find the most common types and focus on those, then assess the most common injury types and counts. In coordination with this, a bottom-up approach was used on the injury data to better understand the causation of injury. Finally, the two approaches were merged to establish and select the most common injury types from which scenarios are used to develop advanced restraints performance requirements.

Top-Down Damage and Injury

A general query was first made of the NASS CDS to estimate the total tow-away crash population and the corresponding restraint usage characteristics to date. Next, vehicles were disaggregated by model year, with the retention of vehicles of model year 1998 and later. The model year served as the surrogate for modern restraint systems, including three-point lap and shoulder belts, presence of pretensioners, load limiters, the advent of the second generation, depowered air bags, and more advanced seat belt and air bag technology. This was done to preserve homogeneity in the restraints available within the late model vehicles.

CDS crash variables were selected to capture vehicle attitude, crash severity, and direction of force. The most severe event is normally based upon vehicle deformation processed through an algorithm to produce delta-V. Delta-V is a measure of crash energy transfer and deemed to form part of a composite crash severity indicator to be studied during this project. However, the algorithm yielding delta-V may fail owing to extreme planar conditions and in all rollover crashes. For planar events, if a researcher is able to provide a quantitative or qualitative value, it will be reported as an estimated delta-V. The decision to report quantitative or qualitative severity is dependent upon the degree of confidence that the NASS CDS researcher is able to assert. In the case of rollover crashes, crash severity may not be calculated using the existing crash algorithm and the estimated crash severity will always take on a qualitative value.

The top-down analysis was based on a model of zone of impacts for the most severe event, as seen in Figure 1. Planar crash events occurred from one o'clock through 12 o'clock and rollover crashes were identified with zero, as seen in Figure 1. For rollover crashes, the type of damage distribution was consulted to ascertain whether the rollover crash was the most severe event. A composite variable was then formed for rollover crashes by consulting both the type of damage distribution and rollover initiation type. The rollover initiation type was further summarized to characterize tripped versus untripped rollover crashes.

The vehicle analysis was an iterative process and yielded commonalities based upon Collision Deformation Classification (CDC). The elements of interest included the principal direction of force

(PDOF), damaged vehicle plane, specific horizontal location, specific vertical location, and the extent of damage. The restriction on the extent of damage was loosened owing to the case representation across the zones of deformation.

The first analysis conducted was for damage to the frontal plane pursuant to force with an, 11, 12, or 1 o'clock direction. This would indicate a head-on collision with full frontal or offset frontal damage. The full frontal crash with a 12 o'clock direction of force was found to be the most prevalent; however, the aggregate of the left frontal and right frontal offset crashes exceeded the full frontal crashes. Further, examination of the cases indicated that everything below the belt line on the vehicle body was prevalently damaged. Finally, an array of extent zones from one to five appeared in the initial analysis. Owing to the integration of injury parameters into this selection process, the extent zone was not specified in subsequent queries. Thus, the database query yielded 12FDEW (**12** o'clock direction of force, **F**rontal damage plane, **D**istributed damage, **E**verything below the belt line, and **W**ide distributed damage) as a prevalent CDC where the extent zone was omitted to generalize the injury search.

This methodology was generalized to consider all crash types at the MAIS 3+ level, as shown in Figures 2 through 4. MAIS 3+ subsumes MAIS 3 (serious), MAIS 4 (severe), MAIS 5 (critical), and MAIS 6 (maximum) injuries. Further, comparison of these figures focusing on frontal crashes shows that MAIS 3+ head injuries trailed thoracic injuries. Abdominal injuries were also examined and summarized in Figure 4. The prevalence of the frontal injuries was seen in the plots for thoracic and abdominal injuries. Comparable head and thorax injury frequencies were seen for tripped rollovers. Frontal crashes resulting in MAIS 3+ head injuries were disaggregated by the specific horizontal location. Frontal offset injuries were the most prevalent for head and thorax injuries. These results are pending further case review.

Figures 2 through 4 clearly show the predominance of frontal crashes as the largest part of the overall MAIS 3+ injury problem. Consequently, the next step was to look in more detail at these frontal crashes to determine how the belted drivers are being injured, in what body regions. Analysis of the mortality rate and injury costs dictated the body regions of interest in defining the crash problem (Eigen and Martin, 2005). The frequency counts for these major body region injuries in frontal crashes are shown in Figure 5. Here, the size of the relative injuries are shown, with the largest being thorax injuries, followed by head, neck, and abdomen.

Bottom-Up Injury and Damage

Using the results of Figure 5, the bottom-up approach to CDS analysis starts with the most common type of injury and seeks to find clues as to how these came about in a kinematic sense to lay a basis for scenario development. The accuracy of this task was corroborated using the Biomechanics Tab (BioTab) found in the Crash Injury Research and Engineering Network (CIREN) database. For example, within the 20,197 weighted cases describing the various types of head injuries, 75% were due to head contact within the vehicle interior and 4% of the head injuries occur despite the lack of contact with the vehicle interior or other occupants (0.6%). Furthermore, injury from contact of the head could be due to one kind of kinematics, while injury without contact may be due to another kind of kinematics. This is assuming that the selection of non-contact by the researcher does not imply that there is a lack of physical evidence supporting contact with the vehicle interior. To avoid misinterpretation and ambiguity in describing the injury causation when incorporating the contact information, the injury parameters from CDS associated with certain and probable confidence were considered. This information was used to supplement and support a similar query using the BioTab. These two databases concurrently provided valuable and accurate clues to vehicle and occupant motions prior to and during the crash event.

Figure 5 shows the major body regions injured in frontal crashes, with the thorax region being the largest problem. Nevertheless, the head region was selected for this initial study. The choice of the head injury in frontal crashes as a focus for the initial bottom-up analysis stemmed from an examination of the relationship between the injured body region and the injury source.

The sources of injury to the head, such as contact with the A-pillar or B-pillar were more distinct than thoracic injuries occurring from the usual contact with the steering hub, rim, and wheel combination and also the belt web or belt buckle. Further, contact with the injury sources specified for thoracic injuries did not involve as much excursion by the driver as that of the head region using the given injury sources of Figure 6. Thus, the motivator for the selection of the head injury data for initial analysis was to understand why and how the belted driver was able to contact the pillars. In addition, the sample size for the head exceeded that of the neck or abdomen.

Thus, more cases were available for preliminary analysis using the head region.

Figure 6 displays several sources of injury for the head and the thorax by total weighted cases. Of note in this figure is the fact that roof contact in frontal crashes resulted in MAIS 3+ head injuries with such a high frequency. 82% of these head injuries in which the roof was stated as an injury source was made with high confidence by the researcher. The specific reasons for this result need to be evaluated before a scenario for such crashes can be detailed.

The second phase of injury analysis identified the top ten head injury types by frequency. Table 2 shows the weighting totals for these head injuries.

Next, the causation of these head injuries was investigated for two reasons. The first was to better understand the circumstances that will result in the head injury. This was performed as a means of validating and supporting the injury source data in NASS CDS. The second reason was to provide a means of aggregating similar injuries, where possible. This step alleviated one of the problems of case limitations from a query focusing only on model year 1998+ vehicles by increasing the cases that were available for analysis. This enabled the explanation of the injury causation in connection with the relationship between the injury and vehicle-level CDS parameters to be understood more comprehensively.

The following example uses both intracerebral and subdural cerebrum hematoma/hemorrhage injuries, vault skull fractures, and orbit fractures to illustrate the caution needed in steps for aggregation. The causation of these four prevalent head injury cases, acquired from Table 2, were examined to justify aggregation. This step must not be overlooked as the injuries vary by mechanisms, which is dependent upon the occupant kinematics in response to the vehicle collision (Takhounts et. al., 2003).

Hematoma/hemorrhage in the intracerebral region is typically due to bleeding directly into brain tissue, pushing the tissues against the bones of the skull. This type of injury encapsulates 31% of the hematoma/hemorrhage category. However, research has shown that 8-13% of all strokes result from intracerebral hemorrhage (Liebeskind, 2006). Although this percentage is relatively small, it is still considered in the analysis of this injury. One should be careful to examine other data in NASS CDS, such as the crash or accident summary to determine whether the intracerebral hemorrhages were due to the crash or the stroke. This detailed selection criteria will prevent the use of cases in which the injury precipitated the crash. A similar analysis should be performed during the study of injuries in other body regions.

Hematoma/hemorrhage in the subdural region is due to swelling in the area between the cerebrum/brain surface and the parietal bone/skull (Jasmin, 2004 & WebMD, 2004). The bleeding can be either minor or severe, causing a slow or rapid increase in pressure within the skull (Meagher, 2005).

All cerebrum hematoma/hemorrhages are the result of one or more blood vessels breaking in the cerebrum tissue. As a result, the influx of blood in the confined region of the brain, where the damage occurred, causes swelling and an increase of pressure within the skull. For example, the head of an occupant may be subjected to a hard blow or impact to the A-pillar during the frontal planar crash. Or, due to inertial effects of the crash, the occupant may suffer an AIS 1 neck injury such as whiplash. This minor neck injury may initiate the vibration of the brain within the skull, resulting in an AIS 3+ head injury (University of Virginia Health System, 2004). This rapid movement of the brain within the skull can also result in cerebrum hematoma/hemorrhages due to bruising, swelling, or tearing of the brain tissue. Without further specifying the type of cerebrum hematoma/hemorrhage (intracerebral small, subdural small, or subdural NFS), the results of this analysis showed that aggregation of these three groups of cerebrum injuries were possible since they all resulted in swelling and an increase of pressure within the brain.

Vault comminuted fractures are bones of the skull that are broken, splinted, or crushed/shattered into a number of pieces (MedicineNet.com, 2003). The bones of the vault skull include: parietal, frontal, squamous temporal, and the squamous part of the occipital (The Johns Hopkins Hospital Center for Craniofacial Development and Disorders, 2000).

Orbit fractures, are any or combination of open (where a broken bone penetrates the skin), displaced (where the fragments are not perfectly aligned), or comminuted fractures of the bone around the eye (The Medical Center Online, 2006). Non-deployment of the air bag increases the occupant contact with the steering wheel, resulting in the orbit fracture (Duma and Jernigan, 2003).

Following the analysis and aggregation, where applicable, three injury groupings resulted for this

example: Cerebrum Hematoma/hemorrhage, Vault skull fracture comminuted, and Orbit fracture open/displaced/comminuted. The vault skull and orbit fractures could not be aggregated because the causes and locations of these injuries differed.

The next step is to aggregate injuries to infer kinematics at the occupant level. For example, suppose in frontal crashes, a severe brain injury with a face injury indicates a head contact causation. On the other hand, a brain injury without a facial injury indicates a non-contact head injury. While these are both head injuries, the restraint countermeasure could be quite different, so they must be separated.

To further strengthen the comprehension of the injury causation following an aggregated grouping scheme, the most prevalent CDC value among the head injuries was obtained. Without application of the extent, this CDC value corresponded to 12FDEW. Next, the most prevalent accident type for 12FDEW was chosen to constrain the given data set to a particular vehicle impact description for a detailed causation description.

Table 3 displays the parameters that are needed to better describe the transition from injury to CDC (occupant to vehicle level) for each of the head injuries, utilizing the outcome of the CDC query and vehicle maneuver constraint.

Beginning with the occupant, the presence of alcohol or drugs is noted as it may affect the biophysical response to insult (Couper and Logan, 2004). This may provide additional locations of contact within the vehicle interior for the restrained occupant, who is under the influence of the substance. Thus, this parameter should be analyzed to determine whether it contributes any new information.

Next, the injury source parameter is examined as it initiates the transition to the vehicle level by connecting the occupant and injury with the vehicle interior. The accuracy of this step is fundamental for the transition to be made successfully. Thus, a combination of the evidence supporting the occupant contact with the vehicle interior, such as scuff mark(s), tissue contact(s), tooth mark(s), and bent structure(s), along with the researcher's level of certainty that the evidence supports the injury sources noted will aid in the selection of the appropriate cases for analysis.

In certain cases, the occupant sustains multiple injuries, in addition to the MAIS 3+ injury initially selected. Such instances require that these injured body regions, regardless of the injury severity, should be included in the analysis along with the corresponding injury source only if they meet the accuracy requirement. Thus, evidence supporting the injury source must also be substantiated by the researcher through their certainty level when determining the relationship between the injury and the injury source.

Next, information regarding the gender, age, height, and weight of the occupant is needed to determine whether the injuries are dependent upon these factors. This is similar to the BioTab's description of other contributing factors that affect the injury causation, mechanism, and severity. Whether these four parameters are related to the injury and injury source through the occupant's seat back position, seat track position, and seat belt anchorage position should also be investigated.

Afterward, all vehicle intrusions and all severe events and corresponding CDC, where applicable, should be included in the analysis. This step clarifies whether or not occupant contact with the vehicle interior occurred on account of the intrusion(s). It is also necessary to include the information describing any pre-event movement that initiated the crash, critical pre-crash event that resulted in the crash, and any avoidance maneuver that the occupant performed leading to the crash.

Finally, to complete the transition from the given injury to the given vehicle-level crash, the heading angle and its corresponding other angle, which describes the vehicle configuration and location of the damage to the vehicle with respect to the North direction is necessary. Inclusion of this parameter is important as different geometry configurations for the given CDC may result in different injury and injury combinations.

From these parameters, the injury causation or scenario can be developed and used to explain the occupant positioning and movement that generated the injury as it relates to the CDC in the event of an imminent collision in time sequence. Through the listed parameters of Table 3, a causation describing the possible series of events that may result in one of the head injuries is possible.

As an aside, this process of injury selection led to vehicle-to-occupant case selection substantiation, as well as providing a complete case overview from the injury-to-vehicle perspective. This method will be applied to all other body regions for occupants in all seating positions (front and back seat passengers).

Although the listed parameters are sufficient to describe the injury causation resulting from the crash, there are other parameters not included in the NASS CDS database that would enhance and provide a more comprehensive scenario description to be used in vehicle testing situations and also to draw more definitive conclusions. For instance, examination of the seat belt material properties in conjunction with the retractor locking mechanism by body type and vehicle model may serve to be useful in understanding the excursion of the driver. Perhaps some combinations of the airbag properties, seat belt properties and retractor types function better than other system combinations (Ridella et. al., 2003). This information, along with the parameters declared in Table 3, may prove to be useful in explaining why occupants in similar crashes sustain different injuries.

Merging top-Down and Bottom-up Data

The research reported in this paper serves as the foundation for merging the top-down data with the bottom-up data into scenarios. This next step will be done first for frontal crash head injuries. The transition from the injury to the vehicle level will be possible through the use of the Collision Deformation Classification. This will both enable and ensure the proper alignment of the two methods prior to the merger.

SUMMARY

The objective of the advanced restraints research was to develop a set of crashworthiness scenarios that capture the timeline of events leading up to and during crashes that result in injury. These scenarios would contain a description of the conditions and events of the crash such that performance requirements for advanced restraints may be specified and benefits computed. Initial study of this problem suggested the use of CDS pre-crash variables and the sequence of harmful events. This would be used in the development of a chronology of what the vehicle sensors would detect and occupants would experience leading up to, and during the crash.

A framework for a top-down approach to the problem has been developed and preliminary analyses performed for model year 1998 and later vehicles in 1997 and later CDS data. Areas of damage and principal direction of force were analyzed. These results showed that the predominant types of crashes where belted drivers are getting injured are frontal and rollover crashes. Frontal crashes were analyzed in more detail showing four predominant injury areas in rank order: thoracic, head, neck, and abdomen.

Head injuries in frontal crashes were examined in more detail to develop a framework for a bottom-up problem definition approach, which would later be extended to all crash types. The most common types of head injuries were found to be cerebrum hematoma/hemorrhage, vault skull fracture, and orbit fractures. These injuries were caused by contact with the A-pillar, B-pillar, roof, and steering hub, rim, and wheel combination.

A taxonomy for crashworthiness scenarios was developed and presented based on an evaluation of all types of crashes. However, the research stopped short of creating the detailed crashworthiness scenarios.

Subsequent Study

Even at this early stage of the research it is clear that many data sources will be needed to develop useful scenarios, not just NASS CDS. Such sources include data from the CIREN, the Fatality Analysis Reporting System (FARS), and NHTSA Special Crash Investigations (SCI), all of which will certainly be needed. In addition, European data will be considered, if available, in the way that CIREN or SCI would be used to supplement the understanding of scenarios found in nationally representative data sets. The specific approach to this data integration will be considered in the context of the cooperative research program that NHTSA is now implementing with carmakers and suppliers.

Much work remains to be done for frontal crashworthiness scenarios, beginning with merging the top-down data with the bottom-up data sets for head injury scenarios. Next, the approach could be extended into thoracic and other injuries in frontal crashes, then similarly into other crash types, especially rollover. For instance, a large number of head contacts with the roof can be found in frontal crashes in which the driver was belted (Figure 6). This phenomenon is also present when examining the rollover problem for belted drivers. Thus, an advanced restraint that keeps the belted driver's pelvis in the seat could have a positive effect in both of these crash types. As these are preliminary results, the injury causation and occupant kinematics must be studied in greater detail before reaching any conclusions relative to frontal crashes and, subsequently, drawing any shared conclusions between frontal and rollover crashes. Nonetheless, it is precisely this type of insight that could lead to substantial benefits for advanced restraints.

Electronic case files may be accessed via the NHTSA website, Electronic Case Access Screen. The hyperlink is as follows: http://www-nrd.nhtsa.dot.gov/departments/nrd-30/ncsa

REFERENCES

Association for Advancement of Automotive Medicine, Abbreviated Injury Scale (AIS) 1990 - Update 98, Barrington, 1998.

Duma, S.M.. and M. Jernigan, "The Effects of Air bags on Orbital Fracture Patterns in Frontal Automobile Crashes." Ophthalmic Plastic & Reconstructive Surgery, 19(2), March: 107-111, 2003.

Eigen, A.M. and P.G. Martin, "Identification of Real World Injury Patterns in Aid of Dummy Development," Paper No. 05-0219, Enhanced Safety Vehicles Conference, 2005.

Jasmin, L, "Subdural Hematoma." Last updated on August 8, 2004. http://www.healthline.com/adamcontent/subdural-hematoma.

Liebeskind, D, "Intracranial Hemorrahge." Last updated on August 7, 2006, http://www.emedicine.com/neuro/topic177.htm.

Couper, F.J. and B.K. Logan, "Drugs and Human Performance Fact Sheets," Report No. DOT HS 809 725, 2004.

Meagher, R.J, "Subdural Hematoma." Last updated on August 5, 2005. http://www.emedicine.com/neuro/topic575.htm

MedicineNet.com, "Definition of a comminuted fracture." Last updated December 26, 2003. http://www.medterms.com/script/main/art.asp?articlekey=8079.

Najm, W. and D.L. Smith, "Definition of a Pre-Crash Scenario Typology," Paper No. 07-0412, Enhanced Safety Vehicles Conference, 2007.

Ridella, S.A., M.J. McCann, R.C. Turnbull, and G.S. Bayley, "Development of Restraint Systems with Considerations for Equality of Injury Risk," Paper No. 05-0403, Enhanced Safety Vehicles Conference, 2005.

Takhounts, E.G., R.H. Eppinger, J.Q. Campbell, R.E. Tannous, E.D. Power, and L.S. Shook, "On the Development of the SIMon Finite Element Head Model," Stapp Car Crash Journal. 47. October: 107-133, 2003.

The Johns Hopkins Hospital Center for Craniofacial Development and Disorders, "Regions of the Skull." Last updated February 2000. http://www.hopkinsmedicine.org/craniofacial/LynmProject/BSC/BSC1.htm.

The Medical Center Online, "Fractures of the Orbit." Last updated 2006. http://www.mccg.org/childrenshealth/content.asp?pageid=P02084.

United States Department of Transportation, National Highway Traffic Safety Administration, National Automotive Sampling System, Crashworthiness Data System, 2002-2005, NHTSA, Washington, D.C.

United States Department of Transportation, National Highway Traffic Safety Administration, "National Automotive Sampling System, Crashworthiness Data System, 2000 Coding and Editing Manual", NHTSA, Washington, D.C.

University of Virginia Health System, "Nervous System Disorders: Head Injury." Last Updated on February 12, 2004. http://www.healthsystem.virginia.edu/uvahealth/adult_neuro/headinj.cfm.

WebMD, "Bleeding within or around the Brain." Last updated July 23, 2004. http://www.webmd.com/hw/health_guide_atoz/not39323.asp?navbar=.

Table 1: Proposed Crashworthiness Scenario Taxonomy					
Crash Mode of Interest	**Subcategory**				
	Case Vehicle General Area of Damage	**Other Vehicle General Area of Damage**	**Object Type**	**Taxonomy Index**	**Resultant Scenario**
Frontal Impacts	Front	Front		1a	Front-vehicle front
	Front	Side		1b	Front-vehicle side
	Front	Rear		1c	Front-vehicle rear
	Front		Wide	2a	Front-wide object
	Front		Narrow	2b	Front-narrow object
Left Side Impacts	Left	Front		3	Left side-vehicle front
	Left		Any	4	Left side-object
Right Side Impacts	Right	Front		5	Right side-vehicle front
	Right		Any	6	Right side-object
Rear Impacts	Rear	Front		7	Rear-vehicle front
Rollover	Tripped			8	Tripped rollover
	Untripped			9	Untripped rollover
Note: Shaded areas denote regions inapplicable to the crash scenario.					

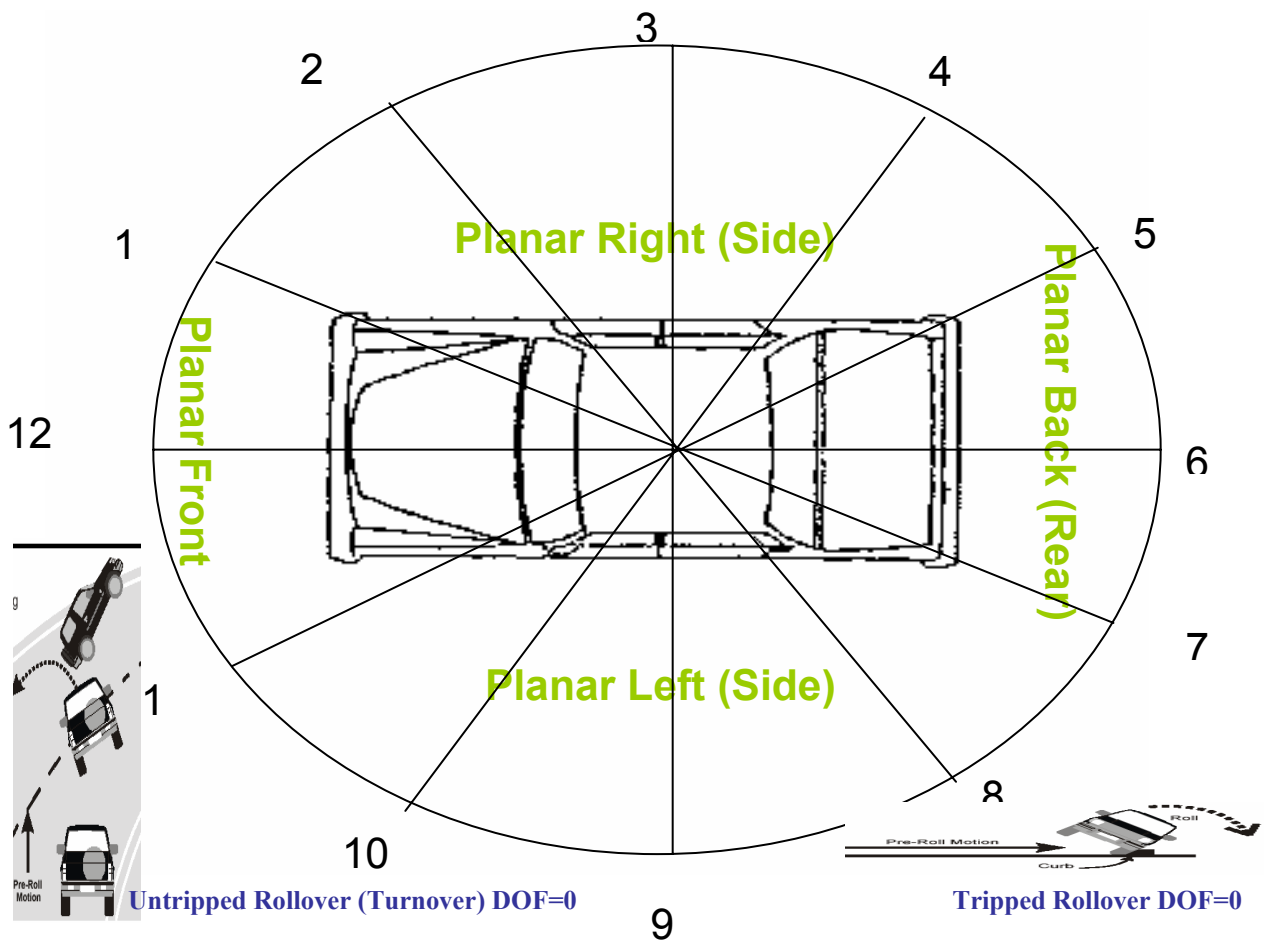

Figure 1. Zones of Interaction

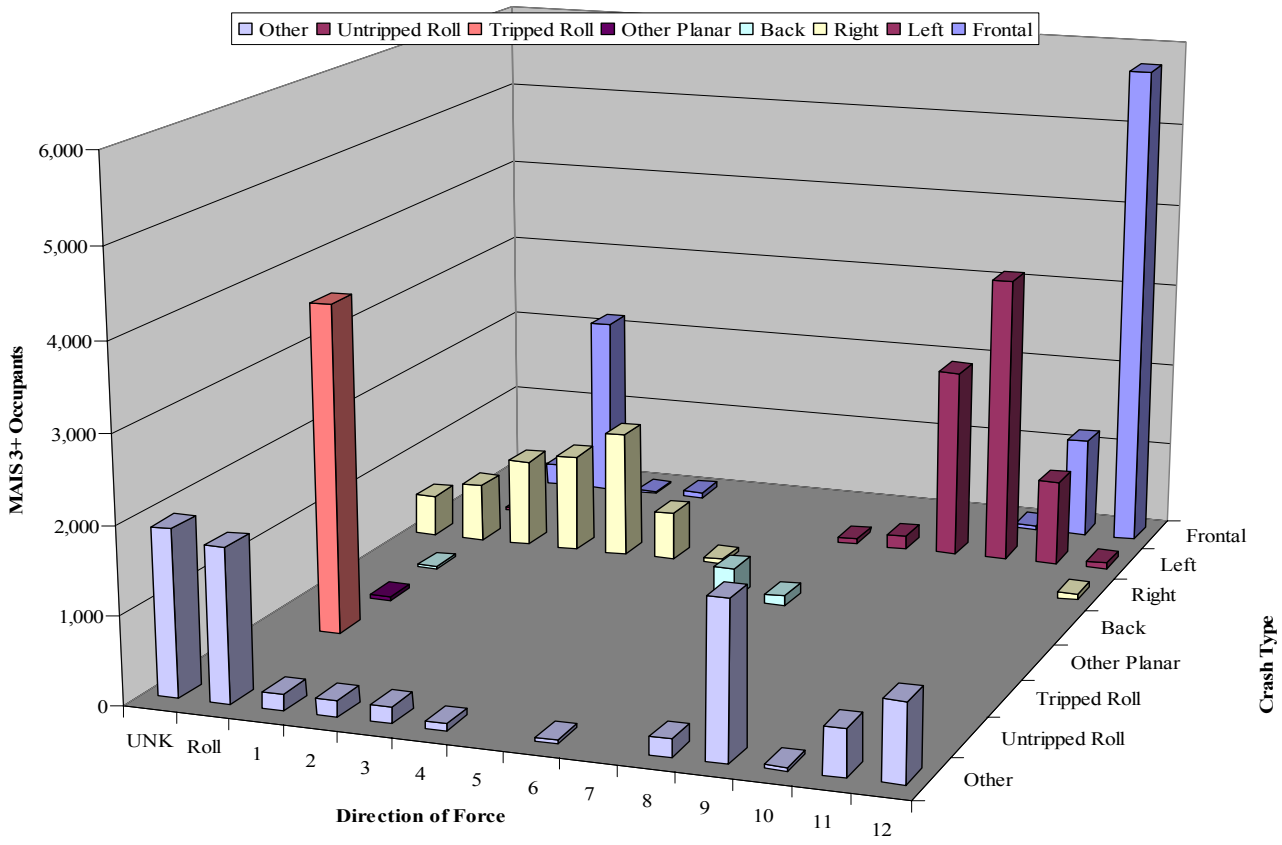

Figure 2. Occupants with MAIS 3+ Head Injury, traveling in Model Year 1998+ Vehicles, involved in Tow-Away Crashes, by Planar Direction of Force or Rollover and Crash Type, Weighted Data

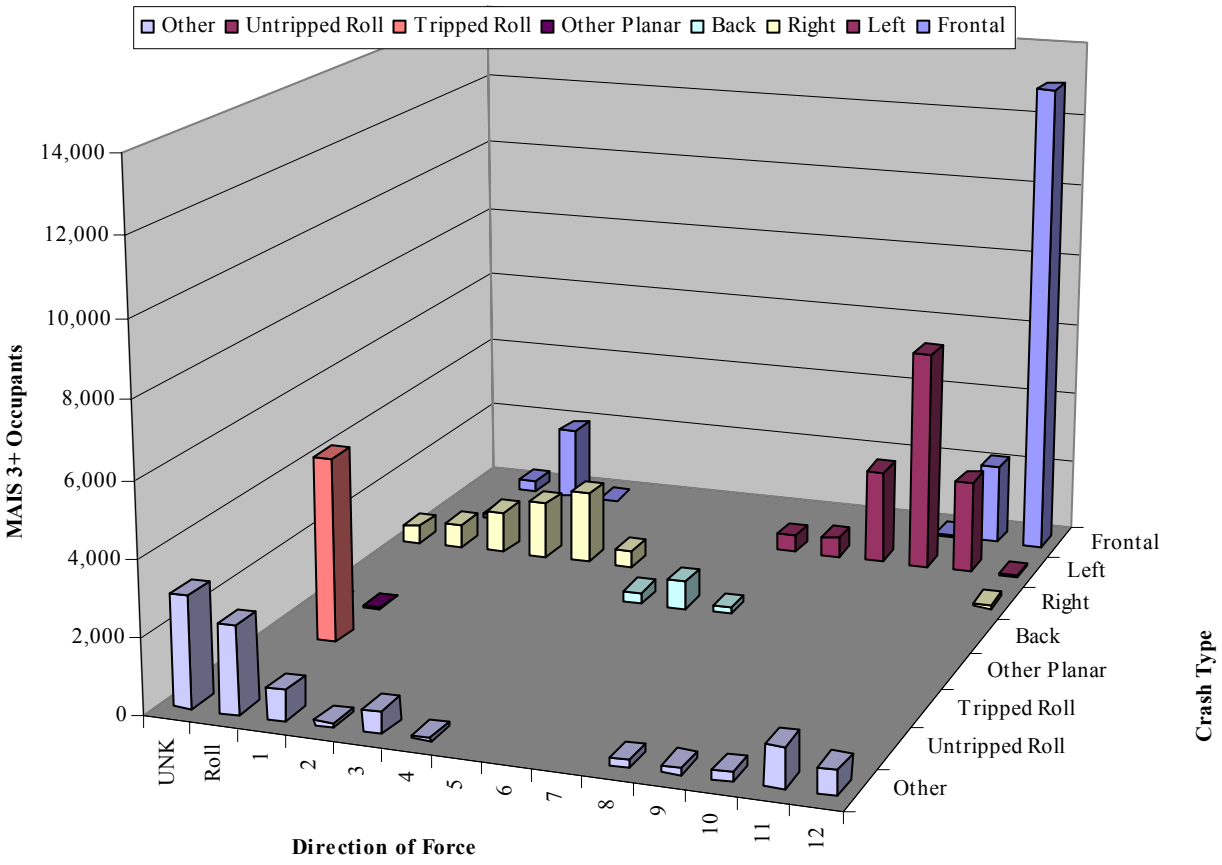

Figure 3. Occupants with MAIS 3+ Thorax Injury, traveling in Model Year 1998+ Vehicles, involved in Tow-Away Crashes, by Planar Direction of Force or Rollover and Crash Type, Weighted Data

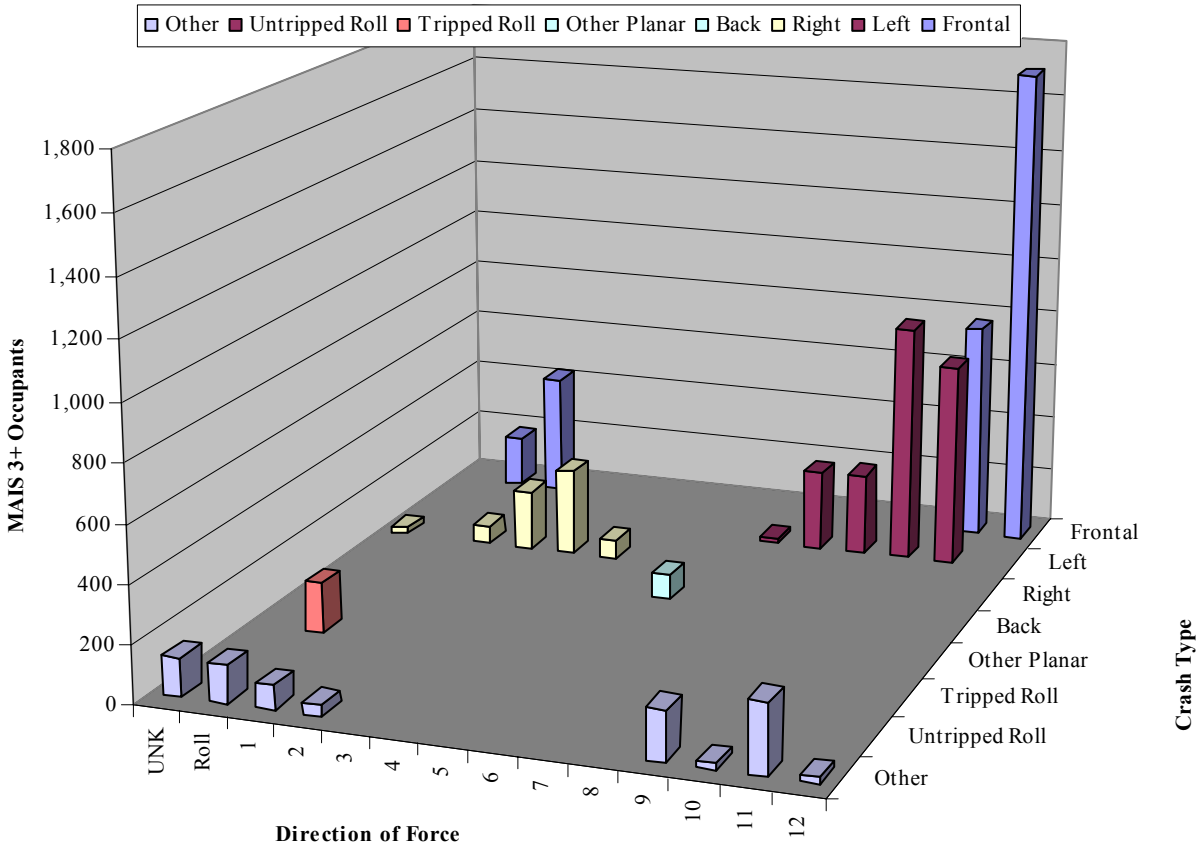

Figure 4. Occupants with MAIS 3+ Abdominal Injury, traveling in Model Year 1998+ Vehicles, involved in Tow-Away Crashes, by Planar Direction of Force or Rollover and Crash Type, Weighted Data

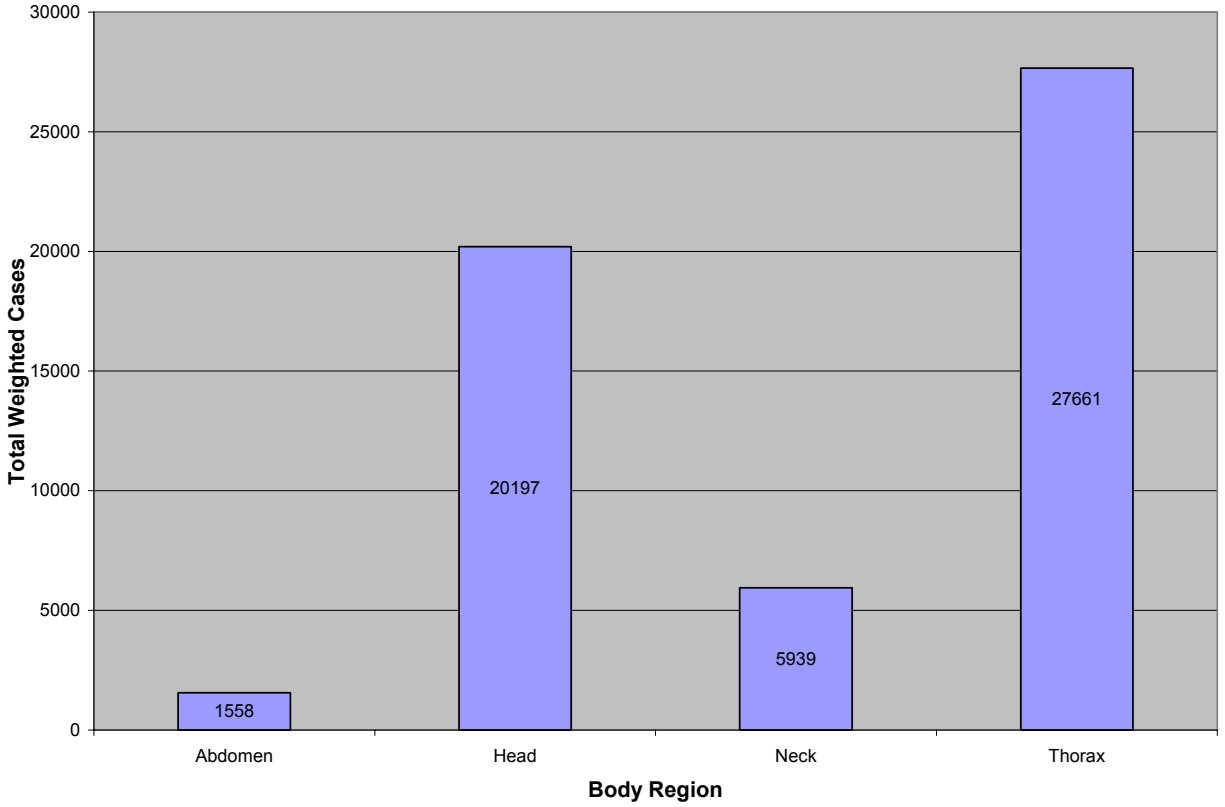

Figure 5. Total weighted cases by body region for drivers with MAIS 3+ injuries sustained in frontal crashes

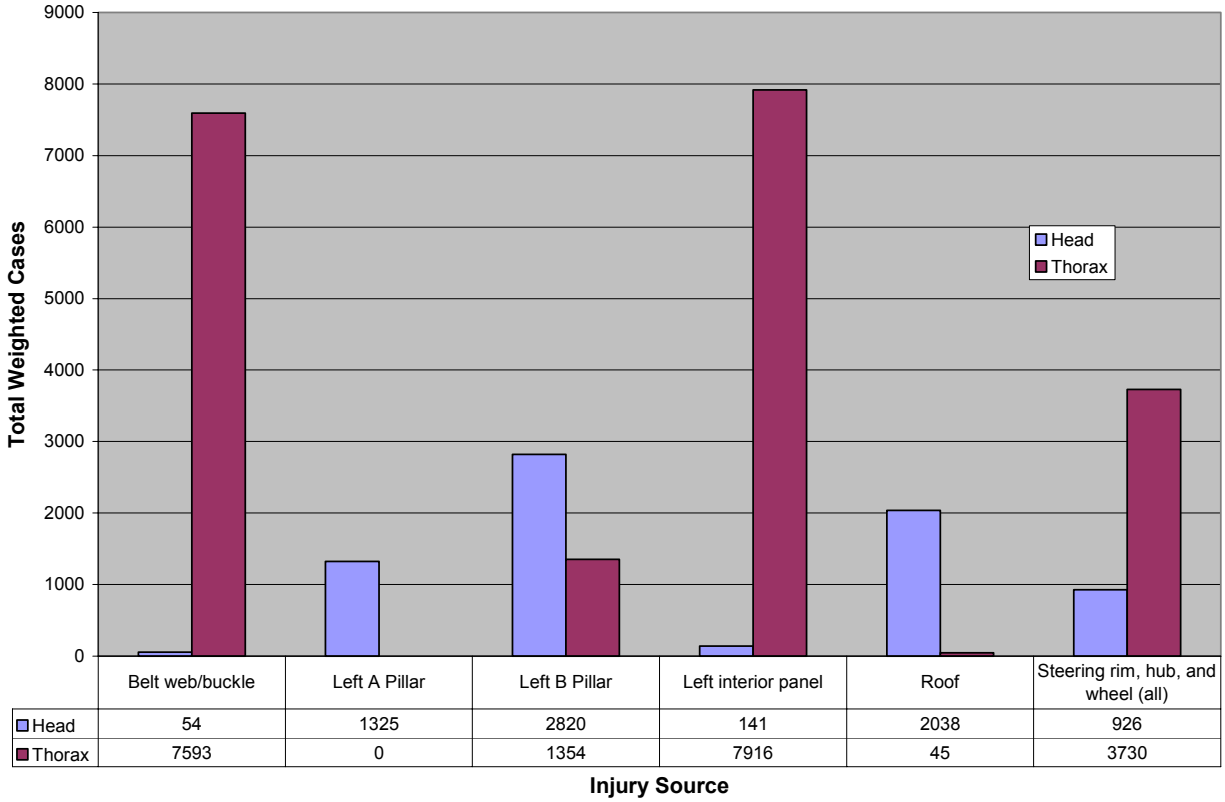

	Belt web/buckle	Left A Pillar	Left B Pillar	Left interior panel	Roof	Steering rim, hub, and wheel (all)
Head	54	1325	2820	141	2038	926
Thorax	7593	0	1354	7916	45	3730

Figure 6. Sample of Several Injury Sources for the Head and Thorax Body Regions in Frontal Crashes, Weighted Data

Table 2: Top ten head injuries for drivers with MAIS 3+ injuries sustained in frontal crashes	Total Weighted Cases
Cerebrum hematoma/hemorrhage NFS - extra axial*	1902
Cerebrum hematoma/hemorrhage intracerebral small	1817
Cerebrum subarachnoid hemorrhage	1673
Orbit fracture open/displaced/comminuted	1212
Cerebrum hematoma/hemorrhage subdural small	1048
Cerebrum diffuse axonal injury (white matter shearing)	929
Vault skull fracture comminuted	806
Cerebrum contusion single small	720
Brain stem laceration	704
Cerebellum hematoma/hemorrhage subdural NFS*	694
*Note: NFS = Not Further Specified.	

Table 3: NASS CDS parameters that will aid in the transition from the occupant to the vehicle level (injury to CDC)
All other injured body regions (regardless of injury severity) and its corresponding injury source (if multiple injuries were sustained)
All severe events resulting from the crash and its corresponding CDC, where applicable
All vehicle intrusions
Avoidance maneuver performed
Critical pre-crash event that resulted in the crash
Gender, Age, Height, and Weight
Heading angle and Other angle to describe vehicle configuration and location of the damage to the vehicle with respect to the North direction, where applicable. These two angles provide a geometric configuration of two vehicles at the point of impact. This information is used to supplement the PDOF.
Injury source
Pre-event movement which initiated the crash
Presence of alcohol or drugs
Seat back position
Seat track position
Seat belt anchorage position

Injuries in Rollovers by Crash Severity

Kennerly Digges
The National Crash Analysis Center,
The George Washington University
USA

Ana Maria Eigen
The National Highway Traffic Safety Administration
USA
Paper Number 07-0236

ABSTRACT

Earlier studies by the authors have examined factors that contribute to rollover crash severity. These factors include: (1) belt use, (2) the number of quarter-turns aggregated according to number of vehicle inversions, and (3) the damage severity from planar impacts with fixed and non-fixed objects that occur before or during the rollover. Further research indicated that rollovers with severe damage from planar impacts should be analyzed separately from other rollovers since the injury rates for these crashes is 2 to 3 times greater than equivalent rollover crashes with less severe damage.

This paper separates rollovers into two categories, based on the presence or absence of severe damage from a planar crash. The research then examines the distribution of MAIS 3+ injuries and harm by body region and contact for belted adult occupants in each rollover category. The rollover categories are further examined using the number of vehicle inversions to quantify rollover crash severity.

Based on the analysis, the magnitude of the opportunities for injury and harm reduction through safety enhancements such as air curtains and safety belts designed for rollover protection is examined.

INTRODUCTION

The NASS CDS (National Automotive Sampling System/ Crashworthiness Data System) is a sample of tow away crashes that occur on US roads each year. The sample is stratified by the severity of the crash. The sample rate for minor crashes is much lower than for severe crashes. In order to expand the stratified sample to the entire population it represents, an inflation factor is assigned to each case in the NASS CDS sample. When the data are processed using the actual number of cases investigated, the data is referred to as "unweighted". When the data are processed using the inflation factors, the results should represent the total population of vehicles and the data are referred to as "weighted".

Earlier analysis by the authors showed clearly that rollovers with 4+ quarter-turns carried a higher injury rate than rollovers with fewer quarter-turns. Prior to 1995, NASS did not code the number of quarter-turns beyond four. Beginning in 1995, the NASS coding was expanded to enumerate the number of quarter-turns up to 16. Rollover extent of damage was also measured and categorized in three severity levels – minor, moderate, and severe. Unlike the extent of damage classified via the Collision Deformation Classification, a reserved phrase and variable name in NASS CDS, this study examines total delta-V and estimated delta-V, as given for the most severe event. For planar crashes, for which a delta-V can be calculated by measurements taken at the crash scene, the numeric or total delta-V is considered. In cases where the algorithm parameters are exceeded, a qualitative or quantitative delta-V is reported as the estimated delta-V. Delta-V is a measure of crash energy transfer and deemed to form part of a composite crash severity indicator. For rollover crash events, however, the reported delta-V is a qualitative indicator of crash severity not energy transfer. It should be noted that, the algorithm fails in extreme or complex planar engagements and rollover crashes. The enumeration of up to 16 quarter-turns in NASS has provided a much more detailed characterization of the rollover. However, it has complicated the analysis because it has created smaller cells with varying amounts of data. As an artifact of sample size and cell size issues, some lower numbers of quarter turns carry higher injury rates than subsequent numbers of quarter-turns. Previous analysis has demonstrated the merit of aggregating quarter turn cells producing increasing injury risk. Owing to the complex nature of rollover crashes, it is desirable to identify the factors other than quarter-turns that contribute to injury risk.

In an earlier study, crash factors that increased the risk of MAIS 3+ injuries in rollovers were examined

[Digges 2006]. The study found that the number of times the vehicle roof faces the ground (number of vehicle inversions) was a statistically significant factor that predicted increased injury risk for single vehicle rollovers. The analysis also examined the extent of damage to the vehicle as an added severity metric for rollovers that are preceded by or interrupted by impacts with fixed and non-fixed objects. Vehicle damage was measured and categorized in three severity levels: minor, moderate, and severe. Rollovers were also coded into four classes : (1) rollover as a single event, (2) rollover as the 1st event of multiple harmful events, (3) rollover preceded by impact with a non-fixed object, and (4) rollover preceded by impact with a fixed object. It was found that the number of vehicle inversions was a good severity metric for rollovers with fixed and non-fixed object impacts so long as cases with severe damage from the object impacts were excluded. The inclusion of the rollovers with minor and moderate damage from fixed object impacts with pure rollovers permits the application of the number of vehicle inversions as a severity metric to about 80% of the rollovers with belted front seat occupants and MAIS 3+ injuries. The remaining 20% are rollovers with severe damage with fixed or non-fixed objects and the planar impact may have contributed to the injury severity. In an earlier study, new NASS codes were used to examine crash factors that increased the risk of MAIS 3+ injuries [Digges 2003]. That study used NASS CDS 1995-2001 data. The variables added in 1995 permitted a more robust examination of how planar damage and number of quarter-turns may influence the risk of injury. These rollovers may require countermeasures to protect against both the planar impact and the rollover.

The earlier study found that the number of vehicle inversions was a statistically significant factor that predicted increased injury risk for belted occupants in single vehicle rollovers and in rollovers with impacts with fixed and non-fixed objects where only minor and moderate damage occurs.

DATA QUERIES

The data set described in this paper was queried from NASS CDS, a database of NASS, years 1995 through 2005. Definitions were prepared below for: occupant selection, quarter turn (rollover) codification, crash configuration, restraint usage, ejection status, injured body region groupings, injury severity, and occupant counts versus injury counts.

Occupant Selection

As described in previous works, occupancy rates of the various vehicle platforms dictated the selection of drivers and right front passengers. It was found that the higher occupancy rates of vans and SUV's tended to bias the results when all rear seat occupants were included [Digges 2003]. Earlier work has shown that belted and unbelted occupants should not be combined when attempting to characterize rollover crash severity [Digges 2003]. In the present study, only belted occupants were considered. Occupants less than 12 years old were excluded from the study because of complications that could be introduced by the presence of a variety of supplemental restraint systems not accounted for by the OEM.

Quarter Turn Codification

In addition to the classification of quantifiable quarter turns, rollover crashes may be defined as end-over-end rollover crashes or rollover with unknown details. The end-over-end rollover crash owing to its severe nature and varying crash dynamics requires an individual severity metric and is not examined in detail. Although reported in the Table 3 for completeness, the rollover of unknown detail was excluded from the analysis since the number of quarter turns was not quantified and it could not be established whether the rollover was lateral or longitudinal.

Crash Configuration

Two types of data queries were run for the analysis. First, all applicable front seat occupants involved in single vehicle rollovers were disaggregated. In this run, all damage levels were included but impacts with fixed and non-fixed objects were excluded. Second, all remaining rollover types were disaggregated and the cases with severe planar damage were excluded. The data runs provided the distribution of crashes and injured occupants by MAIS, Fatality, and Injured Body Regions. The results are presented in the sections to follow.

Restraint Usage and Ejection Status

As reported in Digges [2003], restraint usage and ejection status were applied in this paper. In summary, restraint usage was disaggregated by restrained, unrestrained, and ineffectively restrained occupants with respect to the rollover crash exigencies. The ejection analysis was an underlying element of this research and considered in the data interpretation presented in the Discussion.

Definition of MAIS 3+F and Harm

MAIS 3+ refers to occupants who sustain injuries with classification of serious (MAIS 3), severe (MAIS 4), critical (MAIS 5), or maximum (MAIS 6). In NASS CDS, a treatment variable is coded indicating the occupant disposition pursuant to the crash. One of the possible dispositions is fatality and must be consulted in conjunction with the MAIS score to ascertain occupant outcome.

The MAIS 3+F populations were determined by separating the fatally injured from the survivors. All the fatalities were that added to the survivor data at the MAIS 6 level. The Harm was then calculated using the procedures reported by Malliaris [1982]. The Harm weighting factors were based on the costs in Appendix E of DOT HS 809 203. Both MAIS 1 and 2 injuries were excluded from the MAIS 3+ Harm calculation. AIS 3+ Harm is calculated by applying the Harm weighting factors to the most severe AIS 3+ injury for each body region that sustains a serious injury.

It should be noted that MAIS and AIS might be used interchangeably in this study. Although common NASS CDS practice indicates that the maximum abbreviated injury scale score is applied at the occupant level, this concept may be extended to indicate the maximum AIS injury per body region per occupant.

Analysis Variables

The analysis variables were created using existing NASS CDS variables and attributes. These included groupings for the total delta-V, injury source associated with the maximum injury per body region, and consideration of the sequence of the rollover with respect to the crash events.

The delta-V groupings have been used in previous publications and are based upon total delta-V, and where that is unavailable estimated delta-V. The delta-V has been categorized as minor moderate, or severe. The delta-V is related to the most severe event in the crash, with respect to vehicle damage. This is either a calculated or estimated planar delta-V or and an estimated delta-V. In the case of rollover crashes, delta-V is used very loosely and is synonymous with crash severity. This is an accepted meaning of delta-V but in the planar sense, it involves some sense of change in velocity. The estimated planar delta-V is generally associated with the researcher-assessed delta-V based upon experience. This can take on a numeric, as well as a qualitative value.

The sequence of the rollover and its severity was reported in Digges [2006]. This disaggregation considered rollover as a single event crash, otherwise called pure rollover, and multiple event crashes during which the rollover occurred subsequent to the first event, other rollover, per Table 1. The rollover type and severity inclusion was studied, as seen in Table 1. Consideration was also given to whether rollover occurred pursuant to a fixed, nonfixed contact, or mixed fixed and nonfixed contacts.

Table 1: Rollover Type and Severity Inclusion

Rollover Type	Severity (Extent of Damage)	Injury Severity
Pure Rollover	All	All
Other Rollover	Minor, Moderate	All

The injury source groupings associate occupant contacts to injuries sustained, as shown in Table 2. These groupings are reflective of gross vehicle locations and include: upper vehicle, mid vehicle, safety belt and airbag systems, ground and other vehicle contact, other contacts. The upper vehicle includes roof, headers, windows, frames, and pillars. The mid vehicle consists of side interior, dash board, and steering wheel. The safety belt and airbag systems account for any constituent of the active or passive restraint system exclusive of the knee bolster. Finally, the other grouping considers any contact not listed previously.

The injury source is assessed by comparing physical evidence found within or around the vehicle. Examples of physical evidence may take the form of body fluid residue, tissue transfer, scuffing, denting, or make up traces. The evidence is codified on vehicle diagrams indicating location of transfer. These diagrams are compared with medical records to determine reasonable matching of the evidence with recorded injuries. The injury source is synonymous with injury contact source, as referenced in Table 2, and indicates occupant contact with a vehicle or external component that is associated with an injury sustained by the occupant.

Table 2: Injury Contact Categories

Injury Contact Categories	Description
Upper Vehicle	Window Sills and above, inclusive of frame and glazing
Mid Vehicle	Instrument Panel, Interior Hardware, Steering Assembly
Safety Belt and Airbag System	Active and Passive Restraint System, inclusive of components and hardware
Ground, Vehicle Exterior, Other Vehicle	Any exterior occupant contact, generally associated with some degree of ejection
Other Contact	Any other contact not mentioned in the previous categories.

RESULTS: DATA ANALYSIS

Table 3 shows the distribution of Exposed and MAIS 3+F injuries for relevant belted population in NASS CDS 1995-2005. The relevant population is all outboard front seat occupants age 12 and older. In this table, the authors consider only the relevant belted population involved in rollover without planar impacts and the relevant belted population exposed to rollovers with minor or moderate damage from planar impacts. The raw NASS CDS contains 4,669 belted relevant occupants exposed to rollover and 701 relevant occupants with MAIS 3+ injuries. The weighted numbers are 2,180,113 exposed relevant occupants and 73,340 MAIS 3+F injured occupants.

The columns in Table 3 show the number of vehicle inversions. One quarter turn is represented by "0 Inv". Two to five quarter-turns are included in "1 Inv" and so on. The data in the first six columns of each row adds to 100%. The "% of All" column shows the percent of the total population represented by the sum of the six columns. About 33% of MAIS 3+F injuries in this population occur in single vehicle rollovers without planar impact. The remaining 67% are rollovers with planar impact and minor or moderate damage. As stated above, rollovers with planar impact and severe damage are considered a different severity class and have been excluded from this analysis. Approximately 20% of the MAIS 3+ rollover injuries to belted occupants in NASS occur in these severe damage cases.

The "M3+ Risk" row in Table 3 represents the MAIS 3+F injury rates per 100 relevant occupants exposed to the crash environment as defined by the same column. The "M3+ Risk" in the % of All column is the average risk for the population in the row.

Several observations may be made from the data. First, a substantial fraction of the MAIS 3+F injuries (72%) in single vehicle rollovers without planar impact involve crashes with more than one vehicle inversion. These account for about 33% of the MAIS 3+F injuries. In the cases of rollovers with planar impacts, only 43% of the MAIS 3+F injuries occur in crashes with more than one inversion. It should be noted that 1% of the MAIS 3+ injuries are end-over-end, and 6% have unknown numbers of inversions.

Second, the injury risk for 0 inversions is much higher for rollovers with minor and moderate planar damage than it is for pure rollovers. Earlier papers by the authors have noted that this is partially due to the vulnerability of the vehicle to a roof impact with a fixed or non-fixed object when the rollover is interrupted at one quarter-turn. A more precise benefits analysis may help separate out these cases.

Third, the injury rate for one vehicle inversion is generally higher for the crashes with planar impacts, suggesting that the planar crash may contribute to the injury. However, when examining the influence of vehicle inversion on injury rate, the differences are small in comparison.

Finally, the injury risk for end-over-end rollovers with no planar impact is extremely high. These represent a separate class of rollover severity and will not be considered further in the analysis to follow.

Table 4 shows the similar data to Table 3, but with the injuries disaggregated by body region. In Table 4, the two rollover groupings in Table 3 are combined.

The distribution of MAIS 3+ Harm by body region for the population in Table 4 is shown in Table 5. In this table, the cases with unknown number of quarter-turns and end-over-end classification have been excluded. Table 5 also compares the weighted and unweighted data. The number of unweighted cases with MAIS 3+ injuries was 661. These cases expanded to 69,758 when weighting factors were applied. The principal effect of the weighting factors is to increase the number of chest injuries in pure rollovers while decreasing the number of head injuries in rollovers with planar impacts.

Table 6 provides a further disaggregation of the Table 5 weighted data by two classes of rollover

severity. Table 7 provides the same categories, but with unweighted data.

The distributions of AIS3+ Harm by injuring contacts in rollover crashes are displayed in Table 8. The NASS codes more than 20 different contacts. These were aggregated into 5 categories- (1) Upper Vehicle, (2) Mid Vehicle, (3) Belt & Air Bag, (4) All Other Interior and (5) Ground, and Other Vehicle. The contents of each category are discussed earlier in the paper. The data in Table 8 is based AIS 3+ injuries to all body regions with known contacts. In cases where occupants had more than one AIS 3+ injury, all the injuring contacts that were associated with all injuries AIS 3 and greater were included. The Harm calculation applied the MAIS weighting factors to the equivalent level of AIS injury. There were 719 raw contacts with AIS 3+ injuries. When weighted, these expanded to 75,341. The principal effect of the weighting factors was to increase the Harm from mid vehicle contacts in pure rollovers at the expense of upper vehicle contact Harm in rollovers with planar impacts.

DISCUSSION

Tables 3 and 4 both show an increasing injury rate for increases in number of vehicle inversions. For planar impact, rollovers with minor and moderate damage, the 0 and 1 vehicle inversions carry a higher injury risk than the single vehicle rollovers. The planar impact may contribute to the injuries in some of these cases. However, the differences are small in comparison with the risk increase when 2 or more vehicle inversions occur. Earlier research found that for the selected populations of rollovers, there was a statistically significant relationship between the number of vehicle inversions and the risk of MAIS 3+ injury [Digges 2006].

Table 5 indicates that the Head Grouping has the largest fraction of AIS 3+ Harm for both weighted and unweighted data. The weighted data increases the Chest/Abdomen Harm in pure rollovers while decreasing head injuries in rollovers with planar damage. This trend continues in the Table 6 and Table 7 data. Chest/Abdominal injuries in pure rollovers with 2+ vehicle inversions are considerably more numerous in the weighted data than in the unweighted data. An examination of Table 8 shows that mid-vehicle contacts carry much higher Harm for pure rollovers in weighted data compared to unweighted data.

Tables 6 and 7 indicate that the largest opportunity for injury reduction of the belted rollover population under consideration is in multiple impacts with minor and moderate damage and with low numbers of vehicle inversions. This Rollover Grouping accounts for over 50% of the AIS 3+ Harm. The Head Injury Grouping accounts for about half of the body region Harm within this population. Another observation from these tables is that the second largest opportunity for injury reduction is in pure rollovers with 2+ vehicle inversions. The 2+ rollover severity accounts for more than half of the AIS 3+ Harm in pure rollovers. In the 2+ severity grouping, both the Head and Chest Body Regions offer large opportunities for injury reduction.

Table 8 shows the AIS 3+ Harm from injuring contacts by rollover type. Relatively small amounts of Harm are attributed to the Restraints and to 'Other' contacts. Even for belted occupants, about 10% of the Harm is associated with partial or complete ejection. Systems to reduce injuries from the combined upper interior and external contacts could conceivably address a large fraction of the Harm. An almost equally large opportunity exists in trying to reduce injuries from contacts with mid-vehicle surfaces.

CONCLUSIONS

This paper deals only with belted adult front seat occupants exposed to rollover crashes. The grouping of belted occupants in rollovers according to number of vehicle inversions offers the ability to examine opportunities for reducing injuries in crashes of different types and of different severities. This paper excluded rollovers with severe damage from impacts with fixed and non-fixed objects and end-over-end rollovers. These rollovers need special treatment to reflect their high injury risk. The remaining rollovers account for about 80% of the MAIS 3+ injuries and fatalities. The analysis and conclusions in this paper deal with this remaining population of belted occupants rollovers.

Pure rollovers without damage from other crash events account for about 40% of the Harm. Over half of this Harm occurs in rollover crashes with more than 2 vehicle inversions. The injuring contacts for pure rollovers are about equally distributed between upper and mid-vehicle locations. Each accounts for about 45% of the Harm. About 2% of the Harm is attributed to the restraint systems. About 4% is associated with ejection and 4% other contacts. The head and chest body regions are about equal in accounting for 90% of the Harm attributed to this population.

Rollovers with damage from other crash events account for about 60% of the Harm. About 86% of this Harm occurs in rollovers crashes with less than 2 vehicle inversions. Injuries to the head, face, neck, and spine account for about 65% of the Harm in this rollover category. Systems that could address contacts from the combined upper interior and the ground may offer a large opportunity for Harm reduction. Harm reduction from mid-vehicle contacts offers an opportunity of about the same magnitude – about 40% of the Harm attributed to this population.

ACKNOWLEDGEMENT

Funding for Dr. Digges' participation in this research has been provided by private parties, who have selected Dr. Kennerly Digges [and the FHWA/NHTSA National Crash Analysis Center at the George Washington University] to be an independent solicitor of and funder for research in motor vehicle safety, and to be one of the peer reviewers for the research projects and reports. Neither of the private parties have determined the allocation of funds or had any influence on the content.

REFERENCES

Digges, K., and Eigen, A., "Crash Attributes that Influence the Severity of Rollovers", Paper 231, Proceedings of the ESV Conference, May 2003.

Digges, K., and Eigen, A., "The Injury Risk from Objects Impacted Before and During Rollovers", Paper 231, Proceedings of the IRCOBI Conference, September 2006.

NHTSA, "1995-1997 National Automotive Sampling System/Crashworthiness Data System" NHTSA, DOT HS 809 203, p.152, February 2001

Digges, K., and Eigen, A., "Classification of Rollover According to Crash Severity," 50th Proceedings of the Association for the Advancement of Automotive Medicine", pp. 141-154, October 2006.

Malliaris, A.C., Hitchcock R. and Hedlund, J., search for priorities in crash protection, Proceedings of Society of Automotive Engineers SAE SP-513, p.1–33, (1982).

The opinions, findings, and conclusions expressed in this publication are those of the author and not necessarily those of the Department of Transportation or the National Highway Traffic Safety Administration. The United States Government assumes no liability for its contents or use thereof.

Table 3. Distributions of Exposed Occupants, Harm, MAIS 3+F and MAIS 3+F Injury Risk for Rollover Populations

Single Vehicle Rollover, No Planar Impact - All Damage Severity							
Population	0 Vehicle Inversion	1 Vehicle Inversion	2 Vehicle Inversion	3+ Vehicle Inversion	END OVER END	Unknown	% of All
MAIS 2+Harm	1%	36%	41%	13%	1%	9%	28%
MAIS 3+ Harm	1%	33%	45%	11%	1%	9%	29%
MAIS 3+F	0.2%	23%	66%	6%	2%	3%	33%
Exposed	8%	72%	14%	1%	0.1%	5%	27%
M3+ Risk	0.11	1.01	11.30	14.35	48.74	3.35	2.71
Rollover with Planar Impact - Minor and Moderate Damage							
Population	0 Vehicle Inversion	1 Vehicle Inversion	2 Vehicle Inversion	3+ Vehicle Inversion	END OVER END	Unknown	% of All
MAIS 2+Harm	14%	50%	22%	7%	1%	6%	72%
MAIS 3+ Harm	14%	48%	24%	7%	1%	6%	71%
MAIS 3+F	8%	48%	32%	5%	2%	6%	67%
Exposed	18%	67%	11%	1%	0.2%	3%	73%
M3+ Risk	1.29	2.02	7.98	14.51	18.38	5.78	2.83
Rollover with No Planar Impact + With Planar Impact - Minor and Moderate Damage							
Population	0 Vehicle Inversion	1 Vehicle Inversion	2 Vehicle Inversion	3+ Vehicle Inversion	END OVER END	Unknown	% of All
MAIS 2+Harm	11%	46%	27%	8%	1%	7%	100%
MAIS 3+ Harm	10%	44%	30%	8%	1%	7%	100%
MAIS 3+F	6%	41%	40%	6%	2%	6%	100%
Exposed	15%	68%	12%	1%	0.2%	3%	100%
M3+ Risk	1.09	1.68	9.19	14.44	23.50	4.72	2.79
Note: Rows may not sum to exactly 100 percent owing to rounding.							

Table 4. Distributions of Harm, MAIS 3+F and MAIS 3+F Injury Risk by Injured Body Region with Rollovers with Severe Damage from Planar Impacts and End-over-end Rollovers Excluded

Head, Face, Neck & Spine Injuries						
Population	0 Vehicle Inversion	1 Vehicle Inversion	2 Vehicle Inversion	3+ Vehicle Inversion	Unknown	Ave Risk
MAIS 2+Harm	8%	50%	23%	12%	6%	
MAIS 3+ Harm	6%	48%	26%	13%	7%	
MAIS 3+F	6%	54%	30%	3%	8%	
Exposed	15%	68%	12%	1%	3%	
M3+ Risk	0.31	0.66	1.78	5.44	1.61	0.83
Chest & Abdomen Injuries						
Population	0 Vehicle Inversion	1 Vehicle Inversion	2 Vehicle Inversion	3+ Vehicle Inversion	Unknown	Ave Risk
MAIS 2+Harm	13%	43%	28%	8%	6%	
MAIS 3+ Harm	13%	40%	30%	9%	7%	
MAIS 3+F	6%	35%	43%	5%	7%	
Exposed	15%	68%	12%	1%	3%	
M3+ Risk	0.41	0.48	3.36	4.79	1.91	0.94
Pelvic, Upper & Lower Extremity Injuries						
Population	0 Vehicle Inversion	1 Vehicle Inversion	2 Vehicle Inversion	3+ Vehicle Inversion	Unknown	Ave Risk
MAIS 2+Harm	20%	50%	18%	7%	4%	
MAIS 3+ Harm	19%	48%	19%	8%	4%	
MAIS 3+F	10%	65%	16%	5%	3%	
Exposed	15%	68%	12%	1%	3%	
M3+ Risk	0.63	0.65	1.01	3.96	0.79	0.74

Note: Rows may not sum to exactly 100 percent owing to rounding.

Table 5. Percentage of AIS 3+ Harm by Body Region in All Pure Rollovers and Rollovers with Minor or Moderate Planar Impact Damage by Rollover Type, Weighted and Unweighted Data; End-over-end Rollovers Excluded

Weighted Data			
Body Region	All Pure Roll	Min/Mod Damage	All
Head, Neck, Face, Spine	19%	27%	47%
Thorax, Abdomen	17%	19%	35%
Extremities with Pelvis	4%	14%	18%
Total	40%	60%	100%
Unweighted Data			
Body Region	All Pure Roll	Min/Mod Damage	All
Head, Neck, Face, Spine	19%	36%	55%
Thorax, Abdomen	8%	22%	31%
Extremities with Pelvis	3%	11%	14%
Total	31%	69%	100%
Note: Rows and columns may not sum to exactly 100 percent owing to rounding.			

Table 6. Percentage of AIS 3+ Harm by Body Region in All Pure Rollovers and Rollovers with Minor or Moderate Planar Impact Damage by Rollover Type and Severity, Weighted Data; End-over-end Rollovers Excluded

0 & 1 Inversions - Weighted Data			
Body Region	All Pure Roll	Min/Mod Damage	All
Head, Neck, Face, Spine	10.7%	23.3%	34.9%
Thorax, Abdomen	2.9%	15.3%	18.1%
Extremities with Pelvis	1.7%	12.4%	14.1%
Total	15.2%	51.9%	67.1%
2 & 3+ Inversions - Weighted Data			
Body Region	All Pure Roll	Min/Mod Damage	All
Head, Neck, Face, Spine	8.6%	3.1%	11.7%
Thorax, Abdomen	14.0%	3.3%	17.3%
Extremities with Pelvis	1.8%	2.0%	3.8%
Total	24.4%	8.3%	32.8%
Note: Rows and columns may not sum to exactly 100 percent owing to rounding.			

Table 7. Percentage of AIS 3+ Harm by Body Region in All Pure Rollovers and Rollovers with Minor or Moderate Planar Impact Damage by Rollover Type and Severity, Unweighted Data; End-over-end Rollovers Excluded

0 & 1 Inversions - Unweighted Data			
Body Region	All Pure Roll	Min/Mod Damage	All
Head, Neck, Face, Spine	11.2%	32.7%	43.9%
Thorax, Abdomen	2.5%	18.5%	21.1%
Extremities with Pelvis	1.2%	9.1%	10.3%
Total	14.9%	60.3%	75.3%
2 & 3+ Inversions - Unweighted Data			
Body Region	All Pure Roll	Min/Mod Damage	All
Head, Neck, Face, Spine	7.8%	3.4%	11.2%
Thorax, Abdomen	5.6%	3.9%	9.6%
Extremities with Pelvis	2.2%	1.6%	3.8%
Total	15.6%	8.9%	24.6%
Note: Rows and columns may not sum to exactly 100 percent owing to rounding.			

Table 8. Percentage of AIS 3+ Harm by Injuring Contact in All Pure Rollovers and Rollovers with Minor or Moderate Planar Impact Damage by Rollover Type, Weighted and Unweighted Data; End-over-end Rollovers Excluded

Weighted Data			
Injuring Contact	All Pure Roll	Min/Mod Damage	All
Upper Vehicle	17%	19%	36%
Mid Vehicle	18%	25%	44%
Other	2%	5%	8%
Restraint, Airbag System	1%	4%	5%
Ground, Other Vehicle	2%	6%	9%
Total	40%	60%	100%
Unweighted Data			
Injuring Contact	All Pure Roll	Min/Mod Damage	All
Upper Vehicle	15%	28%	43%
Mid Vehicle	9%	23%	32%
Other	3%	8%	11%
Restraint, Airbag System	1%	3%	4%
Ground, Other Vehicle	3%	7%	10%
Total	32%	68%	100%
Note: Rows and columns may not sum to exactly 100 percent owing to rounding.			

THE APPLICATION OF CAE IN THE DEVELOPMENT OF AIRBAG RESTRAINT SYSTEM PERFORMANCE FOR A CERTAIN VEHICLE

Jang-Mook Lim
Hyung-Wook Park
Seok-Ho Hong
Bum-jin Kim
Kwan-Hum Park
Hyundai Kia Motors
Korea
Paper Number 07-0265

ABSTRACT

If vehicle manufacturers have an airbag sensing algorithm, they could use this algorithm to find optimal airbag sensor locations for the better airbag sensing performance, to get an optimal firing logic for their certain vehicle, and to get the overall good performance by considering both the vehicle structure and the airbag sensing algorithm. One study in this paper shows how to find the optimal locations of front impact sensors (FIS) using in-house airbag sensing algorithm, crash test data and CAE simulation models. For this purpose, three steps are fulfilled as follows. In the first step, the acceleration sensor signals of the crash tests are collected at several positions of the vehicle. In the second step, the full car crash simulations are made and correlated to the crash test data. Using these well defined crash vehicle models and crash test data, the acceleration signals of the FIS candidate locations, such as radiator, front side members, and bumper back beam, are obtained. In the final step, using these acceleration signals and airbag algorithm, the airbag sensing performance are evaluated, and the final candidate positions are selected. The robust FIS positions are selected effectively for various crash conditions and velocities via this approach.

The other study shows how to determine an airbag deployment logic using CAE. From simulation models which have several crash speeds, several crash modes, and several restraint conditions, the airbag deployment logic can be determined to minimize the occupant injury level. In addition, the roles and limitations of CAE simulations are demonstrated in the airbag algorithm calibration process and the airbag restraint system development.

INTRODUCTION

Out of several requirements for airbag sensing performance, it is very important to find the optimal locations of ACU (Airbag Control Unit) and FIS in the early phase of vehicle development. Besides the accelerometers in ACU near vehicle front tunnel, the FIS has very important role, too.

The current vehicle's FIS have various locations such as front side member, radiator upper or lower, bumper back beam and so on; therefore, further survey and research to find optimal sensor positions for airbag sensing must be carried out now and after.

The purpose of this paper is to find the optimal location of FIS in order to prevent airbag malfunctioning from inaccuracy of airbag sensibility under various crash modes and velocities. From this optimization point of view, airbag sensing algorithm and calibration technique were developed and various vehicle crash test data with various crash modes and speeds, and airbag sensing crash simulation data were handled to find our goal for sensor locations.

VEHICLE CRASH TEST DATA ANALYSIS

Requirements for Frontal Crash Airbag Sensing

The so-called advanced airbag system to meet the requirements of FMVSS208 should be able to discriminate crash severity with the help of frontal impact sensor(s) under multiple crash modes and impact speeds. In general, crash signal from FIS should survive at least up to 15ms for the high speed frontal impact and until over 40ms for the offset crash. That sensor survival time could be the necessities against the sensor damage and wiring cutting.

The peak of FIS signal must be larger and earlier than that of ACU. And for the ACU, the signal of lower crash severe modes must not be more than that of higher crash severe modes to prevent firing the airbag in case of Must Not Fire condition, and also to prohibit firing the airbag in case of Must Fire condition, on the contrary.

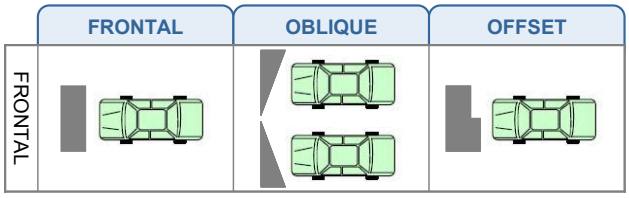

Fig.1 Crash Modes (Frontal, Oblique and Offset)

Crash Test Matrix and Test Conditions

Table.1 shows crash test matrix which has various crash modes and crash speeds for this project.

No.	Speed	Crash Mode	Purpose
1	Low	Frontal	Threshold
3	Low	Frontal	Threshold
2	Low	Frontal	Threshold
4	Low	Frontal	Threshold
6	Mid	Frontal	Threshold/Regulation
5	Mid (25mph)	Frontal	Threshold/Regulation
9	Mid (20mph)	Oblique	Regulation
7	Mid (25mph)	Offset	Regulation
11	High (35mph)	Frontal	Regulation
10	Mid (25mph)	Oblique	Regulation
8	High (40mph)	Offset	NCAP
12	Mid	Others	Due Care
13	Mid	Others	Due Care

Table.1 Crash Test Matrix

To minimize test numbers and costs, indispensable test items were selected from the past vehicle development test results by adjusting test speeds and distributing the number of tests, and using the past crash test data.

FIS Location Candidates

After surveying the FIS locations from many vehicle platforms in the real field, 3 points at the radiator support upper member (left, center, right), 3 points at the radiator support lower member (left, center, right), 3 points at the bumper back beam (left, center, right), 2 points at the front side inner member (left, right), and 2 points at the front side outer member (left, right) were selected and classified into 4 categories and 13 points per crash test. Fig.2 shows one of the FIS location candidates (radiator support upper member).

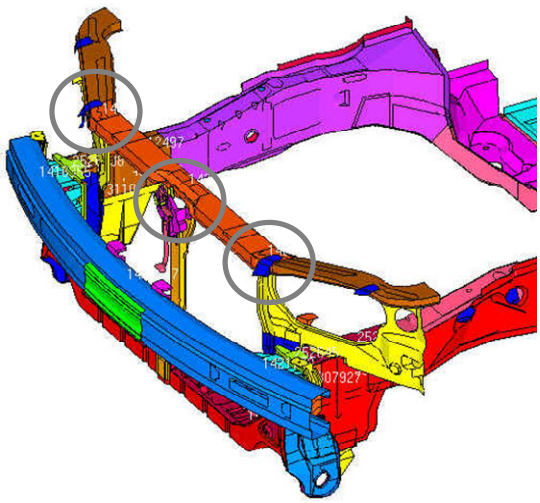

Fig.2 FIS Candidates - RAD SUPT UPR

Validity Analysis of Crash Test Data

The numbers in Table.2 are signal failure number according to crash modes, crash speeds and FIS location candidates including left, center and right positions. Especially failure rate in central positions of radiator support lower panel and bumper back beam plate is higher than other positions, because those positions are the direct crash deformation area. And the rate of the front inner and outer side member is relatively higher than radiator support panels and bumper back beam.

Mode	Speed	RAD SUPT UPR	RAD SUPT LWR	Bumper Back Beam	FR S/MBR INR	FR S/MBR OTR
Frontal	Low	-	-	-	-	-
	Low	-	1	2	-	-
	Low	1	1	4	3	4
	Low	2	1	5	3	4
	Mid	2	3	3	1	-
	Mid (25mph)	1	2	2	-	-
	High (35mph)	4	6	3	2	3
Offset	Mid (25mph)	-	1	1	-	1
	High (40mph)	-	3	-	1	1
Oblique	Mid (20mph)	-	1	-	-	-
	Mid (25mph)	-	-	-	-	-
Others	Mid	-	1	1	-	1
	Mid	-	1	1	-	-
Sum	Failure Rate	10/67	21/67	22/67	10/42	14/42

Table.2 Failure Rate according to Crash Modes and Crash Speeds at FIS Candidates

From a validity view with FIS signal observation, the failure numbers of frontal crash are proportional to the crash speed in the nature of thing. But because most of failure time is fortunately beyond the RTTF (Required Time To Fire) (Fig.3), it almost doesn't matter to airbag sensing performance of crash discrimination. And other crash modes such as oblique, offset etc. have lower failure rates than frontal impact.

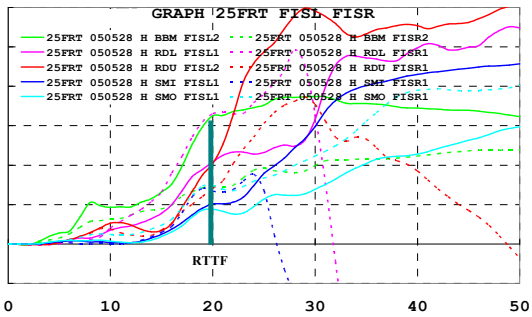

(a) Mid Frontal FIS Signal Failure

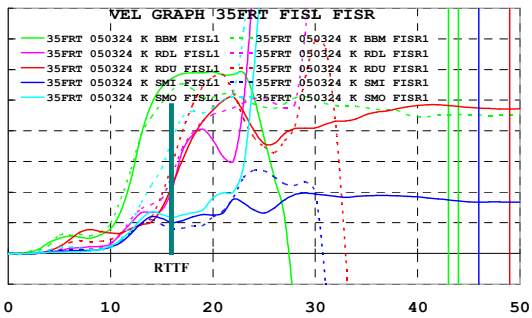

(b) High Frontal FIS Signal Failure

Fig.3 FIS Signal Failure Time Analysis

Threshold Analysis (Stage 1 and Stage 2)

Table.3 and Fig.4 show the discrimination results of threshold stage1 with the crash test data including low speed frontal crash test modes, middle offset and middle oblique crash tests, and other crash modes. Where, 'possible' means that it is possible to discriminate the FIS signals according to the impact speeds, and 'mixed' means that the FIS signals are mixed one another, and 'reverse' literally means that the signals are reversed regardless of crash severity.

		Low Frontal Vs. Mid(25mph) Offset	Low Frontal Vs. Mid(20mph) Oblique	Low Frontal Vs. Other modes
RAD SUPT UPPER	FIS-L/R	Possible	Possible	Possible (Partly)
	FIS-C	Mixed	Mixed	Mixed
RAD SUPT LOWER	FIS-L/R	Possible	Possible	Possible (Partly)
	FIS-C	Offset Fail	Oblique Fail	Mixed
BACK BEAM	FIS-L/R	Possible	Possible	Possible
	FIS-C	Reverse	Reverse	Mixed
FR S/MBR INNER	FIS-L/R	Offset Fail	Possible	Reverse
FR S/MBR OUTER	FIS-L/R	Offset Fail	Possible	Mixed

Table.3 Threshold #1 Discrimination Results

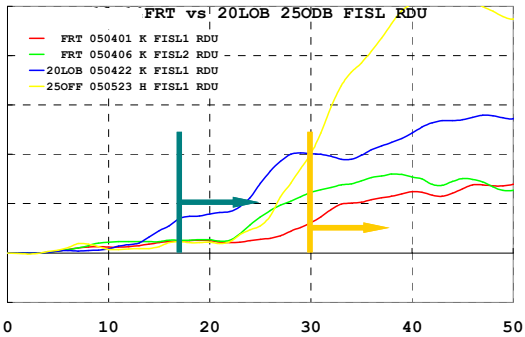

(a) FIS-LH @ RAD UPR

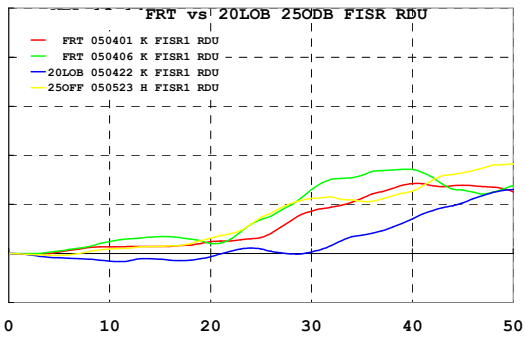

(b) FIS-RH @ RAD UPR

Fig.4 FIS Signal Comparison between Low Frontal and Mid Oblique/Offset

It is possible to classify FIS signals according to crash severity in the offset, oblique and other crash mode using crash test data of FIS-LH and RH at the radiator support upper member, the radiator lower member and bumper back beam. On the other side, it is difficult to divide crash data because of the FIS signal failure in the offset and oblique crash modes at the front side member which is the most general FIS locations, and also difficult to stand in line reversed crash test data according to crash severity. The crash signals from central FIS position can't be arranged as crash severity throughout the crash data set.

Finally, bumper back beam plate is the most likely to discriminate in view of discrimination time, and radiator support lower member, radiator support upper member follows after that position

Table.4 and Fig.5 show the discrimination results of threshold stage2 with the crash test data including low speed frontal crash test modes, high offset and middle oblique crash test modes, and other crash mode.

		Low Frontal Vs. High(40mph) Offset	Low Frontal Vs. Mid(25mph) Oblique	Low Frontal Vs. Other mode
RAD SUPT UPPER	FIS-L/R	Possible	Possible	Possible
	FIS-C	Mixed	Mixed	Fail
RAD SUPT LOWER	FIS-L/R	Possible	Mixed	Reverse
	FIS-C	Mixed	Mixed	Mixed
BACK BEAM	FIS-L/R	Possible	Possible	Mixed
	FIS-C	Mixed	Mixed	Mixed
FR S/MBR INNER	FIS-L/R	Frontal Fail	Frontal Fail	Frontal Fail
FR S/MBR OUTER	FIS-L/R	Frontal Fail	Frontal Fail	Frontal Fail

Table.4 Threshold #2 Discrimination Results

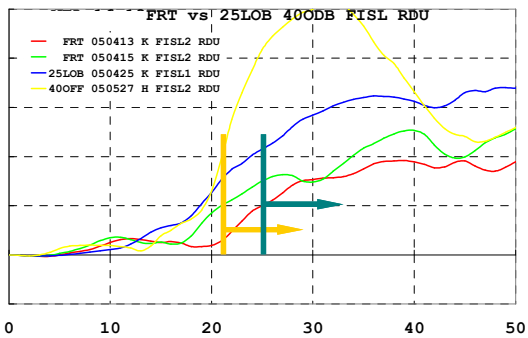

(a) FIS-LH @ RAD UPR

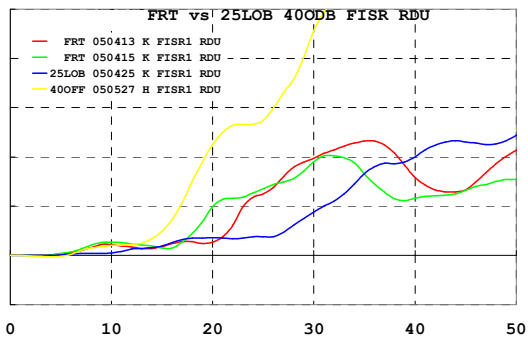

(b) FIS-RH @ RAD UPR

Fig.5 FIS Signal Comparison between Low Frontal and Mid Oblique/High Offset

It is possible to divide FIS signals according to crash severity in the offset, oblique and other crash mode using crash test data of FIS-LH and RH at the radiator support upper member, and also possible to classify signals only in the offset mode using FIS crash data at the radiator support lower member, but impossible to discriminate in the oblique and other crash mode at that position. At the bumper back beam, it is possible to classify in the offset and oblique mode with FIS-LH and RH data. At the front side member, it is impossible to analyze the results because of the FIS signal failure of low speed frontal cash modes. Crash signals from central FIS position also have difficulties in arranging as crash severity from whole crash data set.

Parametric Study and Discussion

First, the evaluation results whether the FIS signal amplitude from various crash speeds is proportional to crash severity or not at the same FIS locations, are in Table.5. From the table, FIS signal discrimination performance from FIS-LH and RH is directly proportional to crash severity at the radiator support member locations (Fig.6), but FIS-CTR is not. Exceptionally, at the bumper back beam, whole FIS candidates have good proportionality.

At the front side member, the FIS signal of low crash speed is bigger than that of high speed in reverse at some locations.

	FIS-LH	FIS-RH	FIS-CTR
RAD SUPT UPPER	Proportional	Proportional	Mixed
RAD SUPT LOWER	Proportional	Proportional	Mixed
BACK BEAM	Proportional	Proportional	Proportional
FR S/MBR INNER	Reversed	Proportional	
FR S/MBR OUTER	Reversed	Proportional	

Table.5 FIS Signals according to crash speed at the same FIS locations

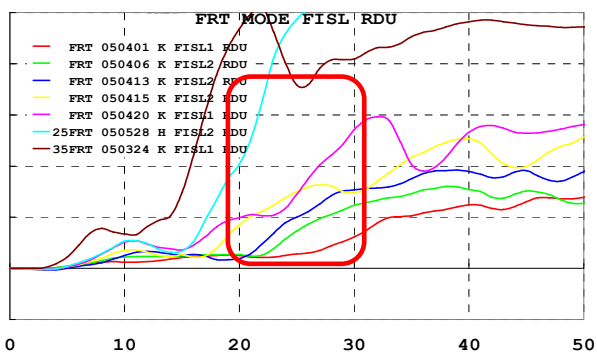

(a) FIS-LH Signals @ RAD UPR

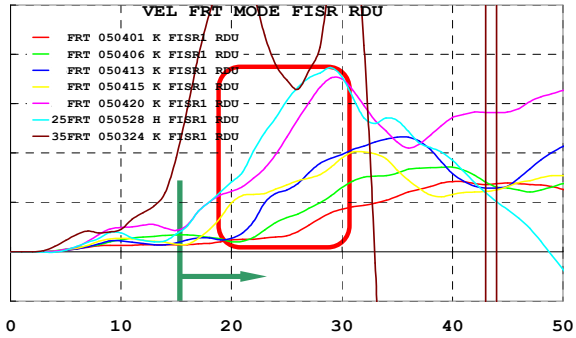

(b) FIS-RH Signals @ RAD UPR

Fig.6 FIS Signals of Frontal Crash Mode According to Impact Velocities @ RAD UPR

Signal amplitude from various locations is in good order at the same cash speed as follows: bumper back beam, radiator support upper and lower member, and front side inner and outer member.

It is noted that after reviewing the comparison results of FIS data analysis and parametric study, the radiator support upper member is the preferred location of FIS mounting.

CALIBRATOIN RESULTS OF FIS CANDIDATES

Calibration Data Set & Test Conditions

Airbag calibration controls the crash performance by decision of airbag firing at a proper time, so calibration results from whole the candidate locations, should be compared and analyzed to find the optimal positions.

Table.6 shows the test set and conditions for this project including 14 vehicle crash tests. And though not listed in Table.6, the other 94 rough road and misuse tests (25 constant road tests, 22 obstacle tests and 47 static tests) are also included in the calibration data set.

		Speed	Mode	Date	Purpose	Remark
Test Site 1	1	Low	Frontal	050401	THRESHOLD	
	2	Low	Frontal	050406	THRESHOLD	
	3	Low	Frontal	050413	THRESHOLD	S/MBR FISL DATA FAIL (S/MBR FISR)
	4	Low	Frontal	050415	THRESHOLD	S/MBR FISL DATA FAIL (S/MBR FISR)
	5	Mid	Frontal	050420	THRESHOLD / Regulation	
	6	High (35mph)	Frontal	050324	Regulation	
	7	Mid (20mph)	Oblique	050422	Regulation	
	8	Mid (25mph)	Oblique	050425	Regulation	
	9	Low	Frontal	030307	THRESHOLD	050401 Frontal FIS DATA
Test Site 2	10	Mid (25mph)	Frontal	050528	THRESHOLD / Regulation	
	11	Mid	Others	050526	DUE CARE	
	12	Mid	Others	050527	DUE CARE	
	13	Mid (25mph)	Offset	050523	Regulation	S/MBR FISL DATA FAIL
	14	High (40mph)	Offset	050527	NCAP	

Table.6 Calibration Data Set & Test Conditions

Calibration Results at Various Locations

(1) Bumper Back Beam

Over 80% (59 over 70, No.3) probability of No

Trigger exists at low speed frontal crash mode, which must be triggered into stage1 condition. And about 40% (42 over 70, No.5) probability of stage2 exists at another low speed frontal crash mode. And at the other modes such as mid speed oblique, mid speed offset, the calibration results couldn't satisfy the requirements. (Table.7)

Investigation of the misuse test margin, O17AS, O20AS and other 3 items have a margin of No Trigger less than 200%.

	SPEED/MODE	INFLATOR OUTPUT			REQ.	TTF's			RTTF
		NT	S1	S2		MIN	NOM	MAX	
1	Low Frontal	70	0	0	NT				
2	Low Frontal	64	6	0	GZ				
3	Low Frontal	59	11	0	S1				
4	Low Frontal	0	70	0	S1				
5	Low Frontal	0	42	28	S1				
6	Mid Others	0	70	0	S1				
7	Mid Oblique	0	16	54	S1				
8	Mid Frontal	0	0	70	S2				
9	Mid Frontal	0	0	70	S2				
10	Mid Oblique	0	0	70	S2				
11	Mid Offset	0	56	14	S1				
12	Mid Others	0	17	53	S2	Max. Delay : 13ms			
13	High Frontal	0	0	70	S2				
14	High Offset	0	0	70	S2				

	TEST	MARGIN
1	C09AS	185%
2	C11AS	180%
3	C15AS	190%
4	O08AS	180%
5	O17AS	125%
6	O20AS	130%

Table.7 Calibration @ Bumper Back Beam

(2) Radiator Lower Support Member

Table.8 shows that the calibration results can't fulfill the requirements at low speed frontal crash, mid oblique, mid offset and other conditions, and O17AS, O18AS, O20AS and the others at misuse tests, also can't meet the requirements.

	SPEED/MODE	INFLATOR OUTPUT			REQ.	TTF's			RTTF
		NT	S1	S2		MIN	NOM	MAX	
1	Low Frontal	70	0	0	NT				
2	Low Frontal	70	0	0	GZ				
3	Low Frontal	0	70	0	S1				
4	Low Frontal	0	70	0	S1				
5	Low Frontal	0	52	18	S1				
6	Mid Others	0	70	0	S1				
7	Mid Oblique	0	16	54	S1				
8	Mid Frontal	0	0	70	S2				
9	Mid Frontal	0	0	70	S2				
10	Mid Oblique	0	0	70	S2				
11	Mid Offset	0	56	14	S1				
12	Mid Others	0	17	53	S2	Max. Delay : 13ms			
13	High Frontal	0	0	70	S2				
14	High Offset	0	0	70	S2				

	TEST	MARGIN
1	C09AS	185%
2	C11AS	180%
3	C15AS	190%
4	O08AS	180%
5	O17AS	125%
6	O18AS	130%
7	O20AS	130%

Table.8 Calibration @ RAD SUPT LWR

(3) Radiator Upper Support Member

The calibration results at radiator upper support member can't satisfy the requirements at low speed frontal crash, mid oblique, mid offset and other conditions like the proceeding locations, and O17AS, O20AS, and so on at misuse tests, also can't meet the requirements. (Table.9)

	SPEED/MODE	INFLATOR OUTPUT			REQ.	TTF's			RTTF
		NT	S1	S2		MIN	NOM	MAX	
1	Low Frontal	70	0	0	NT				
2	Low Frontal	59	11	0	GZ				
3	Low Frontal	0	70	0	S1				
4	Low Frontal	0	70	0	S1				
5	Low Frontal	0	52	18	S1				
6	Mid Others	0	70	0	S1				
7	Mid Oblique	0	16	54	S1				
8	Mid Frontal	0	0	70	S2				
9	Mid Frontal	0	0	70	S2				
10	Mid Oblique	0	0	70	S2				
11	Mid Offset	0	52	18	S1				
12	Mid Others	0	16	54	S2	Max. Delay : 13ms			
13	High Frontal	0	0	70	S2				
14	High Offset	0	0	70	S2				

	TEST	MARGIN
1	C09AS	190%
2	C11AS	180%
3	C15AS	190%
4	O08AS	180%
5	O17AS	125%
6	O20AS	130%

Table.9 Calibration @ RAD SUPT UPR

(4) Front Side Inner Member

Many FIS crash signals are failed at low speed frontal crash test, and so the calibration was performed with other position signal from some other crash modes. As a result, at somewhat more crash types and speeds than other locations, couldn't meet the requirements especially mid speed offset crash mode.

	SPEED/MODE	INFLATOR OUTPUT			REQ.	TTF's			RTTF
		NT	S1	S2		MIN	NOM	MAX	
1	Low Frontal	70	0	0	NT				
2	Low Frontal	70	0	0	GZ				
3	Low Frontal	0	70	0	S1				
4	Low Frontal	0	70	0	S1				
5	Low Frontal	0	47	23	S1				
6	Mid Others	65	5	0	S1	No Trigger and Delay			
7	Mid Oblique	0	16	54	S1				
8	Mid Frontal	0	0	70	S2				
9	Mid Frontal	0	0	70	S2				
10	Mid Oblique	0	0	70	S2				
11	Mid Offset	0	56	14	S1				
12	Mid Others	0	17	53	S2	Max. Delay : 13ms			
13	High Frontal	0	0	70	S2				
14	High Offset	0	0	70	S2				

	TEST	MARGIN
1	C09AS	185%
2	C11AS	180%
3	C15AS	190%
4	O08AS	180%
5	O17AS	125%
6	O20AS	130%

Table.10 Calibration @ FR S/MBR INR

Discussion of Calibration Results

To summarize and compare the calibration results objectively according to FIS location candidates by numerical value, weighting factors are enforced into each crash mode. The weighting values vary from 1 to 5 as the importance of crash mode, requirement margin of crash and misuse test and so on as shown at Table.11

	ITEM	WEIGHT	BACK BEAM	POINT	RAD. LOWER	POINT	RAD. UPPER	POINT	S/MBR INNER	POINT
	Low Frontal Margin	5	1.48	5	1.48	5	1.48	5	1.59	5
	Low Frontal Margin	5	1.38	5	1.38	5	1.37	5	1.38	5
VIOLATED ITEMS	Low Frontal	3	40%	1	25.7%	3	25.7%	3	32.9%	2
VIOLATED ITEMS	Mid Others	2	0%	5	0%	5	0%	5	91.4%	0
VIOLATED ITEMS	Mid Oblique Margin	3	77.1%	0	77.1%	0	77.1%	0	77.1%	0
VIOLATED ITEMS	Mid Offset Margin	4	20.0%	3	20%	3	25.7%	3	20.0%	3
VIOLATED ITEMS	Mid Others	2	24.3%	3	24.3%	3	22.9%	3	24.3%	3
VIOLATED ITEMS	Mid Others	1	84.3%	0	84.3%	0	85.7%	0	84.3%	0
	∑ W X POINT	-	81		87		87		74	
MISUSE MARGIN	C09AS	4	185%	4	185%	4	190%	4	185%	4
MISUSE MARGIN	C11AS	4	180%	4	180%	4	180%	4	180%	4
MISUSE MARGIN	C15AS	4	190%	4	190%	4	190%	4	190%	4
MISUSE MARGIN	O08AS	4	180%	4	180%	4	180%	4	180%	4
MISUSE MARGIN	O17AS	4	125%	2	125%	2	125%	2	125%	2
MISUSE MARGIN	O18AS	4	200%	5	130%	3	200%	5	200%	5
MISUSE MARGIN	O20AS	4	130%	2	130%	2	130%	2	130%	2
	∑ W X POINT	-	100		92		100		100	

Table.11 Summary of Calibration Results

The summary of calibration results explain that the radiator support upper and lower member are the best location for FIS mounting among candidates after investigation of airbag sensing crash test data, and that the locations except only the radiator support lower member get the same marks for the misuse test. In conclusion the radiator support upper member is proved again to be the better FIS candidate after considering all the calibration results.

OPTIMIZATION OF FRONTAL CRASH SENSING PERFORMANCE BY FIS SIMULATION PULSES

Robust Design Concept with Taguchi-Method

To prevent the reversal phenomenon of crash severity between frontal and offset crash pulses, the first peak of FIS signal from low speed frontal crash is defined as one variable, which has the smaller-the-better characteristics. On the other hand, the first peak of FIS signal from mid and high speed offset crash is defined as another variable, which has the larger-the-better characteristics.

After all, the smaller frontal FIS crash pulse and the larger offset FIS crash pulse are preferred, and which have an effect on the improvement of crash severity discrimination. On this method, control factors which have the highest signal to noise ratio are to be determined.

Selection of Control Factor and Noise Factor

For the optimization of FIS sensing performance, control factors with high priority are the number of FIS, position of FIS and the number of FIS mounting in relation to FIS, and other control factors are the material types and thickness of FEM (Front-End-Module). As shown in Table.12, all the control factors except the number of FIS have 3 control levels, and the umber of FIS has 2 levels.

	Design Variable	Level 1	Level 2	Level 3
A	Number of FIS	One	Two	-
B	Position of FIS	1	2	3
C	Number of FIS Mounting	1 pt	2 pt	3 pt
D	Material Type of FEM	All Plastic	All Steel	Hybrid
E	FEM Thickness	0.6mm	0.9mm	1.2mm

Table.12 Level of Design Variables

Table of orthogonal arrays for Taguchi method in this study are L_{18} (2^1X3^4), and the noise factors are like these: the distribution of vehicle weight which is a very important factor for frontal crash test, and that of stiffness and strength of bumper back beam, front side member which are the main parts for vehicle crashworthiness. The noise levels are ±100kg of vehicle weight distribution and ±10% stiffness and strength. The strategies of noise factor are composed of N1 which is toward improving FIS sensing performance and N2 in reverse.

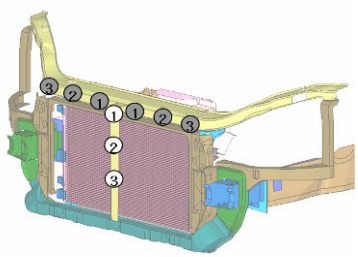

Fig.7 FIS Position According to the Level of Design

Variable

Crash Simulation of Orthogonal Arrays

Reduced crash simulation model was formulated to reduce the simulation time and cost as shown in Fig.8

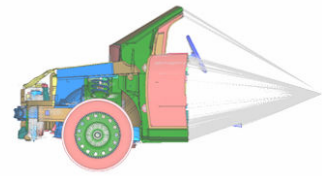

Fig.8 Reduced Crash Simulation Model

With reduced crash model, CPU time was reduced by 41% compared with full vehicle model in case of high speed offset crash simulation. Frontal and offset crash simulation results according to the impact velocities and noise factors represented in the table of orthogonal arrays are listed in Table.12. In general, the signal to noise ratio from radiator support upper panel is relatively higher than other positions.

No	A	B	C	D	E	Low Frontal1		Mid Offset		S/N Ratio
	1	2	3	4	5	N1	N2	N1	N2	
1	1	1	1	1	1	1195.0	1220.0	533.0	554.0	-6.9
2	1	1	2	2	2	1147.0	1119.0	217.0	193.0	-14.9
3	1	1	3	3	3	1196.0	1178.0	504.0	504.0	-7.4
4	1	2	1	1	2	1556.0	1543.0	441.0	656.0	-9.5
5	1	2	2	2	3	1702.0	1693.0	552.0	587.0	-9.5
6	1	2	3	3	1	1534.0	1538.0	555.0	720.0	-7.9
7	1	3	1	2	1	1550.0	1559.0	695.0	989.0	-5.7
8	1	3	2	3	2	1484.0	1482.0	740.0	930.0	-5.2
9	1	3	3	1	3	1474.0	1460.0	899.0	1015.0	-3.8
10	2	1	1	3	3	1054.0	799.0	1941.0	1861.0	6.2
11	2	1	2	1	1	1163.0	1220.0	2064.0	2052.0	4.7
12	2	1	3	2	2	943.0	743.0	1862.0	1949.0	7.0
13	2	2	1	2	3	862.0	626.0	2060.0	2020.0	8.7
14	2	2	2	3	1	1171.0	982.0	2210.0	2337.0	6.5
15	2	2	3	1	2	1062.0	957.0	2379.0	2217.0	7.1
16	2	3	1	3	2	1061.0	636.0	2212.0	2353.0	8.3
17	2	3	2	1	3	992.0	825.0	2110.0	2127.0	7.3
18	2	3	3	2	1	1061.0	773.0	2343.0	2309.0	8.0

(a) Low Frontal 1 vs. Mid Offset Crash

No	A	B	C	D	E	Low Frontal2		High Offset		S/N Ratio
	1	2	3	4	5	N1	N2	N1	N2	
1	1	1	1	1	1	1631.0	1598.0	1084.0	1171.0	-3.1
2	1	1	2	2	2	1698.0	1698.0	1410.0	1068.0	-3.0
3	1	1	3	3	3	1686.0	1774.0	1243.0	1332.0	-2.6
4	1	2	1	1	2	2008.0	2043.0	684.0	938.0	-8.3
5	1	2	2	2	3	2460.0	2341.0	1099.0	978.0	-7.3
6	1	2	3	3	1	2298.0	2285.0	981.0	1159.0	-6.7
7	1	3	1	2	1	2203.0	2241.0	1357.0	1614.0	-3.6
8	1	3	2	3	2	2094.0	2087.0	1308.0	1516.0	-3.5
9	1	3	3	1	3	1946.0	1937.0	1389.0	1587.0	-2.4
10	2	1	1	3	3	1510.0	1393.0	2392.0	2447.0	4.4
11	2	1	2	1	1	1755.0	2409.0	2612.0	3264.0	2.7
12	2	1	3	2	2	2039.0	2351.0	2463.0	3105.0	1.9
13	2	2	1	2	3	1782.0	2259.0	3078.0	3230.0	3.8
14	2	2	2	3	1	1350.0	1358.0	2809.0	3066.0	6.7
15	2	2	3	1	2	1536.0	1324.0	3060.0	3002.0	6.5
16	2	3	1	3	2	1054.0	1016.0	2750.0	3001.0	8.8
17	2	3	2	1	3	1358.0	1260.0	2729.0	2852.0	6.6
18	2	3	3	2	1	1131.0	744.0	2855.0	3033.0	9.7

(b) Low Frontal 2 vs. High Offset Crash

Table.12 Orthogonal Arrays and Analysis Results as Regards the Frontal and Offset Crash

Selection of Robust Optimal Design Specification

From the results of Table.12, response charts of S/N to select the robust optimal design specification are shown in Fig.9. According to the impact velocity of frontal and offset crash, the degree and tendency by which each control factor level has an effect, can be figured out from Fig.9, and from that charts S/N is the most sensitive to the control factor of A(number of FIS) and B(position of FIS).

Therefore, the robust and optimal control factors are chosen as the number of FIS equals 'Two' and the position of FIS is '3(FEM UPR MBR). And the other factor C(number of FIS mounting) is 1 point, D(material type of FEM) is Hybrid, and E(thickness of FEM) is 0.6mm. The summary of these factors are listed in Table.13.

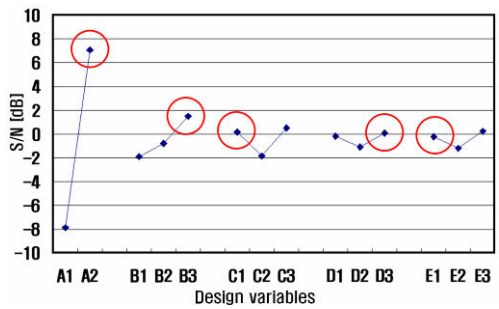

(a) Low Frontal 1 vs. Mid Offset Crash

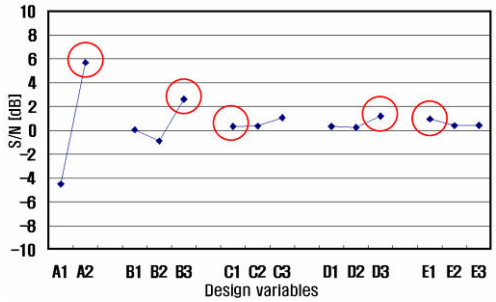

(b) Low Frontal 2 vs. High Offset Crash

Fig.9 Response Chart of S/N

	Design Variable	Current Design	Robust Opt. Design
A	Number of FIS	One	Two
B	Position of FIS	2	3
C	Number of FIS Mounting	1 pt	1 pt
D	Material Type of FEM	Hybrid	Hybrid
E	FEM Thickness	0.9mm	0.6mm

Table.13 Comparison of Initial with Robust Optimal Design

Verification and Discussion of Robust Optimal Design Specification

To verify the FIS sensing improvement, additional crash simulation results which is performed with selected optimal control factors are in Table.14, in which S/N values are summarized from the first peak of each FIS signal.

Low Frontal 1 vs. Mid Offset Crash				
Current Design		Robust Optimal Design		Gain
Predicted	Verified	Predicted	Verified	
-8.03	-9.14	10.15	9.88	19.02
Low Frontal 2 vs. High Offset Crash				
Current Design		Robust Optimal Design		Gain
Predicted	Verified	Predicted	Verified	
-5.80	-8.30	8.43	9.40	17.70

Table.14 Summary of Optimization Results

When comparing between low frontal and mid offset FIS signal, S/N ratio are raised by 19.02dB from current design specification, and S/N ratio are also raised by 17.7dB in comparison between another frontal and high offset crash mode. These results explain that with current base design specification, the crash severity of low frontal crash may be larger than that of mid offset crash, but after optimization, the robust optimal design can drastically reduce the possibility of airbag malfunction. Fig.10 show the FEM sample of optimal FIS position.

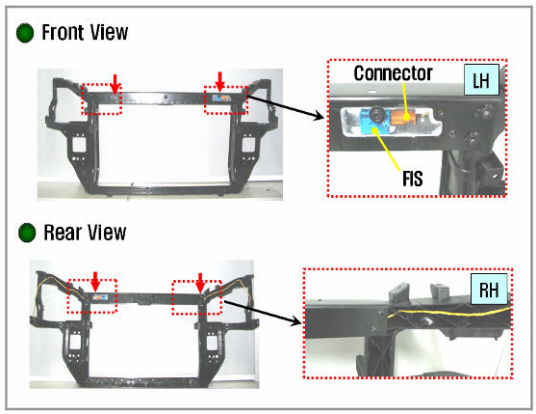

Fig.10 FEM Sample of Optimal FIS Position

DETERMINATION OF AIRBAG DEPLOYMENT LOGIC WITH CAE TECHNIQUE

Development of Unified Crash Simulation Model

Occupant injury simulation generally uses the different simulation model case by case for various crash modes. But in this study, to compare the crash severity between different crash modes in view of occupant injuries, unified occupant simulation model was developed and used. And the model was verified and confirmed through the correlation with the crash test results. Table.15 shows the notation for the unified simulation model used in this study.

Crash Mode / Restraints	Frontal	Offset	Oblique
Bag(Stage2)+PT	FRT bb2	OFF bb2	OBL bb2
Bag(Stage1)+PT	FRT bb1	OFF bb1	OBL bb1
Bag(Stage2) only	FRT bag2	OFF bag2	OBL bag2
Bag(Stage1) only	FRT bag1	OFF bag1	OBL bag1
PT only	FRT PT	OFF PT	OBL PT
Belt only(w/o PT)	FRT noPT	OFF noPT	OBL noPT
No Restraints	FRT nores	OFF nores	OBL nores

Table.15 Notation for the Unified Simulation Model

Fig.11 shows the development procedure of the unified occupant simulation model. Crash simulations with PAM-CRASH to acquire vehicle deceleration and deformation were performed, and as a result the unified occupant simulation with MADYMO followed after that.

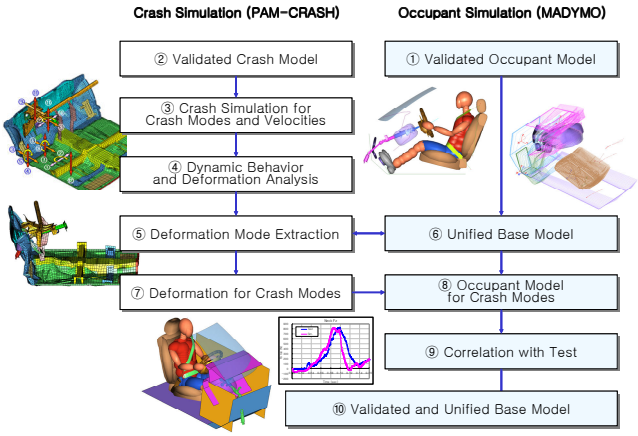

Fig.11 Development Procedure of the Unified Occupant Simulation Model

Based on old occupant simulation model for frontal crash, the unified occupant model was constructed with the utilization of crash simulation deformation results as follows, 1) model geometry and JOINT (vehicle structure, steering system, side plane), 2) lower leg contact model, 3) deformation scale factor. Validation results between the simulation and test using the unified simulation occupant model are listed in Table.16.

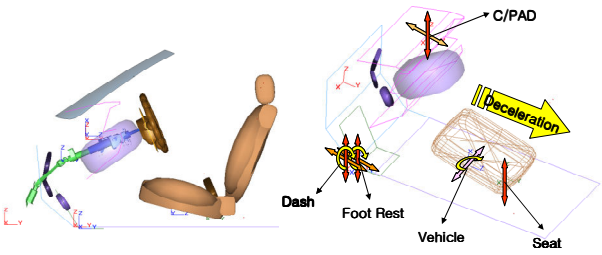

Fig.12 Unified Occupant Simulation Model

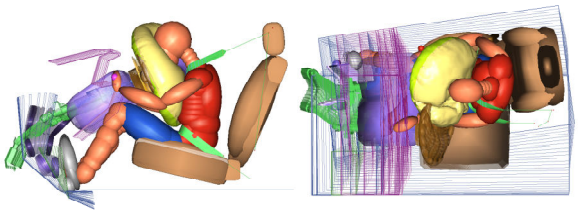

(a) Vehicle and Occupant Behavior

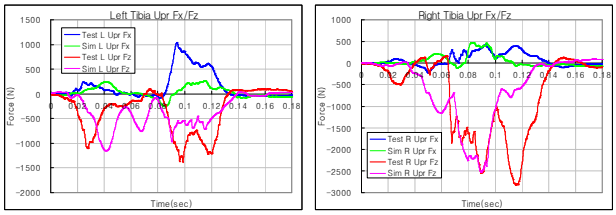

(b) Injury Graph

Fig.13 Validation Results (Offset Mode)

TEST		HIC			Chest G			Femur Load LH			Femur Load RH		
Mode	Speed	Test	Sim	Err	Test	Sim	Err	Test	Sim	Err	Test	Sim	Err
Frontal	Mid	154.4	179.1	16%	35.0	31.9	-9%	1229	1115	-9%	3137	4093	30%
Frontal	High	357.5	329.0	-8%	45.1	43.1	-4%	1344	1459	9%	4130	4771	16%
Others	Mid	377.2	234.5	-38%	34.4	38.7	13%	1952	1752	-10%	4609	4609	0%
Oblique	Mid	106.0	95.4	-10%	21.4	19.3	-10%	598	725	21%	1273	2090	64%
Oblique	High	240.9	341.3	42%	43.2	40.6	-6%	1148	2996	161%	5157	4535	-12%
Offset	High	235.0	408.0	74%	41.1	39.7	-3%	1251	3361	169%	2845	4828	70%

Table.16 Validation Results of the Unified Model

Discussion of Simulation Results with Variable Crash Modes and Velocities

As crash modes and velocities change, corresponding values are put into MADYMO input data file such as body pulse, vehicle deformation graphs, DAB/PT TTF, and so on. (Fig.14), and corresponding occupant simulation model can be classified into 7 groups according to restraint conditions: bagS2+PT, bagS1+PT, bagS2 only, bagS1 only, PT only, belt only and no restraints.

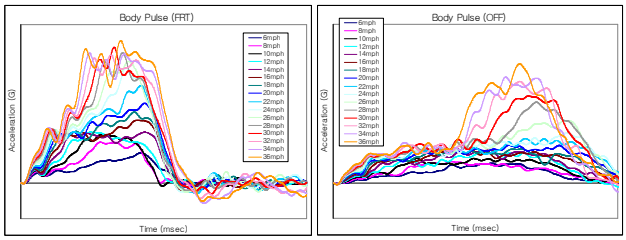

Fig.14 Crash Simulation Body Pulses according to Crash Velocities

After 525 crash and occupant simulations, occupant injuries of 21 items are extracted and selected as 4 representative injuries for this project as like: HIC15, Chest G, Nij and Femur Load, which represent the injury of head, chest, neck and lower leg. Fig.15 shows the injury results graph classified according to occupant injury levels, restraint conditions and crash modes.

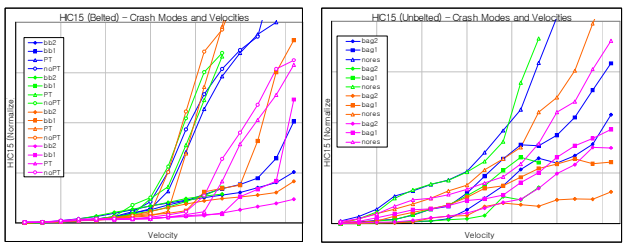

(a) by Occupant Injury Level

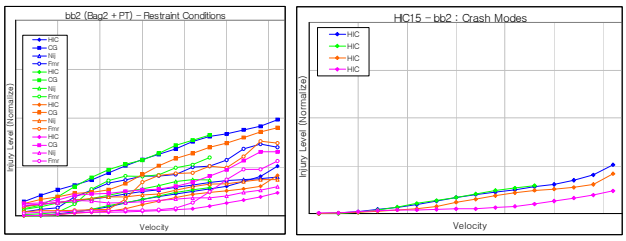

(b) by Restraint Conditions and Crash Modes

Fig.15 CAE Simulation Results

Airbag Firing Decision Logic Determination

To determine airbag firing decision logic, the optimal restraint constraint condition which has a minimum occupant injury level for certain crash modes and impact velocities, must be found, but the optimal restraint varies as the injury items what we focus on.

To solve this problem, new dimensionless and combined injury severity index is used on this study, and which expresses multiple occupant injuries with one number by equation.

$$Index = a \times HIC_{15} + b \times ChestG + c \times N_{ij} + d \times Femurload$$

Where, a, b, c, d are weighting factors, and have different levels as belted and unbelted condition.

Two methods are proposed in this study as the manner to determine the weighting factors, one is an area weighting factor method and the other is a standard deviation weighting factor method.

Area weighting factor method means that the larger the area, the higher the weighing factor, that is the largest weighting factors are granted to the severest injury levels in order to reduce that injuries, so the firing time of airbag and P/T is determined by the weighting factor.

Standard deviation weighting factor method means that the larger the standard deviation of each restraint conditions, the higher the weighting factor, so to speak the largest weighting factors are given to the most sensitive injury levels to determine the firing time of airbag stage and P/T. Table.17 is the weighting matrix for combined injury severity index (where, 30 means the velocity range are from 0 to 30mph, and 24 means up to 24mph).

Belted

	Frontal				Offset				Oblique			
	HIC	CG	Nij	Fmr	HIC	CG	Nij	Fmr	HIC	CG	Nij	Fmr
Area30	0.22	0.34	0.20	0.24	0.15	0.42	0.28	0.15	0.28	0.32	0.20	0.20
Area24	0.12	0.38	0.23	0.27	0.07	0.46	0.36	0.11	0.13	0.39	0.26	0.22
Standard Deviation 30	0.66	0.13	0.17	0.04	0.56	0.18	0.23	0.03	0.81	0.07	0.12	0.01
Standard Deviation 24	0.44	0.19	0.28	0.09	0.13	0.26	0.56	0.05	0.61	0.12	0.24	0.03

Unbelted

	Frontal				Offset				Oblique			
	HIC	CG	Nij	Fmr	HIC	CG	Nij	Fmr	HIC	CG	Nij	Fmr
Area30	0.16	0.20	0.28	0.35	0.12	0.21	0.44	0.23	0.12	0.19	0.39	0.31
Area24	0.13	0.20	0.32	0.35	0.09	0.19	0.45	0.27	0.10	0.18	0.42	0.31
Standard Deviation 30	0.36	0.11	0.51	0.03	0.23	0.15	0.58	0.03	0.30	0.13	0.53	0.04
Standard Deviation 24	0.31	0.10	0.55	0.03	0.19	0.15	0.62	0.04	0.24	0.12	0.60	0.04

Table.17 Weighting Matrix for New Index

To determine the airbag deployment logic, first, crash and occupant simulation results are used, and various crash modes for example frontal, offset, oblique etc. and belt condition such as belted and unbelted are also used. And 6 injury indexes are also used: HIC15, Chest G, Nij, Star rate P_{comb}, and two indexes (area30 and standard deviation30). Methodologies of determination are divided into 2 categories

1) Airbag deployment logic to minimize injury level
2) Airbag deployment logic of Must Fire

Method of minimizing the injury level can use an ideal and definite restraint condition in a certain region, but the firing condition is somewhat lower velocity than needed, that is, restraint system is inclined to fire at lower velocities (Fig.16a). On the other side, the method of Must Fire uses a restraint condition without which the injury level increases rapidly. That condition seems to be the Maginot line for deployment, but the firing comes from higher velocities and is apt to be arbitrary because of indefinite basis (Fig.16b).

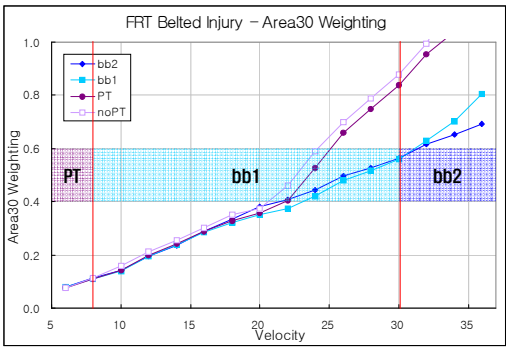

(a) Minimize Injury Level

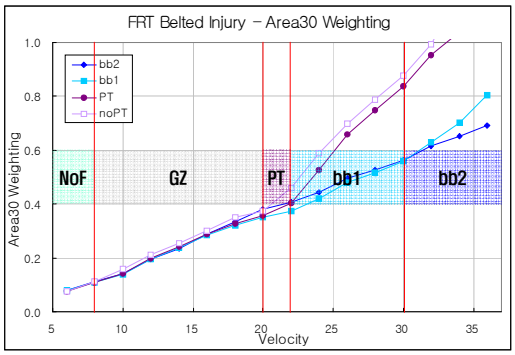

(b) Must Fire

Fig.16 Airbag Deployment Logic

Discussion of Airbag Firing Decision Logic with P_{comb}

Apart from the new methodologies ahead proposed in this paper, however, the airbag deployment logic is constructed using NCAP star rate P_{comb} as an injury severity index, which is already verified and generally used, and with the method to minimize injury level. Fig.17 shows the final logic chart.

Seat Belt	Cash Mode	Crash Speed																																				
		1	2	3	4	5	6	7	8	9	10	11	12	13	14	15	16	17	18	19	20	21	22	23	24	25	26	27	28	29	30	31	32	33	34	35
Belted	Frontal							NF																														
																		PT															S1					S2
	Offset							S1																														
																																						S2
	Oblique																	PT																				
																																	S1					S2
Unbelted	Frontal							S1																														
																																						S2
	Offset																																					
																																						S2
	Oblique							S1																														
																																						S2

Fig.17 Proposed Final Airbag Deployment Logic Chart

CONCLUSIONS

To find out the optimal location of FIS which can enhance the airbag sensing and calibration performance, vehicle crash test results are used and 4 calibration set are carried out. As a result of FIS data analysis and airbag calibration, the relatively superior FIS locations are selected and proposed into the vehicle development process.

From now on, CAE simulation results which have a limitation in accuracy to use in the airbag calibration process must go further in comparison with test results.

To promote FIS sensing discrimination performance, CAE and Taguchi robust optimization design technique were used. At frontal and offset crash mode, the number of FIS and the positions of FIS are the most sensitive control factors for airbag sensing performance. And also the distribution of vehicle weight and stiffness/strength as a noise factor are also considered in this progress.

To determine the airbag deployment logic, crash and occupant simulation techniques are applied and adapted to this project, and as a result, the optimal restraint condition to minimize occupant injury level and to suppress the rapid increase of injuries are proposed. As an injury criterion to determine firing decision logic, two combined injury severity indexes are proposed. But at lower speed region less than about 20mph, there are few differences in injury levels irrespective of restraint condition.

ACKNOWLEDGEMENTS

The authors would like to acknowledge the staffs of this national project for their assistance and support in undertaking this project.

REFERENCES

[1] J. M. Lim et al., “National Transportation Core Technology Development Proposal and Plan (2004~2006)”, the Ministry of Construction and Transportation, Korea, 2004.

[2] H. W. Park, S. H. Hong and J. M. Lim, “Airbag Sensing Test Results Analysis According to Frontal Impact Sensor Location Report”, Advanced Development & Analysis Team, Hyundai-Kia Motors, 2005.

[3] J. M. Lim, “Frontal Impact Sensor Location Inspection Results Report”, Advanced Development & Analysis Team, Hyundai-Kia Motors, 2005.

[4] H. W. Park, “Advanced Airbag Frontal Algorithm Calibration Results Report”, Advanced Development & Analysis Team, Hyundai-Kia Motors, 2006.

[5] K, H. Lee and W. S. Joo, “Robust Design of Driver Airbag with Taguchi Method”, KSME, Vol.12, No.2, pp.131~138, 1999.

[6] Ranjit K. Roy, “A Primer on the Taguchi Method”, Van Nostrand Reinhold inc. 1990.

[7] “Occupant Injury Research Results Report”, Advanced Development & Analysis Team, Hyundai-Kia Motors, 2003.

NHTSA RESEARCH ON IMPROVED RESTRAINTS IN ROLLOVERS

Michael L. Sword
Transportation Research Center
United States
Lisa K. Sullivan
National Highway Traffic Safety Administration
United States
Paper Number 07-0279

ABSTRACT

As part of a comprehensive plan to reduce the risk of death and serious injury in rollover crashes the National Highway Traffic Safety Administration (NHTSA) has reinitiated a program to characterize restraint system response in rollovers. A rollover restraint tester (RRT) is utilized to produce a 180 degree roll followed by a simulated roof-to-ground impact. Recognizing the unpredictability of the real world rollover phenomenon, this test provides a repeatable and consistent dynamic environment for suitable lab evaluation. Similar NHTSA research during the mid-1990s demonstrated an excursion reduction of up to 75% when an inflatable belt was compared to the standard three-point belt with a 50th percentile male [Rains, 1998].

Technologies being considered include integrated seat systems, pyrotechnic and electric resetable pretensioners, four-point belt systems, and inflatable belts. High speed video data are collected and analyzed to examine occupant head excursion throughout the tests and are presented for discussion. Though repeatable, concern about the real world relevancy of the RRT dynamics have been focused toward the absence of a mechanical component for lateral motion. This component is not inbuilt to the test fixture.

This research attempts to determine if reasonably reduced excursion is possible in the simulated rollover. This research has been constrained to examining restraint systems focused to the seat. Future research to include a partial vehicle cab structure is planned to allow evaluation of devices that utilize it for a reaction surface; such as rollover air bags.

Restraint advancements have primarily been focused on frontal and side crash performance. It is believed that many of these advancements can also aid in reducing occupant excursion during a rollover crash. Improving restraint effectiveness in rollovers may further enhance protection for belted, non-ejected occupants in rollovers.

INTRODUCTION

Rollover crashes are a major problem in the U.S. Digges [2002] reported that rollovers constitute about 2.2% of crashes but represent 33% of the total injury cost. Much of this cost is attributed to ejections, especially of unbelted occupants. NHTSA has a research program focused on reducing occupant ejections through side windows and the U.S. Congress has mandated that a new standard be published by October 2009. For non-ejected occupants, rollovers still pose a serious threat of injury; particularly head injuries from hitting the interior of the vehicle. FMVSS No. 216 approaches this issue by requiring roof crush resistance and survivability space in the cabin. Safety belt slack and stretch have been thought to allow occupants to 'dive' toward the roof structure in the rollover crash.

In the mid-1990s, the agency initiated a research program to explore the effectiveness of various restraints in rollovers. A rollover restraint tester (RRT) was developed to simulate rollover conditions. It provided a controlled roll for a seated occupant and was followed by a simulated roof-to-ground impact. Occupant excursions toward the roof were measured for common 3-point belts and other advanced restraints systems. NHTSA has revived this program with the intent to examine the latest restraint technology for the seat belt. Many of these devices have been developed for the more common frontal and side crashes. The goal is to determine if these same devices could be employed to improve restraint of belted occupants in rollovers.

The RRT provides a repeatable dynamic environment suitable for comparison testing of various restraint configurations. It has been criticized for lacking a built in lateral component. No single device can replicate the dynamics of all rollovers because every rollover crash is very different and unique. This device allows for consistent repeatability of a specific dynamic environment. In addition to the physical testing, NHTSA has initiated a cooperative project to use computer simulation to validate the RRT testing with real world accident data and FMVSS No. 208 dolly testing. The simulation will allow for expanded capabilities for evaluating technologies in many different ways.

With anticipated FMVSS No. 216 improvements and previous work highlighting the potential effectiveness of advanced restraints, this research program provides an opportunity to evaluate current and future available state-of-the-art countermeasures for occupant protection during a rollover.

TESTING

Test Device

A device, similar to the original RRT [Rains, 1998], has been developed. The rollover simulated is one in which the vehicle becomes airborne at the initiation of the roll and then impacts the roof structure after rotating approximately 180 degrees.

Figure 1 is a schematic of the new rollover restraint test device. The coordinate system is set to the dummy for excursion analysis. The device has four (4) main features consisting of

1) A support framework,
2) A counter-balanced test platform with rotating axle,
3) A free weight drop tower assembly, and
4) A shock tower.

The test platform, with vehicle seat, dummy and restraint device(s) attached, is mounted to the supporting framework. The free weight drop tower provides energy to rotate the test platform at a desired angular acceleration and peak roll rate. The peak roll rate can be adjusted by changing the weight of the drop tower mass. To simulate the roof impact, the rotating platform impacts an adjustable shock-absorbing tower after approximately 180 degrees of rotation. Rollers are attached to the shock absorbers to accommodate the Nylon impact blocks custom mounted to the table. Figure 2 shows the impact region of the table to the shock tower.

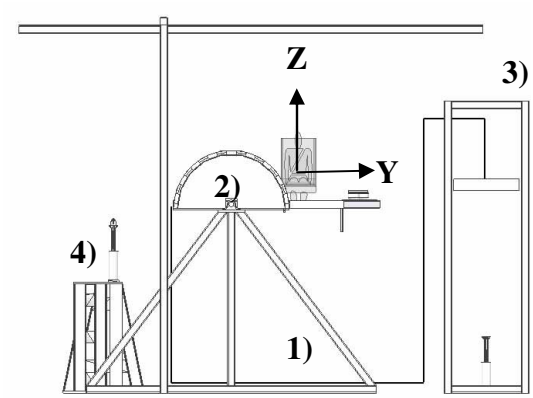

Figure 1. Rollover Restraint Tester (RRT)

Figure 2. Impact area of RRT

Instrumentation

The RRT was instrumented to help characterize the dynamics of the testing. An encoder was used to monitor the roll rate. Two (2) 50,000 lb. load cells were mounted to the roll table at the point of impact to record the impact force. Figure 2 shows how the load cells were mounted between the impact blocks and roll table. A string potentiometer was utilized to measure the shock absorber deflection. A 2,000 g rated accelerometer, mounted to the platform directly

underneath the center line of the seat, was used to collect the acceleration at impact.

The 50th percentile male Hybrid III dummy used for testing contained full head, neck and chest instrumentation, and these channels were collected during testing. Seat belt load cells were used for both the lap and shoulder portion of the belts. Video data were collected with a combination of on-board real time cameras (33 fps) and off-board high speed cameras (500 fps).

Evaluated Restraint Technology

A variety of restraints were selected for testing. They range from current consumer available technologies to prototype devices. Cooperation with automotive suppliers and original equipment manufacturers (OEM) allowed for much of the technology to be assessed. The following devices were selected for evaluation. They have been tested individually and in conjunction with others, depending on feasibility of implementation.

Integrated Seat – The integrated seat has the seat belt hardware incorporated into the seat. Many SUV and other light trucks utilize these seats. These seats are generally reinforced to accommodate the increased loads experienced in a crash event. Figure 3 shows the integrated seat used for the evaluation.

Figure 3. Integrated Seat

Integrated SWAP Seat – The integrated SWAP seat refers to a supplier technology where the restraint, integrated with the seat, comes from the inboard side of the car and buckles on the outboard side.

Non-Integrated Three-Point Seat – This is a standard fleet representative three-point restraint attaching to a B-pillar frame element of the vehicle. A representative B-pillar was fabricated for testing. It was utilized for all non-integrated configurations of various technologies. Figure 4 shows the standard non-integrated seat used for evaluation. This seat was used for all non-integrated seat three-point testing configurations.

Retractor Pretensioner – The retractor pretensioner is a device that uses a pyrotechnic discharge to remove the slack from a seat belt when triggered by a sensor. The action for the removal of slack occurs in the retractor portion of the system. This is currently used in various production vehicles and was purchased as a replacement part. Once the system is ignited, it must be replaced with a new system and is not reusable; similar to an air bag.

Buckle Pretensioner – This is also a pyrotechnic device incorporated in the buckle and is fired to remove the slack near the pelvic region. This is currently used in various production vehicles and was purchased as a replacement part. Like other pyrotechnic devices, it is only usable one time and must be replaced.

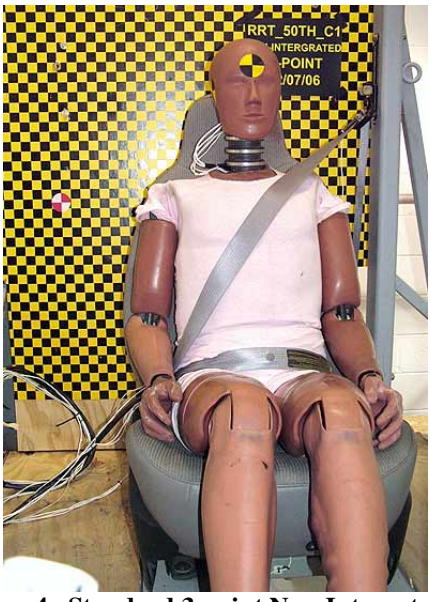

Figure 4. Standard 3-point Non-Integrated Seat

Motorized Retractor – The motorized retractor, sometimes called electric pre-pretensioner, is a reusable device designed to remove slack from the seat belt system. The force rating is generally much lower than the pyrotechnic devices. The reusability of the device allows implementation much earlier when the possibility of a crash is sensed, but the crash is not yet imminent. An example could be one where a car with Enhanced Stability Control (ESC) was activated from an erratic vehicle dynamic; the motorized retractor could be triggered to remove occupant belt slack even if ESC prevented a crash.

Four-Point Seat Belt – The four-point seat belt is a device that has belts coming across both shoulders and buckles at the center of the lap. Two pyrotechnic pretensioners are utilized on each side of the restraint's lower retractors. This is a prototype device being evaluated by suppliers and OEMs for improved restraint performance.

Inflatable Belt – The inflatable belt, similar to the inflatable tubular torso restraint (ITTR) tested in the mid 90s, is a three-point device [Rains, 1998]. It has an inflatable section in the shoulder portion of the belt designed for both pretensioning and cushioning. Previous testing demonstrated reduced dummy excursion when the inflatable belt was compared to a standard three-point system. This prototype restraint is being considered by automotive suppliers and OEMs.

Test Matrix

The test matrix for the restraint evaluation is included as Table 1. The 50th percentile male Hybrid III dummy was used for this series of tests. Configuration code C is baseline treatment for test comparison. It is a standard 3-pt. non-integrated seat without pretensioning. The D-ring position is set in the lowest position.

Pretensioner Deployment

Pyrotechnic and motorized pretensioners were tested for the series. To maintain consistency regarding their use, a switch was mounted to activate at a prescribed angle of table roll. As the table rotated, the dummy began moving out of position, mainly in the Y-direction (lateral). A simulation with an automotive supplier determined a hypothetical dummy motion before a rollover sensor would detect that a rollover was inevitable and would trigger the pyrotechnic devices. For the RRT device this motion amount occurred at about 45 degrees of rotation. This angle was used for firing all pyrotechnic pretensioners used in testing.

Table 1.
Test Matrix for 50th Hybrid III Male

Configuration Description	*D-Ring Position*	*Code*	*REPS*
Integrated Seat	N/A	A	3
Integrated SWAP DURA	N/A	B	3
* 3-pt. Non-Integrated (3PN)	Lower	C	3
3-pt. Non-Integrated	Upper	D	3
(3PN) Retractor Pretensioner	Lower	E	3
(3PN) Buckle Pretensioner	Lower	F	3
(3PN) Retractor w/Buckle Pretensioner	Lower	G	3
(3PN) Motorized Retractor	Lower	H	3
(3PN) Motorized Retractor w/Buckle Pretensioner	Lower	I	3
4pt system w/Pretension	N/A	J	3

** Baseline Configuration for comparison*

For the motorized restraint configurations, the assumption was that they would be used prior to the onset of the roll because of their reusability in the fleet. For instance, if a motion sensor detected irregular vehicle kinematics, it would

engage the motorized pretensioner to remove slack early. From this assumption, motorized pretensioners were activated just prior to the initiation of roll.

Static Test

A static test was conducted for each configuration prior to testing to evaluate the natural system slack. The dummy was first seated to testing position with the restraint configuration. A hydraulically driven gearbox, mounted to the rotating table, was then used to slowly roll the table 180 degrees. The rotated table would just barely touch the rollers mounted on the shock absorbers. Static measurements of the X (longitudinal), Y and Z (vertical) direction for the inverted dummy were recorded. The table was rotated back to the start position and the dummy was reseated for the dynamic test.

Dynamic Test

A test to simulate a 180 degree roll followed by a roof impact was administered. Dynamic testing utilized a free-falling mass to drive the rotation of the table. A cable system connected the free falling mass to the half circle drive feature of the test platform. The mass, housed in the drop tower, was stopped by a series of shock absorbers. Platform kinematics were adjusted by changing the mass weight. The target impact angular rate was 315 degrees/second. Earlier reported testing was conducted around 260 degrees/second [Rains, 1998]. Improved structural design of the latest RRT allowed for increased rates.

Roof impact simulation was achieved through the adjustable shock absorbers. The damping adjustment changes the impact force deflection characteristics. A harder impact resulted in less shock deflection. For all testing reported, only one setting was utilized. The selected setting allowed for some deflection of the table and limited rebound after impact. A very "hard" setting would result in dramatic rebounding and bouncing of the table.

Two event marks were utilized for data collection. The first was when the locking clasp was triggered to initiate the test. The second and main event mark for testing was the impact of the nylon blocks with the roller bearings. Data were collected throughout the entire event. All presented comparison data curves utilize the impact mark for setting a zero time for comparison purposes.

Resting dummy measurements along with pictures were taken post testing. Video data collected at the head area were analyzed with video imaging software for excursion. Real-time (33 fps) cameras mounted on-board were used to measure pre-impact excursion. High speed cameras (500 fps) were setup off-board and collected excursion data post impact. After video analysis, the two views were married to develop excursions curve in the X, Y and Z directions for the entire event.

RESULTS

RRT Device Kinematics

Each test is characterized by an acceleration of roll rate until impact. The acceleration is initially slow and increases with time up until impact with the shock tower. The distinct motion profile for the rotating platform is provided as Figure 5 where time zero is the data mark when the table mechanically begins to roll.

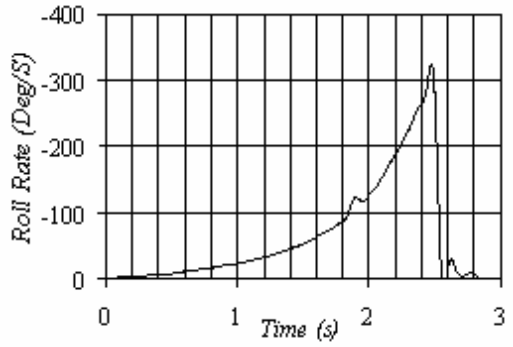

Figure 5. Rotating Platform Angular Speed Profile for Representative Testing of RRT with Target Impact Speed of 315 degrees/second.

The motion is very sensitive to the major weight changes on the table created by certain configuration changes. Changes of the moment about the rotating axle affect the start of the initial roll. The motion profile can be adjusted through changing the drop weight total mass. Sandbags were used to adjust this mass. The aim was to have an angular speed of the table at impact of 315 degrees/second. Average impact roll rate for each tested configuration, with the standard deviation for the 3 repeated tests, is provided in Figure 6. The rates did not deviate

beyond 3% of the target rate. An explanation for the configurations is provided in Table 1.

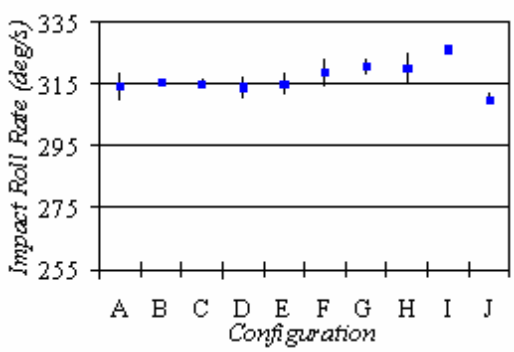

Figure 6. Average Impact Roll Rate w/Std Deviation (50th male test series)

RRT Impact Force

The impact was characterized through a combination of the table-mounted load cells and an accelerometer mounted directly under the seat. Table 2 summarizes these data for all the tested configurations.

Table 2.
Average Impact Force and Accelerometer Data for RRT
50th Hybrid III Male

Restraint Config.	*Avg. Impact Force Max (N)*	*Avg. Impact Accel. Max (g)*
A	95,784	51.9
B	95,370	53.6
C	102,456	46.4
D	102,696	47.3
E	102,277	43.8
F	103,300	45.6
G	104,172	45.5
H	101,402	45.1
I	101,964	45.1
J	93,747	47.4
**Avg.*	*100,820*	*46.7*
**Std Dev*	*3,575*	*3.0*

**Calculated from all tests*

Average impact force and acceleration between the three repetitions on any specific configuration never exceeded ±2% and generally was below ±1% of the average. Differences between configurations generally were noticed after significant table weight changes occurred between configurations. An example is between the integrated seats (A, B) and the non-integrated seats (C-I). In these cases, the seat fixture required changes that resulted in platform weight changes for testing. Non-integrated testing utilized similar seating with restraints utilized in different combinations. 4-point testing (J) also required a seating fixture change leading to differences in RRT impact forces.

Dummy Kinematics

Dummy kinematics were influenced by a combination of platform rotational and gravitational forces. At the onset of the test, the dummy was seated in an upright position. Gravity was the primary initial dummy force for the slow starting action of the rotating platform. As the platform began to rotate, the dummy's course was changed and gravitational forces tended to move the dummy inboard (negative Y-direction).

The angular speed of the platform increased with the centripetal or normal acceleration, creating the appearance of an outward or centrifugal force on the dummy. This outward force pushed the dummy outboard and up (toward the roof) of the vehicle (positive Y-direction, positive Z) during the pre-impact roll event. The dummy tended to start moving back in the positive Y-direction at about 90 degrees of platform rotation. Gravitational forces continued to play a roll for Z-direction (out of the seat toward the roof) past 90 degrees of rotation, until impact.

After impact the dummy immediately changed from outboard and up motion to a dramatic inboard (opposite) Y-direction movement and an amplified Z-direction (positive, toward roof direction) movement. The stopped table eliminated centripetal accelerations leaving momentum and gravity until the dummy came to a hanging rest.

Dummy Head Excursion

Video data of the dummy's head were collected for excursion analysis. X-direction (fore and aft) data have been omitted. The kinematics of the RRT do not have an X-direction motion component, and analysis shows less significance in motion compared to the Y and Z directions. It

is recognized that real world rollovers do have varying magnitudes of X-direction motion that can be significant. However, the presented data will focus only on Y and Z direction motions.

Y-Direction Excursion

Figures 7-10 illustrate the results of specific configurations tested. Not all tested configurations are shown for brevity. These figures offer insight into the testing that was conducted. The figures include results for the Integrated Seat (A), Non-integrated Seat (C), the combination pyrotechnic retractor with buckle pretensioner (G) and the electronic motorized retractor with pyrotechnic buckle pretensioner (I). From these figures, the general Y-direction dummy kinematics are observed. These configurations demonstrate how effective each countermeasure was in altering the dummy head excursion values. They also demonstrate the consistency of dummy head excursion between repetitions within a configuration set.

Time zero is the impact moment, and beyond is the post-impact excursion. The portion of the curve before time zero is the pre-impact excursion while the platform is rotating. Within a configuration, dummy head excursion was relatively consistent. Here the dummy tendencies in the test are noticed. The initial pre-impact Y-direction inboard movement is depicted by a negative value. The subsequent pre-impact outboard movement is noticed from the increasing value of Y before time zero.

The impact stops rotation of the platform. After time zero, the dummy head Y-excursion shifts. This inboard movement peaks and the dummy rebounds to a resting position.

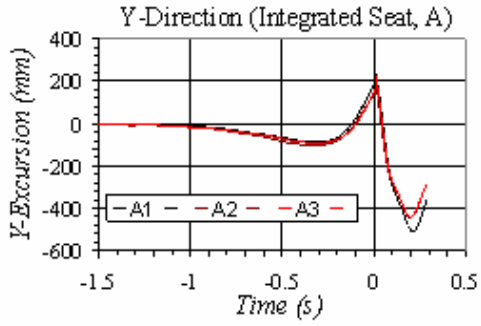

Figure 7. Configuration A Y-direction excursion of 50th male.

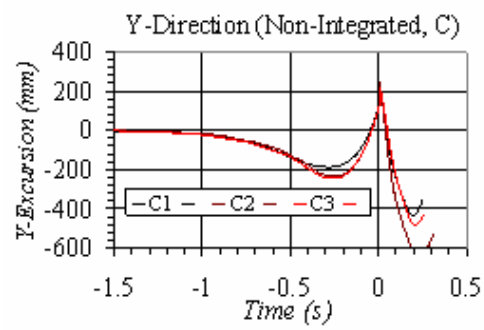

Figure 8. Configuration C Y-direction excursion of 50th male.

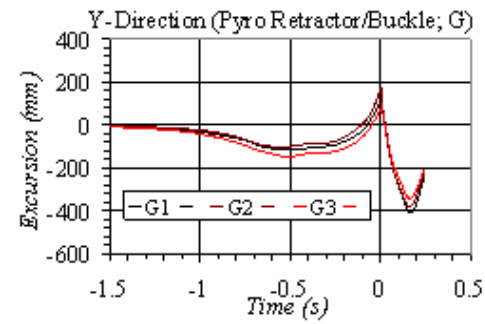

Figure 9. Configuration G Y-direction excursion of 50th male.

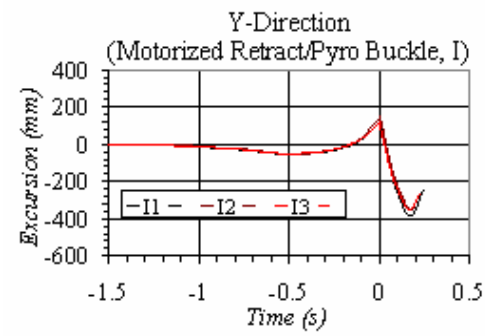

Figure 10. Configuration I Y-direction excursion of 50th male.

Figure 11 plots the average Y-direction dummy head excursion of the four configurations, A, C, G and I. As previously mentioned, configuration C is used as the baseline because it represents a standard 3-pt system with no use of pretensioners. The dummy Y-direction head excursion is reduced when each configuration is compared to the standard 3-pt. belt, C. Pre-impact Y_in (inboard) excursion is reduced from 223mm to 54mm (76%) when the motorized seat belt with buckle pretensioner (I) is compared to

the baseline (C). Pre-impact Y_out (outboard) is reduced from 225mm to 131mm (42%) when the same configurations are compared.

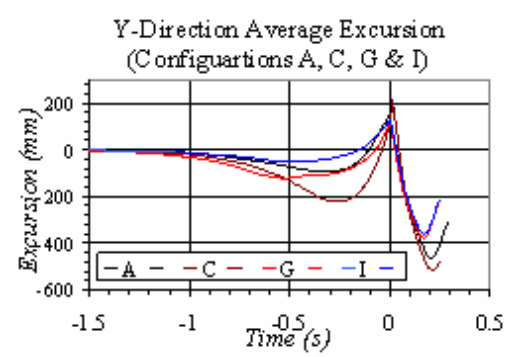

Figure 11. Average Y-direction movement for Configurations A, C, G and I.

Table 3 summarizes the average maximum dummy Y-direction head excursions for all tested restraints. These values are divided into pre and post impact categories. Pre-impact is subdivided for the inboard motion and outboard motion. Configurations with pretensioners were able to reduce dummy head Y-direction excursion.

Table 3.
Average Pre and Post Impact Dummy Y-Direction Head Excursion
50th Hybrid III Male

	PRE IMPACT		*POST*
Restraint	***Y_in***	***Y_out***	***Y***
A	-95	215	-466
B	-83	128	-387
C	-223	225	-518
D	-250	284	-445
E	-102	95	-392
F	-116	159	-458
G	-122	132	-354
H	-44	173	-391
I	-54	131	-362
J	-83	266	-514

A graphical summary of average maximum pre-impact excursion for all treatments is provided in Figure 12. The shaded background distinguishes between integrated (green), non-integrated (yellow) and the 4-pt (blue) configurations. In general, treatments resulting in a lower Y_in also had a reduced pre-impact Y_out when compared to the baseline (C) and the other non-pretensioned 3-pt. test (D). The integrated seats were effective in reducing excursion, with the SWAP configuration performing comparable to pretensioned treatments. It is important to consider that all pyrotechnic pretensioners were fired at a roll angle of 45 degrees (around 0.75 seconds before impact), and the motorized retractors were energized at the initiation of the roll. These devices were utilized in configurations E-J. Y_out of the 4-pt belt (J) was not reduced even though inboard motion was.

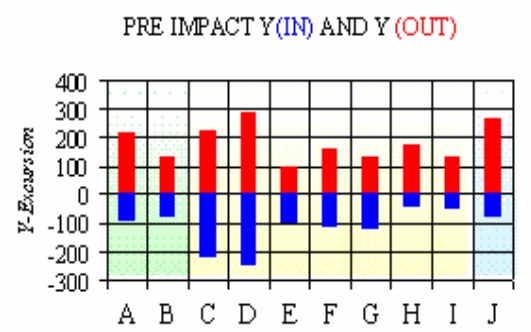

Figure 12. Pre-impact Y_in and Y_out Dummy Head

Post impact average maximum Y-direction dummy head excursions are quite variable between treatments, though pretensioning in 3-pt systems seemed to help reduce the excursion when compared to the baseline (C). The integrated SWAP (B) reduced post impact Y-excursion from 518mm to 387mm (25%) when compared to C. However, post impact evaluation of excursion by the RRT is difficult because dummy motion is very dramatic from the immediate stopping of platform rotation. Similar types of real world crashes are less prevalent and most generally continue to roll beyond 180 degrees and do not immediately stop.

Z-Direction Excursion

The motion of moving up toward the roof is considered Z-direction excursion for this testing. Figures 13-16 summarize each test for the individual configurations illustrated. Similar to the Y-direction plots, time zero is the impact of the table. Typical Z-direction movement in the pre-impact phase is zero until the apparent centrifugal forces begin to force the dummy up out of the seat. At this point, the Z-excursion begins to increase through the pre-impact phase. At impact, the dummy experiences a pointed

spike in the Z-direction. After this spike, the Z-direction begins to decrease and rebound to a resting position. Much of this post-impact spike Z-direction motion occurs because the dummy is pivoting around the lap belt and the dramatic Y-direction inboard motion reduces the dummy Z-direction. At stated earlier, rollover crashes that immediately stop after 180 degrees of roll are less common, making post impact data difficult to interpret.

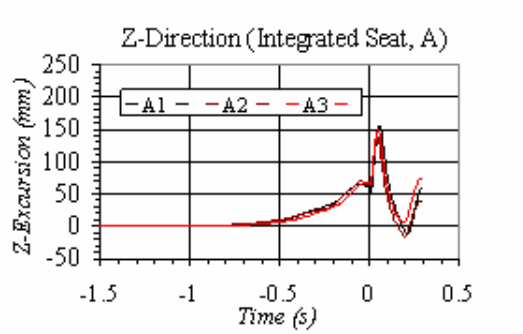

Figure 13. Configuration A Z-direction excursion of 50th male.

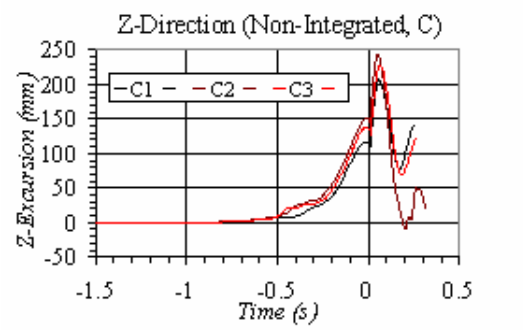

Figure 14. Configuration C Z-direction excursion of 50th male.

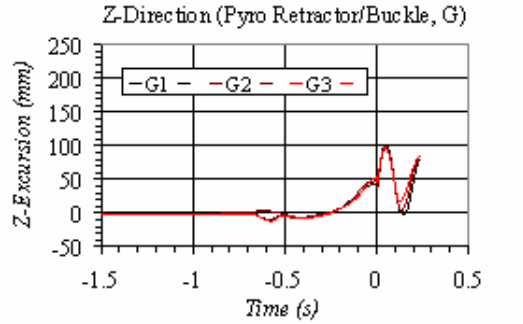

Figure 15. Configuration G Z-direction excursion of 50th male.

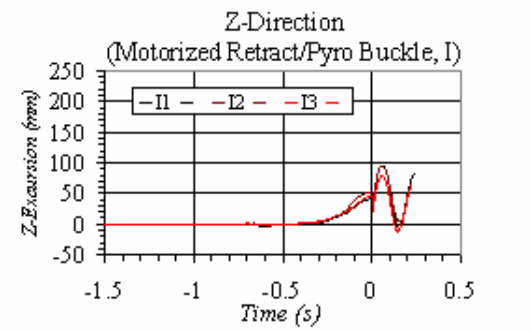

Figure 16. Configuration I Z-direction excursion of 50th male.

Similar to the Y-direction, pretensioners were able to alter the dummy head Z-direction motion between treatments. Figure 17 plots the average Z-direction motion of configurations A, C, G and I. With the baseline configuration as C, each treatment was able to reduce the Z-direction head excursion of the 50th male dummy.

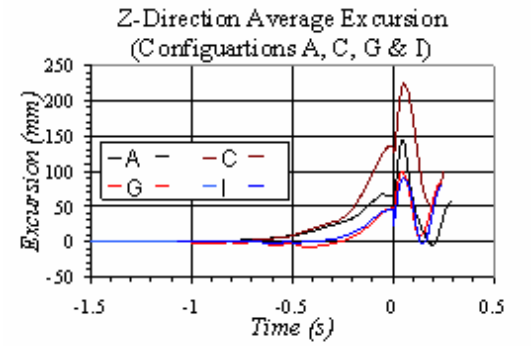

Figure 17. Average Z-direction movement for Configurations A, C, G and I.

Table 4 summarizes the average maximum dummy head Z-excursion pre and post impact for all tested configurations. This is graphically depicted as Figure 18. When compared to the baseline (C), the integrated seat configurations, A and B, had pre-impact Z-direction reductions of 49% and 54%, respectively. The post-impact were reduced 35% and 50%, respectively. No pretensioners were used in the integrated seat configurations.

The 3-pt pretensioner configurations, E-I, show a large reduction of dummy Z-direction head excursion. When compared to C, pre- and post-impact dummy head excursions for the motorized pretensioner and pyrotechnic configuration (I) were reduced 66% and 60%

respectively. In general, reduced pre-impact Z-head excursion led to reduced post impact Z motion. The 4-pt belt (J) had similar performance as the integrated seat configuration (A) in Z-direction excursion.

Table 4.
Average Pre and Post Impact Dummy Z-Direction Head Excursion
50th Hybrid III Male

Restraint	*PRE IMPACT Z*	*POST IMPACT Z*
A	69.0	147.5
B	61.7	113.3
C	135.4	226.0
D	140.1	226.9
E	47.3	89.9
F	61.7	128.9
G	49.9	98.7
H	60.8	117.2
I	45.7	89.8
J	62.7	162.6

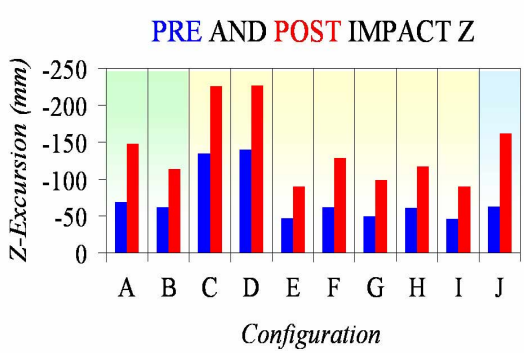

Figure 18. Average Z-direction movement for Configurations A, C, G and I.

SUMMARY

A test series focused on restraint technologies for rollover crashes was conducted with the NHTSA Rollover Restraint Tester (RRT). The 50th percentile male Hybrid III dummy was utilized. Restraints included fleet typical 3-point non-integrated seats, integrated seats, pyrotechnic retractor and buckle pretensioners, motorized pretensioners and a 4-point belt system. Pretensioners were tested in various combinations. Each configuration simulated a roof-to-ground impact at 180 degrees with an angular speed of 315 degrees/second and was repeated 3 times. Occupant excursions in the X, Y and Z direction were recorded utilizing a combination of real time and high speed cameras and analyzed with digitizing software. Configuration C is the baseline used for comparisons between treatments. All pyrotechnic devices were deployed at 45 degrees of table rotation. Motorized devices were activated at the initiation of roll. Observations from this round of testing include:

1. The RRT is a research device that provides a repeatable dynamic environment suitable for evaluating restraints in a rollover scenario.

2. Integrated seats, when compared to the baseline (C), reduced both Y (lateral) and Z (vertical) head excursions in the pre and post impact phase of the test. These reductions were up to 54%.

3. Pretensioners in all configurations effectively reduced maximum dummy head excursions in both the Y and Z-directions in pre and post-impact of the RRT.

4. Motorized retractor pretensioners (H, I) activated at the initiation of roll reduced pre-impact excursion in the Y-direction by up to 76% and Z-direction head excursion up to 66%.

5. The 4-pt belt (J), with 2 pyrotechnic retractors, reduced pre-impact Y_in motion by 63% and Z by 54%, however Y_out motion dummy head excursion increased 18% when compared to the baseline. The post impact Z excursion was reduced 28%, while the post impact Y excursion was essentially unchanged from the baseline configuration.

6. Initial results indicate that restraint technologies tailored for rollover crash events may reduce occupant excursion toward the roof.

CONTINUED WORK

Testing with the RRT is continuing. Other technologies that may have potential for restraint

during a rollover crash are also being considered. One technology is the inflatable belt previously tested in the mid 1990s. Other considerations include adding a partial cab reaction surface to allow for testing of rollover air bags and similar devices being incorporated for rollover protection.

Other testing includes evaluation of the 5th female and 95th male dummies to investigate how occupant size affects rollover crash restraint. Physical limitations of the RRT play a factor in testing the heavier occupant (95th) and adding a cab structure.

New camera equipment has been purchased to improve visual data collection. They are high speed/high g rated cameras allowing all data to be collected on-board the RRT.

A rollover modeling program has also been initiated with goals of correlating dummy kinematics with the RRT to simulated real world rollovers. Physical results from the testing are aiding in developing a computer model. This will allow evaluation of technologies and situations that may be physically restricted by the RRT.

REFERENCES

Digges, Kennerly H. "Summary Report of Rollover Crashes", FHWA/NHTSA national Crash Analysis Center, 2002, p 1-32.

Gopal et al. "Simulation and Testing of a Suite of Field Relevant Rollovers," 2004-01-0035 SAE World Congress, 2004, Detroit United States.

Rains, Glen, Jeff Elias and Greg Mowry. "Evaluation of Restraints Effectiveness in Simulated Rollover Conditions", 16th International ESV Conference Proceedings, 1998, Ontario Canada, p 1897-1910.

Rouhana et al. "Biomechanics of 4-Point Seat Belt Systems in Frontal Impacts," Stapp Car Crash Journal, Vol. 47 (October 2003), p 367-399.

DATA ANALYSIS METHODOLOGY AND OBSERVATIONS FROM ROLLOVER SENSOR DEVELOPMENT TESTS

Bridget M. O'Brien-Mitchell
Stephen J. Cassatta
Melanie A. Giasson
Robert C. Lange
Anthony G. Melocchi
General Motors Corporation
United States
Paper Number 07-0308

ABSTRACT

Although rollover crashes represent a small fraction (approximately 3%) of all motor vehicle crashes, they account for roughly 22% of crash fatalities to occupants of cars, light trucks, and vans (NHTSA Traffic Safety Facts, 2005 (1)). Of the fatally injured occupants in rollover crashes, 57% were ejected (2). With the development of advanced airbag and sensing technologies, General Motors (GM) has introduced systems intended to help mitigate the risk of head and torso ejection during a rollover crash.

The implementation of these systems was preceded by the development of a suite of rollover sensor laboratory tests designed to simulate several types of rollover initiations. Many of these tests were conducted with instrumented Hybrid III 50th percentile Anthropomorphic Test Devices (ATDs) seated in the front outboard seating positions. For tests in which an Injury Assessment Reference Value (IARV) (3) was exceeded, a methodology was developed to provide a detailed summary of the vehicle kinematics, timing of ATD contacts, ATD peak responses, and film observations.

Using this procedure, GM was able to identify common trends of peak ATD responses relative to restraint use and rollover initiation type. IARVs were shown to be exceeded in all test types, with both belted and unbelted ATDs. Although exact ATD motion was unpredictable, test type did have some effect on the location of ATD contact. In addition, the location of contact by leading side ATDs was influenced more by test type than by restraint usage. IARVs were shown to be exceeded with the vehicle at a wide range of orientations. Any impact during which the motion of the ATD head was arrested prior to stopping the ATD body showed the potential for exceeding a neck compression IARV. This was true regardless of vehicle orientation, location of the head contact, or dynamic deformation of the vehicle's structure.

INTRODUCTION

General Motors first introduced rollover crash sensors in 2005 model year mid-sized sport utility vehicles and has continued to develop this technology for other vehicle model lines during subsequent model years. The introduction of these sensors was preceded by the development of a suite of rollover sensor laboratory test types and test procedures that were used to develop the sensor calibrations for production applications. (4)

GM has conducted 176 tests during the development of the suite of rollover sensor signature laboratory test methods as well as the development of production sensor calibrations for 2005 and 2006 model year vehicles. These tests were conducted to generate vehicle sensor signatures as well as ATD kinematics for sensor calibration. The test types included:

1. Trip-over:
    a. Curb trip-over
    b. Soil trip-over
    c. Gravel trip-over
    d. Friction trip-over
    e. Curb trip-over sled
    f. Soil trip-over sled
2. Fall-over:
    a. Ditch fall-over with dirt slope
    b. Ditch fall-over with high friction slope
3. Flip-over: Corkscrew ramp flip-over
4. SAE J2114 Dolly rollover
5. Other:
    a. Half corkscrew ramp
    b. Bounce-over

The data collected were not identical across all tests, but the majority of tests included the following:

1. ATD head accelerations
2. ATD chest accelerations
3. ATD upper neck loads and moments
4. ATD lower neck compression
5. Seat belt loads, on tests with belted ATDs
6. Vehicle accelerations and roll rates

The vehicles tested included:

1. Mid-sized sport utility vehicles
2. Full-sized sport utility vehicles
3. Cross over vehicles
4. Passenger cars

The tests were conducted with belted and unbelted Hybrid III 50th percentile ATDs in the front row outboard seating positions. In many of the tests, nylon-fabric membranes were attached to the vehicle structure across the front side window openings. High-speed cameras were installed in the test vehicles to record the kinematics of the ATDs relative to the vehicle. In addition, high speed cameras were placed outside of the test vehicles to document the kinematics of the test vehicle.

CHARACTERIZATION OF ENTIRE DATASET

Test Type

A comparison of field statistics for the types of rollover initiations in the field to the 176 laboratory test dataset under analysis is shown in Figure 1. The trip-over tests make up the largest proportion of the laboratory dataset and reflect the majority of field rollover initiations (2001-2005 NASS-CDS, Cars + LTV's).

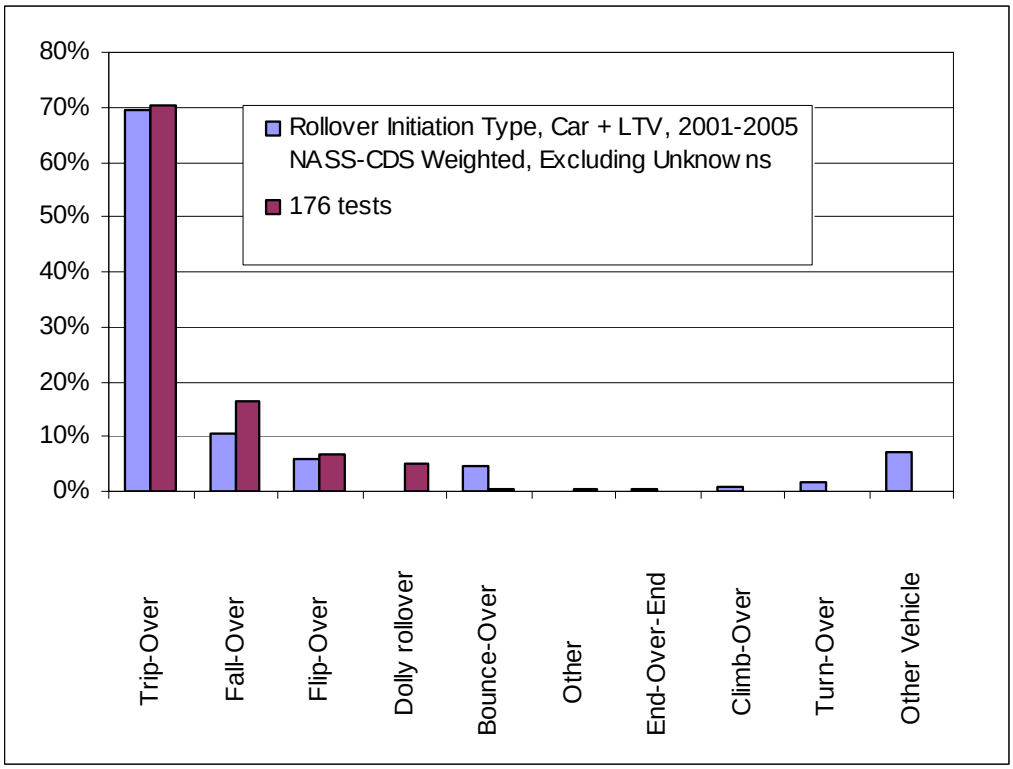

Figure 1. Distribution of test types.

Quarter Turns Achieved

Of the 176 tests under analysis, 95 resulted in a rollover of at least ¼ turn. A comparison of these 95 tests which rolled at least ¼ turn to statistics from field rollovers is shown in Figure 2. The larger proportion of laboratory tests that rolled only ¼ turn is indicative of the objective of the rollover testing itself - to develop a rollover sensing calibration. This puts an emphasis on simulating vehicle kinematics that approach and/or exceed a "threshold" in terms of vehicle rollover.

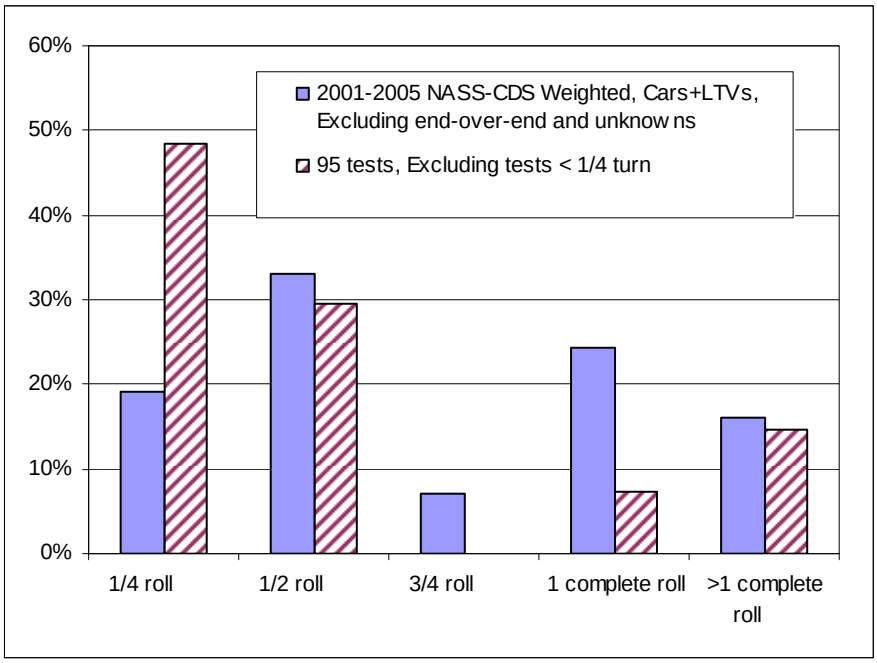

Figure 2. Comparison of field data to test data by quarter turn achieved.

CHARACTERIZATION OF TESTS WITH IARV EXCEEDED

For the 176 tests conducted, the data was sub sampled for tests in which the ATD recorded injury values which exceeded IARVs. It was observed that in the 81 tests which did not achieve at least ¼ turn, no IARVs were exceeded. Of the remaining 95 tests, 48 tests had at least one IARV exceeded.

Quarter Turns Achieved

Tables 1 and 2 show the distribution of the 176 tests conducted with and without an IARV exceeded by test type and by number of quarter turns achieved. The dataset shows 46% (81) of the tests rolled less than ¼ turn, which again reflects the objective to develop a rollover sensor calibration. Although the data shows that an IARV can be exceeded in a rollover of only ¼ turn, the majority of IARVs were exceeded in tests with multiple ¼ turns.

Table 1.
Number of quarter turns achieved – IARV not exceeded

	Number of Quarter Turns Achieved IARV not Exceeded													
	0	1	2	3	4	5	6	7	8	9	10	11	12	Total
Trip-over	68	26	3	0	1	0	2	0	1	0	0	0	0	101
Fall-over	12	5	3	0	0	0	0	0	0	0	0	0	0	20
Flip-over	0	2	2	0	0	0	0	0	0	0	0	0	0	4
Dolly	0	0	0	0	0	0	0	0	0	0	0	0	1	1
Other	1	0	0	0	1	0	0	0	0	0	0	0	0	2
All	81	33	8	0	2	0	2	0	1	0	0	0	1	128

Table 2.
Number of quarter turns achieved – IARV exceeded

	Number of Quarter Turns Achieved IARV Exceeded													
	0	1	2	3	4	5	6	7	8	9	10	11	12	Total
Trip-over	0	9	7	0	3	0	2	0	2	0	0	0	0	23
Fall-over	0	2	7	0	0	0	0	0	0	0	0	0	0	9
Flip-over	0	2	6	0	0	0	0	0	0	0	0	0	0	8
Dolly	0	0	0	0	2	0	0	0	1	1	1	0	3	8
Other	0	0	0	0	0	0	0	0	0	0	0	0	0	0
All	0	13	20	0	5	0	2	0	3	1	1	0	3	48

Restraint Condition

Direct A-to-B comparisons of specific tests were not possible due to the underlying test objective, variation in vehicle models and rollover test types, and the inherent non-repeatability of rollover testing. Therefore, observations focused on the dataset of 95 tests (190 ATDs) in which a rollover of at least ¼ turn was achieved. Table 3 and Table 4 show the distribution of restraint usage for the various test types in tests which rolled at least ¼ turn.

Table 3.
Leading side ATD in tests which rolled at least ¼ turn

	Unbelted		Belted	
	IARV Not Exceeded	IARV Exceeded	IARV Not Exceeded	IARV Exceeded
Trip-over	7	6	41	2
Fall-over	2	3	7	5
Flip-over	0	1	7	4
Dolly	0	3	4	2
Other	0	0	1	0
All	9	13	60	13

Table 4.
Trailing side ATD in tests which rolled at least ¼ turn

	Unbelted		Belted	
	IARV Not Exceeded	IARV Exceeded	IARV Not Exceeded	IARV Exceeded
Trip-over	3	10	33	10
Fall-over	2	3	11	1
Flip-over	0	1	5	6
Dolly	0	3	1	5
Other	0	0	1	0
All	5	17	51	22

For this dataset, 14 of the 44 unbelted ATDs did not have an IARV exceeded, while 111 of the 146 belted ATDs did not exceed an IARV. Therefore, 68% of the unbelted ATDs and 24% of the belted ATDs exceeded an IARV. This suggests the likelihood of an ATD exceeding an IARV decreases with the use of belts, which is consistent with observations of rollover field data (5).

The seat belt types included all-belts-to-seat (ABTS) as well as belt-to-pillar configurations. Retractor pretensioners or buckle pretensioners were included in some belted tests. However, the small size of the dataset precludes analysis of the effects of seat belt configuration, anchor location, and pretensioner type.

DATA ANALYSIS METHODOLOGY

A summary chart was created for each ATD in the 48 tests that had at least one IARV exceeded. This involved a total of 26 leading side ATDs (13 belted, 13 unbelted), and 39 trailing side ATDs (22 belted, 17 unbelted). An example summary chart is shown in Figure 3.

The chart is a tool used to develop a one-page summary of the rollover test. The x-axis represents time in milliseconds, while the y-axis reflects the roll angle of the vehicle. The time at which a peak value occurred is plotted on each chart, along with the appropriate data label. Data labels in bold show peak ATD loads that exceeded the IARV, while those in italics show observations estimated from film. Film observations may include items contacted by the ATD, as well as estimated timing of dynamic vehicle upper structure deformation. Pictures of the vehicle and ATD orientation at the time at which an IARV was exceeded are also included.

In Figure 3 for example, two IARVs were exceeded on the trailing side ATD during a single impact -- head contact to the leading side B-pillar. At this point in the rollover, the vehicle has achieved only 52 degrees of roll angle.

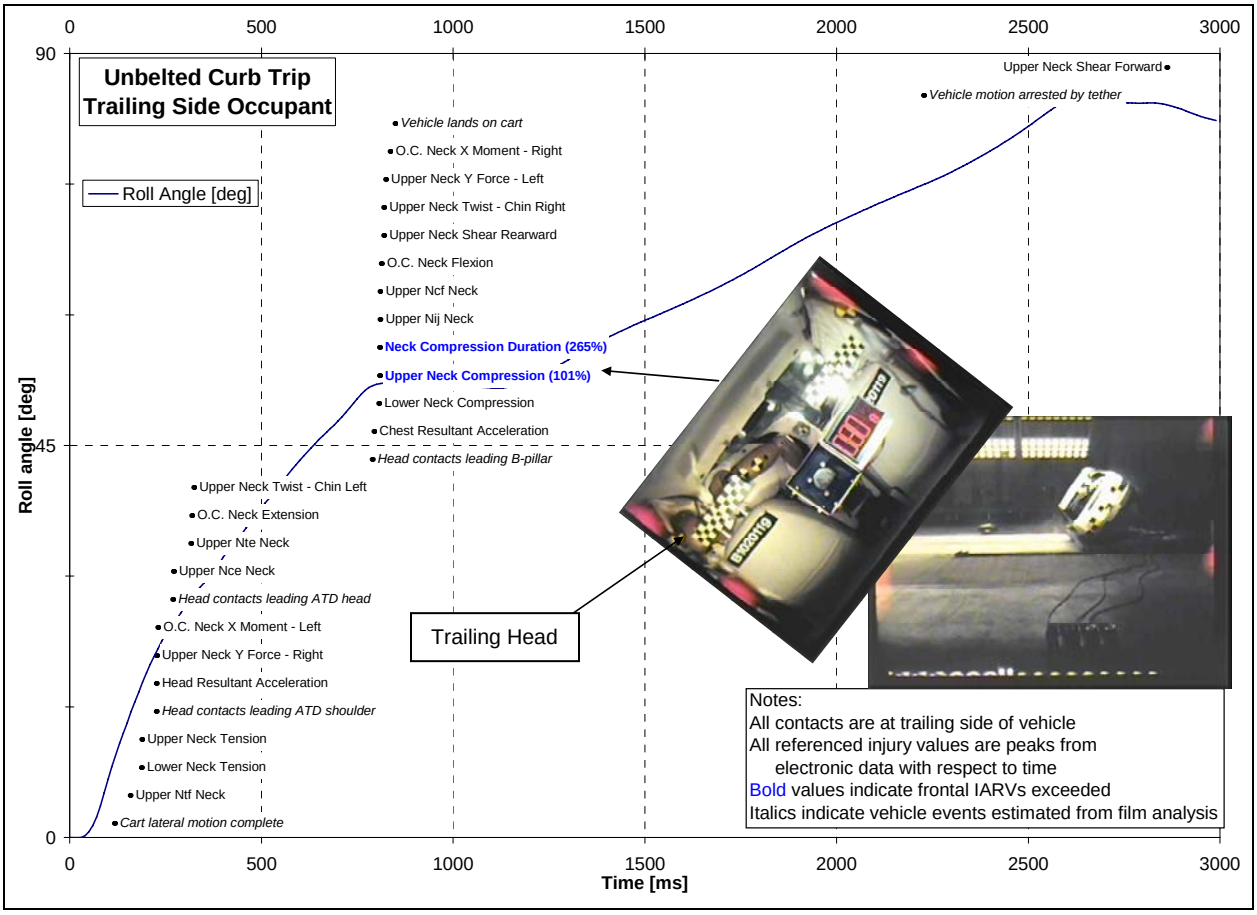

Figure 3. Sample summary chart.

DATASET OBSERVATIONS

The 48 tests with at least one IARV exceeded were analyzed by IARV type, ATD contact location, test type, and restraint usage.

IARV type

The distribution of types of IARVs exceeded on leading side and trailing side are shown in Figure 4 and Figure 5, respectively. For these tests, the following IARVs were grouped as follows:

1. One upper neck compression IARV was 'counted' if an ATD response exceeded the peak upper neck compression IARV and/or the peak upper neck compression time duration IARV.
2. One lower neck compression IARV was 'counted' if a peak lower neck compression IARV was exceeded.
3. One Nij IARV was 'counted' if one or more Nij (i.e. Ntf, Nce, Nte, Ntf) were exceeded.
4. One HIC IARV was 'counted' if a test exceeded the 15ms and/or 36 ms HIC.
5. The 'Other Neck IARVs' included upper neck shear rearward, upper neck occipital condoyle moment left, upper neck occipital condoyle flexion and upper neck occipital condoyle extension.

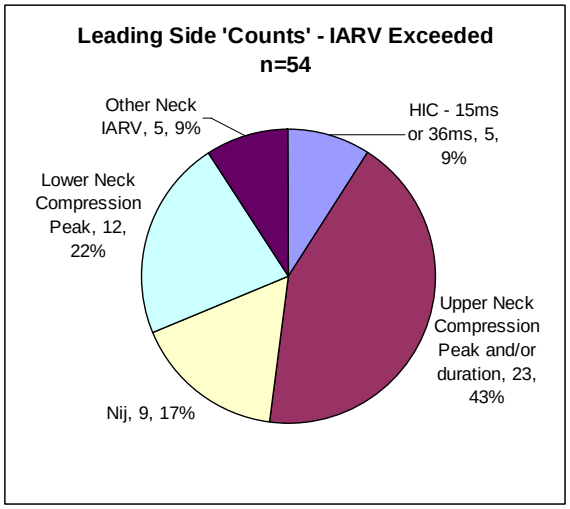

Figure 4. Leading side 'counts' – IARV exceeded.

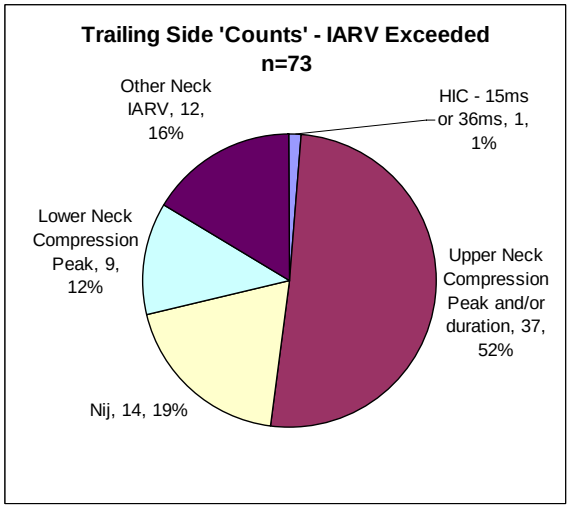

Figure 5. Trailing side 'counts' – IARV exceeded.

Of the 96 ATDs in the 48 tests, 65 ATDs had at least one IARV exceeded for a total of 127 'counts'. The distribution of exceeded IARVs is similar between leading and trailing side ATDs except for Head Injury Criteria (HIC), which has a larger proportion on the leading side. The lone example of a HIC IARV being exceeded by the trailing side ATD was the result of ATD to ATD contact.

ATD Contact Location

A description of the categories used to describe the locations of contact, with associated example photographs showing vehicle orientation and ATD orientation relative to the ground, is as follows:

1. Head contact to leading side door at beltline: The unbelted leading side ATD moved toward the trailing side and then moved back toward the leading side resulting in head contact to the leading side door (Figure 6).

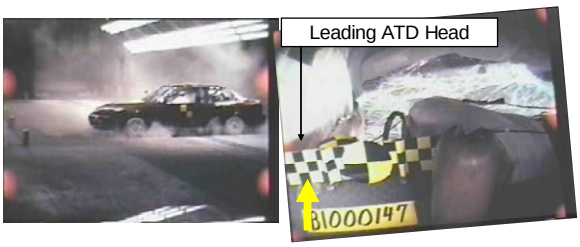

Figure 6. Head contact to leading side door at beltline.

2. Head contact to ground - convertible: The head of the belted ATD contacted the ground through

the open convertible roof. The convertible roof was not in a closed position for the tests.

3. Head to leading/trailing side structure at event arrest: These tests were corkscrew ramp flip-over tests where the vehicle was arrested by contacting a row of jersey barriers that were placed in front of the building wall. The time at which the vehicle contacted the jersey barriers is considered to be the event arrest.
4. Head contact to ground or ground/roof rail on leading side: The head of the leading side ATD either contacted the ground through the leading side window membrane (a more lateral outboard motion) or the contact was to the ground with the head in contact with both the leading side roof rail and membrane (a more vertical outboard motion) (Figure 7).

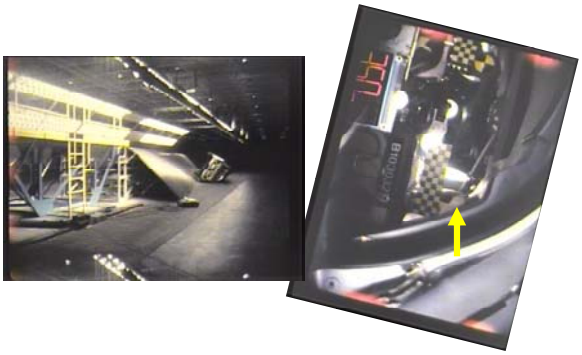

Figure 7. Head contact to ground/roof rail.

5. Head contact to leading/trailing side structure: The head contacted the roof rail, door frame, roof etc. on the leading/trailing side of the vehicle (Figure 8).

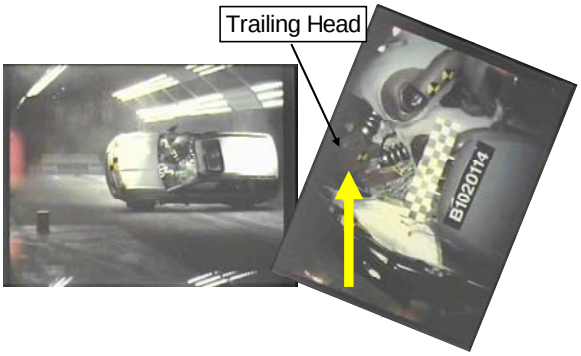

Figure 8. Head contact to leading side structure.

6. Head contact to ground through leading side membrane: The unbelted trailing side ATD moved toward the leading side and contacted the leading side window membrane which was in contact with the ground due to vehicle orientation. (Figure 9).

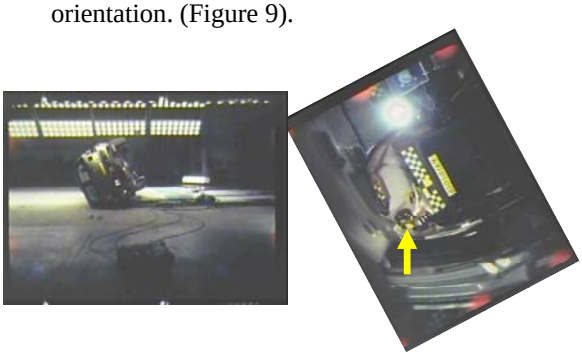

Figure 9. Head contact to ground through leading side membrane.

7. Head contact to leading side window membrane: The unbelted trailing side ATD moved toward the leading side and was arrested by the leading side window membrane when the leading side of the vehicle was not in contact with the ground (Figure 10).

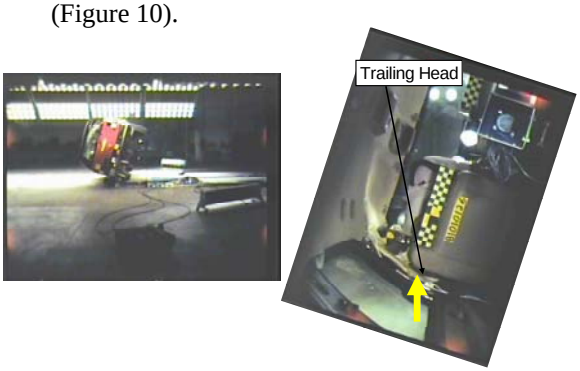

Figure 10. Head contact to leading side window membrane.

8. Head contact to leading side ATD: The head of the trailing side ATD contacted the leading side ATD (Figure 11).

Figure 11. Head contact to leading side ATD.

9. Head contact to ground/roof rail on trailing side: The trailing side ATD contacted the trailing side roof rail and window membrane which were in contact with the ground.
10. Insufficient film length/No onboard lights: In some tests, the onboard camera ran out of film prior to the ATD contact or the onboard lights were lost for the entire test, so ATD contacts were not visible.

A summary of the locations of contact for a leading side ATD impact during which an IARV was exceeded is shown in Figure 12. The summary for the trailing side is shown in Figure 13. It should be noted that multiple contacts during which an IARV was exceeded occurred in some tests, resulting in 71 contacts during which IARVs were exceeded for the 65 ATDs.

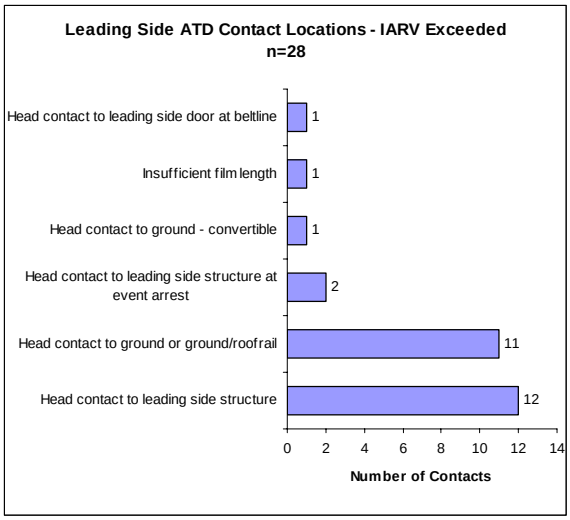

Figure 12. Leading side ATD contact locations – IARV exceeded.

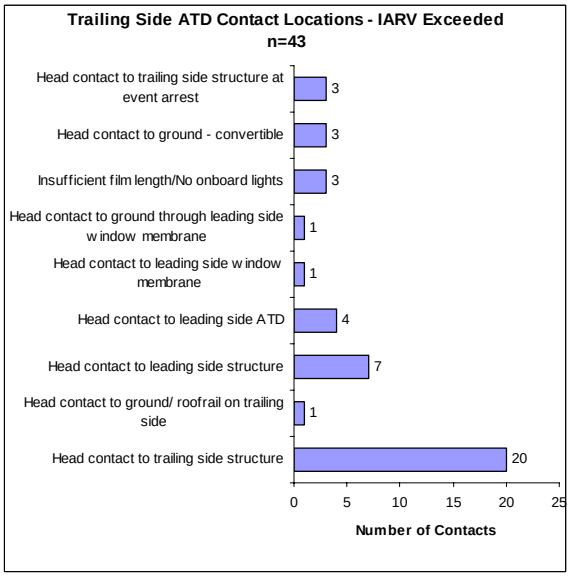

Figure 13. Trailing side ATD contact locations – IARV exceeded.

Figure 12 and Figure 13 demonstrate the complex nature of ATD motion in a rollover. Although 82% of leading side ATD contacts were with structure and/or ground, the location of contact varied. For instance, in one test, the ATD head contact was to the leading side door at the belt line, with the vehicle on its wheels (Figure 6). On the trailing side, 63% of trailing side ATD head contacts occurred with the leading or trailing side structure. IARVs were also exceeded through contact to the leading side ATD and through restraint provided by the leading side window membrane.

ATD Contact Location by Test Type

Table 5 shows the leading side ATD contacts during which an IARV was exceeded for each rollover initiation type.

Table 5.
Leading Side ATD contacts during which an IARV was exceeded – by test type

	Trip-over	Fall-over	Flip-over	Dolly rollover
Head contact to leading side structure	4	0	3	5
Head contact to ground or ground/roofrail	3	8	0	0
Head contact to leading side structure at event arrest	0	0	2	0
Head contact to ground - convertible	0	0	1	0
Insufficient film length	1	0	0	0
Head contact to leading side door at beltline	0	0	0	1

All of the fall-over tests involved ATD head contact to ground or ground/roof rail. This was due to the relatively low vehicle angular rate that is characteristic of this test methodology. In these tests, ATD motion is influenced largely by gravity, leading to motion that is primarily lateral with respect to the vehicle. In contrast, the relatively high angular rates associated with flip-over and dolly rollover tests

resulted primarily in ATD head contact with the leading side structure as the ATD moved upward and outward.

In trip-over tests, leading side ATD contact location was more varied. At trip initiation, the deceleration of the vehicle is primarily lateral, leading to lateral motion of the ATD relative to the vehicle. As the vehicle's lateral motion is converted to angular rotation, ATD motion becomes more upward and outward. For some tests, this resulted in ATD head contact to the leading side structure, while in others the ATD struck the ground or ground/roof rail.

Table 6 shows the trailing side ATD contacts during which an IARV was exceeded by test type. The various angular rates associated with the different test methodologies again played a role in the amount of upward and outward motion of the ATD.

Table 6.
Trailing Side ATD contact locations during which an IARV was exceeded – by test type

	Trip-over	Fall-over	Flip-over	Dolly rollover
Head contact to ground - convertible	2	0	1	0
Head contact to trailing side structure	8	1	4	7
Head contact to ground/ roofrail on trailing side	1	0	0	0
Head contact to trailing side structure at event arrest	0	0	3	0
Head contact to leading side structure	2	3	0	2
Head contact to leading side ATD	4	0	0	0
Head contact to leading side window membrane	1	0	0	0
Head contact to ground through leading side window membrane	1	0	0	0
Insufficient film length/No onboard lights	2	0	0	1

ATD Contact Location by Restraint Usage

Figure 14 and Figure 15 show a comparison between belted and unbelted leading side ATDs in terms of their contact locations. The distribution of contact locations does not appear to be affected by belt usage for the leading side ATD.

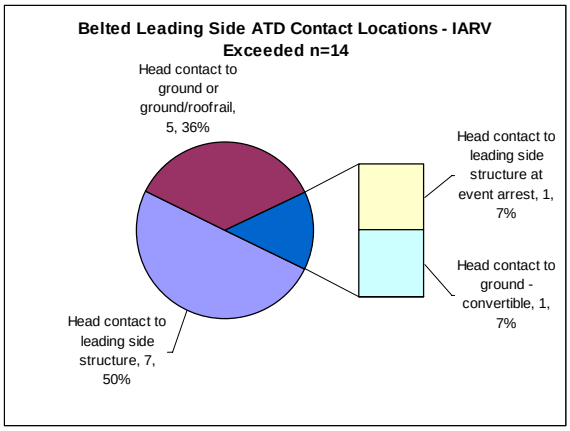

Figure 14. Belted leading side ATD contact locations with IARV exceeded.

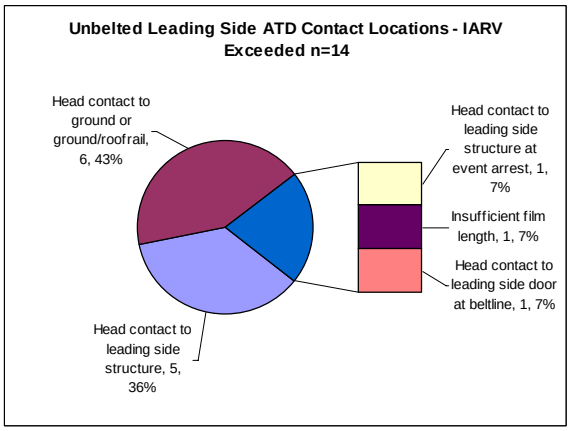

Figure 15. Unbelted leading side ATD contact locations with IARV exceeded.

Figure 16 and Figure 17 show the distribution for contact locations for belted and unbelted trailing side ATDs demonstrating that belt usage strongly influenced the trailing side ATDs contact location.

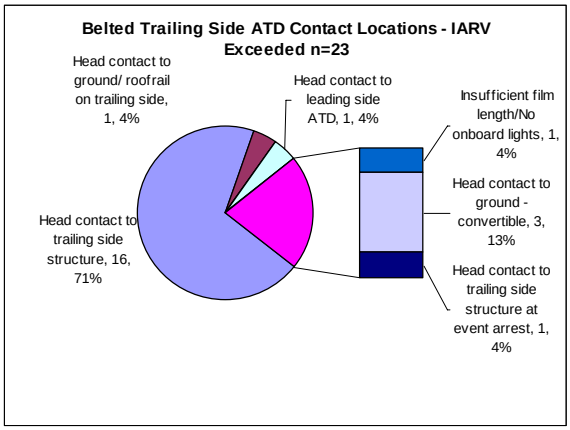

Figure 16. Belted trailing side ATD contact locations with IARV exceeded.

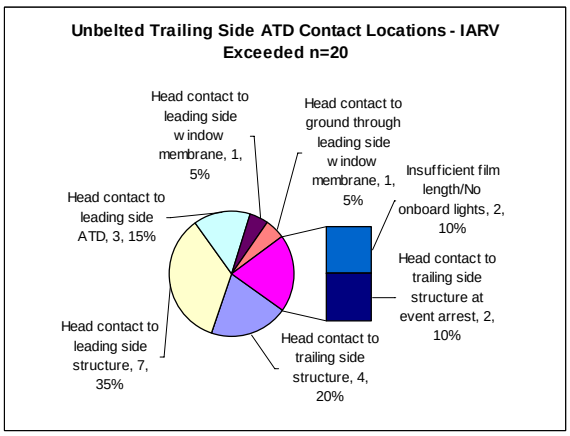

Figure 17. Unbelted trailing side ATD contact locations with IARV exceeded.

For the belted ATDs, contact occurred primarily to the trailing side structure, although belt usage did not preclude head contact with the leading side ATD (Figure 18).

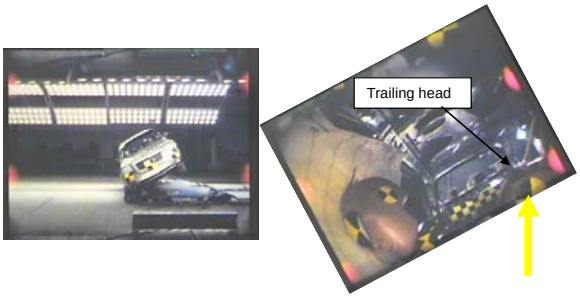

Figure 18. Belted ATD head contact to leading side ATD.

For the unbelted trailing side ATDs, 60% of the contacts occurred on the leading side of the vehicle, while only 20% were to the trailing side structure.

Table 7 shows the number of quarter turns and vehicle orientation for the contacts, summarized by restraint usage. For the leading side ATD, the vehicle orientation at the contact did not show a significant difference for belted or unbelted ATDs. For the trailing side, however, the trend differs. The unbelted trailing side ATDs show the majority of contacts when the vehicle is on the leading side, as the unbelted ATD moves from the trailing side to the leading side, whereas the majority of belted contacts occurred when the vehicle was on the roof.

Table 7. Restraint condition and ATD location in contacts with IARV exceeded by vehicle orientation

	Restraint usage - Contacts by vehicle orientation			
	On wheels	On leading side	On roof	On trailing side
Unbelted Leading Side	1	10	2	1
Belted Leading Side	0	11	3	0
Unbelted Trailing Side	3	15	2	0
Belted Trailing Side	1	3	19	0
Sum:	5	39	26	1

HIC and ATD Contact Location

For leading side ATDs, HIC IARVs were only exceeded during fall-over tests as a result of head to ground contact. However, head to ground contacts occurred during other tests without the HIC IARV being exceeded. In addition, one test demonstrated that it is possible that the HIC IARV could be exceeded without exceeding any additional IARVs.

On the trailing side, the HIC IARV was exceeded once, due to belted trailing side ATD head contact with the shoulder of the leading side ATD (Figure 18).

Upper Neck Compression and ATD Contact Location

As shown in Figure 4 and Figure 5, approximately ½ of the IARVs exceeded were due to upper neck

compression loading. Figure 19 and Figure 20 show the distribution of contact locations during which the upper neck compression IARV was exceeded.

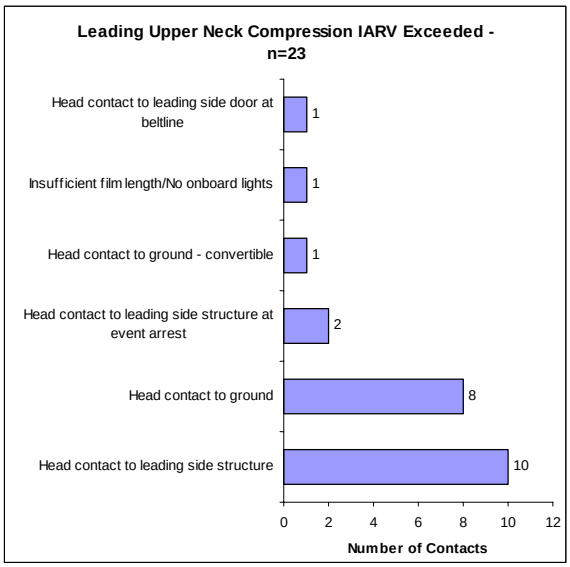

Figure 19. Leading side ATD upper neck compression IARV exceeded – ATD contact location.

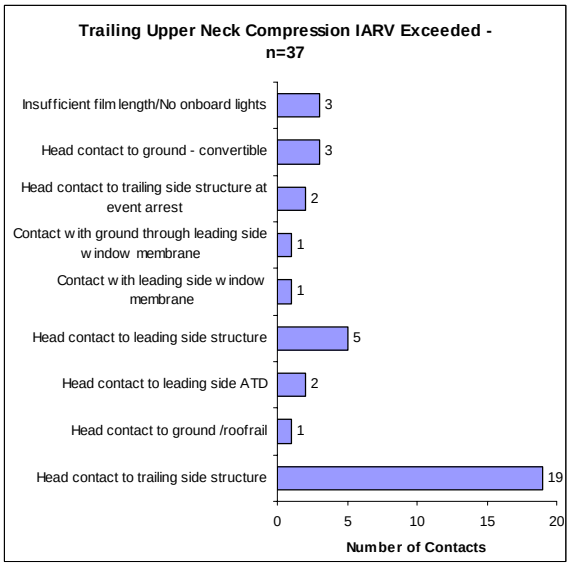

Figure 20. Trailing side ATD upper neck compression IARV exceeded – ATD Contact Location.

Table 8 shows the vehicle orientation for tests during which the upper neck compression IARV was exceeded. As demonstrated in Figure 19 and Figure 20, upper neck compression IARVs were exceeded through contact with the ground, door, roof rail, roof, window membrane or the other ATD. Any contact during which the motion of the ATD head was arrested prior to stopping the ATD body showed the potential for exceeding a neck compression IARV. This was true regardless of vehicle orientation, location of the head contact, or dynamic deformation of the vehicle's structure, as shown in Figures 6 through 11.

Table 8.
Restraint condition and ATD location in tests with upper neck compression IARV exceeded by vehicle orientation

	Restraint usage - Contacts by vehicle orientation Neck compression IARV exceeded			
	On wheels	On leading side	On roof	On trailing side
Unbelted Leading Side	1	9	1	1
Belted Leading Side	0	9	2	0
Unbelted Trailing Side	2	12	2	0
Belted Trailing Side	0	3	18	0
Sum:	3	33	23	1

Lower Neck Compression Peak

For the leading side ATDs with lower neck load cells installed, there were two tests in which the upper neck compression and lower neck compression IARVs were not both exceeded during the same impact. This was likely due to the ATD orientation during loading. In one of these tests, the upper neck aft shear IARVs were exceeded and in the other, the Ncf (Neck compression-flexion) IARV was exceeded, demonstrating the off-axis nature of the neck loading in these impacts. When the loading of the neck was primarily axial, the magnitudes of the upper and lower neck compressions were similar.

For the trailing side ATDs with lower neck load cells installed, lower neck compression peaks did show an associated IARV exceeded for the upper neck compression, due to the more axial nature of loading.

Nij

The Nij IARV was exceeded in 9 impacts for the leading side ATD and a single impact for the trailing side. There were no cases in which the Nij was the only IARV exceeded.

CONCLUSIONS

General Motors has conducted 176 laboratory-based rollover sensor signature tests for developing test methods as well as for development of rollover sensor calibrations for 2005 and 2006 model year vehicles. These tests have a distribution of rollover initiation type that is similar to field frequencies.

The tests were conducted with a combination of restraint characteristics – unbelted, belted with and without retractor and buckle pretensioners, with belts mounted to pillars and with all-belts-to-seat configurations. For this dataset, the likelihood of an ATD exceeding an IARV decreases with the use of belts.

General Motors has developed a method for evaluating ATDs in a rollover test in which an IARV was exceeded. This method distills a complex crash test into a one page summary chart. This summary chart shows the times of peak injury assessment values, the vehicle roll angle, vehicle and ATD contacts, ATD orientation relative to the vehicle and ground, and vehicle orientation relative to ground.

An analysis of ATD contact locations in the vehicle during which an IARV was exceeded demonstrates the complex nature of ATD motion during rollover crashes. IARVs can be exceeded through contact to:

1. The vehicle structure on the leading side of the vehicle (roof, pillars, roof rail, etc)
2. The vehicle overhead structure on the trailing side of the vehicle (roof, pillars, roof rail, etc)
3. The vehicle door at the belt-line
4. The other ATD
5. The nylon-fabric membrane covering the window
6. The ground through an open convertible roof
7. The ground through the window membrane

ATD motion and location of contact during which an IARV was exceeded can be affected by ATD location, test type, and restraint usage.

For leading side ATDs, tests with lower angular rates led to ATD motion that was influenced primarily by gravity, leading to head contact to the window membrane and the ground. For tests with higher angular rates, the ATD motion was primarily upward and outward, leading to contacts with the vehicle structure on the leading side. Restraint usage did not show a significant effect on ATD motion for the leading side ATDs.

On the trailing side, however, the trends differed. The motion of the ATD was influenced primarily by the restraint condition and did not appear to be significantly affected by test type. Belted trailing side ATDs primarily contacted the trailing side structure when an IARV was exceeded. Unbelted trailing side ATDs primarily made contacts on the leading side of the vehicle. Contact locations included impacts to the leading side structure, ATD, window membrane, and the ground through the leading side window membrane.

An evaluation of vehicle kinematics, quarter turn, and orientation during ATD contacts with an associated IARV exceeded showed that an IARV can be exceeded with the vehicle at any orientation and at any number of quarter turns.

An analysis of this dataset showed that it is possible that the HIC IARV could be exceeded without exceeding any additional IARVs. The only ATD contacts during which HIC IARV was exceeded were head to ground contacts through the window membrane.

In addition, the analysis showed that neck compression IARVs could be exceeded with the vehicle at any orientation, independent of belt usage, and through any contact during which the head of the ATD stopped moving prior to the rest of its body. These ATD contacts occurred with the ground, door, roof rail, roof, window membrane or the other ATD.

REFERENCES

1. NHTSA Traffic Safety Facts 2005, National Center for Statistics and Analysis, National Highway Traffic Safety Administration, DOT-HS-810-631
2. 2005 Fatality Analysis Reporting System
3. Mertz, H.J, et. al.., "Biomechanical and Scaling Bases for Frontal and Side Impact Injury Assessment Reference Values." Stapp Car Crash Journal, 2003. 47:p. 155-188
4. O'Brien-Mitchell, Bridget M., et. al. "Rollover Sensor Signature Test Development:, SAE 2007-01-0375, Warrendale, PA. Society of Automotive Engineers, 2007
5. Padmanaban, Jeya, et. al.. "Factors Influencing the Likelihood of Fatality and Serious/Fatal Injury in Single Vehicle Rollover Crashes", SAE 2005-01-0944, Warrendale, PA. Society of Automotive Engineers, 2005

APPLICATION OF NUMERICAL METHODS TO THE SIMULATION OF THE EARLIEST STAGES OF THE AIRBAG DEPLOYMENT.

D. Muñoz[1], J. Carlón[1], A. Negro[1], A. Mansilla[1,2], R. Martín[1]
[1] Fundación CIDAUT
[2] Department of Mechanical Engineering and Engineering of Materials. University of Valladolid
Spain
Paper Number 07-0309

ABSTRACT

The application of numerical techniques to the study of the phenomena that occur during the first milliseconds after the activation of the airbag until recently has remained out of reach, due to the high complexity of the problem. On the one hand, the highly dynamic evolution of the gas produced by the inflator invalidates the hypothesis of uniform pressure within the volume. On the other hand, the simulation of the airbag opening involves problems such as the creation of extremely complex meshes representing the folded bag inside its housing, characterization of the behaviour of strain rate dependent materials, breaking of seam lines, etc.

During the last years several simulation packages have introduced modules to reproduce the gas flow inside the airbag, but experimental methods most commonly used to validate simulations involving airbags are not able to deal with the high speed and lack of accessibility that characterize this stage of the airbag deployment.

The objective of the present studies is the determination of the capability of these simulation tools to be used in the design of parts with attention to the loads produced during the opening of the airbag. This will help us not only to improve the development and integration of components, but, in later steps, also to provide airbag models able to be applied with guarantee in the simulation of OOP. In order to do this, a combined methodology using simulation and instrumentation has been defined, based on the development of numerical models using the FEM software PAM-CRASH and its module for simulation of fluids based on the algorithm FPM. These models have been validated with experimental tests specifically designed for this task. This paper intends to introduce the characteristics of the different stages of the airbag deployment and shows some of the results of the mentioned studies.

INTRODUCTION

As is well known, airbags are devices designed to provide protection to the users of vehicles during crash events. They are part of the so-called restraint system, which includes the different elements that help to reduce the damage to the occupants in case of accident, minimizing the loads necessary to adapt their movement to the movement of the car. Two of the main requirements of the airbags are in conflict. On the one hand, they should remain unseen until they are necessary, occupying as little space as possible. On the other hand, in case of accident they must fill the maximum available volume between the passenger and the parts of the interior of the vehicle that could harm him, in order to allow a progressive transmission of energy. In this case the airbag must reach its working position only a few milliseconds after the vehicle is impacted. To deal with these contradictory functions, the airbag is generally composed of a bag originally folded within a volume defined by mobile parts destined to open, allowing the way out (in order to generalize among the different types of airbag we will refer to them as “cover”), and a more or less rigid surface whose mission is to fasten the base of the bag and to orient its deployment in the desired way (it will be referred to here as “frame”). A very short time after the impact, the airbag receives a trigger signal, which causes an element commonly called generator or inflator to begin to inject gas into the bag. At a certain moment the pressure becomes high enough to open the cover, allowing the bag to unfold to its final position, where it is ready to receive the occupant. During these very rapid processes, the components of the bag, cover and frame can support pressures up to several bars, accelerations of several thousands of g’s and speeds over a hundred meters per second. Additionally, the violence of the deployment makes it potentially dangerous for occupants located in the deployment region. These situations are called “Out Of Position” or simply OOP.

The revision of the American standard FMVSS 208 [1] limiting the aggressiveness of the airbags in OOP situations has led the airbag manufacturers to look for “low risk deployment” properties in their products. This has introduced a higher complexity in the design of the airbag in regard to its opening and deployment functions, as it is expected not only to do it “quickly”, but also “softly”. The number of design parameters related to these functions makes it very desirable to count on numerical tools allowing the simulation of the process instead of testing expensive prototypes.

Finite Elements Method (FEM) based software have been widely employed in the design and development of restraint systems, focusing normally on the function of protecting the occupant once the airbag is deployed. For this task the airbag is simulated as a closed mesh of flat elements affected by a homogeneous field of pressure representing the gas. The hypothesis of uniform pressure within the whole volume of the airbag is quite accurate in this case, but it is very far from being applicable to the first moments of the deployment. To simulate correctly these phenomena we need to reproduce in some way the dynamics of the gas evolving within the folded bag.

Several software developers have accepted the challenge and have introduced modules of simulation of compressible fluids within their simulation packages. The most extended are LS-DYNA (introducing ALE), MADYMO (CFD) and PAM-CRASH (FPM) [2][3]. While the first two are based on the coupling of an eulerian mesh reproducing the fluids with a lagrangian mesh representing the solids, the third one is based on a meshless algorithm called Finite Pointset Method (FPM) [4]. This code fills the volume inside the bag with a cloud of points, as shown in Figure 1, and calculates a set of thermodynamic variables on them, including pressure, density, speed and temperature, relating them by interpolation to the neighbouring points. Finally, it calculates the transmission of momentum between the FPM points and the lagrangian mesh representing the bag.

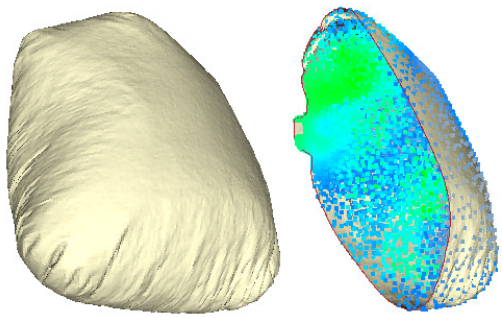

Figure 1. Simulation of airbag using FPM (external skin and section showing FPM points).

The studies presented in this paper were defined according to two main objectives:

1. To evaluate the capability of these numerical methods to be used as tools in the development of airbags, paying attention to three main scenarios: The interaction between the airbag and its surrounding parts during the process of opening, the kinematics during the deployment and, finally, the interaction of the airbag with an occupant in an OOP situation. PAM-CRASH and its module FPM were chosen to perform the simulations.

2. To develop a complete methodology of work, including numerical and experimental tools, designed according to the particularities and needs of each of the three designated scenarios.

METHODS

In order to achieve these objectives, it was necessary to find solutions to an important number of questions related to each one of the scenarios, so it was decided to face each one of them according to their logical order. First of all, we analyzed the problematic of the interactions during the opening of the cover. Once this part was properly solved we proceeded to the deployment analysis, and then we made the airbag interact with a mannequin in OOP. The numerical models used in each of the studies were related to the ones obtained as results in the previous steps and adapted to the needs of the new scenario.

The first step was to analyze the problematic of each of the scenarios using the available information in order to choose the most appropriate way to validate experimentally our numerical models. As a result of these previous analyses, three stages were defined in the deployment of the airbag.

Due to the complexity of the first scenario, which included problems involving the modelling of the folded bag and the inflator on the one hand, and on the other hand the modelling of their environment, including plastic materials and the breaking of seam lines, it was decided to incorporate a prior step in which the assembly bag-generator was validated separately within an environment easier to simulate. This gave us the chance to validate the capability of FPM to reproduce the loads of the deployment in a housing not only easier to simulate, but also easier to measure. These studies were denominated “in Controlled environment”.

The airbag chosen for the analysis was a passenger side frontal airbag, with the particularity of having and integrated cover, which made it unnecessary to use and model the rest of the dashboard. This simplified both the simulations and the tests. The housing was composed of a metallic base and a plastic component in Polypropylene with EPDM, as shown in Figure 2. This element played the roles of being the cover and a part of the frame simultaneously. The design of this element included a set of weakened points with the function of a breakable seam line.

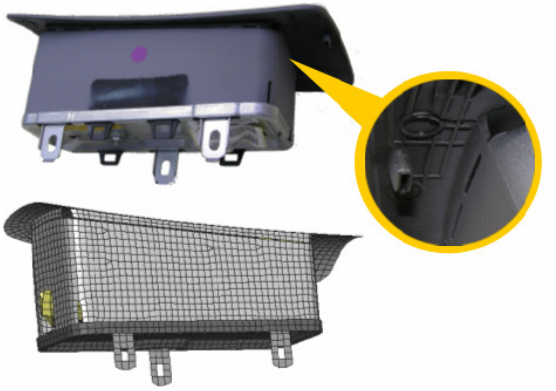

Figure 2. Airbag module with detail of the seam line and numerical model.

The gas generator had only one phase, so it was not possible to include the modification of the mass flow in our studies. It was composed of the inflator itself and a metallic diffuser with a hole allowing for the orientation of the gas towards the cover. The bag was made up of one single volume, with two circular ventings open during the entire deployment and without any strap to control or modify its external shape.

In order to evaluate the capacity of the numerical tools to deal with changes in the design, several modifications were introduced to the models. These modifications were designed taking into account that they should also be easy to perform in the physical components. This allowed us to count on a set of models with the following variables:

1. Folding pattern. Instead of using the original folding pattern of the airbag, Leporello (LE) and Rolling (RO) patterns were chosen because different behaviour was expected during the deployment (Figure 3).

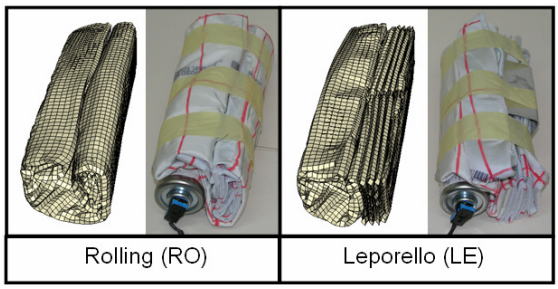

Figure 3. Folding patterns used in the studies.

2. Diffuser. Four diffuser geometries were introduced in order to produce different directions of the gas flow (Figure 4). The first one (Diffuser 1 or Dif 1) was the original one, with radial orientation of the gas flow towards the cover. In the second one (Dif 2) the diffuser was modified in order to get a more or less axial orientation of the gas flow, which should avoid the local concentration of pressure under the cover and produce a more homogeneous distribution of loads. The geometries of diffuser 3 and 4 (Dif 3 and Dif 4) were obtained rotating the original diffuser 54 and 32 degrees respectively with regard to the axis of the generator, in order to redirect the gas flow and originate different zones of concentration of pressure.

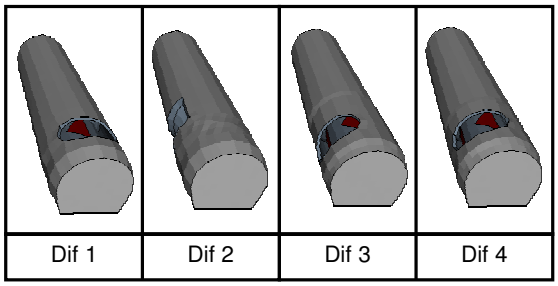

Figure 4. Generators and diffusers employed in the studies.

3. Resistance to the opening of the cover. In order to introduce this variable easily, approximately half of the points that composed the breakable seam line were removed from the model. The original part and the weakened one were named Cover 1 (C1) and Cover 2 (C2) respectively.

The resultant array included 16 cases, which enabled us to evaluate the influence of each variable and to choose the most interesting cases to be performed experimentally. Not all the cases were simulated or tested in each scenario. They were selected according to the particular requirements of the different studies.

The experimental methodologies employed were designed specifically, taking into account the particular needs of each study. Several series of tests were performed in parallel to the development of the numerical works. First of all, a test bench was designed for the tests in controlled environment. Secondly, highly instrumented airbag deployment tests were used simultaneously for the studies of the interaction against real environment and kinematics of deployment. Finally, out of position tests were carried out in several configurations.

On the numerical side, different models were defined according to each scenario. Most of the parameters that helped us to reach good results in the studies of controlled environment were kept in the rest of the models, in order to analyze the

predictability of the method. The smoothing length (associated to the number of FPM points) was modified in the different scenarios in order to keep a balance between accuracy and reasonable calculation times, which varied from an average of eight hours in the simulations of controlled and real environments, more detailed and with only 15 milliseconds of simulation, up to an average of 24 hours in the simulations of out of position tests, less detailed but arriving at 50 milliseconds of simulation. The calculations were performed on a two processors Linux based platform using PAM-CRASH v2005.

STAGES OF AIRBAG DEPLOYMENT

In the process of the deployment of an airbag different phases can be observed. A basic analysis of the processes that occur in each of them will help us to understand the phenomena associated to each of our scenarios.

Observing the evolution of the pressure and volume of the airbag we can define three main stages (see Figure 5):

1. First stage: The first stage begins when the generator starts to inject gas into the bag. At this stage the airbag is contained by its housing and cover, which prevent it from deploying freely. Due to this limitation of the available volume the pressure of the gas within the bag increases quickly, making the fabric push against its environment. At a certain moment the pressure grows enough so as to burst the seam that maintains the cover closed. The loads produced in this interaction depend not only on the gas generated, but also on the resistance opposed by the environment to the growing of the volume of the airbag.

2. Second stage: When the cover begins to open, the bag starts to protrude, being able at this point to increase its volume. Then the second stage begins, in which the bag leaves the case. Due to the difference between the atmospheric pressure and the pressure achieved in the airbag during the first stage, the bag tends to go out of the frame very quickly, producing an expansion of the available volume and, consequently, a drop in the pressure inside the bag. At the beginning of this stage the pressure is still high, and the bag is propelled violently. This situation, known as "Punch Out", is the most potentially dangerous for occupants placed too near the airbag (OOP situations). When the pressure inside the airbag has become closer to the atmospheric pressure, the bag keeps on developing until there is no more folded fabric in the case.

3. Third stage: Once all the fabric is outside the housing, the volume can still grow until the bag is completely filled. This is due to changes in the shape. Then the volume is limited again, this time by the bag, and the pressure grows again, due to the fact that the generation of gas still continues. This time the pressure grows much more slowly and the levels reached are generally lower than the ones reached during the first phase. At this point we can consider that the deployment has finished and that the airbag is ready to receive the occupant. From this stage we can generally accept the hypothesis of uniform pressure within the volume of the bag.

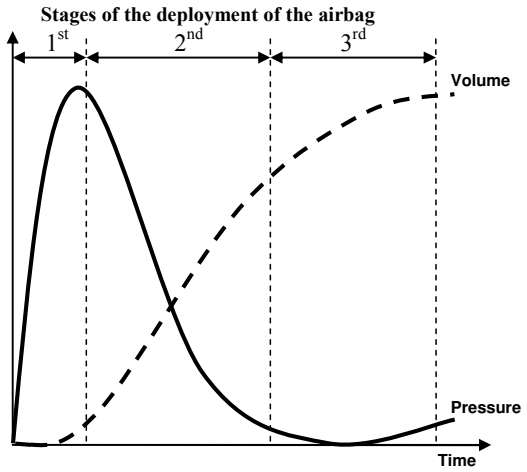

Figure 5. Typical evolution of the pressure and volume of an airbag during the different stages of its deployment.

Following this approach, our first scenario (the interaction of the airbag and its environment up to the opening) includes the entire first stage and the beginning of the second. The kinematics of the deployment (our second scenario) will be linked to the second and third stages, and the Out Of Position will be related mainly to the second stage.

CONTROLLED ENVIRONMENT

The simulation of the opening of a whole airbag includes several points that stretches the limits of the capabilities of the current state of the art techniques. On the one hand, we have the simulation of the folded bag, the generator and the gas itself, whose behaviour at this stage is highly dynamic and cannot be considered in any way as homogeneous. These elements compose what we could call "the active part" in the process of opening. On the other hand, we also need to simulate the housing and the cover, which include plastic components deformed at high strain rates, breakable parts, etc. These components constitute

the "reactive" part of the opening, restraining the deployment of the airbag until the cover is open.

In order to limit the uncertainties of the whole system, a controlled environment was designed, with the advantages of being easy to simulate and with a high degree of instrumentation in order to allow a complete validation of the numerical models. Only airbags with serial diffuser were tested and simulated, using both folding patterns (LE and RO).

The so-called "controlled environment" was composed of a rigid case equipped with transparent walls allowing the acquisition of high speed video images. It was fixed to a rigid support by a six-axis load cell, in order to measure reaction loads. Playing the role of the cover, a guided trolley was used. It was instrumented with an accelerometer and a set of eight small uniaxial load cells with the function of estimating the distribution of contact pressure produced by the airbag against the simulated cover. A pressure sensitive film was also used in order to register the map of maximum pressures achieved during the tests. Some details of the testing bench can be seen in Figure 6.

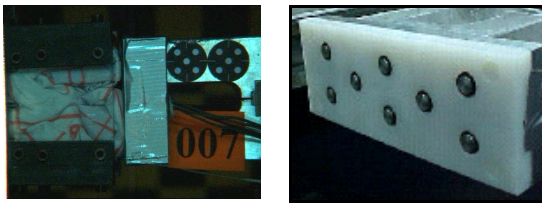

Figure 6. Constructive details of controlled environment tests.

The conclusions of these validations were published in [6]. Figure 7 shows some of the achieved results, comparing the curves obtained using simulation with FPM and experimental results (three tests were performed in each configuration in order to include repeatability factors)

These studies made possible the optimal validation of partial models of folded bags and generator independent of the housing, which allowed us to increase the predictability achieved in later steps. They also established a reference about the capability of FPM to deal with the phenomena associated to the earliest milliseconds of the airbag deployment.

REAL ENVIRONMENT

The interaction between the bag and its real housing during the first stage of the deployment presents some special characteristics that must be taken into account:

- As introduced above, the high dynamicity of the processes invalidates the assumption of uniform pressure of the gas and makes a careful modelization of the behaviour of the materials and breakable seams and their dependencies on the strain rate necessary.

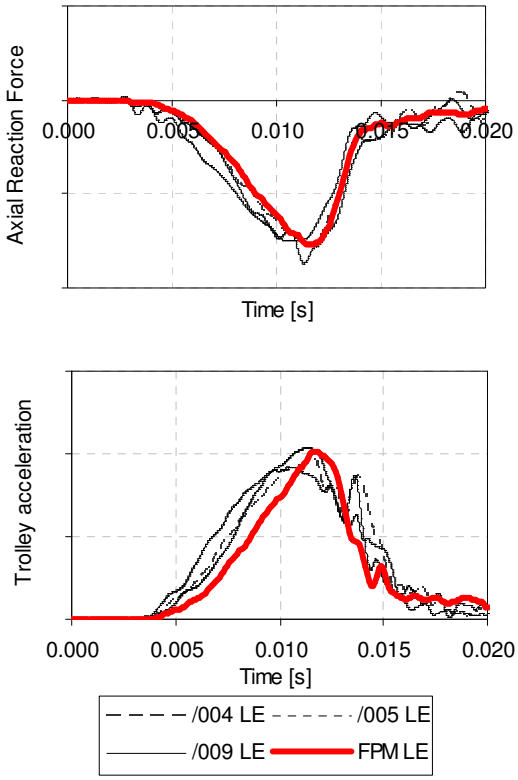

Figure 7. Results in controlled environment (Leporello Folding).

- Experimental tests are characterized by the lack of accessibility and, again, by the high dynamicity. Most of the volume inside the housing is already occupied by the folded bag, and there is no space for standard instrumentation. Besides, the high acceleration that the cover reaches can produce inertial effects that must be taken into account.

- The heterogeneous distribution of pressure within the volume of the airbag, the wide content of frequencies and the presence of phenomena of wave transmission invalidate the use of the pressure sensors commonly used in tests involving later stages of the airbag deployment.

The studies of opening in real environment were divided into two phases. The first of them was oriented to the validation of the numerical models. Six tests were performed using only two different configurations (Leporello and Rolling folding patterns, with serial diffuser and cover). The

instrumentation used in these tests was composed of up to six high speed video cameras at 1000 and 10.000 frames per second (depending on the function of each one), one six axis load cell in order to register the reaction loads at the base of the airbag and a set of eight small load cells in order to analyze the contact pressure between the bag and the cover. These load cells were specifically designed at CIDAUT with this function in mind. The set up of the tests can be seen at Figure 8, next to a diagram representing the position of the load cells under the cover.

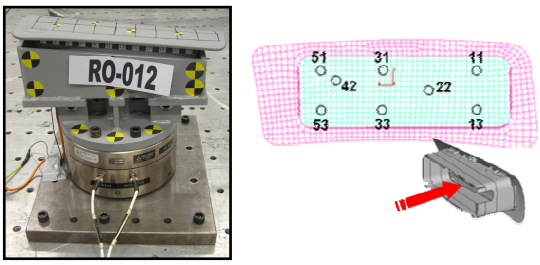

Figure 8. Set up of the deployment tests in real environment and positioning of load cells under the cover.

Numerical models were created from the models of bag and generator used in the previous phase, which were adapted to the new casing. In order to define the sub-model of the real environment, experimental characterisation of materials and seam line was performed, using both quasi-static and dynamic tests. The characterisation of the tearing of the seam line was made by testing the points that composed it separately. In order to do this, special tools were designed to fit to the geometry of the specimens, as shown in Figure 9. Tensile and shear test at several speeds were performed and reproduced in simulation using the different options available in PAM-CRASH, in order to chose the most realistic reproduction of the opening process.

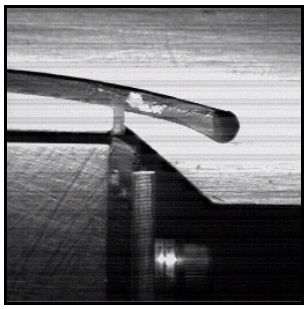

Figure 9. Detail of characterisation tests of seam line.

In addition to the numerical results equivalent to the respective experimental ones, several outputs were defined in the models in order to achieve a better understanding of the opening process. Among these outputs we can emphasize some interesting magnitudes difficult to be measured experimentally, such as the average force made by the bag against the cover or the force opposed by each point of the seam line, which gave us valuable information about the phenomena occurring during the first stage of the airbag deployment.

The results of these studies [7] showed a good numerical reproduction of the phenomena observed in the tests. Figure 10 shows the similarities of the kinematics in both cases.

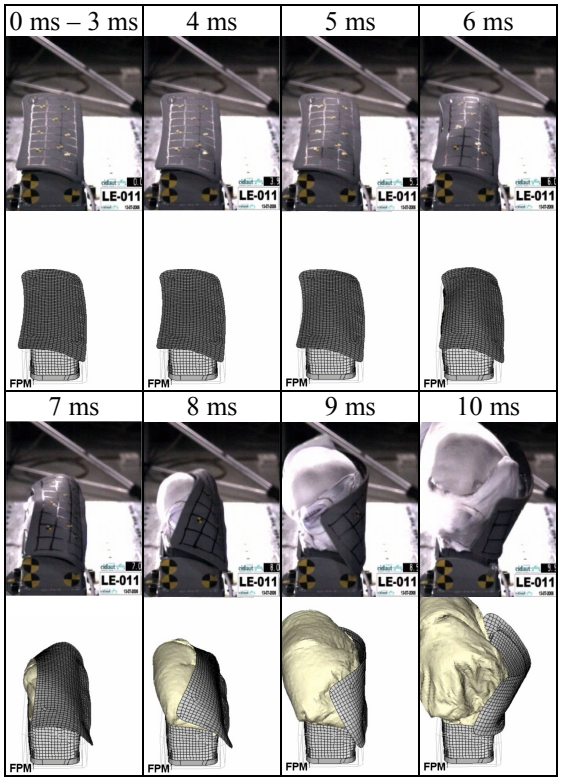

Figure 10. Comparison between experimental and simulated kinematics (Leporello folding).

With regards to the time of the opening, even though we are able to determine the exact time in which the seam line breaks in the simulated models, this was not measured in the experimental tests. The commonest way of estimating this is to consider the time of the frame in which the fabric of the bag is seen for the first time on the high speed video images of the deployment. This method, so called “white spot method” due to the colour of the textile, has also been used in simulation in order to get data comparable to the results obtained in the tests. Table 1 shows the registered values. In it we can see that opening in simulation occurs on average 0.6 milliseconds before. This can be related to the mathematical definition of the gas generated. The most interesting result is that the difference observed

when using both folding patterns has been well predicted numerically.

Table 1. Times of cover opening (white spot)

	Leporello	Rolling
Test 1	5.7 ms	5.6 ms
Test 2	5.7 ms	6.1 ms
Test 3	5.7 ms	6.4 ms
Average	**5.7 ms**	**6.0 ms**
Simulation (FPM)	**5.1 ms**	**5.4 ms**

One of the most promising applications of the use of simulation methods is related to the design of components paying attention to their function during the opening of the airbag. Figure 11 shows how zones with high plastic deformation were detected just in the places where cracks were produced during the tests (failure options were not included in the definition of the material used in the simulations)

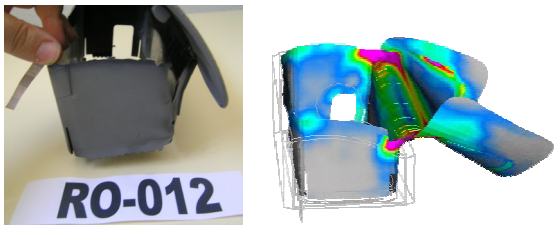

Figure 11. Identification of critical points by simulation (contours of plastic deformation displayed on the right).

With regards to the measurements taken by the load cells under the cover, Figure 12 shows the curves measured experimentally and the corresponding ones obtained by simulation. Numerical curves also reproduce inertial effects equivalent to those registered in the real sensors, in order to allow the comparison between both. The position of the different sensors is the same as displayed in Figure 8.

After the comparison of the local results we can observe that the distribution of pressure has been reasonably well reproduced up to the opening of the airbag (around 5ms in this folding pattern), whereas in later moments experimental deployment produces a sharp concentration of force in the sensor number 42, which is situated just over the outflow of the gas generator. This concentration of pressures is less marked in the numerical case, although still appreciable, as shown in Figure 13. On the other hand, the section displayed in the same figure shows that the pressure calculated in the FPM particles correlates well with the distribution observed experimentally. This fact seems to indicate that there is a loss of accuracy in the pressure distribution, probably associated to the contacts among the layers of folded fabric and with the cover. Still, as seen above, the global behaviour of the simulated cover is very similar to the one observed experimentally.

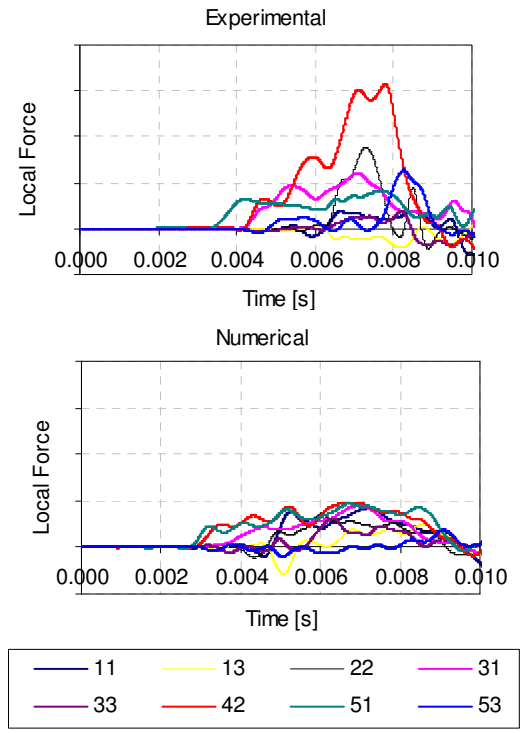

Figure 12. Forces measured under the cover (Leporello folding).

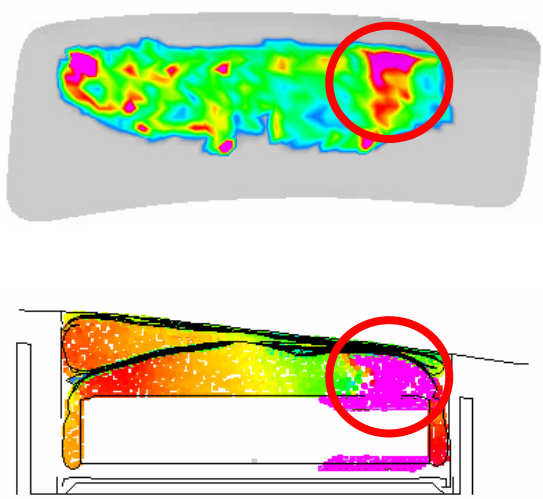

Figure 13. Distribution of contact pressure under the cover, and section with pressure in the fluid (Simulation of Leporello with Diffuser 1 at 5.5 milliseconds). Red circles indicate the position of the gas outflow.

After these studies, the numerical models were considered representative enough so as to proceed to their modification in order to analyze the

influences of the inclusion of different types of diffusers (Dif 1 to Dif 4) and cover configurations (C1 and C2). Two additional simulations were made using a third configuration (Without Cover or WOC), in which the door of the cover was removed in order to provide a reference in the evaluation of the influence of the modifications on the seam line.

Thanks to the specific outputs introduced in the models, it was possible to analyze values that are very difficult to obtain using experimental methods, such as the exact time when the points composing the seam line break, or the force the bag produces against the cover. Figure 14 displays the curves of average pressure inside the airbag and the corresponding forces against the cover in all the simulated cases (obviously, the force against the cover is not represented in the WOC configurations, which have no cover). Figure 15 shows the relation between the maximum values achieved in these curves. After both figures several observations can be made:

- Folding patterns and diffuser geometries are clearly conditioning the average pressure inside the airbag and the time of the opening (marked by the descending slope of the curves). In general, the rolling folding is producing higher pressures and later opening of the cover. It can also be appreciated that the scatter produced by Leporello folding is generally smaller than that produced by Rolling folding.

- Although the opening time is conditioning the shape of the force curves, the maximum values achieved are relatively similar in all the configurations. A certain reduction in the forces is observed when decreasing the resistance of the seam line (C2), although somewhat smaller than expected. We could conclude that this value is controlled mainly by the resistance of opening the door, due both to the seam line and to the energy needed to deform and accelerate the cover. This is easily understandable when thinking about Newton's law of action and reaction forces.

- One of the most interesting findings of the analysis was that, even when the variations of the opening times and average pressure inside the bag were of some importance, the maximum forces registered on the cover did not vary so much, even when the resistance of the seam line was reduced (Configurations C1 and C2). This effect has been related to the folding pattern, which modifies the stresses reached by the fabric and, therefore, the energy stored in it, and to the diffuser geometry, which is related to the concentration of pressure in determined zones of the bag and to the degree of homogeneity of the pressure field that is finally transmitted to the environment.

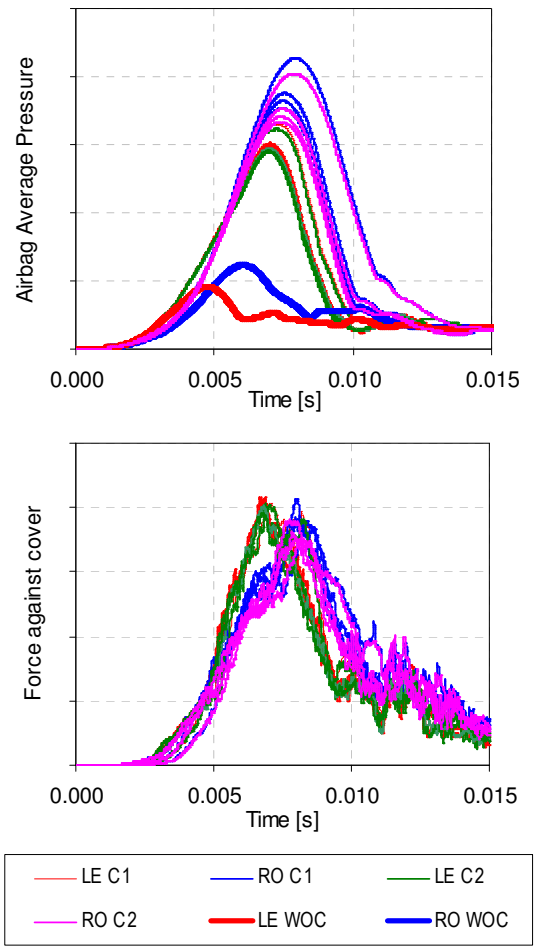

Figure 14. Curves of average pressure and force against cover.

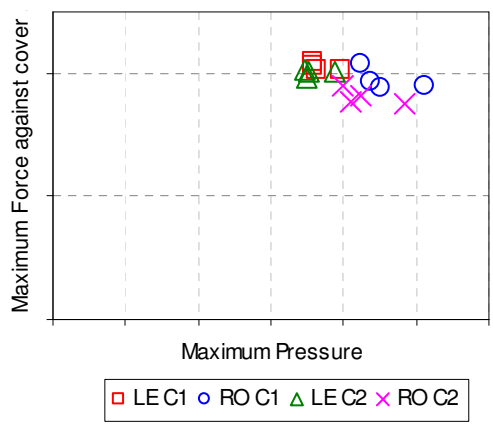

Figure 15. Relation between maximum average pressure in the airbag and maximum forces against cover.

Looking at the different results produced when

changing the diffuser geometry, as expected, the main variations were produced by diffuser 2. The design of this configuration was conceived to produce a more homogeneous pressure distribution, avoiding the concentration of loads on a determined zone of the cover.

Figure 16 shows some of the results achieved by the different geometries of the diffuser. It was observed how the variation of the gas flow direction allowed us to modify the distribution of pressure in the volume and, therefore, the load conditions on the cover. This was seen to affect the time of opening, as shown in Figure 17. The graphs in this figure represent the values of time when the last point of the seam line was broken (end of opening) and the duration from the rupture of the first point to the last. It can be seen how, because of the pressure being more homogeneous in configurations using diffuser 2, the duration of the opening is shorter, which means that the points are breaking almost at the same time, and occurring later than in other configurations.

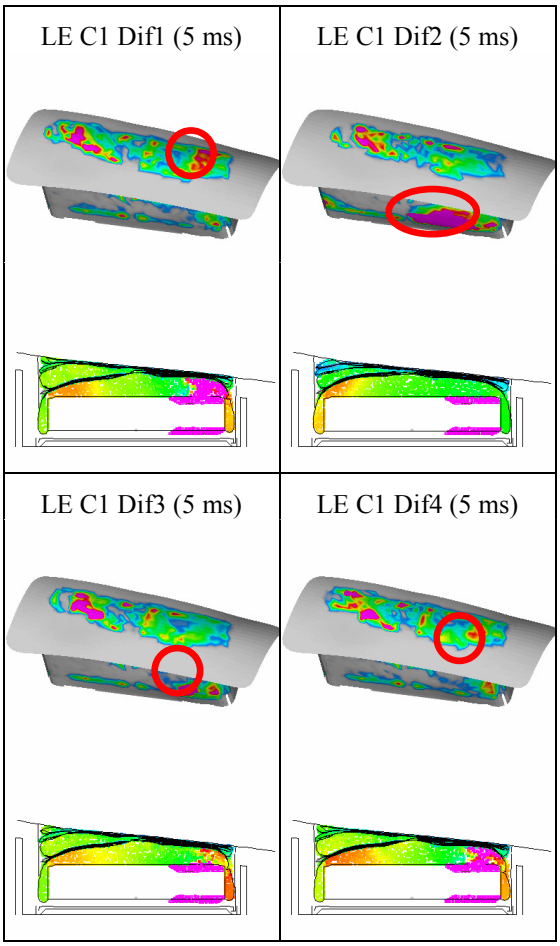

Figure 16. Dependency of contact pressure and gas pressure on the diffuser geometry. Red circles indicate the direction of the gas outflow.

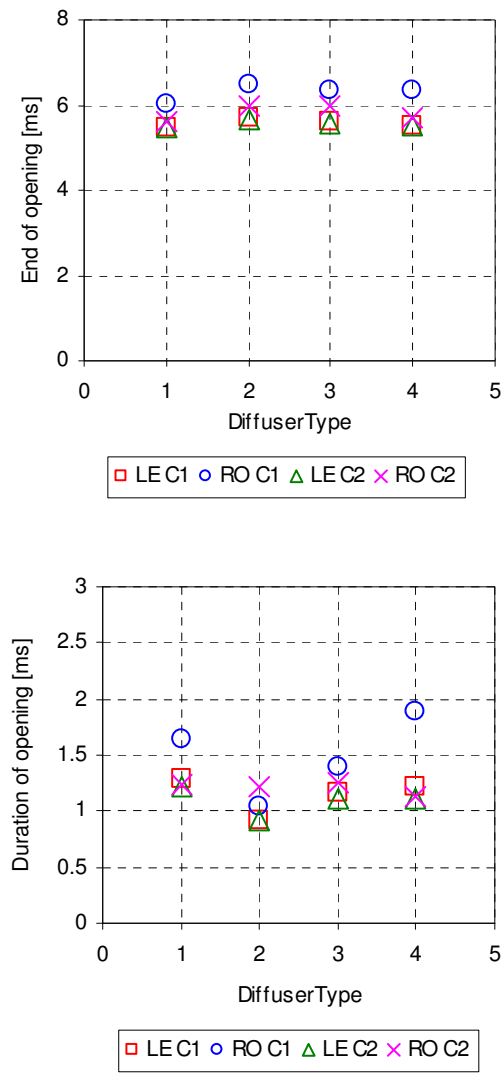

Figure 17. Influence of diffuser on opening time.

A second series of tests were performed in order to provide data for the validation of these results. It was decided to make modifications only in the diffuser, in order to avoid the influences of the folding pattern, which had been seen to be well reproduced before, and to evaluate the capability of FPM to work with different directions of flow. As the biggest differences in the models had been found between the diffusers 1 and 2 the configurations LE Dif1 C1 and LE Dif2 C1 were chosen to be tested. As the repeatability had proved to be good in the previous tests only one test was performed with each configuration. Although the first configuration had already been tested, it was decided to perform the test anyway in order to have exactly the same frame in the video images, which would be essential in the later analysis of the kinematics of deployment.

The main value taken into account for the validation of the models was the time of cover

opening. As experimentally it was difficult to know the exact time of rupture of the points of the seam line, the method of the white spot was employed again. Table 2 shows the obtained values. As had happened in the previous validations, there was a difference of around half a millisecond between experimental and numerical results, but, once more, the difference between the times of opening when using both configurations was well reproduced.

Table 2. Times of cover opening (white spot) with Leporello folding (LE C1)

	Diffuser 1	Diffuser 2
Experimental	5.7 ms	6.6 ms
Simulation (FPM)	5.1 ms	6.1 ms

KINEMATICS OF DEPLOYMENT

During the second and third stages of the deployment of the airbag, the bag is leaving the housing, unfolding and taking the shape required to receive the occupant. Whereas during the previous stage the variation of the pressure was very rapid, in this case, particularly during the second stage, there is a quick evolution of the volume and the pressure at the same time. As the cover is already open, the opposition to the increasing of volume, coming mainly from the resistance of the fabric deforming and the air displacing, is very weak. Consequently, slight variations in the folding or in the gas flow can produce important variations in the overall kinematics. Figure 18 shows how the modification in the gas flow produced by the different geometry of the diffuser is affecting the whole mechanism of deployment.

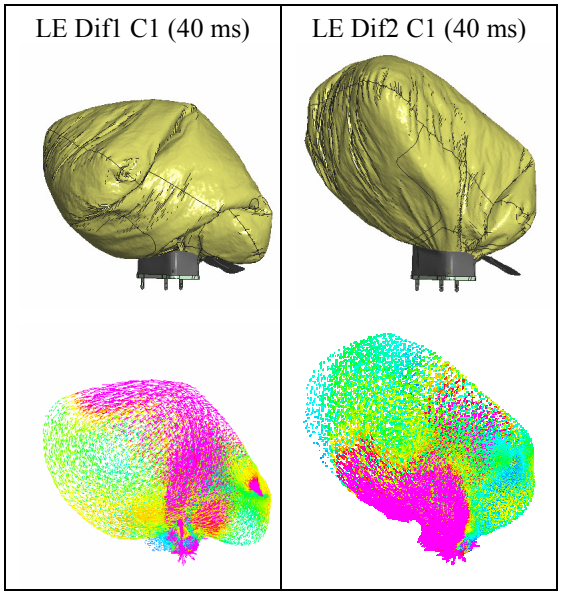

Figure 18. Influence of gas flow in kinematics of deployment (lower images represent the speed of the FPM gas particles).

Only the eight configurations with the serial seam line (C1) were used in the study of kinematics of deployment, showing clear differences in the deployment associated both to the folding pattern and to the geometry of the diffuser. Figure 19 represents the deployment in four of the cases, showing the geometry of the bag and the contour of pressure of the gas inside the bag. We can observe how not only the general kinematics, but also the distribution of pressure is quite different from one case to another. In particular, we can see how the configuration LE Dif2 deploys much less aggressively than, for instance, the configuration LE Dif 1, reducing the "whiplash" effect. On the other hand, we can appreciate also that the Rolling pattern presents less sensibility to variations in the geometry of the diffuser than the Leporello folding.

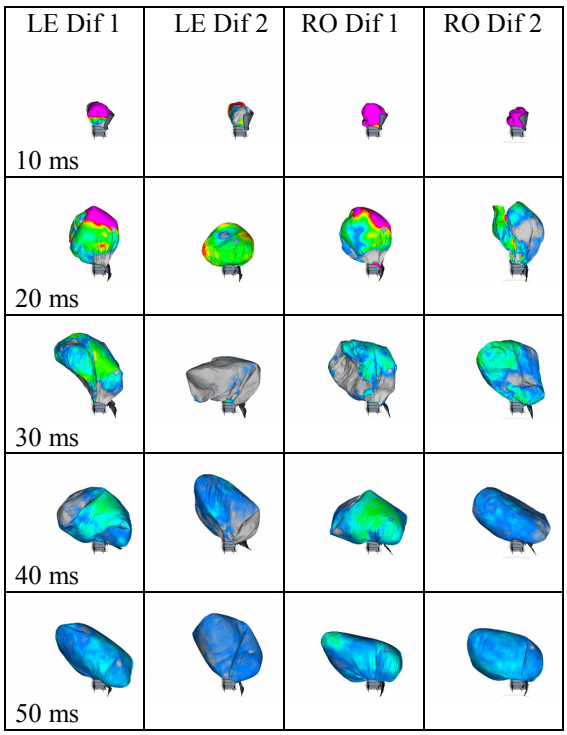

Figure 19. Kinematics of deployment and evolution of pressure distribution in several configurations.

In order to quantify the "whiplash" effect, and to provide data for a quantitative comparison among the different configurations, the values of maximum distance of a point of the bag to the base of the airbag and the time in which this distance was achieved were noted. Table 3 shows these values. In it we can see again how the scatter of the values for the Rolling cases is lower than for the configurations with Leporello folding, particularly looking at the time of maximum displacements. On the other hand, we can see how this time has been highly increased by the configuration LE Dif 2 C1, at the same time that the maximum displacement has been reduced. These values indicate that this

combination is unfolding in a less aggressive way to potential occupants, without the intervention of any tether or additional mechanism to control the geometry of the deployment. Among the other configurations, the one with Leporello folding and diffuser 3, which also directed the flow towards the lateral walls of the housing instead of to the cover, had the most similar results.

Table 3. Time and magnitude of maximum displacement of the bag measured from the base of the airbag

Configuration	**Time of maximum displacement [ms]**	**Maximum displacement from base [m]**
LE Dif 1 C1	26	0.63
LE Dif 2 C1	43	0.54
LE Dif 3 C1	33	0.54
LE Dif 4 C1	27	0.59
RO Dif 1 C1	25	0.63
RO Dif 2 C1	25	0.64
RO Dif 3 C1	25	0.59
RO Dif 4 C1	25	0.58

The tests used for the validation of the models of opening in real environment were also utilized for the validation of the models of kinematics of deployment (configurations LE Dif1 C1 and LE Dif2 C1). Although the frames extracted from the simulations were equivalent to the experimental ones, and therefore photogrammetric studies could have been performed in order to have a quantification of the results, the differences between both deployments were so obvious that a qualitative comparison of the geometries was decided to be indicative enough as to evaluate the capability of the software to simulate the real deployment. Figure 20 shows the comparison between experimental and numerical results. As predicted, the deployment after the modification of the diffuser was quite different to the original one, and followed well the tendencies marked by the simulations. This is particularly clear in the frames corresponding to the milliseconds 20 and 30, where the geometries of both configurations differ considerably.

On the other hand, the new direction of the outflow from the inflator increased the leakage of gas from some holes at the base of the bag, and produced important burns in the fabric next to the generator around the millisecond 40. These effects, which can be noticed in the video images, were not reproduced numerically. At any rate, the correct prediction of the tendencies of the deployment made them negligible to the conclusions of the study.

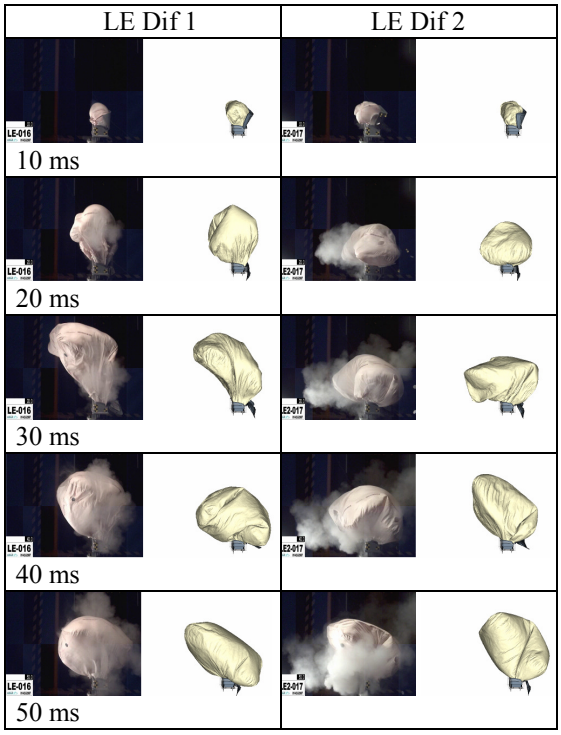

Figure 20. Comparison of experimental and simulated kinematics of deployment.

OUT OF POSITION

The last step of our studies was to check our models in deployments with an occupant placed in Out Of Position. Two configurations were initially selected to be analyzed, one of them looking for the maximum injury on the neck (Chin on module or "CHOM") and the other one trying to produce maximum damage on the thorax (Thorax on module or "THOM"). The dummy chosen for the occasion was the Hybrid III 50%, being the heaviest among those commonly used in OOP tests and, therefore, the one that should produce the maximum difference the static deployment. As no neck skin was present in the numerical models it was not used in testing either.

The standardized testing procedures for OOP testing require the use of elements of the vehicle interior, such as seat and dashboard. When necessary, foams and adhesive tapes are also used in order to maintain the dummy in the desired position. In our case, as our objective was not to simulate a specific type of test, it was decided to use a simplified rigid environment. This provided several advantages. First of all, it was not necessary to simulate these elements. This made it unnecessary to characterize them and eliminated the variability associated with them. On the other hand, the simplification of the environment of the dummy made its positioning much easier, in this way improving the reproducibility of the whole

test.

The tibias and feet of the dummy were removed in order to make the support of the airbag stiffer and easier to construct. The influence of these parts was considered negligible to the overall results of the test. Finally, a flat surface was built around the airbag support in order to avoid the airbag going forward during the deployment instead of pushing against the mannequin. This surface was fixed independently to the airbag, which was supported by the load cell used in the previous tests. The final make-up of the tests can be seen in Figure 21.

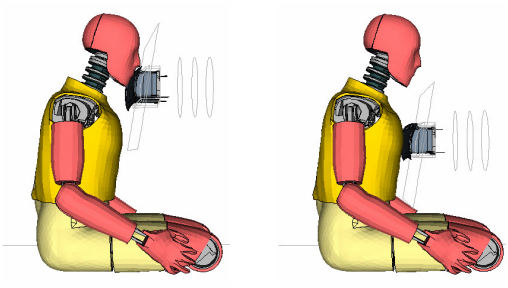

Chin on module (CHOM) | Thorax on module (THOM)

Figure 21. Configurations used in Out Of Position tests.

All the airbag configurations with serial cover (C1) were simulated in both set ups. Additionally, a third OOP scenario was included modifying slightly the distance of the dummy to the airbag in the THOM configuration (from 2 millimetres to 4 millimetres), in order to analyze the sensitivity to modifications in the positioning. Both situations were called "THOM d1" (2 mm) and "THOM d2" (4 mm) respectively.

Eight OOP tests were made for the validation of the models, all of them with serial diffuser (Dif 1) and cover (C1). The four first were "chin on module", performing three tests with airbags with Leporello folding, in order to analyze the repeatability, and a fourth one with Rolling folding, in order to study the sensitivity to the folding pattern. The second group of tests were "thorax on module". In this series there were two tests with Leporello folding placing the thorax at 2 mm (THOM d1), one more with Leporello folding and the thorax at 4 mm (THOM d2), and a last one with Rolling folding with the thorax at 2 mm.

Figure 22 represents the comparison of kinematics observed for the CHOM configuration in both folding patterns. In this image we can observe that the configurations with Leporello folding tended to unfold towards the right side of the dummy, influenced by the asymmetry of the airbag. This tendency, although also existing, was not so defined in the experimental results. On the other hand, in the Rolling configuration the deployment downward takes place some milliseconds earlier in simulation than in testing, while this movement is quite well reproduced by the Leporello folding. As a consequence, the loads in Rolling configuration descend before those observed experimentally (Figure 23). This seems to indicate that Rolling folding is less aggressive than Leporello folding, while experimental results point to the opposite.

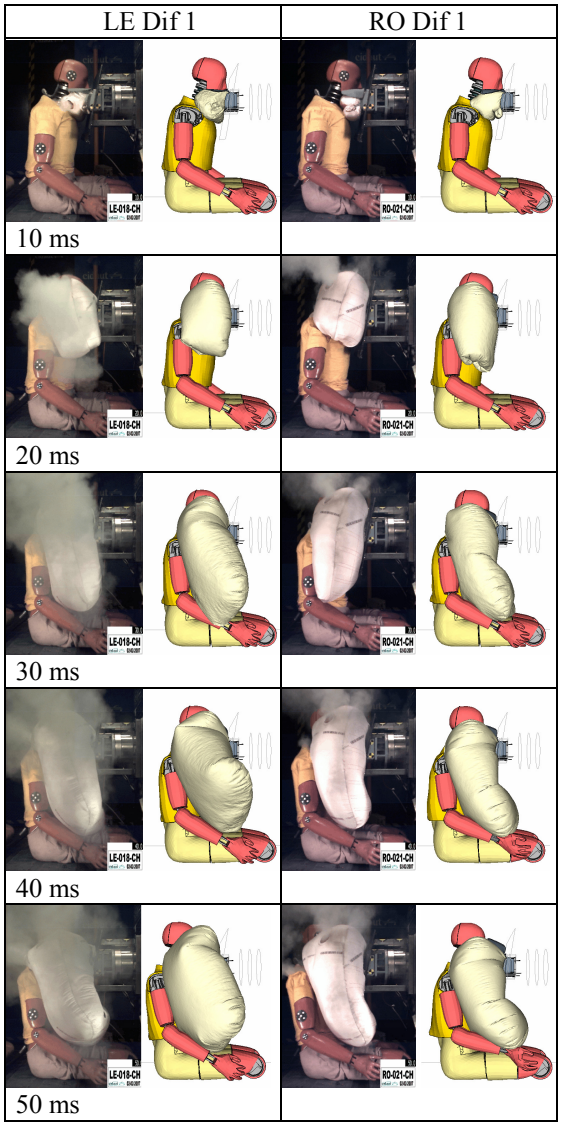

Figure 22. Comparison of experimental and simulated kinematics of deployment (CHOM).

Furthermore, the physical airbags employed in the test tended to break due to the high pressures and temperatures, creating new venting holes not reproduced numerically. This happened generally around the millisecond 20 in CHOM configurations and around the millisecond 30 in THOM configurations.

Some of the most interesting curves of the validation of the CHOM configuration can be seen in Figure 23. If we consider the different graphs separately, we can see that the main parts of the curves have been well reproduced numerically, and that the load levels have been more or less accurately achieved. However, as seen above, the tendencies observed experimentally when changing the folding pattern are not well reproduced by the simulations. Although some parameters were identified to be optimized in order to improve the results, the determination of their influence was left for further research.

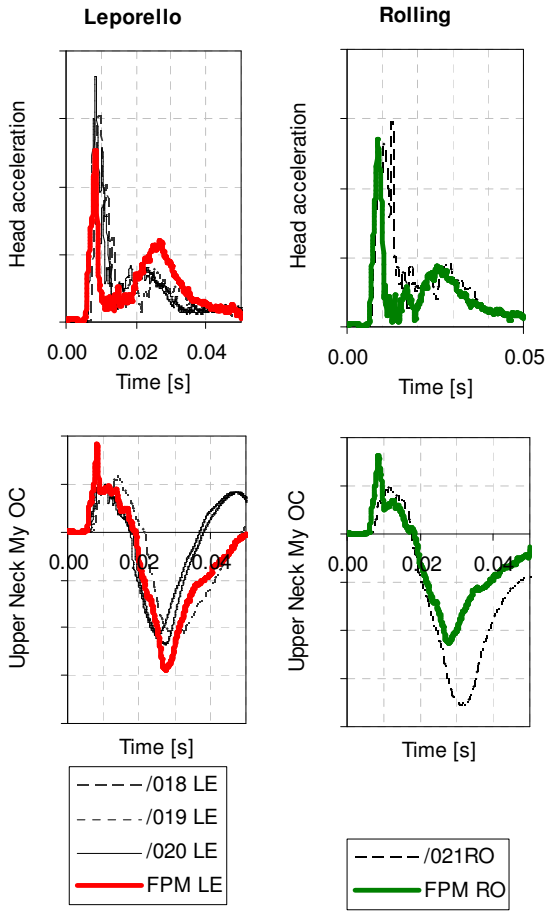

Figure 23. Comparison of experimental and simulated curves (CHOM).

In the case of THOM configuration the kinematics was in general well reproduced by all the numerical models. Observing the curves (Figure 24), we can see nevertheless that the results achieved by Rolling folding seem to be more accurate than the ones achieved when using Leporello folding. Looking at the separated curves, we see that the shape of the curves of thorax acceleration and axial reaction forces are being quite well predicted, particularly in the case of Rolling folding, while the curves of thorax deflection show a worse level of reproduction. This could be related to the numerical definition of the dummy.

With regards to the change of distance from the thorax to the airbag, we can say that the general tendencies have been well reproduced, although perhaps not as strongly as observed in tests.

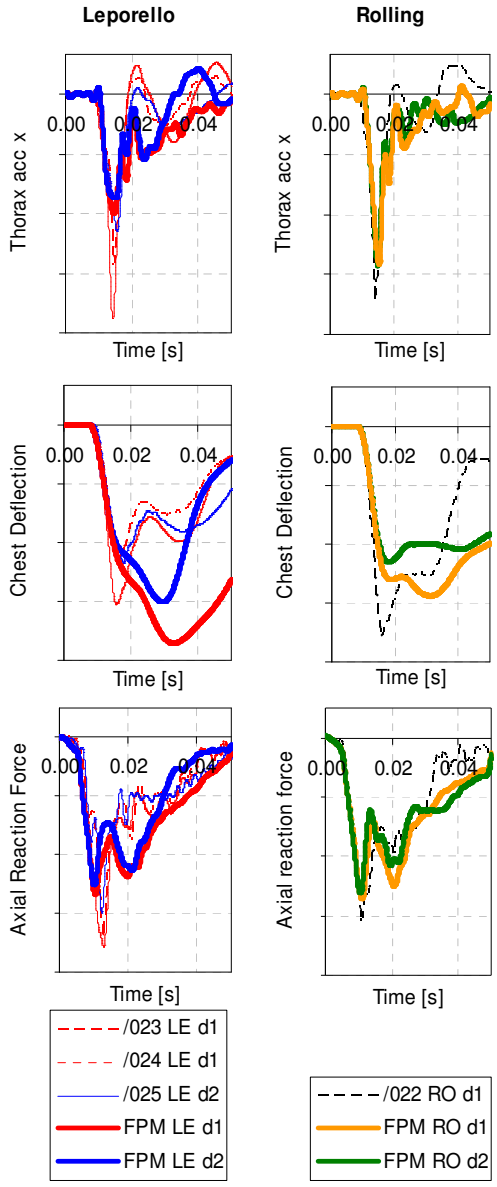

Figure 24. Comparison of experimental and simulated curves (THOM).

Looking at the totality of the simulations performed, different tendencies were observed depending on the airbag configuration. Figure 25 presents some sections of the models with the pressure distribution of the gas inside the airbag. We can observe how the modification in the gas flow due to the variation of the diffusers and folding patterns is producing different zones of concentration of pressure and, therefore, different

kinematics of deployment and different outputs in the dummy. As an example, diffuser 1, which was seen to produce a more aggressive deployment, is now causing lower loads on the neck of the dummy in the CHOM configuration. The explanation of this phenomenon has been related to the deflection of the gas flow produced by the cover, which is prevented by the dummy from opening normally, and that is directing the gas flow to the right side of the dummy when using diffuser 1, while diffusers 2, 3 and 4 are filling the airbag in a more homogeneous way and, at the same time, producing a higher pressure under the chin. This can be seen in Figure 26.

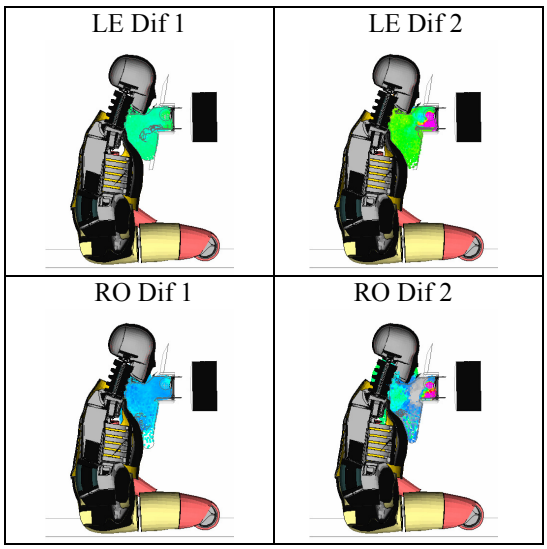

Figure 25. Sections with gas pressure contours (CHOM at 20 ms).

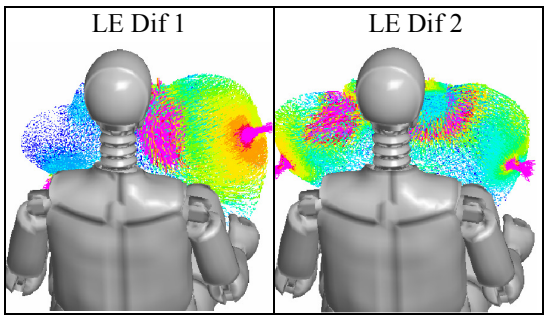

Figure 26. Velocity of the fluid for different diffuser options (CHOM at 20 ms).

One interesting study is the analysis of the relations between results achieved in different stages of the deployment, in order to establish design parameters to predict the behaviour in different situations. The graphs in Figure 27 show the relation between loads achieved in OOP simulations with the maximum average pressure reached in the simulations of opening in real environment. It can be seen that minimum moments of extension (negative values, according to [8]) at the upper neck during the OOP in CHOM configuration depend much less on the pressure during the opening than the thorax acceleration in the THOM configuration. These kinds of studies can help to identify and quantify the causes and effects related to the different factors associated to the airbag design.

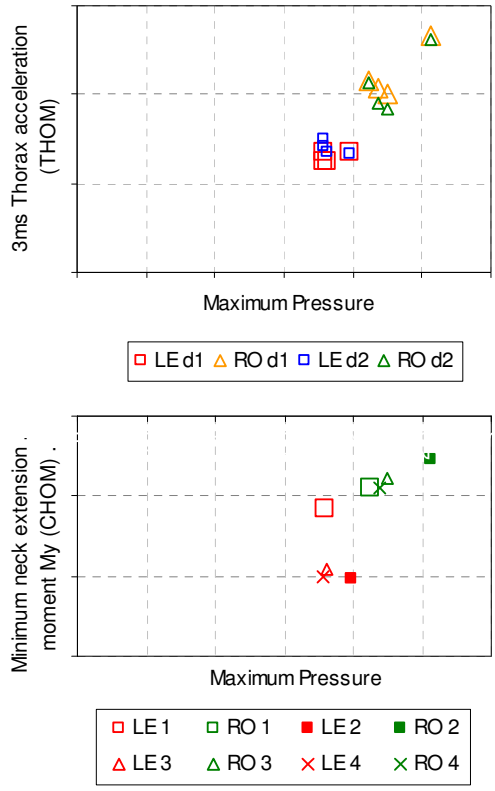

Figure 27. Relation between OOP results and maximum pressure achieved during opening.

DISCUSSION

Up to here we have described the characteristics of the different stages of the airbag deployment, as well as outlined the results obtained in their numerical simulation and experimental validation. The following points summarize the main findings of this group of studies:

- Three stages have been identified in the deployment of the airbag according to the evolution of the pressure and the volume.

- The interactions between the airbag and its environment (housing, cover, supports…) up to the opening of the cover are related to the first stage of the deployment. Numerical and experimental methods have been specifically developed for this phase in order to achieve simulation models as reliable as possible. Although some differences have been

identified in the local distribution of the contact pressure, overall results are very promising, reproducing accurately the general trends and timing observed experimentally.

- Tendencies of kinematics of deployment when using different folding patterns and diffusers have been well predicted numerically. Most aggressive deployments have been correctly identified.

- Good reproduction of load levels and timing has been achieved in the simulation of several OOP situations. In spite of this, some experimental tendencies have not been correctly predicted in simulation when changing the folding pattern. This has been related to the high instability inherent to this kind of events, which means that small variations in the inputs, either experimental or numerical, produce large variations in the results, reducing the reproducibility of the whole process. As a consequence, caution is suggested when using numerical tools to improve OOP results, the validation of the base models with testing still being recommended. Further research is required in order to improve both experimental and numerical methodologies.

CONCLUSIONS

This document outlines the current possibilities and limitations of the simulation of the first stages of the airbag deployment. Studies have been performed in three different scenarios: Interaction with the environment during the opening, kinematics of deployment and OOP. The degree of accuracy of the simulations in each one of them has been evaluated, as well as the sensitivity of the models to modifications of several parameters. Additionally, advantages provided by the use of numerical methods have been shown, such as the possibility of obtaining magnitudes difficult to measure experimentally (e.g. the force made by the bag against the cover during the opening or the distribution of pressure of the gas within the airbag), and the capacity to check different configurations with a high degree of control of the modified parameters. As a result of this, simulation has proved to be a valuable tool to be taken into account in tasks related to airbag deployment.

The studies presented have been performed using a commercial airbag. The numerical models have been developed systematically from the first validation of the generator and folded bag in a controlled environment to their final use in complex OOP scenarios with real cover and housing. At the same time, a complete set of validation tools and methods has been developed.

In conclusion, these technologies are able to be used not only as a tool to solve problems related to the airbag development, but also to help us arrive at a better understanding of the factors that influence the deployment of the airbag and its aggressiveness, and therefore get more efficient and safer designs.

REFERENCES

[1] Federal Motor Vehicle Safety Standards (FMVSS), Part 571.208 (10-1-2001 Edition) “Standard No. 208 ; Occupant protection.”

[2] Zhang H., Raman S., Gopal M. and Han T. (2004) “Evaluation and Comparison of CFD Integrated Airbag Models in LS-DYNA, MADYMO and PAM-CRASH” Society of Automotive Engineers (SAE) Paper Number 933340. USA.

[3] Beesten B., Hirth A., Reinlink R., Remensperger R., Rieger D. and Seer G. (2004) “OOP Simulation – A Tool to Design Airbags? Current Capabilities in Numerical Simulation”. FEA Publications. http://www.feapublications.com.

[4] Trameçon A., Culière P., Kruhnert J. (2003) "Finite Point Set Method: a Mesh Free Approach to Model Airbag Inflation". International Body Engineering Conference (IBEC). Chiba. Japan.

[5] Pyttel T., Thibaud Ch., Floss A. and Goertz C. (2005) “Realistic Simulation Models for Airbags and Humans – new Possibilities and Limits of FE Simulation”. Verein Deutscher Ingenieure (VDI) Kongress. Berlin. Germany

[6] Muñoz D., Negro A., Regidor A. and Hernando L. M. (2005) “Characterisation of Models of Inflator and Bag to be Used in the Study of the Interactions of the Airbag with its Immediate Environment. An Application using FPM”. EuroPAM conferences. Potsdam. Germany

[7] Muñoz D., Carlón J., Regidor A., Negro A. and Mansilla A. (2006) “Simulation and Validation of the First Milliseconds of Airbag Deployment”. EuroPAM conferences. Toulouse. France

[8] (1994) “SAE J1733. Sign Convention for vehicle crash testing. Issued DEC94”. Society of Automotive Engineers (SAE) USA.

STOCHASTIC CRASH ANALYSIS OF VEHICLE MODELS FOR SENSITIVITY ANALYSIS AND OPTIMIZATION

Massimiliano Avalle
Giovanni Belingardi
Andrea Ibba
Politecnico di Torino
Italy
Kambiz Kayvantash
Franck Delcroix
Altair Development France
France
Paper Number 07-0335

ABSTRACT

Within the 6th Framework Programme EU project APROSYS, the Sub-project 7 is fully devoted to virtual testing. The aim is to improve the quality of the crash simulation in order to be able to come to rating and qualification by virtual analysis.

One of the main issues lies in the evaluation of scatter sources and the consequences of scatter on the results of the analysis. Therefore, great effort was devoted in the project to identify and quantify sources of dispersions, and to assess their relevance.

To evaluate the influence of scatter on crash responses a series of stochastic models has been developed. Within the APROSYS project a series of generic car models was developed to perform this task. Generic car models are virtual vehicles, derived from the geometry, layout, and characteristics of the best-in-class models currently available on the market according to EuroNCAP ratings, generated to have commonly shared models to work out towards improvement in crash simulations.

In this work a stochastic analysis developed by using one of these generic car model, called GCM4, a multi-purpose vehicle, will be reported. The stochastic model was generated by considering the stochastic variation of some parameters. In particular, the steel sheet properties were used as stochastic variables (input). Moreover, to evaluate the structure influence on the passenger behavior, a simpler stochastic passenger compartment model was developed.

The simulation runs were managed by a specific tool, called ADVISER, developed within the APROSYS project and its antecedent ADVANCE. The results were analyzed by means of the post-processor included in the same ADVISER tool.

The results give further insight in the problem of the improvement of simulations for passive safety applications.

1. INTRODUCTION

Besides improvement in quality and performance of cars, a major requirement in automotive industry is the reduction of costs by reducing time-to-market. To achieve this goal the use of advanced design methodologies and tools is mandatory. By using improved simulation tools in design, it is possible not only to speed up the project but also to improve it, because many different alternative solutions can be easily analyzed and compared, and it is possible to limit the number of expensive experimental tests, or avoid them at all. Strictly speaking, experiments are not eliminated: physical experiments are replaced by virtual tests. Therefore, this method has been called *virtual testing* (VT) [1].

The greatest advantages of VT in automotive design are certainly in the field of passive safety due to the complexity of crash analyses and the costs implicated with it. In the 5th Framework Programme of the European Union, two projects introduced VT: VITES (VIrtual TESting, [2]) and ADVANCE (ADvanced Virtual ANalysis of Crash Environments [3]). The authors were involved in both projects. In VITES the basic methodologies to develop VT were developed, whereas ADVANCE was mainly focused on the tools to achieve VT.

Further improvements are being obtained within the 6th European Framework Programme APROSYS (Advanced PROtection SYStems), and in particular, in a subproject (SP7) just named *Virtual Testing*.

Final aim, besides developing VT methods and tools, and demonstrating the validity and convenience in using VT methods, is to go towards the use of VT in Regulations [4].

One of the greatest problems in developing VT methods is how to deal with the large number of simulations required to check numerical codes and models, and which models can be used to do this. Car manufacturers are very reluctant, for justified and comprehensible reasons, to share their finite element (FE) models for research purposes. Even developing by scratch a real car model is not accepted by everybody. For that reason, it was decided to create virtual models of virtual cars, that is of cars that do not actually exists, but are like real cars with the best, top-in-their-class, performances in the rating tests like EuroNCAP. These Generic Car Models (GCM) were shared among the APROSYS partners to develop passive safety parametric [5] and stochastic analysis [6], design of advanced passive safety [7] and active safety [8] devices, studies in the protection of pedestrian, cyclists and motor bikers [9-10], and biomechanical investigations [11].

In this work a full vehicle stochastic analysis of a GCM is reported. The aim of this work was to develop and apply a tool for stochastic analysis (ADVISER), examine the feasibility of full vehicle stochastic analysis, and the advantages from using this kind of analysis in car crash design for safety.

Final objective of these research activities is to demonstrate the possibility of using VT in regulations also. There is, in fact, one case of certification that can be already made by simulation, namely ECE R44 regarding bus rollover. In the authors' opinion, VT can be further extended and cover many other possible certification schemes, as it will be developed as a final task of APROSYS Subproject 7 on Virtual Testing.

2. GENERIC CAR MODELS

In APROSYS four generic vehicle models were developed, namely:

- **GCM1** a small city car, like EuroNCAP *superminis* (Fiat 600 and Punto, Renault Clio, Citroën C2 and C3 etc.).
- **GCM2** a small family car, like in EuroNCAP classification (Renault Mégane, Fiat Stilo, Audi A3…).
- **GCM3** a large family car (such as Mercedes C class, BMW Series 5, Audi A4…)
- **GCM4** a multipurpose vehicle (MPV) (such as Renault Espace, Citroën C8, Peugeot 807, Fiat Ulysse, Lancia Phedra…).

The first three GCMs were developed by Centro Ricerche Fiat, whereas GCM4 was developed by Politecnico di Torino. Besides, a heavy truck generic model was developed by the Technical University of Graz. All these are finite elements models, developed both in Radioss from Altair (formerly Mecalog) and LS-Dyna, but the same car models were converted to multibody in the Madymo code from TNO.

Figure 1 shows some snapshots of the four GCMs.

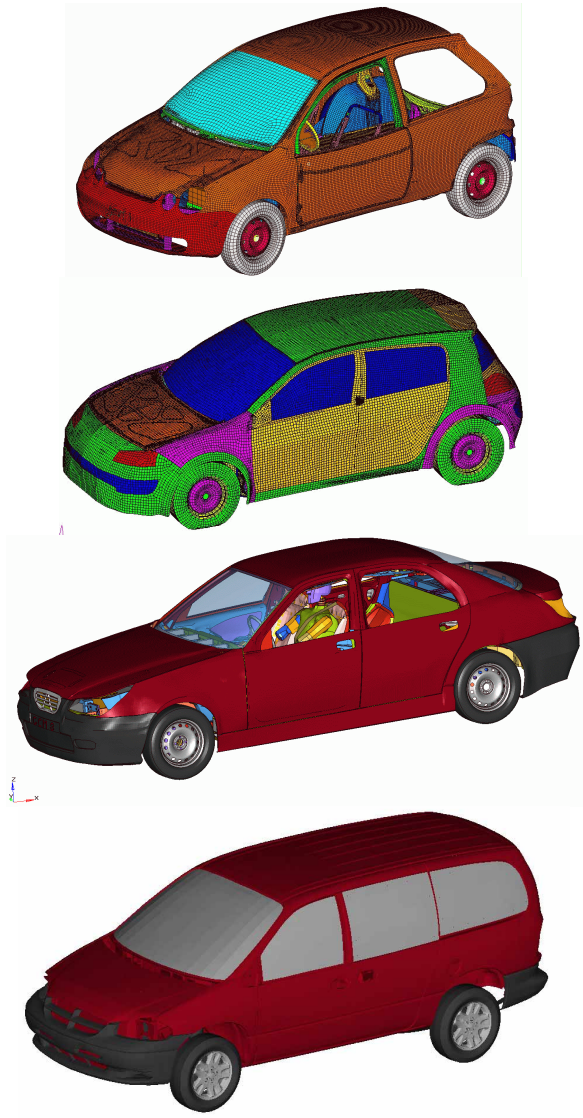

Figure 1. The virtual fleet: the GCMs developed within the APROSYS project.

2.1 The generic car model 4 (GCM4)

The generic MPV model was not started from scratch, but was developed starting from a public domain model of the Dodge Caravan, sold in Europe as Chrysler Voyager, made by the George Washington University and FHWA/NHTSA National Crash Analysis Center (NCAC), and available through the NCAC web site. This initial LS-Dyna

model has no crash environment defined, but a rigid barrier and a US-NCAP frontal crash test environment defined are available. The model includes the whole chassis and body with engine and wheels, but does not include steering system and suspension and also does not include dummies, seats, seatbelts, airbags, nor any other restraint system.

The model was first converted to Radioss with some automatic tools:

- Hypermesh translator for "LS-Dyna Key" to "Radioss block format ver.44".
- M-Crash translator from LS-Dyna to Radioss (under development, performed by Mecalog Italia)

Both translators have some limitations (especially the Hyperworks one when defining material laws and element types). By mixing together the translated files and adding a great amount of manual editing work, a good initial translation of the model was obtained.

However, the model generation did not stopped there for a series of reason. It was decided to have a car model mostly close to the best-in-class models according to EuroNCAP tests. These 5 stars vehicles were, in 2004 when this work begun, the Citroën C8, the Peugeot 807, the Fiat Ulysse, and the Lancia Phedra (that are built on the same platform and are structurally very similar), and the Renault Espace.

Therefore, a series of modifications were made on the virtual model to make it more resembling to these real cars. Modifications include:

- overall external size
- basewheel reduction to 2850 and forward translation of the front wheels and slight rearward translation of the back wheels to match the more usual current styling of European cars
- mass reduction of the body-in-weight to 1271 kg
- many structural modifications to improve impact strength by reinforcement of structural parts, especially in the front area

The front rails were straightened and sheet thickness was increased. Figure 2 show front rail modifications. Fenders were also modified.

Then, the steering line, the front suspensions, the seats, the dashboard, the interior panels were added to obtain the full vehicle model shown in figure 3.

Figure 4 show an example of a simple AMUS crash test against a rigid barrier.

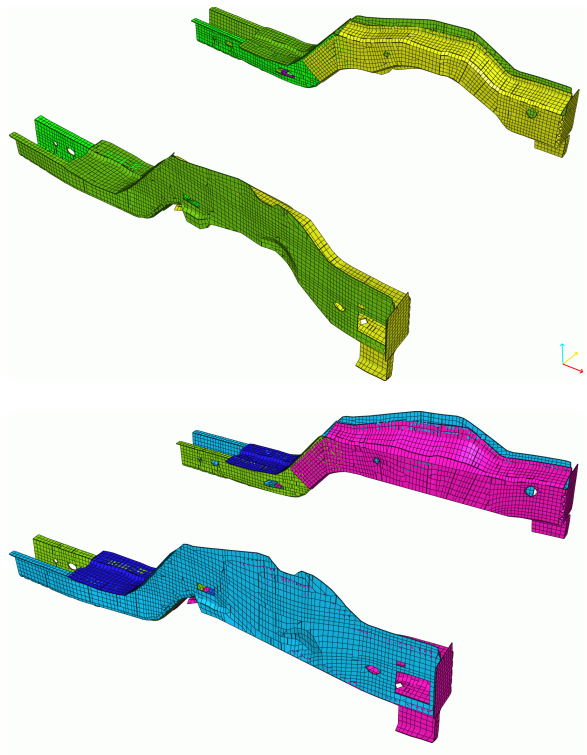

Figure 2. Front rails modifications, above original, below the improved version.

2.1 Validation of the GCM4

An important issue in the development of the GCMs was model validation.

Validation in its usual technical connotation is the process that tries to demonstrate the validity of a numerical (or also theoretical or analytical) model. The most widely accepted validation process comes from the comparison of a series of experimental test results (numerical values of some chosen physical quantity or specific index, characteristic curves, time histories or spectra of some definite signal, and so on) with the equivalent results from the numerical model. Usually validation is considered at the global system level, also including interactions with the external environment (boundary conditions in the most general sense, in the case of a car crash barriers and interaction with the soil, in the case of some simple mechanical test the interaction with environment and the external constraints) but it can be at the component level also [4]. In some cases validation of a series of components at their component level can be accepted for validation of the assembly also: this bottom-top validation process is not without inconvenient and must be used with careful attention, but is acceptable under cautious examination.

However, other forms of validation can be foreseen and are sometimes used and accepted: for example the validation of a numerical model from a former theoretical analysis (typically the comparison of numerical results with the results from widely accepted mechanical theories like Saint Venant's beam model or thick shell theory, that were previously experimentally verified; this is like Nafems process).

Figure 3. The GCM4 exterior and, below, a view of the interior parts (seats are not shown but are included in the model).

The difficulty in the case of GCMs comes from the fact that there is no physical sample to compare with. Since GCMs are fully virtual cars, there are not and there will not be a physical system nor component at all. Therefore, no experimental test will be available to check. Besides the costs involved with the production of such a prototype, it is not sure that the unique or almost unique sample will be significant and useful.

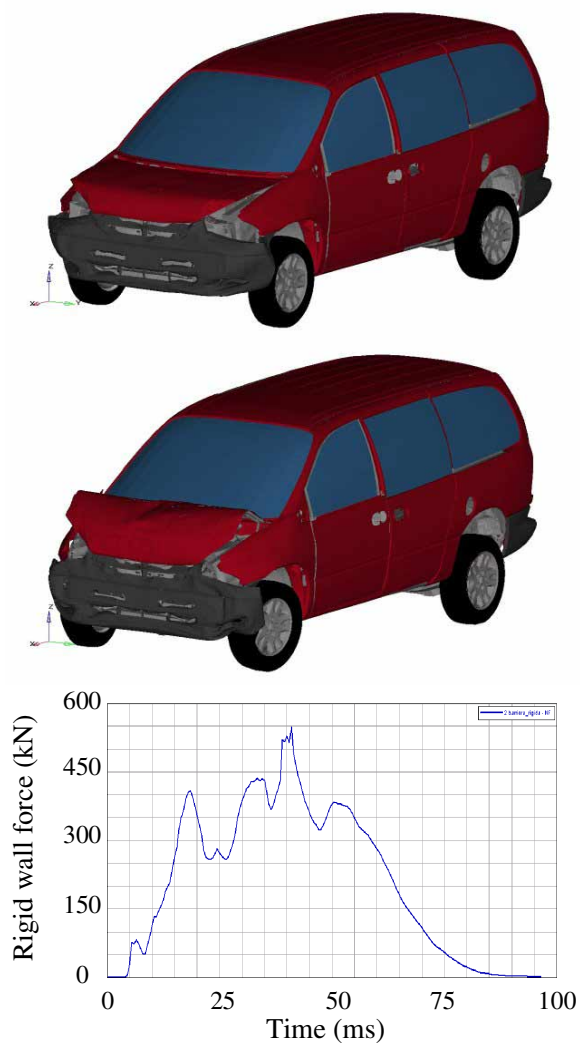

Figure 4. Crash test of the GCM4 against a rigid barrier, deformed structure after 50 ms and 100 ms, and the associated force time history.

However, some validation criteria was to be defined in the most efficient and convincing way. The most acceptable approach to validate the GCMs was agreed to be the comparison with the most wide number of experimental tests coming from external independent sources.

Such a comparison can be done with recent results from EuroNCAP tests of cars of the same class, that for the GCM4 is MPVs, as shown for example by Huibers and de Beer [12].

The GCMs were then tested in various conditions. The results from the EuroNCAP 60% offset crash test on deformable barrier [13] are shown in figure 5. The structural deformation is reasonable, and there are not serious critical deformations.

Figure 6 show the comparison in terms of forces exchanged with the barrier. The reference curves are from [12].

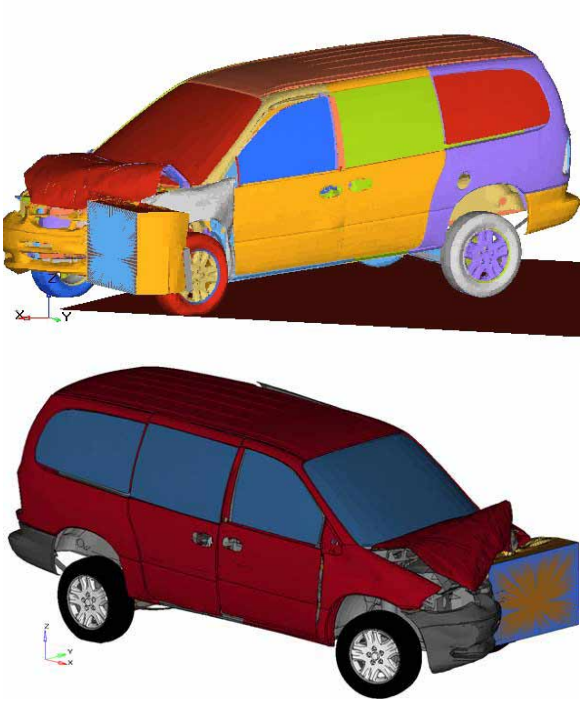

Figure 5. Crash test of the according to EuroNCAP standard for offset impact against deformable barrier [13].

In figure 6, below, the comparison is also shown in terms of a corridor defined from the envelope of all the seven reference curves. The force-displacement curve of the GCM4 is about 86% of the time inside the corridor (strictly inside is 70%; this discrepancy is partly related to uncertainty at the first impact and the shorter length at the end of the impact). The final displacement is slightly less than the average, but this is justified by the fact that the vehicle was without dummies: therefore the overall mass was smaller than the average, even if the body-in-white mass of the GCM4 compares well with the other cars of the class.

Therefore, the GCM4 can be considered validated and acceptable.

It is worth noticing that this validation is important and sufficient for the scope of the APROSYS project to have numerical models available for research purpose, to develop advanced protection systems and the virtual testing methodology and protocols.

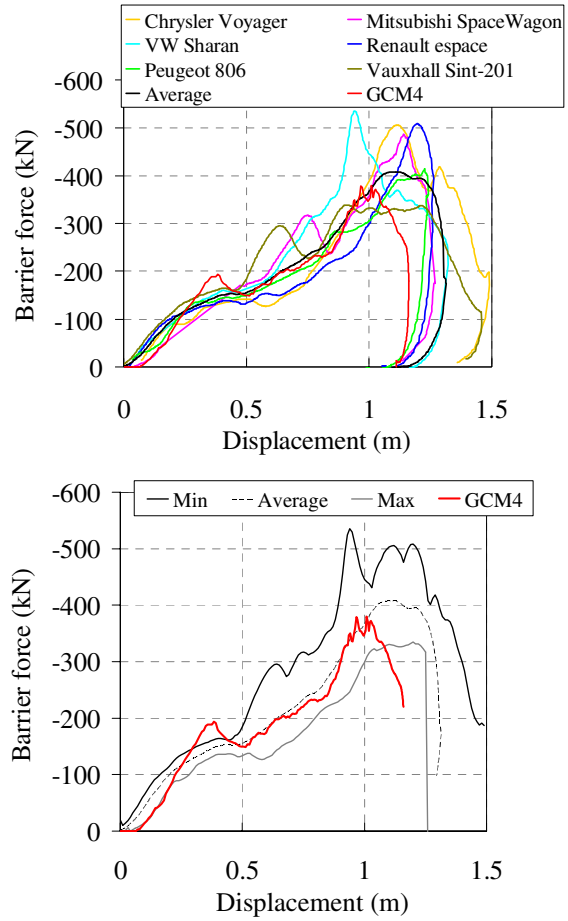

Figure 6. Comparison of the force-displacement curves from EuroNCAP experimental tests on similar cars of the same class (MPVs) with GCM4. Below, the curve is compared with the corridor obtained from the envelope of all the test curves.

3. STOCHASTIC MODEL

A probabilistic approach can be used to evaluate the uncertainties in simulated responses of a system [14-15]. This is extremely important to evaluate the results coming from virtual models. There are, in fact, uncertainties coming from modeling material behavior, material data, geometrical parameters, contact definition, but also uncertainties due to the numerical tools as for example validity limits of the elements formulation. Boundary conditions are also known with a certain degree of uncertainty.

Stochastic analyses give also much information on the influence of the various parameters of influence and their relative importance. These results can be used for optimization and robustness analysis of the vehicle in the design process.

In the following sections the results from a stochastic analysis carried out on the GCM4 are described. The results are analyzed by means of the ADVISER [16-17] software, developed jointly by Mecalog (now Altair Development France) and TNO during the ADVANCE project.

Stochastic variables and analyzed responses

A stochastic model is based on the analysis of the distribution of some output response due to the stochastic variations of some input variable, affected by random variations.

The material properties and the sheet thickness are among the main sources of dispersion that affect the structural behavior of the vehicle body. The thickness variation is typically very small and has an effect analogous to a variation in the stress-strain curve of the material. Therefore, it has been chosen to examine the variation of the material characteristics. The range of variation accounts for both the natural material variations and the thickness dispersion.

Two variables were then defined, one for the variation of the properties of the material of the front rails and the other for the variation of the material properties of the remaining GCM4 body.

The range of variation is reported in table 1, whereas figure 7 gives a graphical representation of the variability of the stress-strain characteristic.

Table 1.
Steel properties and range of variation

Stochastic variables	*RailsYieldStress*	*CabinYieldStress*
Nominal value (GPa)	0.365	0.250
Standard deviation (GPa)	0.035	0.040
Upper value (GPa)	0.40	0.29
Lower value (GPa)	0.33	0.21

The two variables were considered with a normal distribution. The samples for the simulations were generated by ADVISER, by using the Optimal Latin Hypercube algorithm. The experimental plan is shown in figure 8.

The responses used in the analysis are acceleration curves from selected characteristic points within the passenger compartment (figure 9), the force transmitted by the car to the barrier, and the intrusion on the vital space of the driver (figure 10), as follows:

- Maximum value of the acceleration on the base of the left B-pillar;
- Mean value of the acceleration on the base of the left B-pillar;
- Maximum value of the acceleration on the centre of the passenger compartment between the front seats;
- Mean value of the acceleration on the centre of the passenger compartment between the front seats;
- Maximum value of the normal contact interface force between car and barrier;
- Mean value of the normal contact interface force between car and barrier;
- Maximum value of the X component of the normal contact interface force between car and barrier;
- Mean value of the X component of the normal contact interface force between car and barrier;
- Total displacement of the centre of the passenger compartment between the front seats;
- X component of Displacement on the base of the left B-pillar;
- Intrusion on the vital space of the driver; measured as the reduction of the distance between the base of the B-pillar and the knee of the A-pillar.

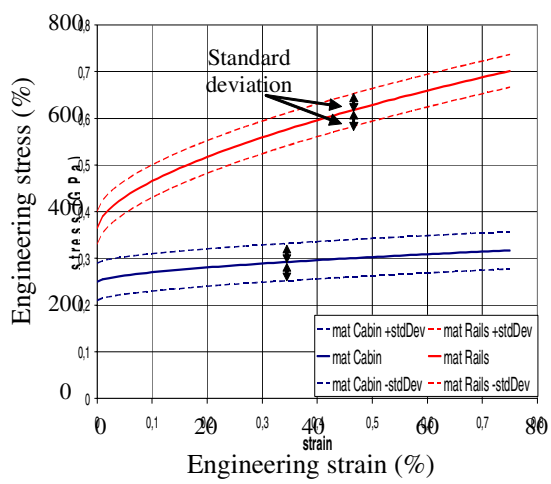

Figure 7. Material characteristic of the steel of the front rails and the GCM body overall, with the range of variation.

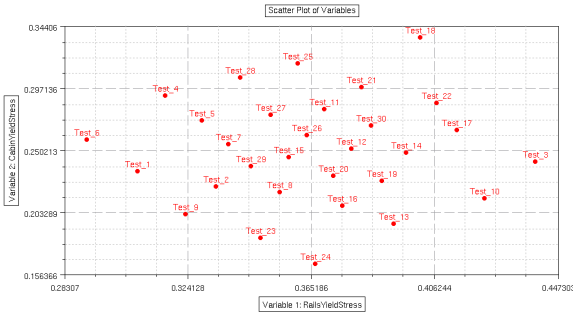

Figure 8. Scatter plot of the two analyzed variables.

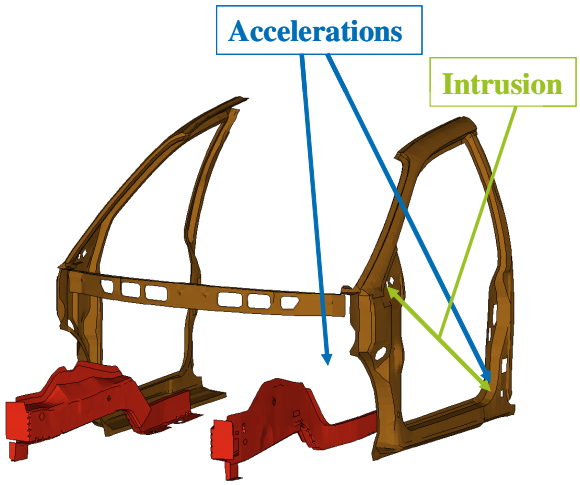

Figure 9. Measurement points of the acceleration and of the intrusion.

Stochastic analysis

The results from the simulation runs were analyzed by means of the ADVISER software. The results are put in the form of tables. Each run (row) is associated to a series of responses (columns) as described above. Some statistical descriptor useful for the analysis can be calculated (mean value, relative range of variation, standard deviation, variance, skewness, and kurtosis).

A graphical representation of the raw figures is shown in figure 10. Some simple consideration can be drawn from the observation of these charts. The responses linked to the acceleration of the B-pillar, and especially its maximum values, have a wide range of variation and seem to be quite sensitive to the variables variation. Moreover, the maximum value can not be considered to have a normal distribution and its histogram shows a possible bifurcation of the response.

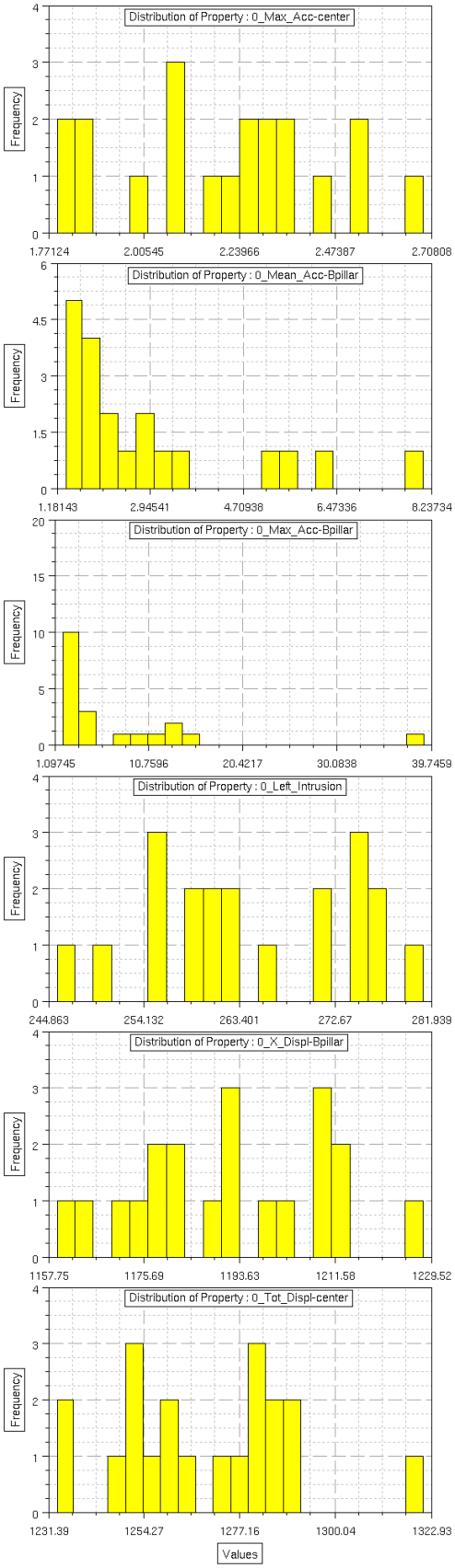

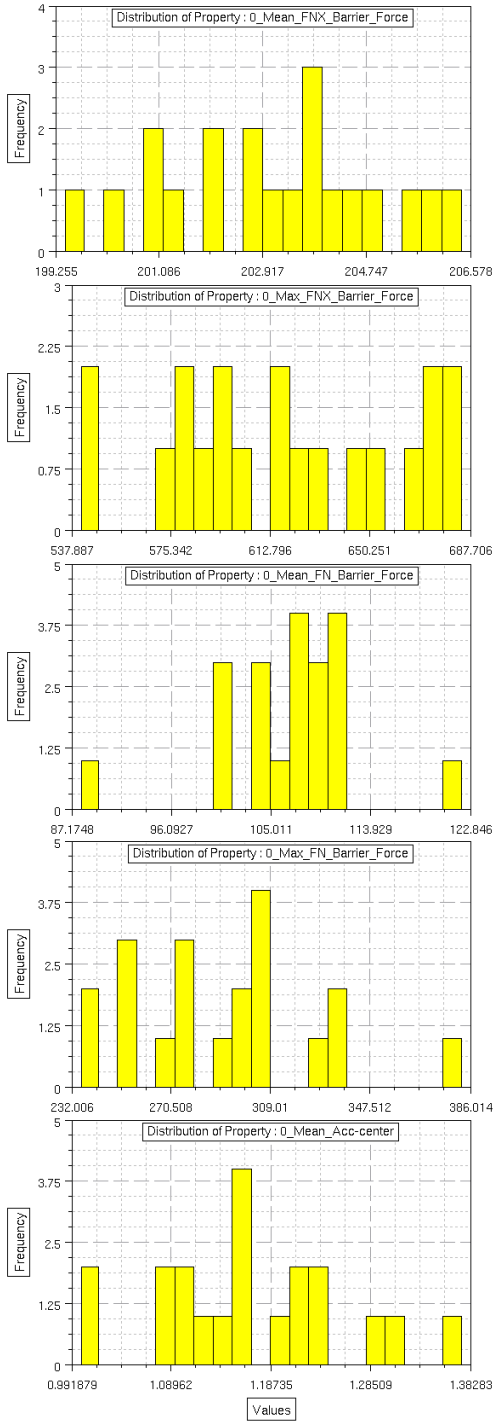

Figure 10. Histograms of the distribution of the responses.

The analysis of the scatter in the responses highlights how a relatively small variation of the input, in the order of magnitude of 10%, can produce greater effects, up to some 20%. This is a very critical issue, to be considered even for physical crash tests which have very few or no repetitions. Scatter in experimental crash it is not known, as sources of dispersion cannot be taken into account.

Further insight in the parametric response of the system is given by the linear and quadratic correlation matrices (figure 11) [18-19]. It appears that the variable yield stress of the steel has high direct correlation with the intrusion on the left side, and high inverse correlation with the maximum and mean values of the acceleration in the centre of the passenger compartment. The variable yield stress of the steel of the rails has only a moderate direct correlation with the responses related to the contact interface force. The maximum and mean values of the B-pillar acceleration, instead, are the only responses with a quite low correlation with both input variables. Finally, it has to be noted that most quadratic correlation coefficients are higher than the corresponding linear ones.

The linear correlation coefficient of the various parameters can also be computed [18].

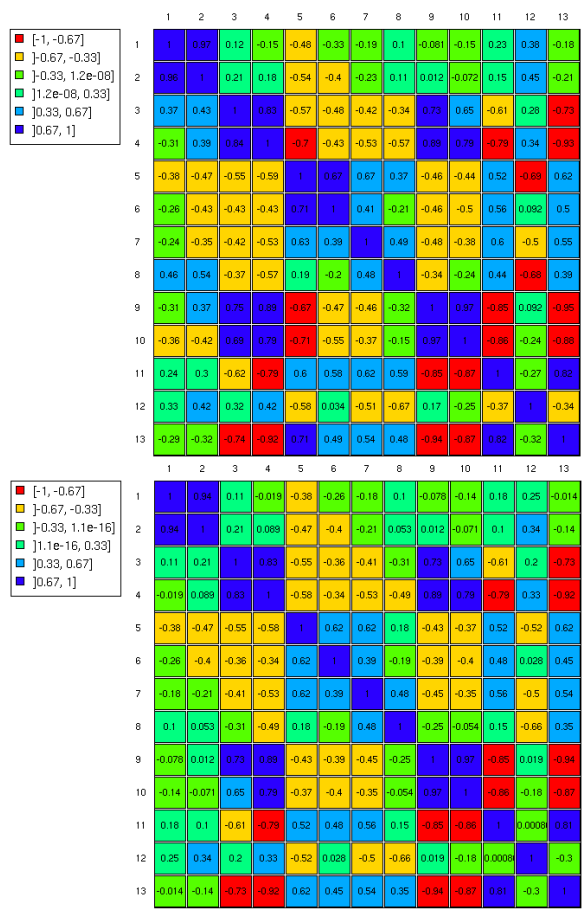

Figure 11. Linear and quadratic correlation matrices for the stochastic parametric problem analyzed.

Confirmation of the results from the correlation matrices comes from the principal component analysis (PCA). It was performed with ADVISER and shown in terms of the distance bi-plot (figure 12) and of the correlation bi-plot (figure 13). Both are representations of variables and responses in the plane of the first two principal components and confirm the previous observations. In this plots direct correlation corresponds to parallel vectors in the same direction, inverse correlation corresponds to parallel vectors in the opposite direction. Perpendicular directions mean lack of correlation. In the distance bi-plot the main role of the *CabinYieldStress* variable is shown: its vector is almost coincident to the first principal axis. The correlation bi-plot shows the high direct or inverse correlation of a lot of responses with the *CabinYieldStress* variable, and highlights that the only response which have a quite good inverse correlation with the *RailsYieldStress* variable is the mean X component of the contact interface force. The absence of correlations for the maximum and mean values of the B-pillar acceleration is also visible and the uncertain correlations of the maximum values of the total and X contact force can be revealed.

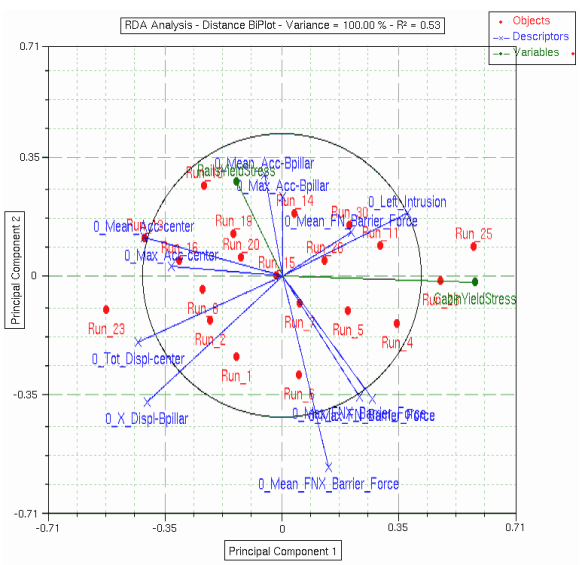

Figure 12. Distance bi-plot: the yield stress of the cabin steel shows high inverse correlation with the mean and maximum acceleration in the centre of the passenger compartment (the related vectors are almost parallel, but in opposite directions). The front rail steel yield stress has direct and inverse correlation with many outputs.

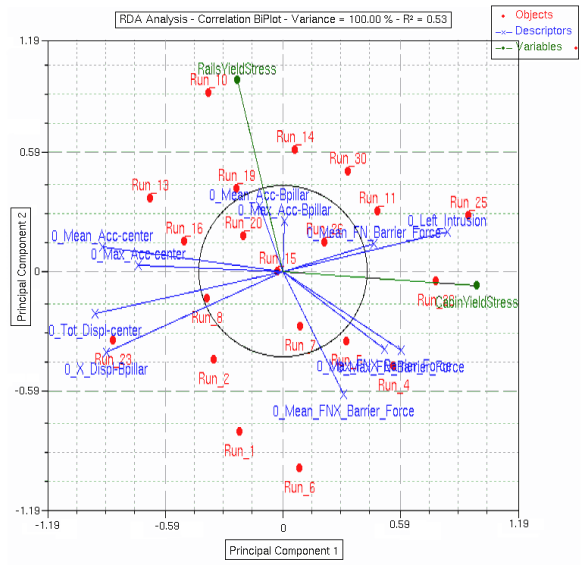

Figure 13. Correlation bi-plot: the results are similar to the distance bi-plot, but it gives also a quantitative measure of the correlations.

From the analysis of the correlation matrices and correlation bi-plots, the main results can be summarized as follows:

- All responses can be considered to have a normal distribution with the exception of the maximum and mean B-pillar accelerations, which have quite high ranges of variation and seem to present bifurcated behaviors.
- From both the linear and quadratic correlation matrices, high correlations of a lot of responses with the yield stress of the passenger compartment steel were found, while the yield stress of the frontal rails steel is only moderately correlated with some responses related to the interface contact force.
- The coefficients of the linear regression confirm the correlations revealed by means of the correlation matrices. Furthermore the first order interaction coefficients are quite low for all responses, except for the left side intrusion which is affected by a strong interaction of the two variables.

Finally the principal component analysis (PCA), by means of the distance bi-plot and of the correlation bi-plot, confirms the main importance of the yield stress of the passenger compartment steel and its high direct or inverse correlation with a lot of responses.

To identify what are the main influences and how they are grouped together, the cluster analysis can be performed. The cluster analysis by means of a

single linkage grouping of response variables is shown in figure 14.

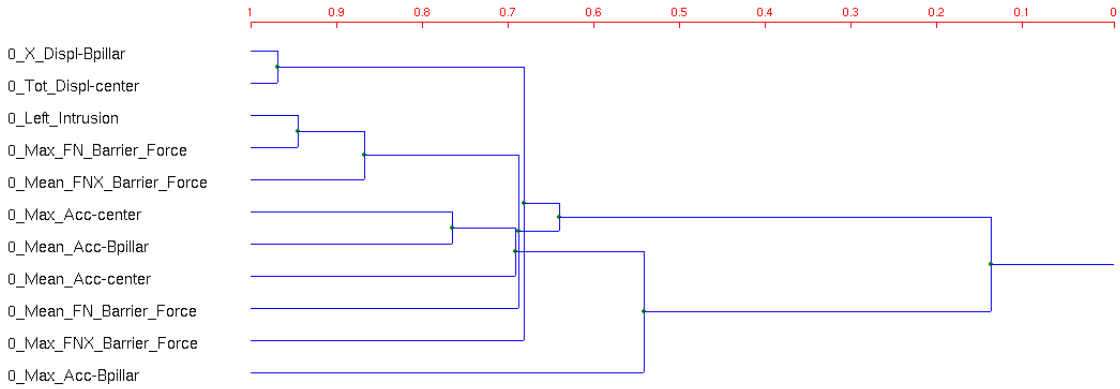

Figure 14. Cluster analysis: it helps to identify how the influence on the various responses can be grouped together.

5. CONCLUSIONS

One of the important topics addressed in the 5th and 6th European FP projects ADVANCE, VITES, and APROSYS is the development of the virtual testing (VT). Validated and fully reliable virtual testing methods and tools have been improved, and the use of virtual testing will not be restricted to the design of vehicles for crash, but it is possible to foresee its utilization, hopefully, also in regulations.

An essential tool to build validated and safe VT models is based on the stochastic analysis. Stochastic analysis allows examining the sources of influence and the correlation with the structural responses. It can help identifying correlations, but also their relative influence, the distributions of the outputs and their statistical parameters, and even show whether there are unpredictable behavior. For example, bi-modal distribution of a response can be related to bifurcations.

A numerical example has been used to demonstrate this approach. The example used a generic car model (GCM) developed within the APROSYS project. The GCMs are virtual cars specifically developed to be used for advanced researches, to be shared among the APROSYS partners to address all the necessary studies for VT. The GCM4, a multipurpose vehicle, developed by Politecnico di Torino was used.

The analysis was carried out by means of the ADVISER software, developed by Mecalog and TNO, during the above mentioned projects.

The effectiveness of the provided tools has been demonstrated. The correlation matrices, both linear and quadratic, give a first glimpse to the main factor of influence, by ranking in a scale from 0 to 1.

Direct and inverse correlations can be made clear with the use of the correlation and distance bi-plots. These are graphical tools that represent the correlations of a couple of input parameters with the output responses. When many input parameters are considered, several correlation bi-plots will be created, even if this will complicate the analysis of the results.

To help the analysis, in the case of multiple input and output, the cluster analysis help in identifying the main mutual connections between responses and will point the analysis in the right direction.

The availability and the continuous improvement of these tools is an important contribution to the assessment of up-to-date analysis methodologies to improve the passive safety of vehicles of any type.

ACKNOWLEDGEMENTS

The authors kindly acknowledge the European Commission that, by funding the APROSYS project through contract TIP3-CT-2004-506503, made this research activity possible. Thanks are also due to the other APROSYS partners, especially Mr. Roberto Puppini of Centro Ricerche Fiat, Italy, Workpackage 7.1 leader.

REFERENCES

[1] APROSYS. 2007. “Description of work – SP7 Virtual Testing.” APROSYS SP1 report, Deliverable AP-SP11-001.

[2] VITES. 2004. “Virtual Testing for Extended Vehicle Passive Safety.” Final Technical Report.

[3] Delcroix, F. et al. 2004. “Parametric studies and evaluation.” ADVANCE report of Task 7.1, Deliverable D20.

[4] Meijer, R. and R. Happee. 2006. “Virtual Testing in Regulations.” APROSYS SP8 Workshop proceedings, Delft, Deliverable AP-SP81-003.

[5] Delcroix, F. et al. 2004. “Scatter of data, stochastic analysis and design robustness.” APROSYS report of task T7.2.1, Deliverable AP-SP7-WP7.2-0003-A.

[6] Diez, M., F. Delcroix et al. 2005. “Sources of dispersion and ADVISER templates for stochastic analysis.” APROSYS report of task T7.2.1, Deliverable AP-SP72-0009-B.

[7] VV.AA. 2005. “Report on main factors in side impact compatibility.” APROSYS report of WP1.1, Deliverable D1.1.5.

[8] VV.AA. 2005. “Preliminary system simulation results and estimation of the pre-crash systems potential.” APROSYS report of WP6.3, Deliverable D6.3.4.

[9] VV.AA. 2005. “Cost / benefit analyses of proposed systems [for Advanced vulnerable road user protection systems].” APROSYS report of WP2.1, Deliverable D2.1.2C.

[10] VV.AA. 2006. “Optimisation methodologies to improve existing protective equipment [for motorcyclists]. Analysis from in-depth studies and simulated reconstructions.” APROSYS report of WP4.3, Deliverable D4.3.1A.

[11] VV. AA. 2007. “New head injury mechanisms.” APROSYS report of WP5.1, Deliverable D5.1.1D.

[12] Huibers, J. and E. de Beer. 2001. “Current front stiffness of European vehicles with regard to compatibility.” In Proceedings of the 17th ESV conference, Paper No. 239.

[13] EuroNCAP. 2001. “Frontal impact testing protocol.” Version 4.1, http://www.euroncap.com

[14] Lyle, K.H., S.L. Padula and A.E. Stockwell. 2003. “Application of probabilistic analysis to aircraft impact dynamics.” American Institute of Aeronautics and Astronautics, Paper No. 1482.

[15] Lyle, K.H., A.E. Stockwell and R.C. Hardy. 2003. “Application of probability methods to assess crash modeling uncertainty.” American Institute of Aeronautics and Astronautics, Paper No. 59.

[16] ADVISER user’s manual, MECALOG/TNO.

[17] Van Hoof, J., R. Puppini, H. Baldauf, C. Oakley and K. Kayvantash. 2003. “ADVISER: a software tool for evaluation and rating of numerical models in crash safety analyses.” In Proceedings of the 18th ESV conference, Paper No. 483.

[17] Legendre, P. and L. Legendre. 1998. “Numerical Ecology.” Second English Edition, Elsevier.

[18] Rapallo, F. and M.P. Rogatin. 2003. “Statistica descrittiva multivariata.” CLUT, Torino, Italy.

CHARACTERIZATION OF ADVANCED AIR BAG FIELD PERFORMANCE USING EVENT DATA RECORDERS

Hampton C. Gabler
Virginia Tech
United States

John Hinch
U.S. National Highway Traffic Safety Administration
United States

Paper Number 07-0349

ABSTRACT

This paper characterizes the field performance of occupant restraint systems designed with advanced air bag features including those specified in the US Federal Motor Vehicle Safety Standard (FMVSS) No. 208 for advanced air bags, through the use of Event Data Recorders (EDRs). Although advanced restraint systems have been extensively tested in the laboratory, we are only beginning to understand the performance of these systems in the field. Because EDRs record many of the inputs to the advanced air bag control module, these devices can provide unique insights into the characteristics of field performance of air bags. The study was based on advanced air bag cases extracted from NASS/CDS 2000-2005 with associated EDR data. The paper presents the characteristics of advanced air bag deployment (number of stages and trigger time) as a function of crash severity and seating location, the characteristics of delayed deployments, and the frequency and characteristics of frontal crashes in which the air bag did not deploy.

INTRODUCTION

In the U.S., automakers have introduced a new generation of advanced occupant restraints, including those specifically introduced in response to the requirements for advanced air bags, as specified in the FMVSS No. 208 upgrade [49 CFR 571.208 (65FR30680)]. These advanced systems are characterized by multi-stage air bag inflators, pretensionsers, advanced occupant sensors, and complex air bag deployment algorithms. Although these systems have been extensively tested in the laboratory, we are only beginning to understand the performance of these systems in the field. Because EDRs record many of the inputs to the advanced air bag control module, these devices can provide unique insights into the performance of air bags in the field.

OBJECTIVE

The objective of this study is to characterize the performance of advanced frontal air bags in real world crashes. The paper will include both vehicles certified to the FMVSS No. 208 advanced air bag regulation, and vehicles having dual-stage frontal air bags.

APPROACH

The analysis was based upon EDR records extracted from the Virginia Tech EDR (VT EDR Database) database. The VT EDR Database contains the records from over 2,200 EDRs downloaded as part of National Automotive Sampling System / Crashworthiness Data System (NASS/CDS) 2000-2005 crash investigations. All cases were downloaded by NASS investigators in the field using the Vetronix Crash Data Recorder (CDR) retrieval system.

CHARACTERIZATION OF DATA SET

This study included only EDR cases from vehicles having a dual-stage frontal air bag. The resulting sample contained the EDR records from 106 vehicles having air bags of the advanced type, also referred to as certified advanced compliant (CAC) air bags. CAC air bags are defined as air bags in those vehicles certified to the FMVSS No. 208 upgrade. The sample was composed entirely of General Motors (GM) passenger cars, light trucks, and vans. Table 1 shows the distribution of cases by EDR module type.

Table 1. Distribution of CAC Air Bag Cases by EDR Module Type

EDR Module Type	Deployment	Non-Deployment	Total
SDMDW2003	3	3	6
SDMGF2002	44	56	100
Total	**47**	**59**	**106**

GM EDRs record longitudinal delta-V versus time for up to two events. Figure 1 presents the distribution of maximum longitudinal delta-V recorded by each of 47 the CAC EDRs in which the frontal air bag deployed. The median longitudinal delta-V in our sample was approximately 15 mph.

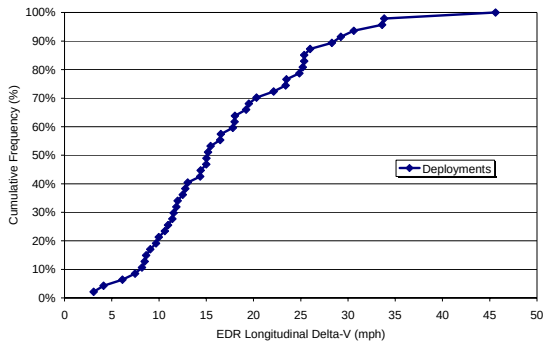

Figure 1. Distribution of Longitudinal Delta-V Values in Deployment Events

As shown in Figure 2, a frontal impact was the most harmful event in over 90% of the CAC air bag deployment cases.

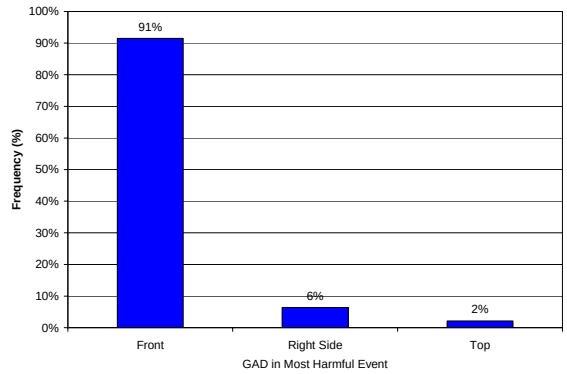

Figure 2. General Area of Damage in Most Harmful Event in Deployment Crashes

More useful than knowing the General Area of Damage (GAD) of the most harmful event however would be to know the GAD of the event which triggered the air bag. The most harmful event may not be the event which triggers the airbag. Unfortunately, in a multiple event crash, the event which triggered the air bag cannot always be determined. As shown in Figure 3, NASS investigators recorded that over 50% of the CAC air bag deployment cases involved multiple events. Not all of these events necessarily have a longitudinal component of sufficient magnitude to deploy the air bag.

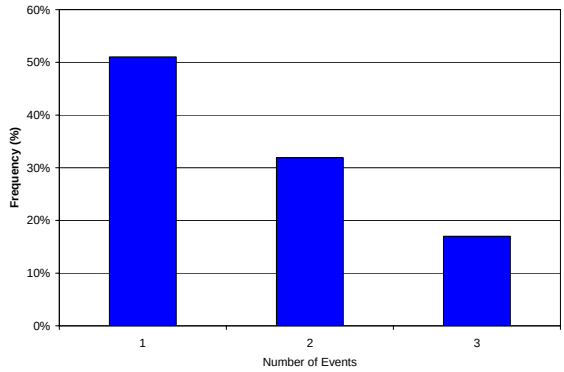

Figure 3. Number of Impact Events in Each Crash Involving a Frontal Air Bag Deployment as Observed by NASS investigator

The EDR data indicated that the majority of the deployment cases in our sample involved only a single event having a longitudinal component of delta-V. The SDMGF2002 module records a count of the number of events in each crash which involved a longitudinal component of delta-V. In our sample of 47 deployments, 44 were SDMGF2002 modules. Figure 4 below shows that in over 80% of the cases, the EDR detected only a single impact with any longitudinal component. This observation does not however mean these events were frontal impacts. Although events with strong longitudinal components are typically frontal impacts, it is possible for other crash modes including side impacts to have a significantly severe longitudinal component to deploy the air bag.

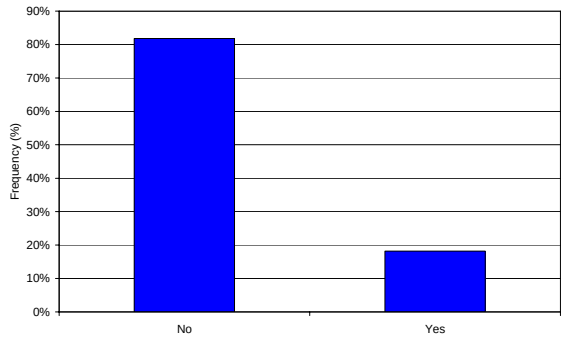

Figure 4. Number of Deployment Crashes with Multiple Events Involving Longitudinal Delta-v Component as Recorded by EDR

Belt Use and Air Bag Deployment

Table 2 presents the distribution of driver belt buckle status in deployment cases. In approximately half of the cases, the EDR recorded that the driver belt was buckled. In our sample, the EDR driver seat belt buckle status frequently did not agree with the belt use status determined by the NASS investigator. In 9

of the 31 cases in which NASS investigators believed that the driver was belted, the EDR recorded that the driver belt was unbuckled.

Table 2. Driver Belt Buckle Status

EDR Buckle Status	NASS – Belted	NASS - Unbelted	Not Inspected by NASS	Total
Buckled	22	1	2	25
Not Buckled	9	12	1	22
Total	31	13	3	47

Table 3 shows that in half of the cases in which a right front passenger was present, the EDR recorded that the passenger was buckled. Because the EDR passenger buckle status is not a data element recorded by the SDMDW2003 module, the three SDMDW2003 cases are not tabulated in Table 3.

Table 3. Right Front Passenger Belt Buckle Status

EDR Buckle Status	NASS – Belted	NASS - Unbelted	Total
Buckled	2	1	3
Not Buckled	2	1	3
Total	4	2	6

Table 4 compares the records of driver air bag deployment as indicated by the NASS investigator and recorded by the EDR. In all but one of the deployments, the EDR and NASS investigators agreed the air bag deployed. In all non-deployment cases, EDR and NASS investigators agreed that the bag had not deployed.

Table 4. Driver Air Bag Deployment Status

EDR Deployment Status	NASS- Not Inspected	NASS- Bag Deployed	NASS- No Deploy	Total
Deployed	3	43	1	47
Non-deploy	15	-	44	59
Total	18	43	45	106

In case 2002-12-150, a 2003 Chevrolet Suburban was involved in a crash in which the EDR recorded that the driver air bag was deployed. NASS investigators observed however that the driver air bag did not deploy. Inspection of the photos from the investigation confirms the NASS observation that the bag did not deploy.

Vehicle Speed just Prior to Impact

The GM EDRs in our dataset recorded 5 seconds of precrash data in one second intervals on vehicle speed, engine speed, engine throttle setting, and brake status. The vehicle speed data at one second before algorithm enable provides an estimate of vehicle speed approximately one second before impact. Figure 5 provides a distribution of vehicle speed at t = - 1 second for the CAC deployment cases in our sample. Although the EDRs in our dataset did not record impact speed, this measure provides an estimate of vehicle speed just before impact. The median vehicle speed approximately 1 second before impact was 38 mph.

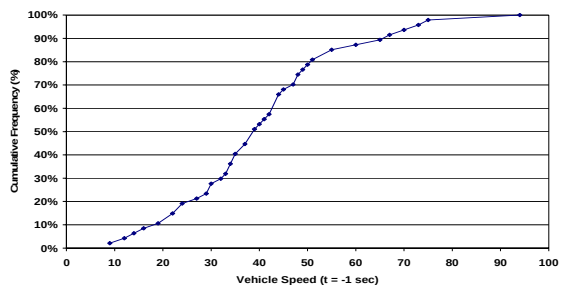

Figure 5. Distribution of Vehicle Speed approximately One Second before impact in Deployment Events

RESULTS

Figure 6 compares the distribution of the driver air bag deployments and non-deployments by peak longitudinal delta-V. All cases in this analysis had incurred a frontal impact in the most harmful event. The cases were aggregated into three groups: 1) those crashes which resulted in a deployment, 2) those crashes not sufficiently severe to deploy the airbag, and 3) split deployments. Split deployments are those cases in which the driver air bag deployed, but the right front passenger air bag did not deploy despite the presence of a passenger. There were no cases in which the passenger air bag deployed, but the driver air bag did not deploy. Of the 106 CAC cases, there were 41 deployments, 2 split deployments, and 19 non-deployments in which the general area of damage was frontal.

The driver frontal air bag was observed to deploy in crashes having a longitudinal delta-V as low as 3-4 mph. The driver bag was observed to not deploy in a crash having a longitudinal delta-V of 26 mph. This crash was a long duration crash of approximately 275 milliseconds into an earth and rock embankment. Logistic regression was performed to determine the probability of driver air bag deployment as a function of longitudinal delta-V. For this sample, the

probability of driver air bag deployment was 50% for a longitudinal delta-V of 8 mph.

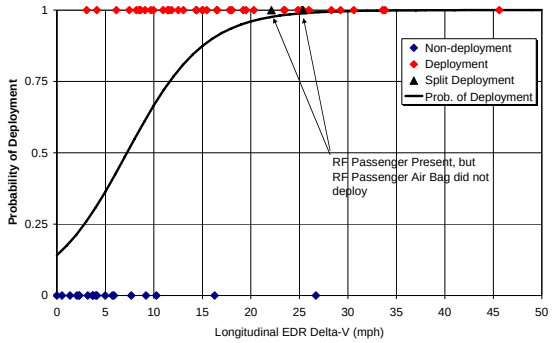

Figure 6. Probability of Deployment of Driver Air Bag by Longitudinal Delta-V

In our dataset of 106 CAC cases, there were 20 right front passengers involved in a crash in which a frontal impact was the most harmful event. This 20 case set consisted of 11 deployments, 2 split deployments, and 7 non-deployments. Figure 7 presents the distribution of the right front air bag deployment decision by longitudinal delta-V for these cases. The right front passenger air bag was observed to deploy in collisions having a longitudinal delta-V as low as 6 mph. In general, the passenger air bag did not deploy in low delta-V crashes. In one crash however, the right front passenger air bag did not deploy in crashes having a longitudinal delta-V of 26 mph. Because our dataset contained only a limited number of right front passenger cases, a logistic regression computation was not possible for this data subset.

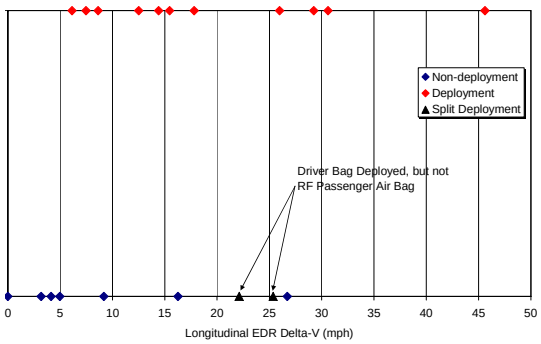

Figure 7. Distribution of Right Front Passenger Air Bag Deployment Decisions by Delta-V

All CAC air bag systems in our data set contained dual stage inflators. Dual stage inflators allow the air bag deployment characteristics to be tailored to the particular crash severity and occupant configuration of a collision. Of the106 CAC cases, there were 43 driver air bag deployments and 19 non-deployments in which the most harmful event was a frontal impact. In the 43 deployments, both the first and second stage fired in 9 of the crashes. Only the first stage fired in the remaining 34 cases. In general as shown in Figure 8, both inflator stages were triggered only in higher delta-V crashes.

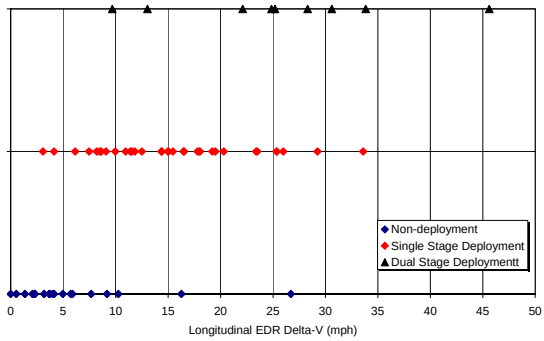

Figure 8. Distribution of Driver Air bag Dual-Stage, Single-Stage, and Non-deployments vs. Delta-V

Figure 9 presents the relationship between longitudinal delta-V and the vehicle speed just prior to impact. In the majority of cases, vehicle speed greatly exceeds longitudinal delta-V.

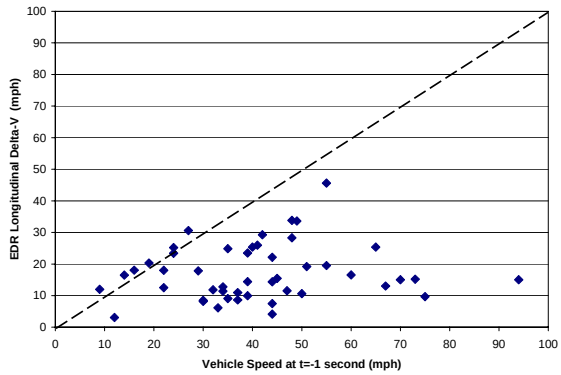

Figure 9. Longitudinal Delta-V vs. Vehicle Speed just before collision in CAC deployment cases

Time Interval from Algorithm Enable to Deployment

Air bag deployment is controlled using a microprocessor. Typically vehicle acceleration, often measured at a central vehicle location and near the front of the vehicle, is processed to determine when the vehicle's frontal air bags should be deployed as well as which air bag stage should be utilized. The air bag processor wakes up after it senses a predetermined acceleration threshold has been exceeded. This wake up is defined as algorithm enable (AE) [Chidester et al, 1999]. After AE occurs, the processor continues to monitor and

analyze the vehicle's deceleration profile and determines if and when the air bags should be deployed. The time the processor deploys the air bags is often referred to as air bag deployment time and is referenced to AE as a time zero. For instance, if the air bags deployed 25 milliseconds (msec) after AE, common notation would consider this an air bag deployment time of 25 msec.

To provide context for real world air bag deployment times, EDRs have been used to assess that air bag deployment times during NHTSA's frontal barrier tests, conducted for Federal motor vehicle safety standard (FMVSS) No. 208 and New Car Assessment Program (NCAP). Data from over thirty vehicles, model year 2002 through 2006, were examined. Deployment times are shown in Figure 10. For these tests, the average deployment time for the first stage driver air bag was 7 msec, with a range of 2.5 to 17.5 msec. Generally, the driver and right front passenger air bags (both first and second stages) deployed at the same exact time.

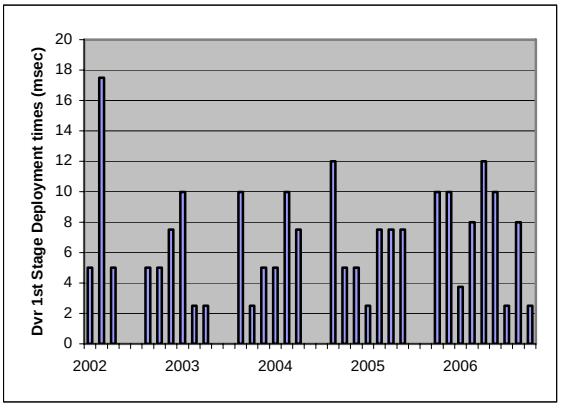

Figure 10. 1st Stage Deployment Times vs. Model Year in Frontal NCAP Tests

Analyses of air bag deployments from real world crashes would allow full range analysis of deployment times under many circumstances. Since there were only 47 CAC deployment cases, we extended the analysis of deployment times to include pre-CAC vehicles with dual stage air bags. NASS cases from years 2000 to 2005, which included a complete EDR record, and a GM vehicle with a dual stage air bag system which deployed, were compiled into a subset of the VT EDR Database. A total of 132 cases met these criteria. Using the EDR data, air bag deployment times were used to form a cumulative distribution, as seen in Figure 11.

In this sample of GM vehicles, with complete EDR records and equipped with dual air bags, the 50th percentile deployment time is 20 msec while the 75th percentile is 35 msec.

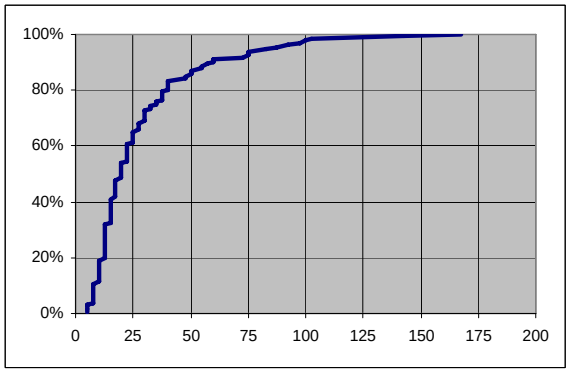

Figure 11. Cumulative Distribution (%) of Driver 1st Stage Air Bag Deployment vs. Deployment Time (msec)

DELAYED DEPLOYMENTS

The VT EDR database contained 132 cases involving deployment of an advanced dual stage air bag. Twelve vehicles had driver deployment times recorded by the EDR of 72.5 msec and longer. Four of the vehicles were CAC. Eight cases were pre-CAC vehicles with dual stage air bags. For each of these vehicles, the NASS and EDR data were reviewed to determine common characteristics. The GM vehicle model year, make, and model for these cases as reported by NASS are presented in Table 5.

Table 5. Vehicle Model Year, Make and Model (* = CAC Vehicle)

NASS Case Number	Model Year	Make	Model
2004-75-126 *	2003	Chev	Avalanche
2004-50-087 *	2004	Chev	C/K-series Pickup
2004-12-052	2001	Pont	Bonneville/Catalina
2005-04-062	2005	Chev	Caprice/Impala
2001-41-133	2001	Chev	Monte Carlo (FWD)
2004-08-108	2004	Saturn	Ion
2004-11-082	2004	Saturn	Ion
2003-12-162	2002	Chev	Caprice/Impala
2005-76-009 *	2004	GMC	C,K,R,V-series P/U
2005-12-149	2005	Chev	Equinox
2004-48-181	2001	Chev	Caprice/Impala
2003-50-110 *	2003	GMC	C,K,R,V-series P/U

For each of these cases, the EDR data were reviewed to determine the driver seat belt status, longitudinal delta-V of the case vehicle, and the driver's air bag deployment time. These data are provided in Table 6.

Table 6. Driver Belt Status, Vehicle Longitudinal Delta-V, and Driver Air Bag Deployment Times (* = CAC Vehicle)

NASS Case Number	Dvr Belt Stat	Delta-V (mph)	Dvr A/B Dep Time (msec)
2004-75-126 *	Buckled	-6.13	167.5
2004-50-087 *	Unbuckled	-19.21	142.5
2004-12-052	Buckled	-28.62	102.5
2005-04-062	Buckled	-58.41	100
2001-41-133	Buckled	-26.21	97.5
2004-08-108	Unbuckled	-10.99	92.5
2004-11-082	Unbuckled	-30.46	87.5
2003-12-162	Buckled	-7.64	82.5
2005-76-009 *	Unbuckled	-17.81	75
2005-12-149	Buckled	-8.10	75
2004-48-181	Buckled	-7.93	75
2003-50-110 *	Unbuckled	-20.31	72.5

NASS Case Discussion

The following presents a short description of the crash, vehicle speed and longitudinal delta-V as reported by the EDR, multi event as reported by the NASS investigator or the EDR, and some potential reasons for the long reported driver's air bag deployment times. In the discussions which follow, PDOF refers to the principal direction of force, expressed in degrees, where 0 is direct frontal. GAD refers to the general area of damage. GAD = F indicates frontal damage.

2004-75-126

Impact description: Minor vehicle impact, followed by curb hit (EDR N/D event) and then subsequent vehicle impact (EDR D event).
Vehicle speed: EDR @ -1 sec = 33 mph
D event delta-V = 6 mph
GAD/PDOF: Frontal/350deg
Multi event: yes
Potential reasons for late reported deployment time:

- Low delta-V event
- Closely spaced D and N/D events

2004-50-087

Impact Description: Multi event crash – sideswiped small post, offset impact on utility pole (D event) followed by curb hit.
Vehicle speed: EDR @ -1 sec = 51 mph
D event delta-V = 19 mph
GAD/PDOF: F/0deg
Multi event: yes
Potential reasons for late reported deployment time:

- Extreme low overlap with pole (soft)
- May miss satellite sensor on lower radiator support
- Abnormal delta-V increases at 100 msec

2004-12-052

Impact Description: Vehicle front contacted a mailbox and a utility pole and came to rest against the pole.
Vehicle speed: EDR @ -1 sec = 42 mph
D event delta-V = 29 mph
GAD/PDOF: F/0deg
Multi event: yes
Potential reasons for late reported deployment time:

- Narrow impact (soft)

2005-04-062

Impact Description: Vehicle struck a street sign and a large diameter tree.
Vehicle speed: EDR @ -1 sec = 76 mph
D event delta-V = 58 mph
GAD/PDOF: F/0deg
Multi event: yes
Potential reasons for late reported deployment time:

- Narrow impact (soft)
- Delayed start of delta-V data. No vehicle acceleration from AE to ~40 msec

2001-41-133

Impact Description: Vehicle departed the left side of the road, hit curb, and contacted a concrete utility pole on the median with its front.
Vehicle speed: EDR @ -1 sec = 48 mph
D event delta-V = 26 mph
GAD/PDOF: F/350deg
Multi event: yes
Potential reasons for late reported deployment time:

- Narrow impact – pole (soft), with broad damage
- Delta-V recording shows no vehicle acceleration from AE to ~30 msec

2004-08-108

Impact Description: Vehicle struck a wooden utility pole with its front, shearing the pole, which resulted in the vehicle rolling 6-quarter turns.
Vehicle speed: EDR @ -1 sec = 61 mph
D event delta-V = 11 mph
GAD/PDOF: F/20deg
Multi event: no (yes subsequent to D event)
Potential reasons for late reported deployment time:

- Low delta-V event
- Narrow offset impact (soft)

2004-11-082

Impact Description: Vehicle rear-ended stopped vehicle in roadway at stop sign.
Vehicle speed: EDR @ -1 sec = 49 mph
D event delta-V = 30 mph
GAD/PDOF: F/0deg

Multi event: no
Potential reasons for late reported deployment time:

- Broad damage
- Delta-V recording shows no vehicle acceleration from AE to ~20 msec

2003-12-162
Impact Description: Vehicle struck another vehicle on roadway (sideswipe), struck a fire hydrant with its front plane (D event), and then struck a steel sign pole
Vehicle speed: EDR @ -1 sec = 17 mph
D event delta-V = 8 mph
GAD/PDOF: F/10deg
Multi event: yes
Potential reasons for late reported deployment time:

- Low delta-V event
- Narrow impact

2005-76-009
Impact Description: Other vehicle swerved to miss debris on roadway and impacted subject vehicle head on with small overlap
Vehicle speed: EDR @ -1 sec = 29 mph
D event delta-V = 18 mph
GAD/PDOF: F/340deg
Multi event: yes
Potential reasons for late reported deployment time:

- Narrow offset impact
- May miss satellite sensor on lower radiator support
- Abnormal delta-V increases at 30 msec
- Delayed start of delta-V data. No vehicle acceleration from AE to ~ 50 msec

2005-12-149
Impact Description: Vehicle contacted a signpost, 2 wooden boxes, another post, and a third wooden box.
Vehicle speed: EDR @ -1 sec = 45 mph
D event delta-V = 8 mph
GAD/PDOF: F/0deg
Multi event: yes
Potential reasons for late reported deployment time:

- Low Delta-V event
- Narrow offset impact (soft pliable planter box)
- Delayed start of delta-V data No vehicle acceleration from AE to ~ 20 msec

2004-48-181
Impact Description: Other vehicle crossed center and hit subject vehicle with extreme offset engagement.
Vehicle speed: EDR @ -1 sec = 43 mph
D event delta-V = 8 mph
GAD/PDOF: F/0deg
Multi event: no
Potential reasons for late reported deployment time:

- Low delta-V event
- Offset to left side
- Narrow impact
- May miss satellite sensor near hood latch
- Velocity change trace starts at 8 mph at 10 msec

2003-50-110
Impact Description: The right front fender was struck by another vehicle at an intersection followed by the subject vehicle hitting a signal pole
Vehicle speed: EDR @ -1 sec = 19 mph
D event delta-V = 20 mph
GAD/PDOF: F/0deg
Multi event: yes
Potential reasons for late reported deployment time:

- Pole impact (soft)
- Misses frame rails
- Offset impact (away from satellite sensor, if equipped)

Discussion

Abnormal delta-V traces**:** On at least two of the twelve cases investigated, the EDR recorded the vehicle's speed increasing during the impact. In case **2004-50-087**, this was observed. Figure 12 shows these data.

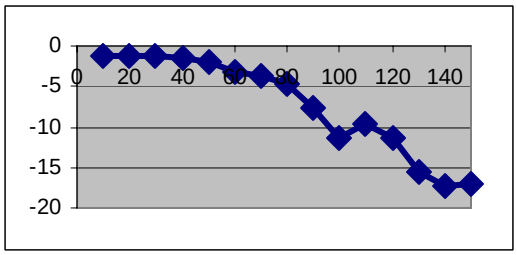

Figure 12. Case 2004-50-087 EDR Delta-V (mph) vs. time (msec)

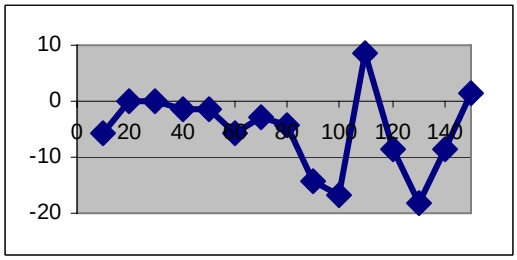

Figure 13. Case 2004-50-087 Differentiated EDR Delta-V (mph) vs. time (msec)

A closer examination can be made by differentiating these data to obtain a rather crude representation of the vehicle deceleration. This is shown in Figure 13.

From these data there is clear vehicle acceleration at 110 msec. While it is not unusual to see positive acceleration in the high frequency acceleration data, it is unusual to see it in low frequency data. Since these data represent very low frequency data, an occurrence of this type should be considered abnormal. A review and validation of this process is found in the Appendix.

Delayed start of delta-V data: In several cases the data captured and recorded are part of the EDR record related to the deployment file show rather long delays between AE and significant changes in vehicle delta-V. An example of this is found in case **2001-41-133**, where the delay was about 50 milliseconds. Figure 14 shows the first major separation from 0 mph to be at 60 msec.

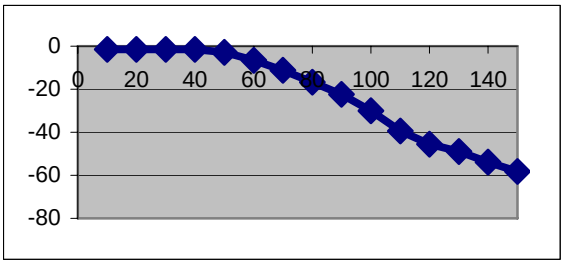

Figure 14. Case 2001-41-133 EDR Delta-V (mph) vs. time (msec)

Findings

The following is a discussion of these twelve cases. Because this is a very small sample and because case counts are used, rather than weighted data, generally only qualitative statements are made.

A review of the model years for these twelve case vehicles shows fairly even distribution, given the small sample and the fact that newer vehicles were not available for selection in the earlier case years. These data are shown below.

Table 7. Distribution of Model Years in Delayed Deployment Cases

Vehicle MY	Number of Cases
2001	3
2002	1
2003	2
2004	4
2005	2

A review of the vehicle type also shows no trends. Both trucks and passenger vehicles had long recorded driver's air bag deployment times. Also, several GM brands were found in the list, as were various sizes of passenger vehicles. Furthermore, driver seat belt status varied between the cases as did crash severity, ranging from 6 mph to nearly 60 mph.

Several common characteristics were found among these twelve cases.

Narrow/Offset: In many of the cases, the vehicle impacted something narrow, such as a pole. Others had significant offset impacts, typically engaging a small portion of the vehicle. Narrow impacts tend to be softer because they may not involve the frame rails. Figure 15 and Figure 16 present examples of these impacts.

Figure 15. Case 2004-12-052 Impact with Small Sign and Pole

Figure 16. Case 2003-12-162 showing fire hydrant damage on vehicle's right

Low Delta-V: Several cases had low delta-V crashes. These crashes are in the zone where the air bag may or may not deploy. For some of these more time may be needed for the air bag controller to predict the need for air bags deployment, hence the longer deployment times.

Abnormal data: As mentioned in the case description section above, some cases had what might be construed as abnormal or unexpected data. There were at least three categories of abnormal data. Two

of these were discussed earlier in the Discussion section.

- Delayed onset of significant changes in velocity after time zero, also referred to as AE.
- Reversal in the delta-V characteristic
- High starting point for the delta-V trace, as reported as the 10 msec data point.

Multi Impact: Many of these twelve cases have earlier non-deployment impacts, as reported by both NASS and the EDR. Table 8 summarizes these characteristics by NASS case number.

Table 8. Summary of Delayed Deployments (* = CAC Vehicle)

NASS Case Number	Narrow / Offset	Low DV	Abnormal data	Multi Impact
2004-75-126 *	✓	✓	✓	✓
2004-50-087 *	✓		✓	✓
2004-12-052	✓			✓
2005-04-062	✓		✓	✓
2001-41-133	✓		✓	✓
2004-08-108	✓	✓		✓
2004-11-082			✓	
2003-12-162	✓	✓		✓
2005-76-009 *	✓		✓	✓
2005-12-149	✓	✓	✓	✓
2004-48-181	✓	✓	✓	
2003-50-110 *	✓			✓

ADVANCED AIR BAG SUPPRESSION PERFORMANCE

The driver and front passenger restraints can operate independently in an advanced air bag system. Deployment of the driver air bag does not always imply that the passenger air bag will also be deployed. Deployment of the right front passenger air bag can be suppressed under certain conditions. A manufacturer may choose, for example, to not deploy the passenger air bag if there is no occupant seated in the right front passenger location. More importantly, the air bag may be suppressed if a child is detected.

Table 9 shows the frequency of suppressions for right front passenger air bags in crashes sufficiently severe to deploy the driver frontal air bag. All cases in this table involve CAC vehicles. In three of the cases, occupant descriptions were not available as the vehicles were not inspected by NASS investigators. Right front passengers were present in 14 of the 44 remaining cases.

Table 9. Frequency of Right Front Passenger Air bag suppression in crashes in which the driver air bag deployed in CAC vehicles

Right Front Passenger	RF Air bag Deployed	RF Air bag Suppressed	Total
Adult	12	1	13
Child	-	1	1
None	3	27	30
Total	**15**	**29**	**44**

When the passenger seat was vacant, the passenger air bag did not deploy in the majority of the cases (27 of 30). This indicates the presence of sophisticated occupant sensors which are characteristic of advanced air bag systems. This behavior however can be dependent on the air bag control module as automakers have the flexibility to implement or not implement this non-safety related feature. Only the SDMFG2002 module suppressed the air bag if the passenger seat was vacant (27 of 27). The SDMDW2003 module on the other hand deployed the right front air bag despite the fact that no occupant was seated at that location (3 of 3).

Air bag Suppression in the Presence of a Right Front Passenger

Deployment of the driver air bag does not always imply that the passenger air bag will also be deployed. Table 9 shows two particular cases of interest in which the passenger air bag was suppressed despite the presence of a right front passenger. In both cases, the driver bag deployed. In both cases, the passengers were subjected to a longitudinal delta-V of over 20 mph. Earlier in this paper, these cases were referred to as split deployments.

In the first case (NASS/CDS case **2005-42-106**), the right front passenger was a 5 year old male child weighing 20 kg. The child was not seated in a child seat. The subject vehicle, shown in Figure 17, was a 2004 Chevrolet C/K-series pickup truck which struck a guardrail and then suffered a rollover. The EDR recorded a longitudinal delta-V of 25.3 mph in the guardrail impact. NASS investigators estimated a PDOF of 30 degrees. The NASS investigator indicated that the child was restrained by a 3-point belt. The EDR however recorded that the right front passenger belt was not buckled. The air bag on/off switch was in the 'auto' position. However, when a child is detected, CAC vehicles are designed to either suppress the airbag or deploy the air bag in a low risk manner. In this case, the system appears to have

detected the child and correctly suppressed the passenger air bag.

In the second case (NASS/CDS case **2003-09-224**), the right front passenger was a 29-year old male restrained by a three-point belt. The subject vehicle was a 2003 GMC C/K-series pickup truck which was subjected to a frontal crash with a longitudinal delta-V of 22 mph at a PDOF of 10 degrees. As with the previous case, three reasons were investigated for air bag suppression: air bag on/off switch, failure of weight sensor, and a forward-located seat.

NASS investigators noted that the air bag on/off switch was in the 'auto' position. Vehicle interior photos also showed the switch clearly in the 'auto' position. The passenger had a weight of 79 kg and height of 175 cm. There is little chance that a weight sensor would not have detected this occupant. The EDR recorded that the passenger seat position was in the rearward position making this also an unlikely reason for air bag suppression. One other possible scenario is that the auto/off switch status was tampered with post-crash. Unfortunately, the EDR data as downloaded with the Vetronix reader only indicates that the right front passenger air bag was suppressed. The EDR does not indicate whether the suppression was due to the auto/off switch being set in the off position or whether the nature of this particular crash did not meet the air bag deployment criteria.

(a) Frontal and Rollover Damage to 2004 Chevrolet Silverado Subject Vehicle	(b) Passenger Air bag On/Off Switch in Auto Position

Figure 17. Frontal Crash followed by a rollover in which Driver Air bag deployed, but Passenger Air bag did not deploy for a child in the right front seat (NASS 2005-42-106)

(a) Frontal Collision Damage of a 2003 GMC Sierra Pickup	(b) Passenger Air bag On/Off Switch in Auto Position

Figure 18. Frontal Crash in which Driver Air Bag Deployed, but Passenger Air Bag did not in the Presence of an Adult Right Front Passenger (NASS 2003-09-224)

LIMITATIONS

This study has several limitations described below:

- The study was based on a limited data set vehicles having an advanced air bag. Because of the small sample currently available, the conclusions of this analysis should be regarded only as an initial indication of the more conclusive findings that can be expected from follow on studies with a larger EDR sample.

- All vehicles were manufactured by General Motors. The results may not apply to other automakers.

- The frequency distributions presented in this paper apply only to the study data set. Because the study has not used NASS/CDS case weights, the results should not be interpreted as necessarily representative of the U.S. national crash environment.

CONCLUSIONS

This paper has investigated the field performance of occupant restraint systems, designed with advanced air bag features, including criteria specified in the US FMVSS No. 208 for advanced air bags. The analysis was based upon EDR records extracted from the VT EDR database for 106 NASS/CDS cases involving CAC vehicles. The CAC sample was composed of 47 air bag deployments and 59 non-deployments. A separate analysis of air bag deployment times was conducted using 132 cases of both CAC and pre-CAC vehicles having an advanced air bag which deployed.

The findings were as follows:

1. Deployment Characteristics. For this sample, there was a 50% probability of driver air bag deployment a longitudinal delta-V of 8 mph. The driver air bag was observed to deploy at longitudinal delta-V as low as 3-4 mph. The driver air bag was observed to not deploy at longitudinal delta-V as high as 26 mph.

2. Delayed Deployments. In twelve advanced frontal air bag cases, driver air bag deployment times recorded by the EDR exceeded 72 milliseconds. Examination of these cases revealed that frequently these delayed deployments were associated with narrow impacts, multiple impacts, lower delta-V crashes or cases with abnormal crash pulses.

3. Passenger Air Bag Suppression when no Passenger was present. The CAC air bag systems in this study suppressed the passenger air bag in the majority of cases (27 of 30) in which the passenger seat was vacant.

4. Air Bag Suppression in Presence of a Right Front Passenger. In two of the CAC vehicles, the passenger air bag did not deploy despite the presence of a passenger. In both cases, the driver air bag deployed and the air bag on/off switch was in the auto position. One case was for a 5-year old child and the other case was for a 29 year old adult.

This study has demonstrated the feasibility of using Event Data Recorders to evaluate the performance of advanced occupant restraint deployment algorithms. Because this study was based upon a small number of cases, the conclusions should be revisited when additional EDR data is available from CAC cases. Our initial examination of CAC deployment algorithms has shown that a first priority of future studies should be to investigate the potential safety issues of delayed deployments and suppression of the right front passenger air bag.

REFERENCES

1. Chidester, A., Hinch, J., Mercer, T.C., Schultz, K.S., “Recording Automotive Crash Event Data”, National Transportation Safety Board (NTSB) International Symposium on Transportation Recorders, Washington, DC (1999)
2. NHTSA Vehicle Crash Test Database, http://www-nrd.nhtsa.dot.gov/database/nrd-11/veh_db.html (2007)

APPENDIX

To determine the efficacy of differentiating the delta-V data from the GM EDR to determine the vehicle's deceleration, a case where the vehicle's acceleration was known was examined. During NHTSA's NCAP program, vehicles are always instrumented with accelerometers. This analysis used the data from an NCAP test of a 2005 Chevrolet Equinox. These data are found in the NHTSA Vehicle Crash Test Database, located on the NHTSA web page [NHTSA, 2007].

The vehicle deceleration is shown in Figure 19. These data were filtered using SAE J211 Class 60.

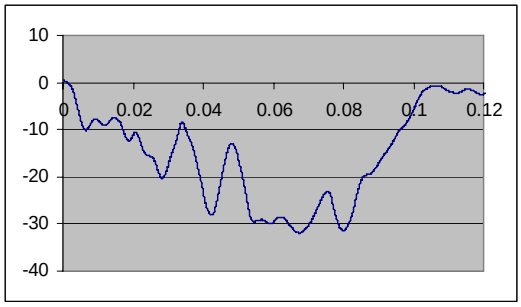

Figure 19. Vehicle longitudinal deceleration (G's) from an NCAP test of a 2005 Chevrolet Equinox vs. time (msec)

The EDR data from this test were extracted and downloaded from the NHTSA Vehicle Crash Test Database. Those data are also available on the NHTSA web page. The deployment file crash delta-V is shown in Figure 20.

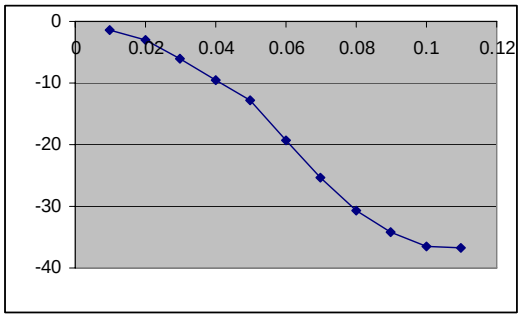

Figure 20. Vehicle EDR longitudinal velocity change (mph) from an NCAP test of a 2005 Chevrolet Equinox vs. time (msec)

These data were differentiated (using a simple difference method and applying a mid point time value to each point) to obtain a representation of the vehicle's deceleration. Because the time between samples is 10 msec, the fidelity seen in the vehicle's accelerometer cannot be replicated. Hence we see a somewhat smoothed characteristic. Figure 21 presents these data.

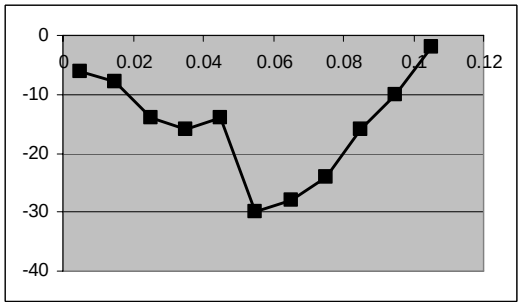

Figure 21. Differentiated vehicle EDR longitudinal velocity change (G's) from an NCAP test of a 2005 Chevrolet Equinox vs. time (msec)

The vehicle accelerometer signal and the differentiated EDR data are compared in Figure 22 .

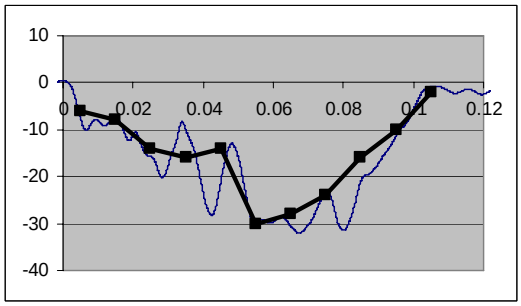

Figure 22. Differentiated vehicle EDR longitudinal velocity change (bold) compared with vehicle accelerometer (G's) from an NCAP test of a 2005 Chevrolet Equinox vs. time (msec)

As can be seen in these data, the 10 msec delta-V data from the GM EDR crash data can be used to generally reconstruct the actual crash pulse, as seen by the vehicle accelerometer. The main different in shape is the loss of the higher frequency content.

EXPERIMENTAL INVESTIGATION OF THE ENERGY ABSORPTION CAPABILITY OF CONTINUOUS JOINED CRASH BOXES

Lorenzo Peroni
Massimiliano Avalle
Giovanni Belingardi
Politecnico di Torino
Italy
Paper Number 07-0350

ABSTRACT

In the design of vehicle structures for crashworthiness, there is a need for rigid subsystems that guarantee an undeformable survival cell for the passengers and deformable subsystems able to efficiently dissipate the kinetic energy. The front rail is the main deformable component dissipating energy in a frontal crash, which is the most dangerous crash situation, and for which the structural behaviour is mostly affecting.

The design of the front rail, usually consisting of a thin walled prismatic column, requires definition of the geometry, that is, of the shape and dimension of the cross section, of the thickness of the material, and of the material itself.

In this work the analysis of the effect of different cross sections of the front rail, and of the joining system is carried out. Furthermore, the collapse during crash is influenced by the loading rate since the loading speed has substantial influence on the mode of collapse and on the material behaviour. In fact, the structural materials used in this application are known to be strain-rate sensitive.

Within the work, different types of sections are compared. Different non-common continuous joining technologies are examined: three different types of adhesive an acrylic, one component epoxy and two components epoxy and laser welding. Adhesives and laser welding can be used as an alternative to the widely used spot-welding to improve the structure performance due to the continuous joint.

The effects of the loading speed are taken into account by comparing quasi-static crush tests to dynamic impact tests. Dynamic tests have been performed under a drop tower testing apparatus built within the campus of the II Faculty of Engineering of Politecnico di Torino.

1. INTRODUCTION

A very important issue in car design nowadays, is the trend in using new, smart materials. In the next future, well known and widely used materials like deep-drawing steels will be discarded in favor of high-strength steels (dual-phase, TRIP steels…), aluminum alloys, magnesium alloys and various grades of polymeric materials and composites [1-2]. The reasons for this choice are many: the weight reduction to allow for more accessories and safety components, the strengthening of the structure and, last but not least, cost reduction. Moreover, even the lowest priced common steels suffered great costs rise due to increased demand from emerging countries.

Many problems are linked to the introduction of new materials: their properties are still not completely known, the technologies usually adopted sometimes fail, and new environmental and protection problems can arise. Additional problems relate joining systems. For several years car body assembly was fully dominated by spot-welding. Resistance spot-welding is a very cheap and affordable technology to join steel sheets. It is highly customizable, it can be extremely automated, it is very quick, and it does not require preparation of the parts before joining. However, there are also some drawbacks: first, as in all the welding systems there is a heat affected zone that can affect the material strength; second, it is a spot connection system that causes high stress concentrations near the spot, and cannot be used to join different materials (unless very difficult procedures are adopted, whenever possible).

Among the various alternative solutions the most promising are probably laser welding and adhesives.

Laser welding, although still a welding technology, is a continuous joining method. It is yet a very flexible solution that can be easily made automatic by means of robotics. It is even possible to join different metals.

Recent developments in high-power CO_2 lasers and robotic control have accelerated the application of laser beam welding (LW) to vehicle structure fabrication and assembly in the automotive industry. Additionally, it has been shown to offer many advantages if compared with other welding processes: a low heat input, a small heat-affected

zone, low welding distortion, welding in an exact and reproducible manner, and welding at high speed. With the advent of new laser technology, such as high power Nd:YAG and CO_2 lasers and fiber-optic beam delivery systems, the automotive industry is re-evaluating manufacturing systems in the body. However, it cannot be used to join other materials like plastics and composites.

The most promising joining solution when dealing with different materials is bonding. The use of structural adhesives in car body construction has a lot of advantages: the joint is not localized in small areas eliminating stress concentrations, the adhesive layer can perform as insulating, protecting and damping material, it is possible to join different materials of almost any kind. The main problems in using adhesives are the loss of strength that comes from the differences in the coefficient of thermal expansion of the adherends and of the adhesive itself (generating residual stresses in it) and their relatively low peel strength. However, up to date structural adhesives have gained very high peel strength sufficient to guarantee very robust designs. Many other, supposed, drawbacks can be worked around by using state-of-the-art knowledge on adhesive joints construction. Surface preparation is little nowadays nor necessary anymore: modern structural adhesives can be applied directly on untreated surfaces, even dirty and greasy. The long curing time can still pose some problems, but, using bonded joint together with other mechanical fastening methods or with provisional fasteners [3], this can be effectively solved: the usual oven treatment for car body paints is then exploited for adhesive polymerization too, if necessary. Probably the main concern in using adhesives, as for many polymer materials, relates to long term endurance, which is still not completely known, especially in severe environments.

There is, maybe, a sort of *cultural* difficulty in designers and manufacturers attitude. They are, comprehensibly, worried by the necessity to introduce dramatic modifications in components design to be suitable for bonding, as it was necessary in the past [4], and expensive changes in manufacturing equipments. As will be shown in the present paper, this is not of concern since recent structural adhesives have so excellent properties to be able to overcome most possible inconvenient.

Main aim of this paper is then to compare results on the use of structural adhesives in structures subjected to crash. Comparison with traditional methods and the obtainable structural improvements have been already demonstrated [4-7]. A wide-ranging comparison, coming from a lot of experimental tests in the Politecnico laboratories, will be addressed here. Three different adhesives and laser-welding technology for joining thin walled metal structures will be considered in the work, and compared to the usual spot-welded solution. Moreover, different sections will be examined to show whether direct substitution of a technology with another one is possible or not, and the greatest advantages of innovative geometries when dealing with new joining methods.

STRUCTURAL COMPONENTS

The basic component addressed in this work is a simplified crash box for frontal impact with square section, made of a common deep-drawing low alloy steel (Figure 1). The steel is DC02 EN10130 (Table 1), and it was chosen on the basis of several considerations: the availability of previous results with the same material [5-6, 8-10] to allow for comparisons, the still relatively widespread use of this steel in car body constructions and, last but not least, accessibility and low cost of this material.

Table 1.
Steel properties

Property	Value
Material	DC02 EN10130
Yield strength, R_e	170-280 (nominal)
Tensile strength, R_m	270-400 (nominal)
Elastic modulus, E	200×10^3 MPa
Plastic modulus, E_p	950 MPa (measured, avg.)
Yield strength, S_y	190 MPa (measured, avg.)

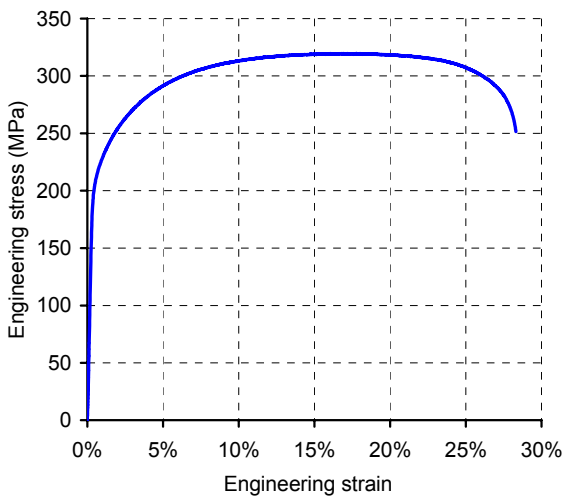

Figure 1. Stress-strain curve for theDC02 steel used in the experimental analysis.

The crash box columns were built by joining two half-shells obtained by plastic deformation. Side of the enclosed square section was 40 mm, and the total length 300 mm for all the examined geometries of the cross section.

When dealing with spot-welds, there are not many possibilities. Since the two face-sheets must be accessible, the box must be provided with flanges (Table 2) and the common solution are as marked with the letter A and B (there are slight variations possible, by shifting the flange position of the B shape with an offset; it is even possible to have asymmetric solution with a different offset in the two flange sides).

Table 2.
Analyzed sections

	Geometry	Spot-weld	Laser	Bonding 330 9514
A	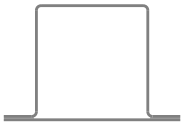	×	×	×
B	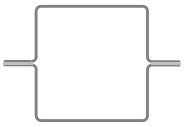	×	×	×
C	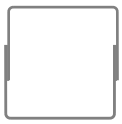	–	× *	×
D		–	×*	×**
E		–	×*	×**

Note:
*it exhibits some manufacturing problems: it is difficult to fix the two parts of the structure during the welding process.
** it exhibits serious manufacturing problems: when inserting one half shell into the other, there is unavoidable adhesive removal that can bring out incomplete bonding.

Several design configurations for bonded square boxes are possible. Again Table 2 shows some of the possible configurations. Fay and Suthurst [3] examined even more possibilities.

Configurations A and B have some problems when obtained by bonding. Peel loads occur between the flanges, and this can lead to premature failures. Configurations C, D, and E are more suitable for bonding, since an opening load will stress the joint in shear, with reduced peeling.

For laser welding, even if it is theoretically possible to adopt almost all possible configurations, there are in practice many manufacturing constraint. The two sheets to be joined must be clamped together: as a result, only solution A and B can be easily manufactured.

The flanges width in A and B configurations and the sheet superposition in C, D, E were chosen to have the same area (9000 mm²), while maintaining the same square section (40×40×1 mm).

JOINTS CHARACTERISTICS

The characteristics of the spot-welds, adhesives and laser welds are described in the following sections.

Spot-welds

Spot-welded crash boxes were joined by means of 6 mm spots, positioned in the middle of the flanges. The spot pitch was of 30 mm, and it was chosen after careful considerations about the maximum strength allowed and reduction of the peak load. Triggers to start stable collapse were introduced by means of small holes near the top end of the column.

Table 3.
Laser welds characteristics.

Brand and model	Haas HL 3006d,
Working mode	CW, continuous
Beam transport method	Optic fiber, ϕ600 µm
Focusing system	Focusing lens
Pumping system	With lamps
Wavelength λ	1064 Nm
Max output power	4000 W
Max work power	3000 W
BPP	25 mm×mrad

Laser-welds

Most known industrial laser sources are CO_2 and Nd:YAG. The first type of lasers is used in light constructions, with penetration depth less than 10 mm. The second type is used for small sized components with limited thickness because of the small spot size. In this work the sheets, 1mm thick,

were joined by means of an Nd:YAG laser source.

The used laser was a Haas HL 3006d. Its main characteristics are reported in Table 3 (Figure 2).

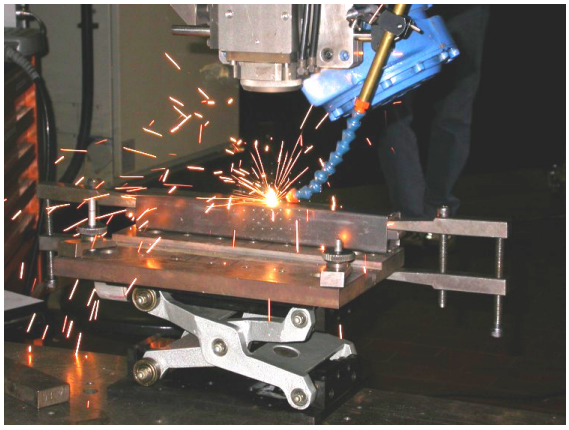

Figure 2. Laser joining of one of the analyzed samples

Adhesives

After a selection phase, taking into consideration previous experiences [5-6, 11] made with various kinds of adhesives, including Araldite®, Dow® and various Loctite®, three types were chosen:

- a urethane metacrylate ester, Loctite® 330 Multibond
- an epoxy resin, Loctite® Hysol® 9466
- an epoxy resin, Loctite® Hysol® 9514

Nominal strength of these adhesive are summarized in Table 4.

Table 4.
Nominal strength of the used adhesives.

Adhesive	Shear strength, MPa (ASTM D1002-94)	Peel strength, kN (ASTM D1876-95)
Loctite® 330 Multibond	16 ÷ 22	1.1 ÷ 1.2
Loctite® Hysol® 9514	52 ÷ 53	4.8 ÷ 5.7
(Loctite® Hysol® 9466)	30 ÷ 39	0.6 ÷ 0.8

The acrylic ester 330 Multibond is a general purpose structural adhesive with good characteristics. Differently from traditional acrylic adhesives it has a much greater toughness that makes it useful for energy absorbing applications. Nominal shear strength according to ASTM D1002 is 15 ÷ 30 MPa, whereas tensile peel strength (DIN 53288) is 12 ÷ 22 MPa. Main limitation of this adhesive is the low temperature applicability: since it is for curing at ambient temperature, maximum operational temperature is relatively low (120°C, but with progressive loss of strength already from 60°C).

The Hysol 9514 epoxy is a high performance structural adhesive. Shear strength can be up to 45 MPa (depending on adherends), with a peel strength of 9 MPa. Temperature limit is quite high: strength reduction is important only above 120°C. It has superior performance with respect to Hysol 9466 that was initially considered.

A series of preliminary tests on the used adhesives were performed to measure the strength obtained with the specific sheet material. Shear strength single-lap tests (Figure 3), and T-peel strength tests (Figure 4), were performed.

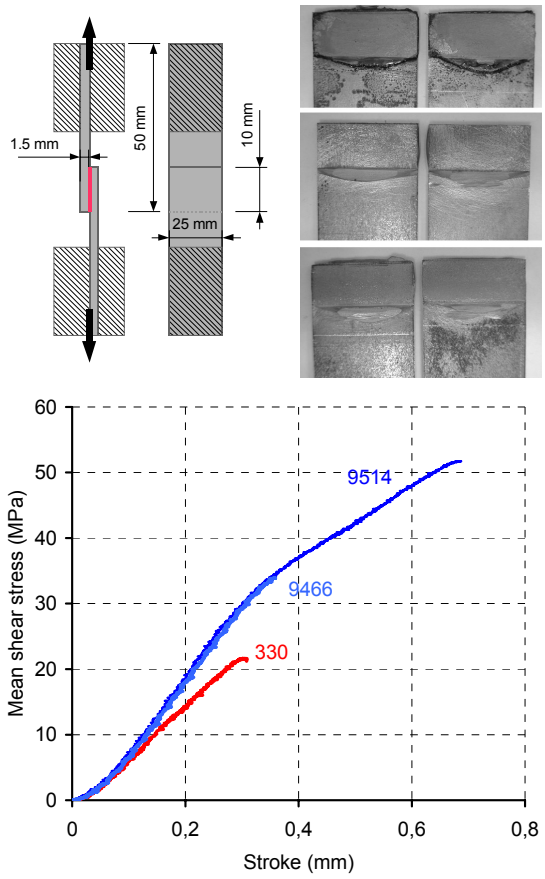

Figure 3. Shear strength tests.

Shear tests were not performed according to ASTM standard, because the strength of the adhesive was in excess of the strength of the steel. In this case

a specimen with only 250 mm² bonded area, instead of 625 mm², was used (25 mm wide, 10 mm superposition length; the bonded pieces were 1.5 thick, 50 mm long).

All the adhesives showed cohesive type failures, resulting in very high strength and capacity of energy absorption. However, Hysol 9514 was found much better especially in terms of peel strength: the increase, with respect to the other adhesives, is from 300% up to 400%.

The Hysol 9466 has not been successfully used in crushing tests because some preliminary samples put in evidence a too brittle behavior of the adhesive and a reduced capacity of plastic deformations.

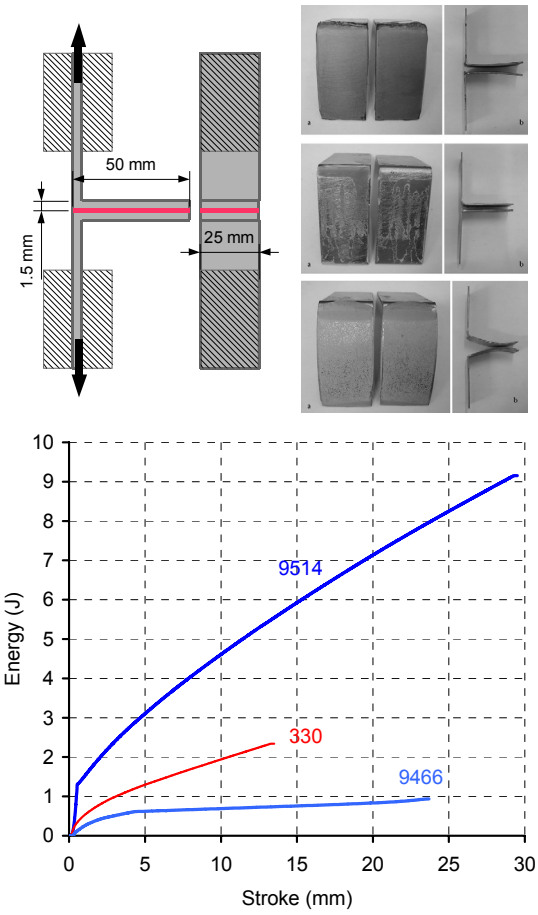

Figure 4. Peel strength tests.

EXPERIMENTAL TESTS

A series of experimental tests in axial compression was performed on the square box columns.

Some quasi-static and dynamic impact tests were performed. Even if the chart will show results of single, representative tests, several repetitions were done for each case. Over 100 tests were performed.

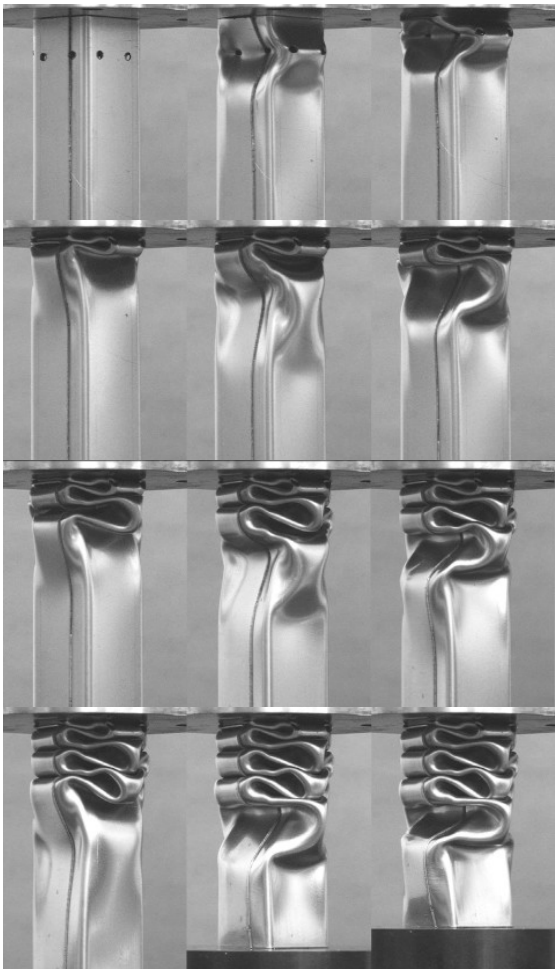

Figure 5. Crushing sequence of a bonded column, quasi-static loading, C solution.

Quasi-static tests (Figure 5) were performed by means of a general purpose hydraulic material testing machine (DARTEC HA100, 100 kN maximum load, 100 mm/s maximum speed). The specimens were placed centrally in the test machine, without any further support, and between two very hard steel end plates, which were bolted to the crossheads of the testing machine. The compressive force was recorded during crushing, together with the crosshead displacement, giving a load-stroke curve of the crushing process. The quasi static tests were stopped after reaching a prescribed crushing distance which was approximately 200 mm. The expected structural behavior of a thin-walled beam submitted to an axial load is a progressive collapse characterized by the regular progressive formation of plastic folds.

Figure 5 shows a pictorial sequence of progressive folding during a quasi-static crushing test.

Adhesively bonded crash boxes

Both solutions A and C performed quite satisfactorily (Figures 6 to 9). However, due to the inferior peel strength, some problems of debonding were encountered with Multibond 330 in configuration A.

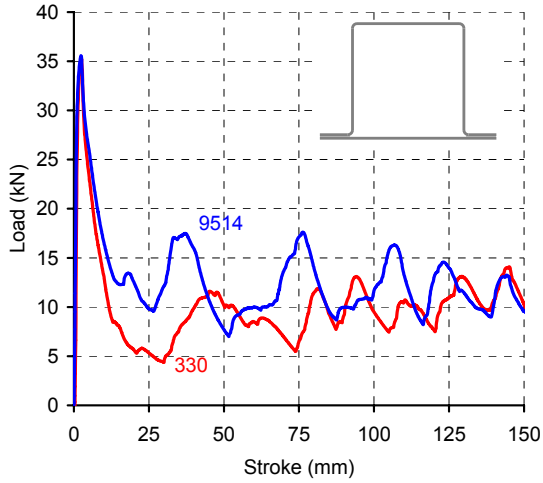

Figure 6. Quasi-static tests comparison, load-stroke curves for A specimen and the two adhesives, without trigger.

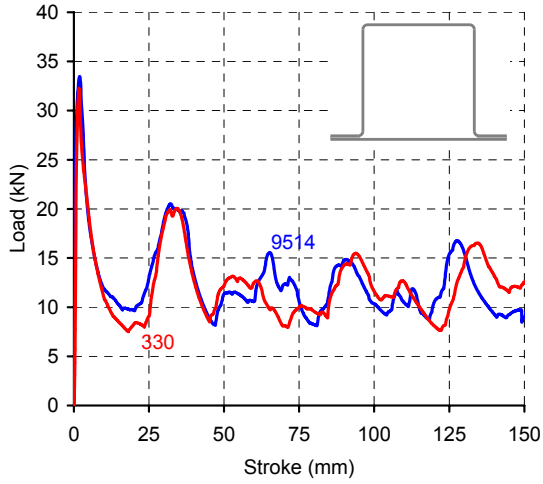

Figure 7. Quasi-static tests comparison, load-stroke curves for A specimen and two adhesives, with trigger.

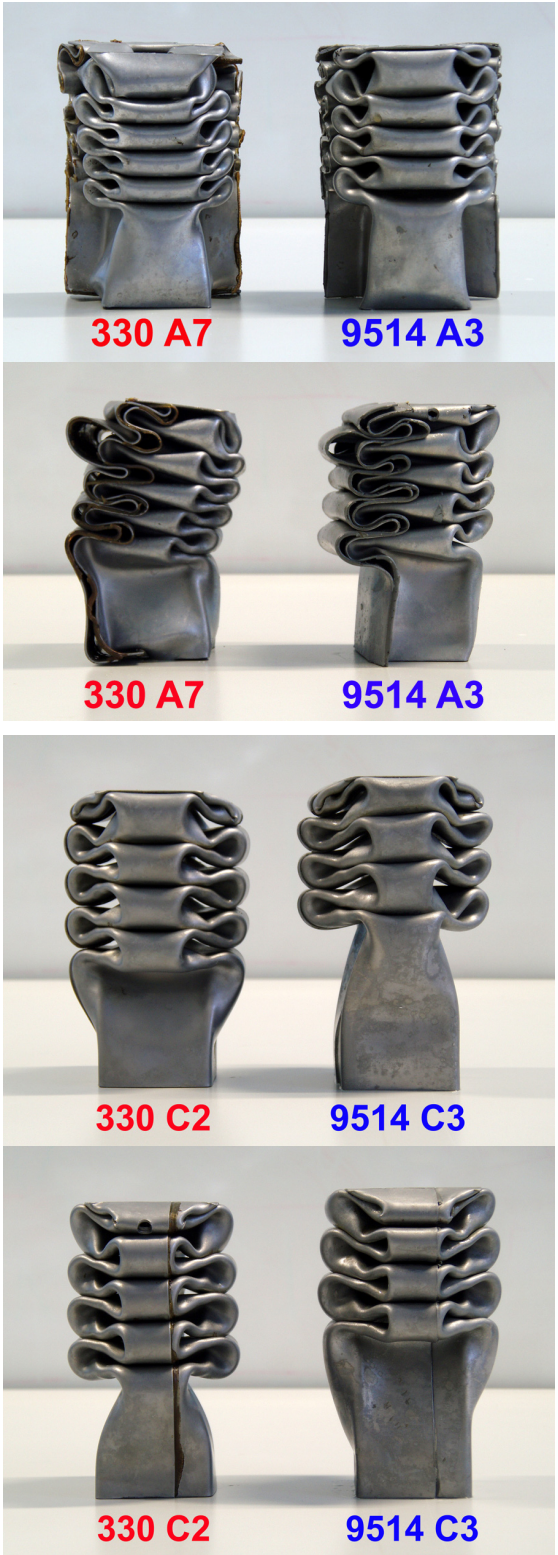

Figure 8. Folding patterns (views from two sides) in quasi-static tests on bonded crash box columns (A and C geometry).

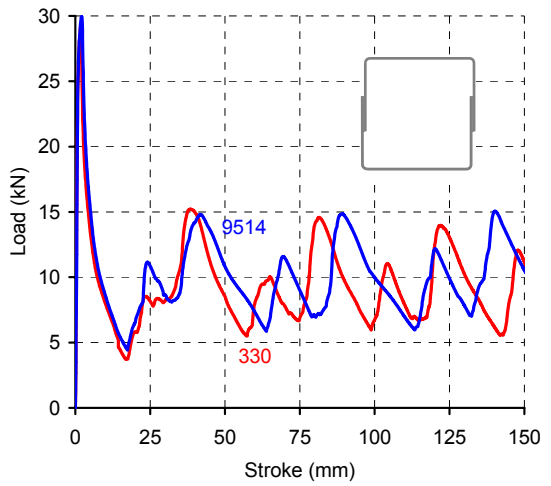

Figure 9. Quasi-static tests comparison, load-stroke curves for C specimen and two adhesives.

This caused a 30% energy absorption reduction. By triggering the initial collapse phase by means of a series of transverse holes at the top of the column, this problem was avoided: the difference was then reduced to some small percent.

The alternatives for overlapped bonded columns were as indicated in Table 2 as C, D, and E. Solution C is simpler and easier to bond: in fact D and E exhibit serious manufacturing problems: when inserting one half shell into the other there is unavoidable adhesive removal that can bring out incomplete bonding. From the structural point of view the differences are not significant.

Also for configuration C, triggering gave improvement in efficiency.

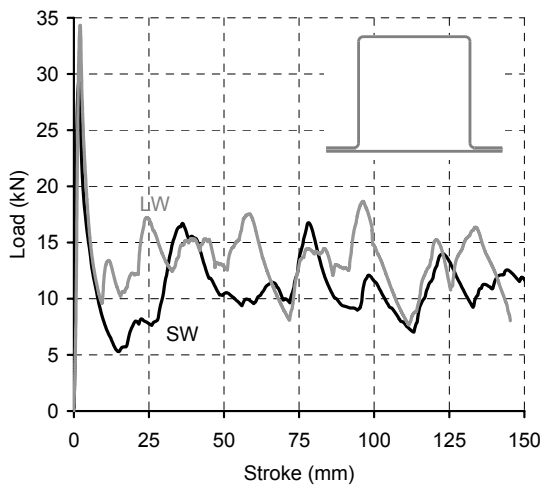

Figure 10. Load-stroke curves for LW and SW crash boxes, A solution.

The final result was that almost no difference was found in the two configurations, with both adhesives. Avoiding debonding, the crash boxes behave very well in quasi-static compression, with very regular folding pattern, as shown in Figures 5 and 8.

Differently from Figure 6 samples, all the test results reported in following paragraphs are about triggered samples.

Laser welded and spot-welded crash boxes

Laser welded and spot-welded columns were also tested under quasi-static compression loading. The results in terms of the load-stroke curves and folding patterns are reported in Figures 10 to 13.

Generally speaking, the spot welds and laser weld resisted the loading and deformation well. There was no interfacial failure of the weld.

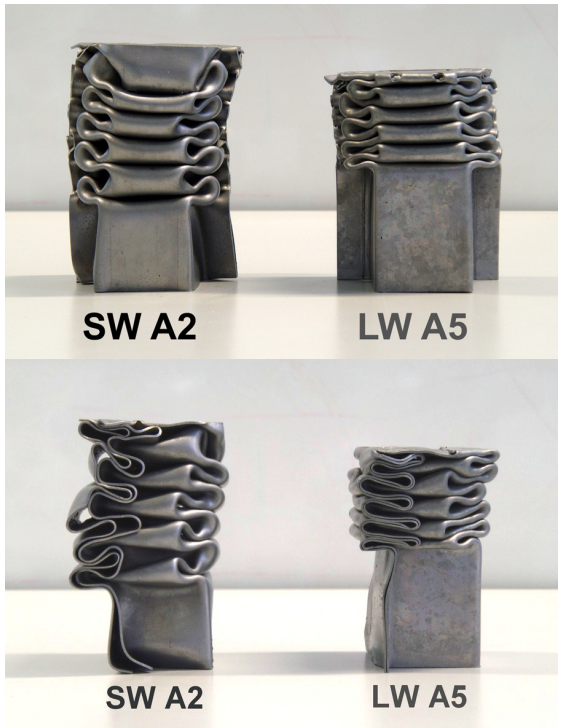

Figure 11. Folding patterns in quasi-static tests on spot welded and laser welded crash box columns, A solution.

For A and B configuration, laser welding produces a folding length shorter than spot welding.

In the laser welded structures the energy absorption is higher also because much material of

the flanges collaborates to the crushing resistance (Figures 11-14).

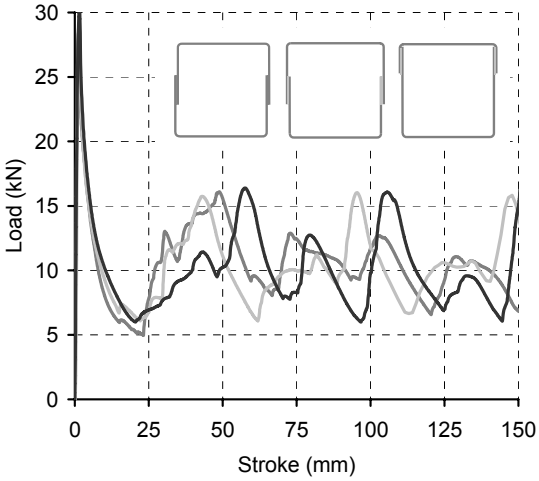

Figure 12. Load-stroke comparison for three laser-welded solutions C, D, and E.

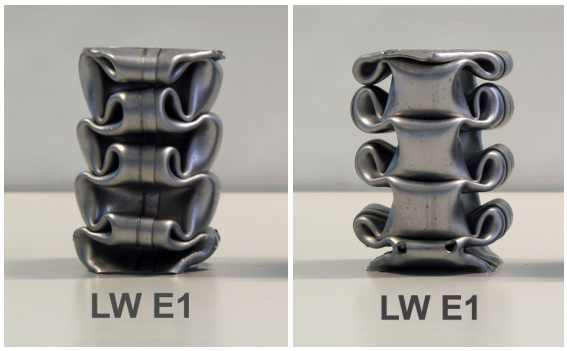

Figure 13. Folding patterns in quasi-static tests on laser-welded E crash box columns.

A simple observation of Figure 10 makes clear the advantage in laser-welding versus spot-welding: the first joining method gives more energy absorption capability and more stable collapse.

This is also clear from Figure 11, in which two crushed boxes are compared: the laser-welded one gave a very regular folding patter with a shortest fold length, which is advantageous for energy absorption. Figure 12 reports the results on tests on C, D and E configuration for laser welded samples. Even if the folding pattern is a little bit different for the three solutions and with respect to the bonded solutions, the energy absorption is almost the same.

In Figure 13 a laser-welded E type column is shown. The collapse is still very regular and stable, however if compared with the bonded C solution in Figure 9, it appears that the E laser-welded has a longer fold pattern

Figure 14. Folding pattern in quasi-static tests on laser-welded and bonded crash box columns.

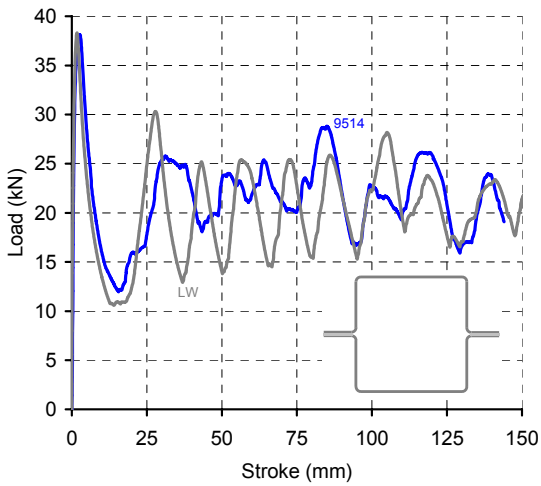

Figure 15. Comparison of laser-welded and bonded crash box columns, B solution.

Figure 14 shows a comparison of the laser welded solution with the adhesively bonded one. Even if there are substantial differences, especially in the first collapse, the bonded solution assure a more uniform load during collapse. The average load is also slightly higher (Figure 15).

Impact tests

Impact tests were performed with a drop tower device installed at the II Faculty of Engineering of Politecnico di Torino (Figure 16). This falling weight test device [3, 9-10] has a drop height of 12 m and a maximum speed of 13 m/s approximately.

The falling mass could be adjusted in small step up to a maximum value of 200 kg.

The falling mass does not impact directly on the specimen: the crushing action is guided by a special rig (Figure 17).

No end constraints were provided to the specimen and special care was taken to provide flat parallel faces of the specimen and test rig.

The load is measured with PCB piezoelectric load cells, the stroke with an optoelectronic encoder.

Figure 16. Twelve meter drop tower for impact tests.

All impact tests were conducted at ambient temperature and the drop height and drop mass were adjusted to crush test specimens by approximately 50-70% of their initial length with speed of 10 m/s.

The importance of triggering was much greater than in quasi-static tests. In some cases, with configuration A namely, transverse holes were not sufficient. Some rivets added at the top of the column helped in reducing debonding.

If debonding is avoided, the two adhesives give similar results, and the folding pattern is sufficiently regular (Figure 18).

Configuration B was found less problematic, as expected. Transverse holes were sufficient to initiate a very regular folding (Figure 19). It comes out that the two adhesives perform quite the same way.

Figures 20 and 21 show a comprehensive comparison of joining methods and types of sections in dynamic impact conditions (thick line) compared to static test results (thin line).

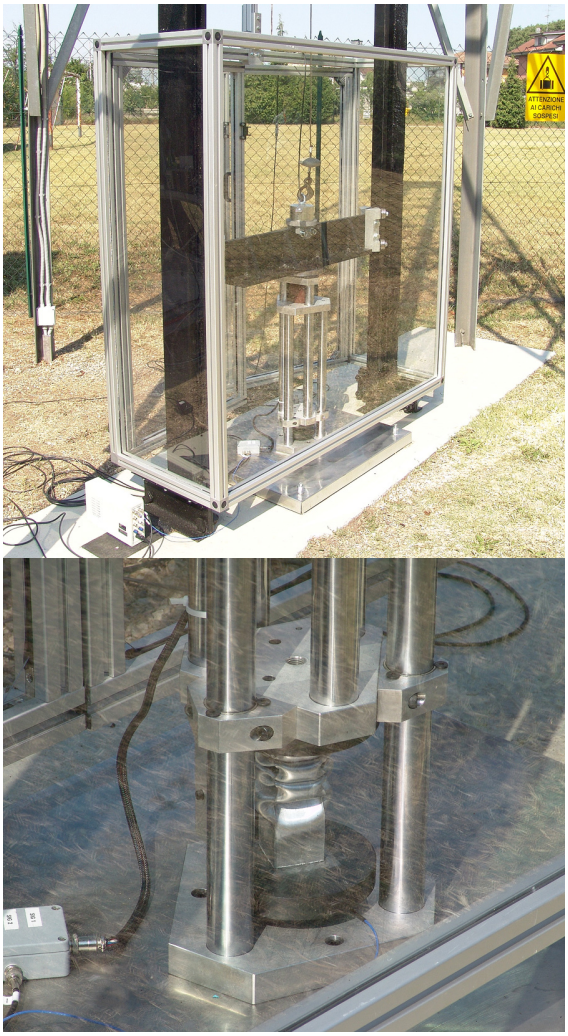

Figure 17. Impact test rig.

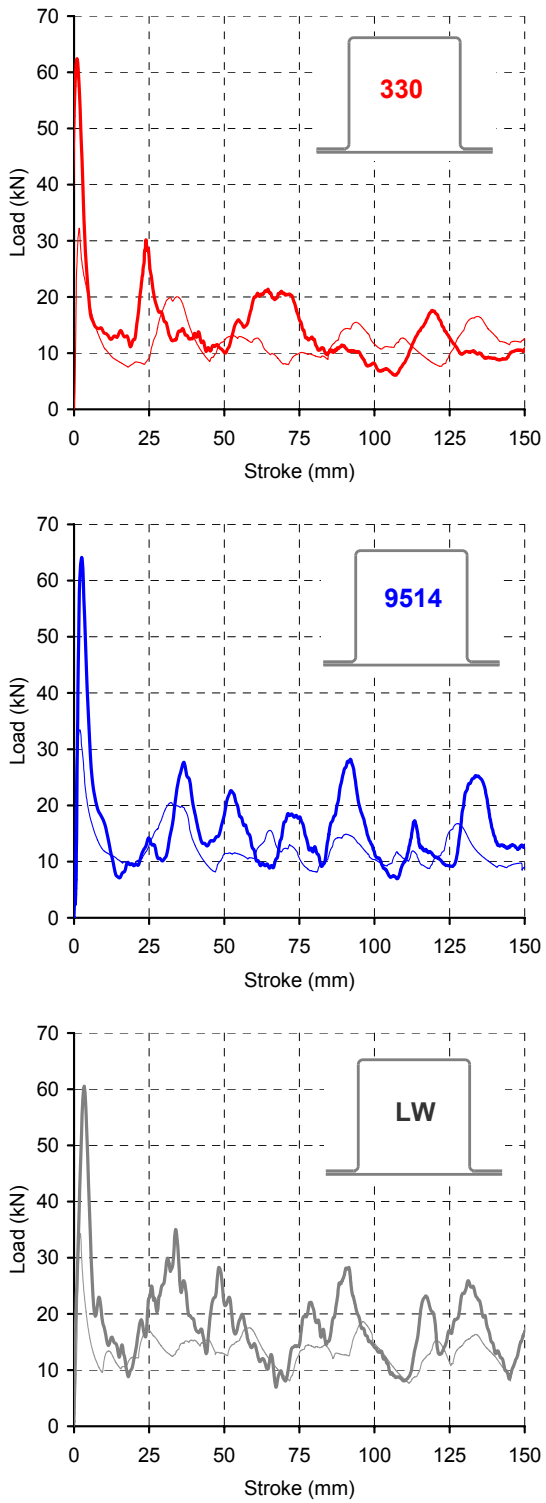

Figure 20. Test results for top-hat A solution: impact loading vs. static.

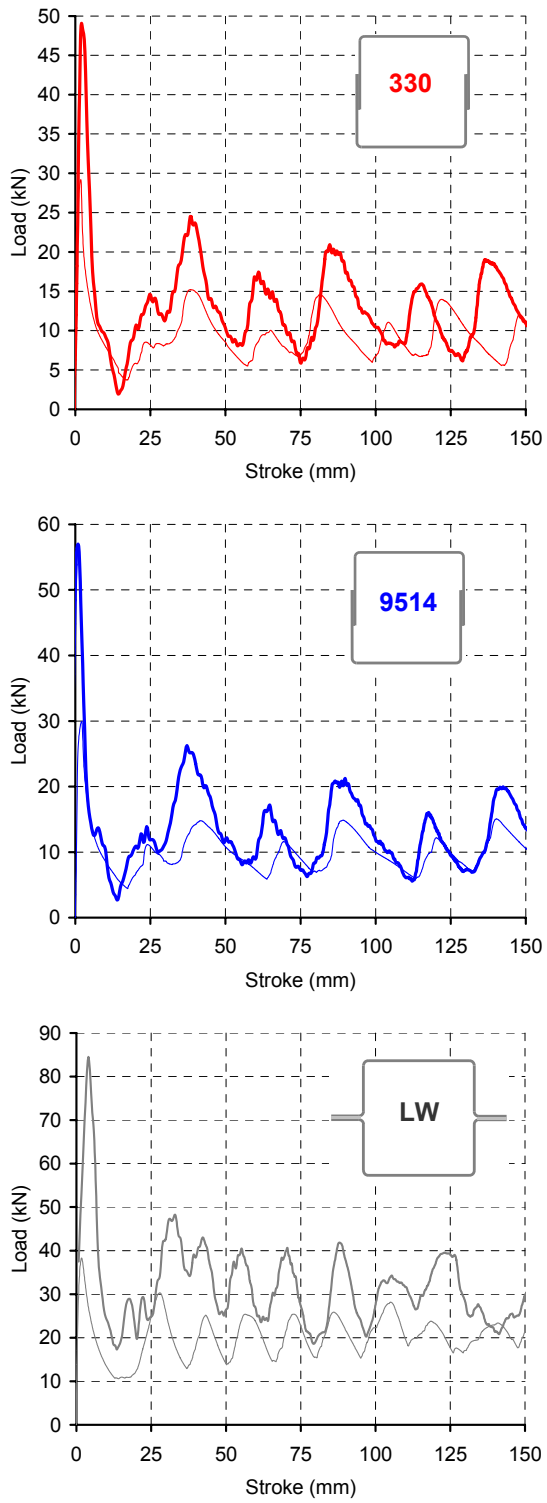

Figure 21. Test results for top-hat B and C solution: impact loading vs. static.

Figure 18. Dynamic, impact tests on crash box columns, configuration A, 9514 adhesives.

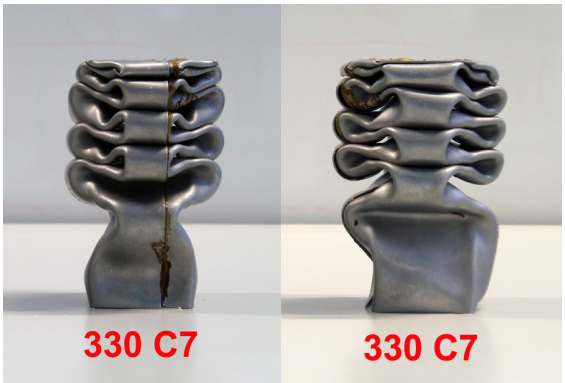

Figure 19. Dynamic, impact tests on crash box columns, configuration C, 330 adhesives.

In general terms, in all tests the diagram of the crushing force is that typical for thin-walled beams.

It can be observed that the crushing force increases significantly with the test speed, although it is important to remember that static tests are performed at a constant velocity, while dynamic tests are impact tests at non constant velocity (the initial velocity is progressively reduced by the energy absorption). The DC02 steel used for the beam construction is a strain-rate sensitive material and this fact can explain this increment of the force values. All the dynamic tests indicated a strong influence of the loading speed on the components behavior.

For all solutions and for the three different joining technologies there is a significant increase in energy absorption of the crash-box with speed (Figures 20-21). If the joining does not fail (as in some A bonded sample) the folding pattern in static and dynamic tests is quite similar. Continuous joining technology (LW and bonding) usually produce a regular crushing with energy absorption greater than spot-welded solution. The energy absorption obtained with this two techniques and the same geometry is similar.

C, D and E geometries, thanks to the absence of flanges, produce very regular and progressive folding pattern in static and dynamic condition. However, if the collapse is regular, the energy absorption is greater for A and B solution due to a smaller folding length and a greater cross section. Even considering the specific energy (energy/weight), the A and B solutions are more efficient than C, D and E.

Comparison of the joining methods

The comparison of the results found with two analyzed configurations, and with the two adhesives (the 9466 was discarded due to its scarce strength especially in peeling) is shown in Figures 6 to 9. All the geometries of bonding were found acceptable, provided that proper measures are taken to avoid unstable collapse.

The comparison of spot-weld and laser-weld for this application is in Figures 10-11. Laser-welding is superior both in terms of stability and energy absorption. Laser-welding can substitute spot-welding without many changes, except the equipment to make the welds.

Then the comparison with impact tests is shown in Figures 20 and 21, for two adhesives and laser-welding. Spot-welded columns were not reported in impact testing conditions, since it was clear the advantage with bonding or laser-welding.

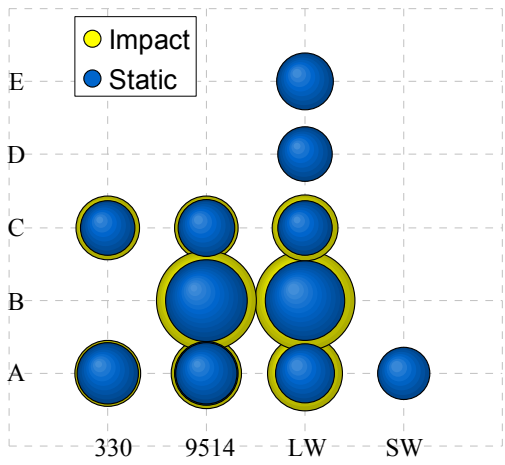

Figure 22. Summary of the results from the different joining methods and geometry in terms of the average crush load

As previously said, for configuration A, provided that a proper folding initialization is achieved, the two adhesives behave similarly both in quasi-static

and impact conditions. Looking at the energy absorption it comes out that there is a 20% dynamic increase, mainly due to the strain-rate sensitivity of this material [9].

Equivalent results were obtained with configuration B. The dynamic effect, in this case, is even greater (around 35%).

In both cases Hysol 9514 behaved better than Multibond 330 but differences are, depending on the case, of a few percent (namely, from 1% to 11%).

In Figure 22 a graphical representation of the most significant results in terms of average load is shown. Average load is a good indicator of energy absorption capability. The chart indicates the average load as the size of the bubbles. The joining method is the abscissa, while the ordinate represents the geometry of the section. It comes out that laser-welding is the more efficient solution for energy absorption. However, all joining methods are comparable, and better than spot-welding. Despite the trend to minor stability of the geometry without flanges, greater energy absorption comes still from geometries with flanges (A and B).

Therefore, there are many alternative efficient solutions to spot-welding that can give valid solutions to the problems posed by new car construction technologies (new materials, joining different materials).

CONCLUSIONS

The behavior of square box bonded columns subjected to axial crushing was investigated. A couple of up to date high performance structural adhesives and the laser-welding technology were compared to classical spot-welding.

Main objective of the work was to demonstrate the advantages of using adhesive bonding and continuous welding in structures subjected to crash, and that very efficient structures with high capacity of energy absorption can be obtained. Moreover, this result can be obtained without additional effort in terms of preparation of the components, surface treatment, etc.

Five series of square boxes were considered: a classical top-hat section, a double-hat section, and three variations of closed square obtained by joining two C shaped half-shells on the sides.

When appropriate countermeasures are provided to avoid debonding, mainly by triggering and, in some cases, adding some additional fasteners like rivets, the top-hat solution has more or less the same performance. This is an important practical result: for instance in car manufacturing it is not necessary to fully redesign the closed section thin walled parts of the car body. At the same time, if debonding can be avoided, even a weaker adhesive can give excellent results. The advantage lies in the fact that the adhesive gives a continuous connection of the sheets, with much more energy absorption. Impact affects negatively the bonded column behavior: debonding is much likely to occur, and proper countermeasures are extremely important to avoid catastrophic failure, with very little energy absorption.

Laser-welding is another very interesting solution: it gives results similar or even better when compared to spot-welding, and results similar to adhesive bonding. Stability is usually much improved with laser-welding compared to the all the other joining solutions.

In conclusion, nowadays many joining solutions for structures and components subjected to crash loading are available. They can give better performance or irreplaceable solution to joining problems (e.g. different materials), and this without the past problems that prevented their use (pre-treatment or cleaning of the surfaces, important design changes).

Acknowledgements

The authors wish to acknowledge the everlasting enthusiastic support of Mr. Piero Mauri of Henkel Loctite®, who also provided materials for the study.

Thanks to Mr. Stefano Chiaussa of RTM for the production of laser welded structures.

Thanks also to Alessandro Salvalaggio and Andrea Ferraris, for their help during the preparation of the samples and execution of the tests.

REFERENCES

[1] Davies, G. 2003. “Materials for Automobile Bodies.” Elsevier, Oxford, UK.

[2] Belingardi, G. and M. Avalle. 2004. “Advanced materials for automotive applications.” Mobility and Vehicle Mechanics, No. 30(2–3): 51–65.

[3] Avalle, M. 2004. “Experimental comparison of different innovative joining system for thin walled structures.” In Proceedings of the ICEM12, 12th International Conference on Experimental Mechanics, paper No. 253.

[4] Fay, P.A. and G.D. Suthurst. 1990. “Redesign of adhesively bonded box beam sections for improved impact performance.” International journal of adhesion and adhesives, No. 10(3): 128–138.

[5] Avalle, M., G. Belingardi and R. Vadori. 2001. "Sul collasso assiale di travi in parete sottile realizzate con adesivi: primi risultati sperimentali." In Proceedings of the XXX AIAS National Conference, paper No. 016.

[6] Belingardi, G., L. Goglio and M. Rossetto. 2002. "Sul comportamento strutturale di travi scatolate con giunzioni incollate: risultati sperimentali di prove d'impatto." In Proceedings of the XXXI AIAS National Conference, paper No. 073.

[7] Schneider, F. and N. Jones. 2004. "Impact of thin-walled high-strength steel structural sections." Proceedings of the Institution of Mechanical Engineers, No. 218 Part D: 131-158.

[8] Avalle, M., G. Belingardi, R. Vadori and G. Masciocco. 1999. "Caratterizzazione dinamica del comportamento flessionale di acciai da stampaggio." Proceedings of the XXVIII AIAS National Conference, 629–638.

[9] Peroni, L., M. Avalle, V. Petrella and G. Monacelli. 2002. "Strain-rate effects on the energy absorption capability of crash boxes with different geometry." In Proceedings of the SUSI VII, eds. N. Jones, C.A. Brebbia and A.M. Rajendran, 259–268.

[10] Peroni, L. 2004. "Evaluation of dynamic characteristic of materials by uniaxial tensile impact." In Proceedings of the ICEM12, 12th International Conference on Experimental Mechanics, paper No. 252.

[11] Goglio, L., L. Peroni, M. Peroni and M. Rossetto. 2005. Caratterizzazione sperimentale in campo dinamico di un adesivo epossidico bicomponente. In Proceedings of the XXXIV AIAS National Conference, paper No. 129.

RESULTS FROM TWO SIDED QUASI-STATIC (M216) AND REPEATABLE DYNAMIC ROLLOVER TESTS (JRS) RELATIVE TO FMVSS 216 TESTS

Donald Friedman
Center for Injury Research
Xprts, LLC.
United States
Carl E. Nash, Ph.D.
National Crash Analysis Center of the George Washington University
Center for Injury Research
United States
Justin Caplinger
Xprts, LLC
United States
Paper Number 07-0361

ABSTRACT

In an attempt to find a test protocol that characterizes the rollover occupant protection capability of a passenger vehicle better than the test used in Federal Motor Vehicle Safety Standard 216, we developed equipment and protocols for a modified, quasi-static roof crush test (M216, a test conducted sequentially on both sides of the roof over the A pillars at a pitch angle of 10º and roll angles of 25° and 40° respectively) and for a repeatable, dynamic rollover test called the Jordan Rollover System (JRS).

We have conducted M216 and JRS tests on 17 production vehicles to determine roof crush and crush velocities at a number of points in the interior. These tests included complete production vehicles, body bucks at reduced weight to increase the effective roof strength-to-weight ratio, and pairs of identical vehicles where one has had the roof reinforced in a manner that is entirely hidden by the vehicle's sheet metal and upholstery. Data from the JRS tests and the M216 tests are compared with the results of FMVSS 216 tests.

Analyses of the data highlight the relative value and validity of each test methodology, its ability to predict roof performance in actual rollovers, its use in vehicle roof structure design, and its potential contribution to regulation or consumer information. Based on the roof crush and crush speed in the vicinity of front seat occupants' heads, we propose a rollover crashworthiness ranking system. While static tests measure the force and deformation of the roof on the outside, the dynamic tests measure the crush on the inside during the sequence of rollover roof impacts, where it is directly related to the occupant's survival space and injury potential.

INTRODUCTION

One third of all light vehicle fatalities are in rollovers. In rollovers, roof crush causes side window failures creating ejection portals. The largest number of casualties in rollovers are from ejection. Roof crush also causes a significant number of head and neck injuries: typically the most severe consequences of rollovers. These two key issues in rollover were recognized by auto safety specialists in the 1960s. They were formally recognized in 1970 when NHTSA established the FMVSS 208 unbelted dolly rollover test[1] (ejection) and proposed FMVSS 216 (roof crush).[2] Current accident statistics which are a basis for this research are shown in Figures 1, 2 and 3.

SUVs have the highest rollover rate and rollover fatality rate. The unbelted front seat dummy in the FMVSS 208 dolly rollover test was intended to be contained by passive means, such as with laminated side window glazing, as was demonstrated in the 1978 Minicars Research Safety Vehicle[3]. A popular misconception, created to encourage belt usage, is that ejection injury is an inevitable consequence for unbelted occupants. The fact is that in typical weak roof vehicles, roof crush creates ejection portals by breaking tempered glass side windows, allowing partial or complete ejection. In addition, weak roof vehicles make belted occupants more vulnerable to serious head, face and spinal injuries from intruding roof components in rollovers. On the other hand, serious injuries to other body parts such as thorax, pelvis, limbs and soft tissue injuries may be the result of an unbelted body position in close proximity to the roof at the moment of roof impact, crush and crush speed.

The U.S. Rollover Injury Problem

- Annual Number of Rollovers 258,000
- Number of Occupants Involved 467,000
- Number of Fatalities 10,000 (2.1%)
  Severe to Critical injuries** 12,000 (2.6%)
- Serious Injuries** 18,000 (3.9%)
  (90% of serious to fatal injuries occur within two rolls.*)
- Not Seriously Injured 427,000 (91.4%)

*NHTSA 2003 estimates. **estimated distribution from Ciren and GWU

Figure 1. Rollover Accident Statistics.

TABLE 1.—ANNUAL AVERAGE NUMBER OF FATAL AND SERIOUS OCCUPANT INJURIES IN TOWAWAY CRASHES BY CRASH TYPE IN THE 1995–1999 NASS AND FARS CRASH DATABASES*

Crash type	Total occupants	Fatalities	Fatalities per total occupants	Fatal and serious injuries	Injuries per total occupants
Rollover	418,371	10,149	0.0243	27,057	0.0647
Frontal	2,921,864	12,384	0.0042	62,536	0.0214
Side	1,359,538	8,169	0.0060	33,610	0.0247
Rear	467,559	1,023	0.0022	2,701	0.0058
Other	36,978	432	0.0117	580	0.0157
Totals	5,204,309	32,157	0.0062	126,484	0.0243

*Adjusted for unknowns

Crash Type	Total Occupants	Injury Rate per Occupant	Fatality Rate per Occupant
Rollover	418,371	0.065	0.024
Frontal	2,921,864	0.021	0.004
Side	1,359,538	0.025	0.006
Rear	467,559	0.006	0.002
Other	36,978	0.016	0.012
Totals	5,204,309	0.024	0.006

Figure 2. Rollover Injury and Fatality Rates (2001).

Still another quantitative misconception is that accident severity is the cause of injury. NASS data makes clear that 80% of rollovers and 65% of serious to fatal injuries occur in less than 4 quarter turns and 95% of rollovers and 95% of serious to fatal injuries occur in 8 quarter turns as shown in Figure 4. Rollovers of less than 4 quarter turns involve trip speeds of less than 15 mph and 8 quarter turn rollover trip speeds are in the range of 20+ mph. Further more many of these low speed rolls are the result of pre-rollover collision as indicated in another companion paper in this conference "What NASS Rollover Cases Tell Us" by Nash[4]. This data makes clear that if there are serious injury consequences in 15 to 20+ mph, one or two roll accidents, something is wrong with the occupant protection system and the number of additional rolls adds opportunity but is irrelevant.

Table 1.4 -- Fatal Glazing Ejections

Annual Average for 1995-1999 NASS, Fatalities Adjusted to 1999 FARS

	Rollover	Planar	Total
Complete Ejection	3,295	1,516	4,812
Partial Ejection	1,476	1,348	2,824
Total	4,772	2,864	7,636

Table 1.5 Glazing Ejections by Vehicle Type

Annual Average for 1995-1999 NASS, Fatalities Adjusted to 1999 FARS

	Partial Ejection	Complete Ejection	All Ejections	All Occupants in Crashes	Glazing Ejections per 1,000 Occupants
passenger car	9,917	8,501	18,417	3,782,316	5
utility vehicle	2,326	3,182	5,508	449,353	12
vans	468	1,772	2,340	409,336	6
pickups	4,014	5,023	9,036	531,590	17
other/unknown	60	31	91	12,366	7
total	16,784	18,509	35,293	5,209,380	7

Figure 3. Ejections in the United States.

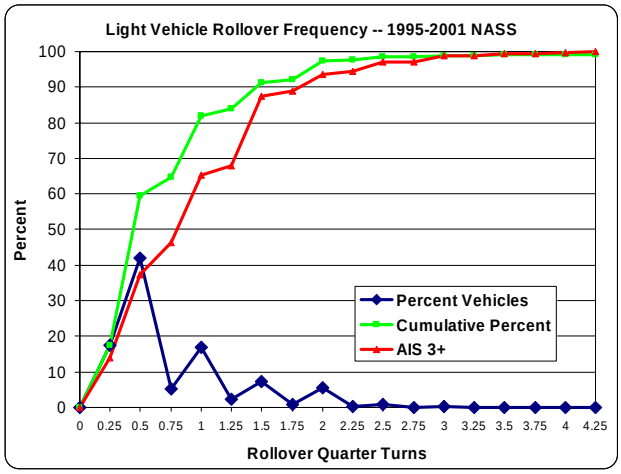

Figure 4. Rollover Frequency and Fatalities.

The most common perception about injury in a rollover accident is that injury increases with the amount of roof crush damage. Actually injury, as in all other accident modes, is caused by the speed of the occupant's second collision with the vehicle interior. In a rollover, that second collision speed is a combination of the structural intrusion or crush speed in combination with the occupants falling (or as manufacturers like to say "diving") speed creating a much higher contact speed at the injury site. This subject is discussed in some detail in a companion paper at this conference "Human/Dummy Rollover Falling (Excursion) Speeds" by Friedman, et. al.[5]

Another misconception comes from the lack of reliable data from accident statistics separating serious (non-permanently debilitating) injury and severe to fatal (permanently debilitating) injury. Several attempts from NASS data suggests (with

substantial uncertainty) that serious injury accounts for about 45% (of the 40,000 serious to fatal injuries) or 18,000 and severe to fatal about 55% or 22,000 (including 10,000 known fatalities) of what otherwise are considered "serious to fatal" injuries. These numbers are important since the economic loss and emotional consequences of these two levels of injury differ greatly. This subject is discussed in some detail in two companion papers in this conference "A Rollover Human/Dummy Head/Neck Injury Criteria" by Friedman and Nash,[6] and "What NASS Rollover Cases Tell Us" by Nash[4].

Crash tests and accident data have clearly shown that the greatest roof damage in a rollover is typically on the initially trailing or far side of a vehicle in a rollover. This coincides with the frequency of head, neck and spinal injuries to occupants seated on the far side of the vehicle. Roof strength designs which limit dynamic roof crush to less than 4" avoid creating side window ejection portals and reduce the potential for complete and partial ejection as well as exposure to external injury.

This paper addresses the issue of head impact on head, neck and thoracic spine injury from roof crush. We will present new data from dynamic rollover tests conducted on the Jordan Rollover System (JRS) on a selection of vehicles that show the mechanisms of roof crush in contemporary vehicles, the mechanisms of injury, and the criteria that can be used to assess the injury potential in dynamic rollover tests. Properly designed vehicles that show the portal creation ejection problem are also discussed. The vehicles tested included those with typical contemporary roof structures and with structures that have been reinforced to improve crush resistance.

SELECTION OF VEHICLES FOR TESTING

Because of their substantial overrepresentation in rollover crash statistics and their use as private passenger vehicles, we instrumented and tested eleven different SUVs. We also tested four different passenger cars and two pick-ups. Their FMVSS 216 Strength to Weight Ratios (SWR) ranged from 1.6 to 3.6.

There have been three series of tests. The first series of six vehicles was for general and regulatory SWR research and was documented in a paper "Observations from Repeatable Dynamic Rollover Tests" in the proceedings of the International Journal of Crashworthiness [7]. Some of those vehicles were tested on the two-sided M216 static roof crush fixture and then on the JRS. Photos of the M216 and JRS fixtures are shown in Figures 5 and 6.

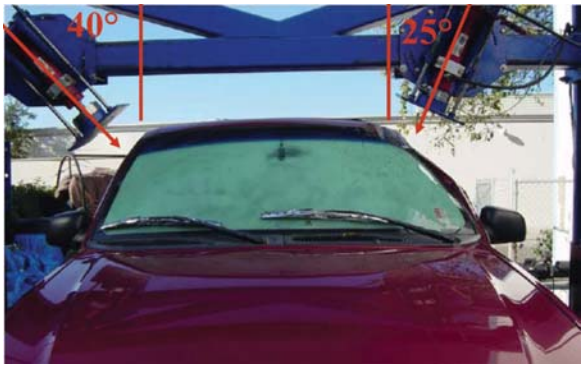

Figure 5. Vehicle in M216 test fixture.

Figure 6. Vehicle in JRS fixture.

Some of the SUVs that were tested were equipped with roof racks. Testing vehicle bucks at reduced weight simulated testing vehicles with higher SWRs. The tests were conducted at a low severity 15 mph and most at 5 degrees of pitch. For comparison purposes we also tested three similar vehicles with reinforced roofs.

A second series of 10 vehicles were tested only on the JRS with a similar low severity 15 mph, 5 degree of pitch protocol. A third series of vehicles is in process to develop a real world protocol suitable for regulatory compliance or NCAP testing with the 15 mph low severity protocol but with the pitch increased to 10 degrees. Three pre-tested vehicles were retested to preliminarily investigate this protocol

The reinforced vehicles and the production XC90 might be considered as the current state of the art reference standard roof: one that performs well and doesn't buckle under known rollover conditions.

DESCRIPTION OF M216 TESTING

The M216 test presses a 30.5 cm wide 61 cm long platen into the corner of the roof over the A-pillar at 10° pitch and 25° roll. It is pressed to a depth of 12.7 cm while measuring roof resistance. Then a similar platen is pressed into the opposite corner of the roof over the A-pillar at 10° pitch and 40° roll to a depth of 12.7 cm.

The test on the second side emulates the impact of the far side of the roof (after a near side impact in an actual rollover) because when the far side is in contact with the ground, the vehicle is rolling onto its side. This test provides a measure of roof strength which is expressed as the strength-to-weight ratio (SWR) which is the ratio of the maximum roof resistance force to the curb weight of the vehicle. Figure 7 compares the second side forces of tested vehicles as a percentage of weight (strength to weight ratio).

The generic effect of these measurements in comparison to FMVSS 216 measurements are shown in Figure 8. The far side strength of the roof is about half of that indicated in the FMVSS 216 test and therefore often only comparable to the weight of the vehicle. This results from the increased pitch angle of the loading platen (which exerts force primarily on the A-pillar) and the fracturing of the windshield which acts as a shear web between A-pillars and header.

The large size of the FMVSS 216 platen and the shallow 5 degree pitch angle combine to transfer the initial loading of the A-pillar to the roof rail and B-pillar within a couple of inches of platen displacement. Since the SWR requirement must be reached in five inches, the A-pillar design strength can be limited in spite of the fact that when the vehicle is rolling with 10 degrees of pitch the A-pillar takes most of the load (2 to 3 times the vehicle weight) to about 5 inches by which time the roof panel buckles from far side lateral forces. Unfortunately we can't predict the way and the extent to which the buckle will propagate from a static test.

A further limitation of the FMVSS 216 test is that roof racks and other appurtenances are removed before the test because they interfere with the large

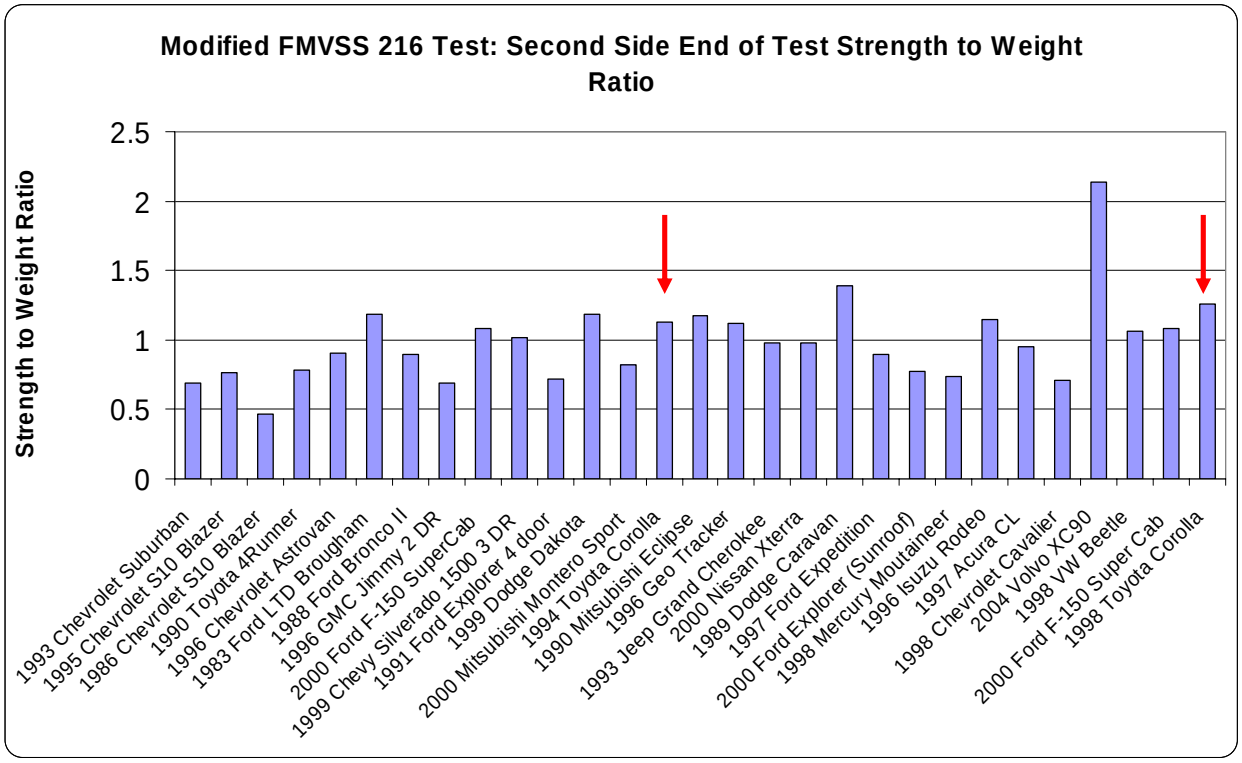

Figure 7. Second side M216 Strength to weight ratio highlighting 2 generations of Toyota Corollas

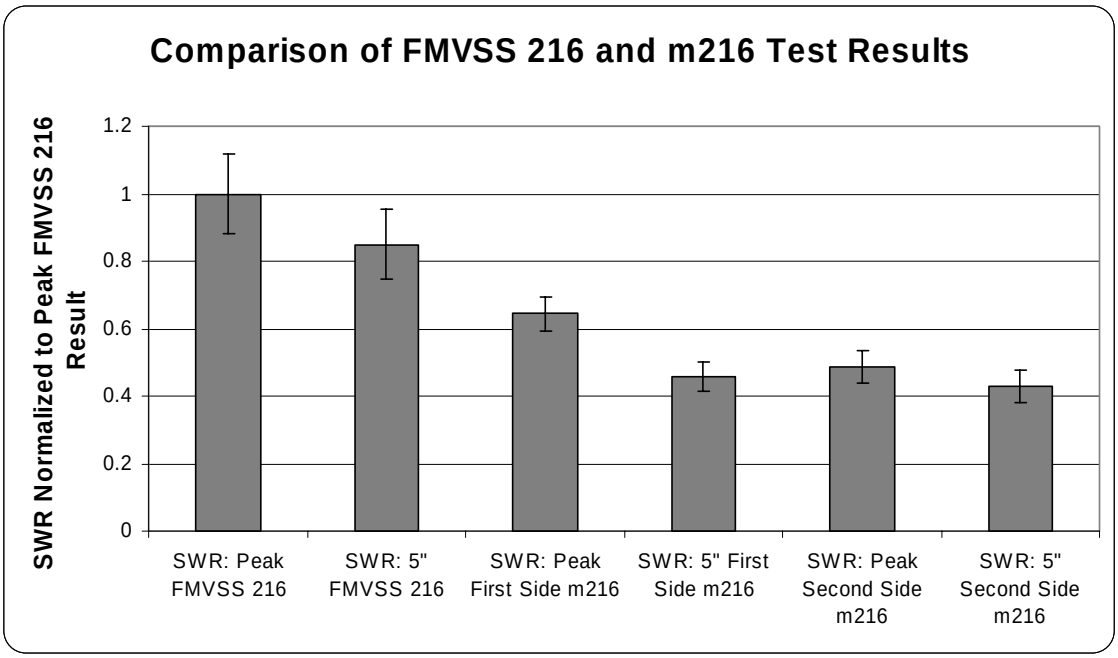

Figure 8. Comparison of FMVSS 216 and M216 tests at peak and 5" of displacement.

platen and shallow angle. In a crash or a dynamic test these things are pushed into the roof panel by the ground and precipitate a buckle whose intrusion speed is then amplified by lateral forces.

The size of the M216 platen was chosen to limit bending loads on the single hydraulic cylinder which provides the platen force. We have run a validation test using a standard FMVSS 216 machine in which the vehicle was attached and supported to the ground at 5 degrees pitch to create a 10 degree platen pitch angle. The conclusion was that the platen size can be as large as is convenient as long as it doesn't compromise the measurement of roof strength in an orientation representing contact with the ground of modern front wheel drive vehicles which roll with increased pitch.

M216 and FMVSS 216 performance has been roughly correlated through XC90 JRS testing. Volvo had an objective to achieve, but did not achieve, a SWR of 3.5 in 2" of platen displacement and at least maintain it to 5" in a FMVSS 216 test. This is roughly equivalent to increasing A-pillar strength as required to resist 10 degree pitch forces. Had it achieved its objective the M216 SWR would have been 2.5 and the ability to maintain structural integrity and low injury potential in 10 degree pitch rollovers would be significantly enhanced. Should NHTSA in its final FMVSS 216 rulemaking require such performance, roof buckles are unlikely and quasi-static test performance can continue as a regulatory requirement. Such static tests could then be verified by dynamic repeatable NCAP tests using the JRS.

HEAD AND NECK INJURIES

The current compressive neck injury criteria value is based on studies by Mertz and Nyquist conducted in 1978.[8] That study examined two high school football practice cervical spine injuries from contact with a tackling block that had 15 cm of foam padding. Based on 1990 and more recent Hybrid III dummy experiments, the consensus catastrophic level of force neck injury measures of 2003 authored by Mertz and Prasad [9], correspond to a Hybrid III dummy impact speed of 3 mph, a level which no one currently claims is seriously injurious.

Accordingly the authors have used six different studies as the basis for head and neck injury potential and criteria in these repeatable dynamic rollover (JRS) experiments. Those studies and conclusions are in a companion paper at this conference [6].

From these studies, we concluded that for rollover research, design and occupant protection evaluation tests the following Injury Criteria should be used:

The onset of serious neck injury occurs at a head impact speed of 3.1 m/sec (7 mph) which produces a force of 7,000 N at the base of a Hybrid III dummy's

head. The onset of severe to fatal neck injury is 4.5 m/sec (10 mph) which produces a force of 10,000 N at the base of a Hybrid III dummy's head. The onset of head and brain injury occurs at an impact speed of around 7 m/sec (16 mph).

DESCRIPTION OF REPEATABLE DYNAMIC JRS ROLLOVER TESTING

The test conditions for the original JRS research test series [10] were derived from various sources. The conditions of a typical next-to-last and last roll of dolly rollover tests (which, in the Malibu tests produced the most serious head/neck injuries) as recorded from instruments and on film suggested testing parameters. Examination of the conditions of actual rollovers from the National Accident Sampling System (NASS) and other sources also suggest aspects of test conditions.

The vehicle to be tested (either the complete vehicle or just the occupant compartment with weighting to emulate a complete vehicle) is balanced around its longitudinal roll axis with the approximately correct roll moment of inertia. It is suspended from drop towers at a fixed pitch and yaw above tracks supporting a mobile roadbed segment that can move under the vehicle as shown in Figure 6.

When the test is initiated, the vehicle is rotated at a fixed speed, freely falling a fixed distance to contact the near side of the roof at a given roll angle on the roadbed moving at a fixed speed under it. The vehicle continues to roll, moving freely as the roadbed moves beneath it so that the far side of the roof strikes the roadbed. After the far side impact, the roadbed moves beyond and the vehicle is caught by the drop towers so that it suffers no further damage.[10] The roadbed is instrumented to record vertical and lateral impact loads. String potentiometers record resultant roof displacement and speed during roof impacts at several roof locations inside the vehicle. A number of high speed and real time cameras record the impact.

Qualification tests in the range and at the limits of the various angles and speeds of the flexible impact parameters were conducted. Since the basic functions are controlled by coordinated mechanical linkages and triggers, repeatability of impact conditions are very good [11]. Repeatability of injury measure potential however is governed by the non-linearity of typical weak roof designs which buckle in unpredictable ways. Based on the research results (with underweight compartment bucks), roofs with M216 far side SWRs in the range of about 2.5 and/or FMVSS 216 SWRs in the range of 3.5 within 2 inches of platen displacement would not be expected to buckle and should be highly repeatable in JRS measured injury potential.

Preliminary examples are the XC90, Xterra and Corolla tests of Table 1. Although these are sequential tests on the same vehicle notice that the first two XC90 and Corolla tests are within about 30% of each other and well under the injury criteria. Both suffer from inadequate A-pillar strength when sequentially subjected to a 10 degree of pitch test although the geometry of the XC90 causes it to roll at 5 degrees while the geometry of the Corolla causes it to roll at 10 degrees. The Xterra when M216 and JRS tested, buckled at the roof rack panel mounting and performed consistently poorly independent of pitch, indicating that the buckle rather than the pillar strength caused the injury potential.

Table 1
JRS Tests at 5 and 10 degrees of pitch.

Vehicle	FMVSS 216 SWR	Initial Pitch Angle (deg)	Dynamic Maximum Crush (in)	Maximum Residual Crush (in)	Maximum Crush Speed (mph)
2004 Volvo XC90 Roll 1	3.6	5	1.5	0.4	2.3
2004 Volvo XC90 Roll 2	3.6	5	2.6	0.7	3
2004 Volvo XC90 Roll 3	3.6	10	7.0	4.1	7.0
2000 Nissan Xterra Roll 1	3.3	5	5.8	2.8	10.4
2000 Nissan Xterra Roll 2	3.3	10	5.9	2.9	10.2
2000 Nissan Xterra Roll 3	3.3	5	5.2	2.0	9.1
2002 Toyota Corolla Roll 1	4.2	5	3.0	1.6	4.1
2002 Toyota Corolla Roll 2	4.2	5	3.5	1.0	5.1
2002 Toyota Corolla Roll 3	4.2	10	5.1	1.8	7.1
2002 Toyota Corolla Roll 4	4.2	10	6.7	2.9	10.2

These research tests were not all conducted with identical protocols. The tests were designed to maximize the collection of experimental data. The road speed, drop height and roll rate were kept the same but the impact angle and weight were varied as was the sequence and number of rolls. Some judgment therefore was involved in combining and generalizing the results.

An occupant's head position and the location of roof crush buckles are relatively unpredictable. The preferred protocol therefore was to study the over-the-seat potential injury environment with an array of several string potentiometers measuring the crush of roof elements relative to the rotational axis of the vehicle. Even so, the measurements were usually not at the peak of the buckles.

BASIC RESEARCH RESULTS FROM JRS TESTING

An examination of the early test results gives insight into the rollover protection capabilities of several roof structures over a variety of test conditions. The data includes the crush and crush speed at several points on both the near and far side of the roof structure and the vertical loads as measured on the roadway.

Although there were some differences in the test protocol for each of the seventeen vehicle tests, a comparison can be made between peak roof crush speed and roof strength for the same point on each vehicle. Figure 9 and 10 illustrates these analyses respectively.

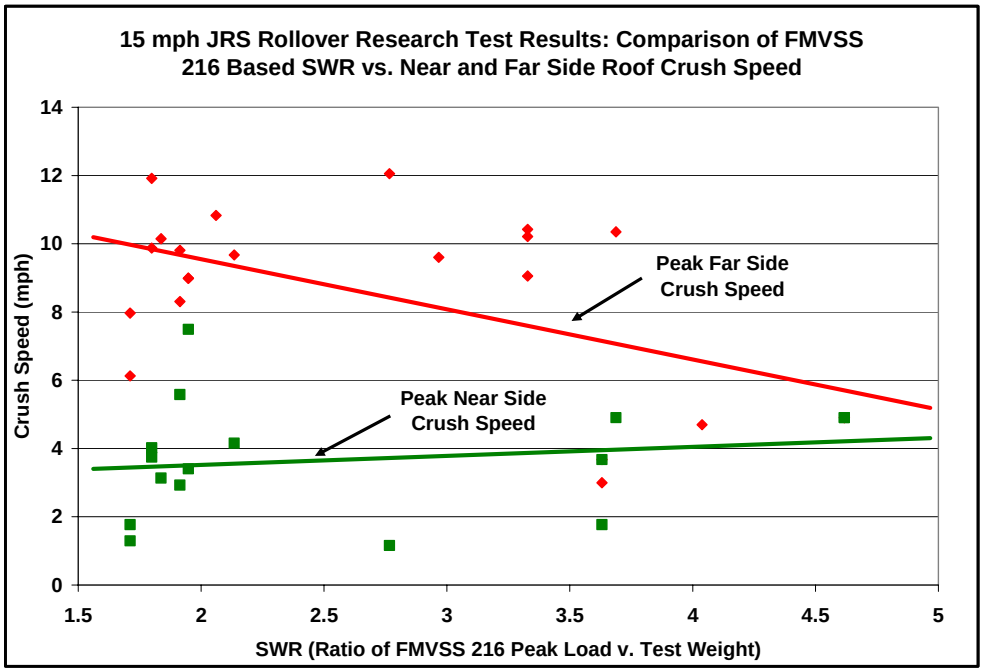

Figure 9. Peak roof crush speed of near and far side measurements vs. SWR at test weight.

There is some correlation between the SWR in FMVSS 216 testing and the results of JRS testing. Since the FMVSS 216 test does not initiate the buckles and collapse that are common in actual rollovers (and in JRS tests) it does not give results that correspond to the actual behavior of a roof in a rollover. However, if the roof were required to be strong enough to preclude buckling the correlation would be good.

The roof crush speed and roof crush indicated in Figure 9 and 10 is as measured in each impact and is not cumulative. From these tests it becomes very clear, that different roof structure designs have grossly different cumulative and residual crush characteristics, which are unknowable and misrepresented by post crash investigators without such JRS one roll at a time dynamic measurements.

As expected, the stronger the roof, as measured by the current FMVSS 216 test, the lower the far side roof crush speed as measured at the middle of the roof rail. For the near side as measured at the A-pillar the average crush speed is low and constant with SWR.

The near side roof crush at the 5 degree pitch impact angle was typically less than 4 inches, a level at which tempered glass resists fracturing and at which retained security (composite) glazing precludes portal creation (even when fractured by the side mirror).

Increasing the SWR, as demonstrated in either the FMVSS 216 or M216 test, does not necessarily ensure that the roof will not intrude to a dangerous degree in a rollover. A dynamic test (either the dolly rollover or the JRS test) will demonstrate whether a roof will buckle or collapse. The conclusion was reached that the failure mode (whether plastic or

elastic deformation) is more important than the actual SWR so long as the latter is above a threshold level.

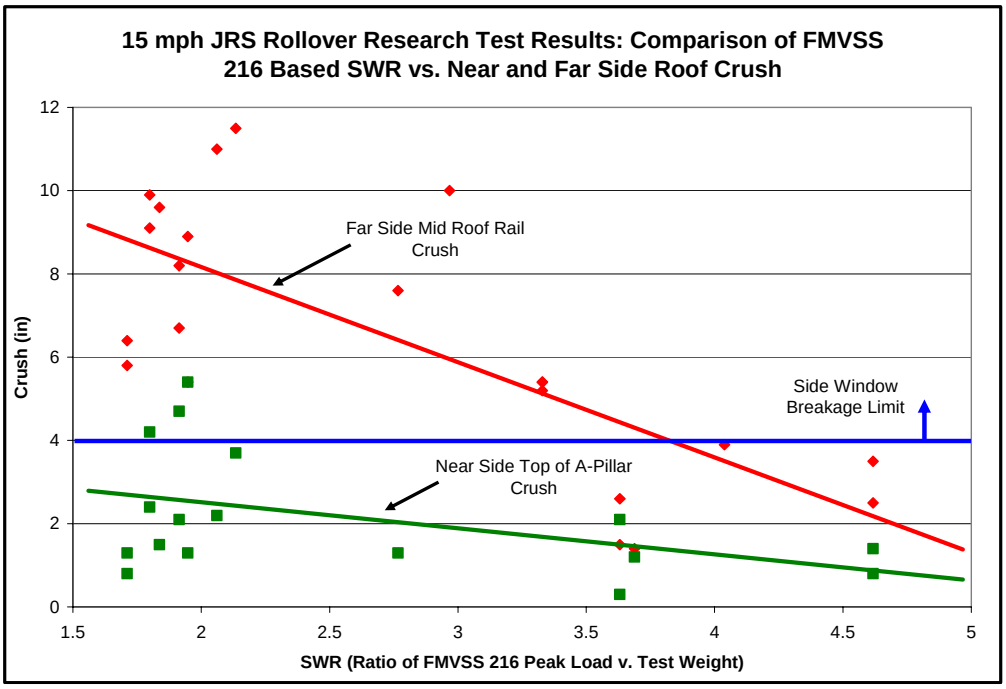

Figure 10. Comparison of Vehicle SWR and Far and Near Side Crush.

In the 5 degree pitch testing, it was found that the peak far side roof impact force in a JRS test in which roof crush is minimal, correlates with a SWR as measured in the FMVSS 216 test of at least 3.5, and a SWR as measured in the far side M216 test of at least 2.2.

The M216 near side peak roof strength is about three-quarters of that found in an FMVSS 216 test. The far side roof strength of a typical contemporary vehicle at 12.7 cm is roughly equal to its weight and about half the FMVSS 216 measured peak strength. For a production vehicle with a FMVSS 216 SWR of two, the near side strength may be adequate, but the far side strength is about one third of that needed to limit crush and crush speed.

SPECIFIC RESULTS FROM THE SECOND SERIES OF PRODUCTION JRS TESTING

A Production Vehicle Comparison

The test of the most popular SUV in the US (the 2000 Explorer) is compared to the Volvo XC90 claimed to be specifically designed to be reasonably safe in all accident modes. The XC90 in these tests shows that multiple roof impacts at 5 degrees pitch (a geometric rolling characteristic of the XC90 design) can be sustained by a well designed roof structure without compromising its ability to protect occupants.

The Explorer and the XC90 vehicles after two rolls are shown in Figure 11.

A comparison of the crush and crush speed between the two Ford production vehicles shows a dramatic difference between the rollover designed XC90 and the Explorer roof structures. In the XC90 there was a dramatic decrease in both of these crucial metrics; 82% in crush and 50% in crush speed. Figure 12 illustrates the reduction in crush speed and crush that is possible with a rollover designed vehicle (the XC90) as compared to a typical production roof vehicle (the Explorer).

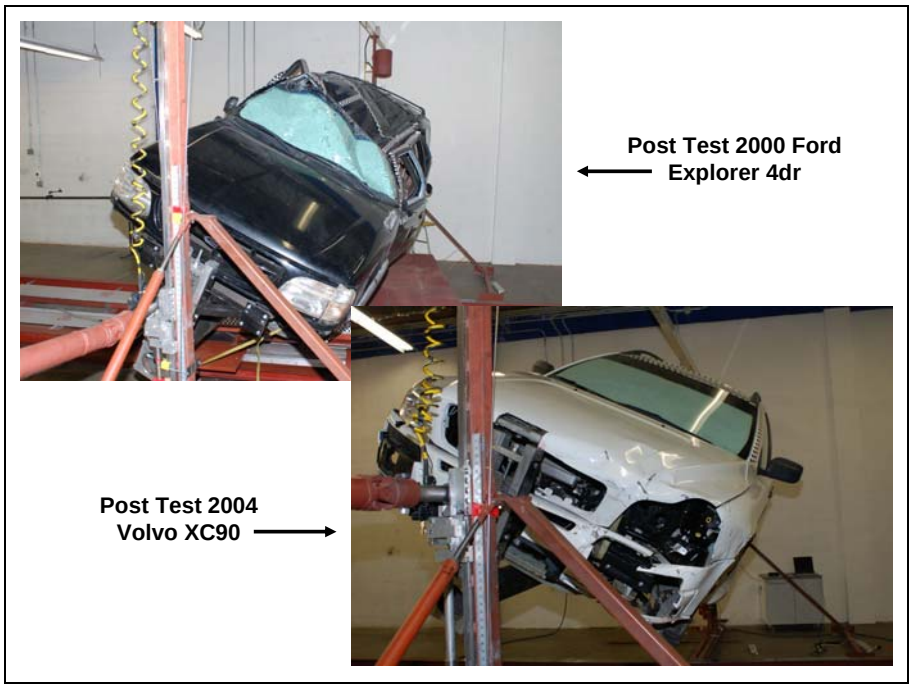

Figure 11. Post-Test Photographs of the Explorer and XC90.

2000 Ford Explorer 4dr Roll 1	Crush (in)		Peak Crush Speed
Location	Peak	End of Test	(mph)
A-Pillar	-8.7	-5.9	-6.3
Mid Point Between A and B Pillar	-9.1	-5.9	-6.7
B-Pillar	-6.7	-3.9	-5.5
Inboard of A-Pillar	-7.0	-4.9	-5.8
Inboard of Roof Rail Midpoint	-11.5	-8.5	-12.1
Inboard of B-Pillar	-8.7	-6.2	-9.1
Center of Roof	-8.2	-6.3	-7.6
Near Side A-Pillar	-4.2	-2.0	-3.8

2004 Volvo XC90 Roll 1	Crush (in)		Peak Crush Speed
Location	Peak	End of Test	(mph)
A-Pillar	-1.0	-0.1	-1.5
Mid Point Between A and B Pillar	-1.5	-0.3	-2.2
B Pillar	-1.2	-0.1	-1.9
Header Inboard of A-Pillar	-0.6	0.0	-1.2
Front of Sunroof	-1.1	-0.4	-1.8
Side of Sunroof	-1.5	-0.3	-2.3
Near Side A-Pillar	-2.1	-0.9	-3.3
Near Side B-Pillar	-3.2	-1.1	-3.7

2000 Ford Explorer 2 Roll JRS Tests
Peak Dynamic Crush – 11.5 inches
Peak Cumulative Crush – 14.5 inches
Peak Crush Speed – 12.1 mph

2004 Volvo XC90 2 Roll JRS Tests
Peak Dynamic Crush* – 2.6 inches
Peak Cumulative Crush* – 1.1 inches
Peak Crush Speed* – 3.0 mph

* Far side only

2000 Ford Explorer 4dr Roll 2	Crush (in)			Peak Crush Speed
Location	Peak	End of Test	Cumulative	(mph)
A-Pillar	-9.2	-6.4	-12.3	-9.6
Mid Point Between A and B Pillar	-9.9	-7.0	-12.9	-9.3
B-Pillar	-9.9	-6.7	-10.6	-8.8
Inboard of A-Pillar	-6.3	-4.2	-9.1	-7.0
Inboard of Roof Rail Midpoint	-9.5	-6.0	-14.5	-9.9
Inboard of B-Pillar	-8.9	-5.6	-11.8	-8.1
Center of Roof	-5.7	-3.1	-9.3	-8.5
Near Side A-Pillar	-2.4	1.0	-1.0	-4.1

2004 Volvo XC90 Roll 2	Crush (in)			Peak Crush Speed
Location	Peak	End of Test	Cumulative	(mph)
A-Pillar	-1.9	-0.5	-0.6	-2.0
Mid Point Between A and B Pillar	-2.6	-0.7	-1.0	-2.9
B Pillar	-2.6	-0.7	-0.9	-3.0
Header Inboard of A-Pillar	-1.2	-0.3	-0.3	-1.4
Front of Sunroof	-1.6	-0.5	-0.8	-2.1
Side of Sunroof	-2.5	-0.7	-1.1	-2.9
Near Side A-Pillar	-0.3	0.2	-0.7	-1.1
Near Side B-Pillar	-0.9	0.3	-0.8	-1.8

Figure 12 Comparison of XC90 and Explorer test results.

In the production and reinforced vehicle tests the maximum crush speed and corresponding crush values were selected from the six locations measured on the far side. Any of the points where roof crush was measured could have been used. However, the roof crush and crush speed is not uniform between vehicles and is affected by localized buckling and component failure, sometimes between measuring locations.

A Production Comparison by maximum crush speed

Given the Injury criteria previously described a sample rollover crashworthiness injury potential ranking system was developed as indicated in Figure 13. For this comparison we chose 10 tests conducted with equal severity on full production vehicles and the same initial conditions and test protocol. Since most of these tests were conducted on behalf of victims of rollover crashes the victim's injury under the deformed roof is indicated. For many of these vehicles such as the Explorer and Blazer the results are representative of dozens of cases the authors have investigated. The ranking basis was to assign labels of Unacceptable for a maximum crush speed of 10 or more mph, Poor for more than 8 and less than 10 mph, Good for less than 6 mph and Best for less than 6 mph and no created ejection portals.

JRS 15 mph Low Severity Dynamic Rolls Ordered by Max. Roof Crush Speed at any Point for Injury Potential Evaluation

Model Years	Make/Models	216 SWR	Max Crush (Inches)	Maximum Speed (MPH)	Injury Probability	Case Injury
2002-2006	Volvo XC90 SUV	3.6	3.2	3.7	Best	NA
1999-2005	Hyundai Sonata Sedan	1.8	6.4	8.0	Fair	Quadriplegia
2003-2006	Kia Sorrento SUV	1.9	6.9	9.0	Poor	Quadriplegia
1995-1999	Nissan Sentra Sedan	3.2	9.1	9.6	Poor	Quadriplegia
1995-2001	GMC Jimmy SUV	2.4	6.7	9.8	Poor	Quadriplegia
1995-2005	Chevy Blazer SUV	2.4	9.6	10.1	Not Acceptable	Quadriplegia
1999-2001	Isuzu VehiCross SUV	NA	6.8	11.1	Not Acceptable	Brain Injury
2001-2006	C2500 HD Reg Cab Pickup	2.2	9.9	11.2	Not Acceptable	Fatal
1995-2001	Ford Explorer SUV	1.6	11.5	12.1	Not Acceptable	Quadriplegia
1994-1999	Mitsubishi Eclipse	2.5	7.6	12.1	Not Acceptable	Fatal

(Criteria: Best = < 6mph and no ejection portals; Good = < 6 mph; Fair = < 8 mph; Poor = < 10 mph; Not Acceptable = > 10mph)

Figure 13. Comparison of far side maximum crush and crush speed of production vehicles.

PRELIMINARY RESULTS FROM THE THIRD SERIES OF JRS REAL WORLD PROTOCOL TESTING

Having demonstrated the repeatability of the JRS in accurately duplicating initial impact conditions and the ability to distinguish between roofs with and without acceptable injury potential crush speed, the next step is to develop a realistic real world protocol useful for regulatory compliance, New Car Assessment Program (NCAP) and crash victim injury severity investigations. The alternative protocols considered were:

A two roll test emulating a two roll crash encompassing 95% of serious to fatal Injuries is:

- 18mph, 240°/s Roll Rate, 10° pitch, 4" drop, 125° initial Roll angle. Stresses the leading side.
- 12mph, 180°/s Roll Rate, 10° pitch, 4" drop, 145° initial Roll angle. Stresses the trailing side.

A one roll test to emulating a one roll crash encompassing 65% of serious to fatal Injuries:

- 15mph, 200°/s Roll Rate, 10° pitch, 4" drop, 135° Roll Angle. Stresses both sides equally (similar road load).

Concerns about repeatability of injury measures, interest in matching or correlating the JRS and M216 performance for a minimum regulatory requirement, and a desire for simplicity, suggest the one roll test, possibly with a 145° roll angle. The study is ongoing with very preliminary results shown in Table 1, comparing the dynamic crush and crush speed results of 5 and 10 degree tests for two SUVs and a passenger car.

Injury potential repeatability may be inferred from the sequential results at 5 degrees of pitch with these high SWR roofed vehicles. A buckle in the Xterra roof accounts for the dangerous injury potential.

The study is now considering the correlation between FMVSS 216, M216, the JRS tests and with NASS residual crush. The main issue is the inability of a static test to induce buckling. Preliminarily, if the static 216 SWR criteria were high enough, say 3.5 in two inches of platen displacement, or the M216 SWR were 2.5, the likelihood of a buckle forming in a one roll real world JRS compliance test is unlikely unless induced by a roof rack or similar object.

WEIGHT AND COST OF ROOF STRENGTH IMPROVEMENT

Two generations of Toyota Corolla roof structures (1994 to 1997 and 1998 to 2002) were carefully inspected and compared. The FMVSS 216 and M216 test results are shown in Table 2.

The second generation roof structure was JRS tested with both 5 and 10 degree pitch protocols as shown in Table 2, although this front wheel drive vehicle is known to roll at 10 degrees of pitch. The roof structure inspection and comparison showed that the two roof structures were identical except that the inner surface of the 2002 roof rail had been reinforced on either side of the B-pillar to just before the A and C pillars with a single stamped steel panel, probably of high strength steel, 41 inches long, 3 inches wide and 0.038 inches thick. The estimated weight for both sides is approximately 3 pounds. The 1994 FMVSS 216 test SWR was about 2.5 and the 2002 SWR was about 4.2. The 1994 M216 test results are a little low because of rear test damage, since the vehicles seem identical. The far side 1994 SWR was 1.2 and the 2002 M216 test SWR was 1.3. The JRS tests with the 5 degrees of pitch resulted in 4.1 and 5.1 mph crush speeds and confirmed the FMVSS 216 SWR improvement at the B-pillar. The JRS tests with the 10 degree protocol resulted in a 7 mph crush speed at the A-pillar (amplified by a buckle at the header and rain gutter which was not measured) that confirmed the M216 lack of improvement at the A-pillar. It was estimated that had the reinforcement been carried around the roof rail, A-pillar intersection and across the header, at an additional weight of 1.5 pounds and a cost of a few dollars, the crush speed of 4 mph could have been maintained when rolling with 10 degrees of pitch.

Table 2
Toyota Corolla SWR results

	1994-1997 Toyota Corolla SWR	1998-2002 Toyota Corolla SWR	Percent Increase
FMVSS 216 - Peak	2.5	4.2	68%
FMVSS 216 - 5"	2.3	2.95	28%
M215 1st side - Peak	1.89	2.3	21%
M216 1st side – 5"	1.43	1.8	25%
M216 2nd side – Peak	1.24	1.33	9%
M216 2nd side – 5"	1.13	1.25	10%

OTHER JRS TEST OBSERVATIONS

Approximately 50 JRS tests have been conducted with a wide variety of vehicles and under a wide range of test conditions. The focus and scope of this paper precludes detailed discussion of those observations but they include:

ROOF STRENGTH, GLAZING AND PORTAL CREATION AS IT EFFECTS PARTIAL AND COMPLETE EJECTION

M216 and JRS tests indicate that near and far side tempered glass windows break after about 4" of roof

crush. Near side crush in these tests seldom reached this level even in a vehicle with a SWR as low as 2.5 but windows often broke from side mirror impacts. Far side windows almost always break even in bucks simulating a 3.5 SWR. Vehicles reinforced or simulated at SWR of 4+ that we tested with tempered windows rarely broke except for side mirror impact. Side window breakage can be reduced by redesigning the window frame shape, size, location and strength and relocating the side mirrors.

OCCUPANT SIZE AND RESTRAINT EFFECTS

In spit tests using the JRS at rates to 220 degrees per sec with various size restrained humans and several different conventional belt systems, most 50th% and 95th% occupants reached the roof panel adjacent to the middle of the roof rail. Fifth percent females were able to reach the underside of the roof rail. When the sum of the excursion in the belts and the occupants seated height was greater than the head room the neck flexed such that it could not be effectively loaded axially.

PITCH EFFECTS ON ROOF LOADING AND CRUSH SPEED.

All tests have been conducted with 10 degrees of yaw. Variations in pitch from 10 degrees to zero resulted in similar far side crush and crush speed at the middle of the roof rail. Higher initial pitch angles resulted in more window breakage as well as roof panel and open section roof rail buckling over the far side occupant.

IMPACT ROLL ANGLE AND VEHICLE GEOMETRY AS THEY AFFECT ROAD LOAD AND CRUSH

The peak road load force and energy for far side roof crush varied as a function of roll angle. At 135 degrees the near and far sides were about equal, while at 155 degrees the far side load and duration (energy) was 2 to 4 times higher than the near side. Due to the web strength of the compartment rear closure panel and bonded rear window as well as the high aspect ratio of the corners of the roof in some pickups, only high initial near side roll angles will result in far side collapse.

CONCLUSION

A strong roof is critical both to prevent head impacts at a speed above 11.3 to 16.1 km/h (7 to 10 mph) that can cause head or neck injury. A strong roof will also protect side glazing so that it continues to provide a barrier to partial or complete ejection. Both the Malibu and JRS tests show that the basic conditions of a rollover are sufficiently benign that even if there is some head contact with the roof under rollover conditions, it will not produce serious injury so long as the roof performs well. This will particularly be true if the vehicle has the head impact area padding now required by FMVSS 201.

The performance of the Volvo XC90 and the Toyota Corolla shows that there is no inherent problem in providing this level of protection in a light passenger vehicle. In fact, the use of advanced materials such as high strength steel and plastic inserts to control buckling of structural elements, could mean that adequate roof strength could be achieved with little or no net weight increase.

It is clear that we now have the testing tools and the vehicle technology to achieve a major reduction in rollover casualties even if rollover rates do not change significantly. In fact, the use of electronic stability controls will reduce the rate of rollovers in the future as well.

REFERENCES

1 49 C.F.R. 571.208.

2 Federal Register, Doc. 71-17936, December 7, 1971.

3 Ausherman, V.K, Kadikar, A.V, Syson, S.R., Strother, C.E., Struble, D.E., "Technical Final Report, The Minicars Research Safety Vehicle Program", September 1981 RSV Paper.

4 Nash, C.E., "What NASS Rollover Cases Tell Us", 2007 ESV Conference.

5 Friedman, et. al., "Human/Dummy Rollover Falling (Excursion) Speeds" 2007 ESV Conference.

6 Friedman, D. and Nash, C.E., "A Rollover Human/Dummy Head/Neck Injury Criteria," 2007 ESV Conference.

7 Friedman, D., Nash, C.E., Bish, J., "Observations From Repeatable Dynamic Rollover Tests", International Journal of Crashworthiness 2007, Vol. 12, No. 1, pp. 67-76.

8 Mertz, H., Nyquist, G., et al., An Assessment of Compressive Neck Loads Under Injury-Producing Conditions, Nov. 1978.

9 Mertz, H.J., Irwin, A., Prasad, P., "Biomechanical and Scaling Bases for Frontal and Side Impact Injury Assessment Reference Values", STAPP Car Crash Journal Vol. 47, October 2003.

10 Friedman, D., et al., “Repeatable Dynamic Rollover Roof Test Fixture”, ASME 2003.

11 Jordan, A. and Bish, J., “Repeatability Testing of a Dynamic Rollover Test Fixture”, ESV Conference, Washington, D.C. 2005.

INTELLIGENT SEATBELT REMINDERS: DO THEY CHANGE DRIVER SEAT BELT USE IN EUROPE

Anders Lie
Karolinska Institutet and Swedish Road Administration
Sweden
Anders Kullgren, Maria Krafft
Folksam Research and Karolinska Institutet
Sweden
Claes Tingvall
Swedish Road Administration
Sweden
Monash University
Australia
Paper number: 07-0388

ABSTRACT

The objective was to study if there were differences in driver's seat belt wearing rates between cars with and without Seat Belt Reminders (SBRs), and if there were differences in wearing rates between some different European countries indicating that the potential in saving lives could vary between the counties.

The influence on seat belt wearing rates of SBRs fulfilling the Euro NCAP specification was studied in seven EU countries; Belgium, Denmark, France, Germany, Italy, Spain and Sweden. The same observer performed all observations and he noted if the seat belt was used and the car model observed. In total 11160 cars were observed. The measurements were only made in cities and did only concern driver SBR.

For all observations the total seat belt wearing rate was 97.5% in cars with SBR, while it was 85.8% in cars without. The results indicate that the number of unbelted car occupants is decreased by 80% independent of the wearing rate. The highest wearing rate in cars with SBRs was found in Paris, 99.8%, and the lowest in Brussels, 92.6%. The results support previous estimations that more than 7000 lives could be saved every year in the EU if all cars were fitted with SBRs. Therefore actions aimed at increasing the fitment rates of SBRs are desirable.

Previously it has been estimated that SBRs are one of the most cost effective measures to save lives. The results in this study support the estimation.

BACKGROUND

It is widely recognised that the seat belt is one of the most important safety inventions. Kahane (2000) estimates the risk reduction associated with seat belts in cars to 45 percent in passenger cars and 60 percent in light trucks. The current wearing rate saves thousands and thousand of lives every year.

Most countries has a mandatory use of seat belt legislated. In Europe there is a seat belt directive. However the seat belt use is not 100% in those countries. The seat belt wearing rate for drivers and front seat passengers in Europe was estimated to an average of 76 % in 2003 (ETSC 2003). For passengers in the rear seat the estimate is 46%. The variations are significant. For front seat occupants in Europe in 2004 it varied from 59% and 96% (ETSC 2006a).

It is clear that significant safety gains could be achieved if more or all car passengers were to use the seat belt.

The European Transport Safety Council (ETSC) has previously calculated the potential of seat belt reminders. In the European Union (EU-15) 7600 lives could be saved per year in 1996 if all used seat belts. In the USA the potential is also high and it has been shown that another 8000 lives would have been saved if all used their seat belts (Glassbrenner 2003). Even in countries with a high seat belt use the remaining potential is high. In Sweden with a 92% seat belt use, almost 40% of those killed as car occupants were unrestrained SRA (2005 & 2006). In Australia, with an overall seat belt use of 95%, 33% of those killed in car crashes were unrestrained Fildes et al (2002).

After some initial work performed by Folksam research in Sweden, the Swedish Road Administration together with Swedish car manufacturers and research institutes started a co-operation around improved seat belt reminder systems in 1995. The joint effort resulted in a shared understanding that improved seat belt reminders could play an important role to increase seat belt use (Turbell et al 1996).

Based on the Swedish experience the European Enhanced Vehicle-Safety Committee (EEVC) initiated a work around seat belt reminders. The working group 16 (EEVC/WG16) reported a set of recommendations in 2002. These recommendations formed the basis for Euro NCAP when developing the first seat belt reminder protocol

Before introducing the smart seat belt reminder, studies were conducted to analyse reasons for non-belt use. In Sweden, Dahlstedt (1999) showed in a combination of an observational and interview study, that only a very small fraction (less than 0,1% of the whole population and approx 1% of the nonusers) was against seat belts on a more principal level. The most common reasons for not using seat belts were simply that they were forgotten, or that the trip was short.

There are similar results from the USA, where it has been reported that approximately only four percent of the drivers are against using a seat belt, and where 87% strongly agree that they would want to be wearing a seat belt in a crash (TRB report 278). Ferguson et al. (2006) found that nearly 90% of drivers having cars with seatbelt reminders would like one in their next car.

Since 2002 the consumer crash protection programme in Europe, Euro NCAP, gives premium to cars having seat belt reminders. The requirement is that a loud and clear light and sound signal should be active for at least 90 seconds if the seat belt is nor worn. Euro NCAP gives separate points for the driver, front seat passenger and rear set passenger. The demand for the rear seat is lower and does not demand audio signal.

In June 2002, the first car with such a system for the driver was introduced, quickly followed by more. In all, Euro NCAP has given points to 96 cars (Nov 2006). ETSC has estimated the proportion of new cars sold with seat belt reminders in EU. In 56% of the cars sold in 2005 there was a seat belt reminder (ETSC 2006b). ETSC found large differences between the different countries. Sweden had almost 70% of the new cars sold in 2005 having seat belt reminders and the Czech Republic only around 30%.

Krafft et al. (2005) reported a study on the effect of seat belt reminders in Sweden in 2005. That data set is a part of this study. The analysis showed that seat belt reminders made a significant difference in seat belt use in Sweden. The seat belt use for cars not equipped with sear belt reminders was 82,3 +/- 1,9%. For cars with seat belt reminders the seat belt use was found to be 98,9 +/- 0,8%.

Ferguson et al. at Insurance Institute for Highway Safety reported in 2006 a study on the seat belt use in Honda cars. They compared the seat belt use in models without seat belt reminders from 2002-04 and cars with seat belt reminder 2004-06 model year. The research sowed a change in seat belt use from 84% to 90%.

The aim of the present study was to evaluate if the presence of a smart seat belt reminder (SBR), increase the driver seat belt wearing rate in traffic in some European cities.

METHOD/MATERIAL

The study was performed in two steps, in July 2005 (Sweden) and in May 2006 (Europe). Using Swedish experience it was assumed that the seat belt use is lower in built up areas than in rural areas. To find the minimum effect of seat belt reminders the observations were conducted in built up areas. The observations were conducted in seven countries within the European Union. In Sweden, the observations were made in five cities spread across Sweden, see Table 1. In the other six countries the observations were made only in one city in each country, see Table 1.

To avoid any inter-observer bias all observations were performed by the same observer,. The observer was trained to discriminate between different car models, and was also instructed to note what car that was observed. The observer was also instructed to only note cases that were clear. Any uncertainties about seat belt use and car model were omitted from the observations. Car model and driver seat belt use was recorded.

Table 1. Countries and cities where the observations were made.

Observation	**Country**	**City/cities**
May 2006	Belgium	Brussels
May 2006	Denmark	Copenhagen
May 2006	France	Paris
May 2006	Germany	Berlin
May 2006	Italy	Milan
May 2006	Spain	Barcelona
July 2005	Sweden	Karlstad, Örebro, Luleå , Sundsvall and Stockholm

Three groups of cars were defined (the cars studied in each category are listed in the Appendix):

- The first group contains cars that fulfil the Euro NCAP protocol for the driver's seat and have been approved by Euro NCAP (Euro NCAP 2004). They all have seat belt reminders that have a visual signal and a loud and clear audio signal. If the driver is unbelted the signals must be active for at least 90 seconds.
- The second group contains cars with visual reminders and some low intensity audio signal. The sound signal does not fulfil the Euro NCAP protocol's demands for loud and clear.
- The third group contained cars without any reminder. The latter group was defined in such a way that it should be similar as to size and age, when compared with the group with reminders.

No control for driver age, gender or socio-economic status was performed in this study.

In total 11160 cars were observed, where the seat belt use of the driver was noted. Statistical tests were carried out comparing the proportion of seat belt usage (student's t-test for proportions).

RESULTS

A significant difference in seat belt wearing rate was found. For all observations the total seat belt wearing rate was 97.5% in cars with SBR, while it was 85.8% in cars without, see Table 2. The results indicate that the number of unbelted car occupants is decreased by 80% independent of the wearing rate.

The wearing rate in cars with mild reminders was 93.2%, indicating that the levels of the audio and visual reminder signals are of importance. The highest wearing rate in cars with seat belt reminders was found in Paris, 99.8%, and the lowest in Brussels, 92.6%. The results are presented in Table 2.

In cars fitted with seat belt reminders and still with unbelted drivers, some manufacturers appear to be over-represented, see Table 3. The differences are, however, not statistically significant.

Table 2. Numbers of observed drivers for cars with and without a seat belt reminder (SBR), drivers with seat belts used, and the associated seat belt use in percent.

	Denmark/Copenhagen			Belgium/Brussels			France/Paris			Spain/Barcelona		
	total n	belted n	belt use %	total n	belted n	belt use %	total n	belted n	belt use %	total n	belted n	belt use %
Cars with SBR	326	319	97,9	526	487	92,6	512	511	99,8	491	484	98,6
Cars with mild SBR	42	39	92,9	42	36	85,7	19	19	100,0	21	19	90,5
Cars without SBR	652	580	89,0	869	605	69,6	897	869	96,9	757	690	91,1

	Italy/Milan			Germany/Berlin			Sweden/5 cities			Total		
	total n	belted n	belt use %	total n	belted n	belt use %	total n	belted n	belt use %	total n	belted n	belt use %
Cars with SBR	463	452	97,6	446	431	96,6	734	726	98,9	3498	3410	97,5
Cars with mild SBR	35	34	97,1	35	35	100,0	729	678	93,0	923	860	93,2
Cars without SBR	894	770	86,1	1044	932	89,3	1626	1339	82,3	6739	5785	85,8

Table 3. Numbers of belted and unbelted drivers in cars fitted with SBR for the included car models.

Make	Model	Year	All cities		
			seat belt used	seat belt not used	un-belted %
Alfa Romeo	159	2005	16	1	6
Audi	A3	2005-	159	4	2
Audi	A4	2005-	174	7	4
Audi	A6	2004-	175	9	5
Citroën	C4	2004-	105	4	4
Citroën	C5	2005-	54	5	8
Ford	C-Max	2005-	105	4	4
Ford	Focus II		168	0	0
Nissan	Micra	2003-	120	4	3
Peugeot	407	2004-	179	2	1
Toyota	Avensis	2003-	131	3	2
Toyota	Prius	2004-	12	0	0
Renault	Megane	2003-	402	13	3
Renault	Scenic	2003-	319	10	3
Renault	Espace	2003-	142	2	1
Saab	9-3	2003-	73	3	4
Volvo	S40	2004-	17	1	6
Volvo	V50	2004-	74	1	1
Volvo	XC90	2002-	54	2	4
VW	Touareg	2003-	64	4	6
VW	Passat	2005-	141	1	1
Total			2684	80	3

DISCUSSION

The seat belt is one of the most important safety devices in a modern car. Even if the belt has saved thousands of lives per year there is a huge potential left. By making all occupants in the cars and trucks wearing their seat belts many thousand lives could be saved also in societies with relatively high seat belt use. Setting the seat belt use target at 100% seems the only logical way ahead.

Seat belt reminders are playing an important role in changing the seat belt use. This study is indicating that more than 80% of the non-wearers of seat belts put their belt on in a car with seat belt reminders.

While seat belts have been found to be very effective for a long time, and several methods have been applied to stimulate and increase seat belt use, there is still a major potential in increasing the use of seat belts to 100%. This also applies to countries with a very high seat belt use, between 90 and 95%. There seems to be a positive marginal benefit, which is associated with that those not using seat belts are also more likely to be involved in crashes, especially in serious crashes. On the other hand, there is little, if any, resistance to use seat belts in countries where this issue has been researched. The modern seat belt reminders have been developed with this in mind, i.e. the force that is applied to the driver does not need to be in the order of an interlock, but it has to be persistent enough and acting with sufficient time duration.

The results of this study show remarkable results. While the seat belt use for a control group was 85.8 %, the use of seat belts was 97.5 % in the group with the most advanced reminders. While the control group would have had a higher use if the observations were conducted outside built up areas, the use of seat belts for those in a car with SBR would probably not be lower. The results were also consistent in that cars with mild reminders had a significantly higher seat belt use than cars without, and a significantly lower use than cars with SBR according to Euro NCAP protocol. This is also consistent with earlier results Kraftt et al (2005) and Bylund and Björnstig (2001) and might be consistent with studies made in the USA Williams et al (2002).

The case and control car models in this study were selected to be as similar as possible in size and age. However, as often in transition phases, a perfect match is very hard to achieve.

The cars equipped with seat belt reminders are slightly younger than the control cars. It is therefore important to follow the seat belt use in those cars over time. In this study no attempt was made to control for potential differences in driver profiles between the case and control groups. This is an important factor that could change the results if significant differences would occur in driver age, gender or socio-economic status.

The study group with mild reminders included different levels of reminding signals. Volvo S60 and V70 changed during the period 2001 to 2005 where the intensity of the sound signal increased. It was not possible to further study the importance of the light and sound in this study, but it is evident the seat belt use was lower for the mild systems, and for the cars individually that had different, but mild reminders.

A study from Australia within the SafeCar project (Regan et al 2005), where specially equipped cars where SBR was turned on and off in a controlled experiment during a long observational time, and where the cars logged all data, it was found that the proportion of time when the driver or passenger was not using seat belts in speed over 40km/h was reduced from 6% to almost 0. In these cars, the reminder system was designed according to the principles of Euro NCAP.

This study looks at seat belt use in traffic. Previous studies have shown a major difference in seat belt use between normal traffic and serious crashes. It is important to perform studies of seat belt use in crashes also for cars with SBR. Such studies should be possible to conduct at this stage or very soon, as the market penetration of SBR is large.

The results show that SBR is one of the most cost effective measures available. In Sweden approximately 150 unbelted car occupants are killed every year. With a 50% effectiveness of the seat belt in reducing fatalities, approximately 60 lives in Sweden annually (14% of the total number of fatalities) could be saved. On a European level more than 7000 annually could be saved, which supports earlier estimates by ETSC. For a small investment into every new car, the benefit cost ratio (BCR) should be much higher than 1 to 10, based on earlier calculations (Fildes et al 2002).

The results presented in Table 3 raised some concerns about possible disconnection of the SBR for specific car models in some countries. The data is however, too limited to draw any conclusions about it. In the Euro NCAP protocol, one of the requirements is that the system should not be easy to disconnect, and that if this is possible, that instructions how to do so should not be available in the owners manual. The owner would therefore be forced to contact the dealer or a workshop with a manual for the car. Hopefully, the automotive sector will be very restrictive in disconnecting reminder systems, as they have strong arguments for not doing so. In the present case, the head office of the car importer was contacted, and a message was sent out from the head office to all dealers and workshops to be very restrictive to disconnection of seat belt reminders. Activities, such as the vehicle inspections, should have an important role to prevent disconnection of SBR.

In the present study, taxi cars were not observed. In Sweden, the use of seat belts among taxi drivers is lower than in the rest of the population (79%). While taxis in Sweden normally are cars up to three years of age, most of them today will have a seat belt reminder. It is important to follow such a group. Also front and rear seat occupants should be studied further, as a growing proportion of new cars have seat belt reminders also for front passenger seat and rear seat.

CONCLUSIONS

It was found that the seat belt wearing rate in cars with seat belt reminders that fulfil the Euro NCAP protocol was 97.5 % in the European cities studied, while the rate was 85.8% in cars without reminders.

The results indicate that the number of unbelted car occupants is decreased by 80% independent of the wearing rate.

Smart seat belt reminders are highly effective in increasing seat belt use, and that the results support previous estimates that more than 7000 lives in Europe and 8000 lives in the USA could be saved each year. Therefore actions aimed at increasing the fitment rates of SBRs are desirable.

ACKNOWLEDGEMENTS

The authors wish to thank Mr Fredrik Bagge, Uppsala, for conducting the observations.

REFERENCES

Brabander BD, Vereeck L. (2003) Cost-benefit analysis for road safety investments in Belgium. Case study for a seat belt reminder system. Report RA-2003-16. Universitaire Campus. Diepenbeek.

Bylund PO, Björnstig U. (2001) Use of seat belts in cars with different seat belt reminder systems. A study of injured cars drivers. In Proc AAAM 45:1-9

Dahlstedt S. (1999) Non-users motives for not wearing the seat belt. VTI report 417. Linköping.

Eby DW, Molnar LJ, Kostyniuk LP, Shope JT. (2005) Developing an Effective and Acceptable Safety Belt Reminder System. Paper No. 171. Proceedings of the 18th International Technical Conference on the Enhanced Safety of Vehicles (CD–ROM). National Highway Traffic Safety Administration, Washington, DC.

EEVC Working Group 16 (2002) Technical Means to Increase Seat Belt Use—Belt Reminder systems specification. Unpublished report. European Enhanced Vehicle Safety Committee, Bron.

ETSC. (2003) Cost Effective EU Transport Safety Measures. ISBN 9076024162. Report from European Transport Safety Council, Brussels.

ETSC. (2005) In-Car Enforcement Technologies Today, ISBN 9076024200, Report from European Transport Safety Council, Brussels.

ETSC. (2006a) Seat Belt Reminders - Implementing advanced safety technology in Europe's cars. ISBN 9076024251. Report from European Transport Safety Council, Brussels.

ETSC. (2006b) Road Safety Performance Index - Flash 3. Getting car users to belt up. ISBN 9076024251. Report from European Transport Safety Council, Brussels.

Euro NCAP. (2006) Seat belt reminder assessment protocol. Version 1.1, July 2006. Euro NCAP Brussels. Available at http://www.euroncap.com

Ferguson S, Wells JK, Kirley B. (2006) Effectiveness and Driver Acceptance of the Honda Belt Reminder System. Insurance Institute for Highway Safety. Arlington VA

Fildes B, Fitzharris M, Koppel S, Vulcan P. (2002) Benefits of Seat Belt Reminder Systems. Monash University Accident Research Centre and ATSB report CR211a. Clayton, Australia.

Glassbrenner D. (2003) Estimating the Lives Saved by Safety Belts and Air Bags. Proc. of the 18th International Technical Conference on the Enhanced Safety of Vehicles (CD–ROM) in Nagoya. Conf Paper No. 500. National Highway Traffic Safety Administration, Washington, DC.

Harrison AH, Senserrick TM, Tingvall C. (2000) Development and Trial of a Method to Investigate the Acceptability of Seat Belt Reminder Systems. Report No 170. Monash University Accident Research Centre, Clayton, Australia.

Kahane, C.J. (2000) Fatality reduction by safety belts for front-seat occupants of cars and light trucks: updated and expanded estimates based on 1986-99 FARS data. Report no. DOT HS-809-199. Washington, DC: National Highway Traffic Safety Administration.

Kamren B, Kullgren A, Lie A, Tingvall C. (1994) The Construction of a Seat Belt System Increasing Seat Belt Use. Proc. of the 14th International Technical Conference on the Enhanced Safety of Vehicles in Munich. ESV Paper 94-S6-W32. National Highway Traffic Safety Administration, Washington, DC.

Krafft M, Kullgren A, Lie A, Tingvall C. (2006) The Use of Seat Belts in Cars with Smart Seat Belt Reminders—Results of an Observational Study. Traffic Injury Prevention, 2006 7:125–129.

ReganM, Triggs T, Young K, Tomasevic N, Mitsopoulos E, Stephan K, Tingvall C. (2005) On-Road Evaluation of Intelligent Speed Adaptation, Following Distance Warning and Seat Belt Reminder Systems: Final Results of the Australian TAC SafeCar Project.MUARC, Clayton, Australia.

SRA Swedish Road Administration. (2005) Bilbältesanvändning och förekomst av alkohol och droger i dödsolyckor (Seat belt use and drugs in fatal crashes). Publication 2005:69. Borlänge, Sweden.

SRA Swedish Road Administration. (2006) Annual Report 2005. Publication 2006:21e. Borlänge, Sweden.

TRB (Transport Research Board). Buckling up. (2004) Technologies to increase seat belt use. Special report 278. TRB, Washington, DC.

Turbell T, Larsson P. (1998) A new generation of seat belt reminder systems. Swedish Road and Transport Institute (VII), Linköping, Sweden.

Turbell T, Andersson T, Kullgren A, Larsson P, Lundell B, Lövsund P, Nilsson C, Tingvall C. (1996) Optimizing Seat Belt Usage by Interlock Systems. In Proc 15th ESV Conference. Melbourne. paper 96-S1-O-07. National Highway Traffic Safety Administration, Washington, DC.

Williams AF,Wells JK, Farmer CM. (2002) Effectiveness of Ford's belt reminder system in increasing seat belt use. Injury Prevention, Vol. 8, pp. 293–296.

APPENDIX

Table 4. Car models included in the study

Car models with SBR			Car models with mild SBR		
Alfa Romeo	159	2005	Saab	9-3	1998-2002
Audi	A3	2005-	Volvo	V70	2001-
Audi	A4	2005-	Volvo	S60	2001-
Audi	A6	2004-	**Car models without SBR**		
Citroën	C4	2004-	Audi	A2	2000-
Citroën	C5	2005-	Audi	A3	2003-
Ford	C-Max	2005-	Audi	A4	2001-
Ford	Focus II	2004-	Audi	A6	1998-2003
Nissan	Micra	2003-	Citroën	C5	2001-
Peugeot	407	2004-	Citroën	Picasso	2000-
Toyota	Avensis	2003-	Ford	Focus I	1999-2003
Toyota	Prius	2004-	Ford	Mondeo	2001-
Renault	Megane	2003-	Peugeot	307	2001-
Renault	Scenic	2003-	Peugeot	607	2000-
Renault	Espace	2003-	Renault	Scenic	1997-2002
Saab	9-3	2003-	Smart	Fortwo	1999-
Volvo	S40	2004-	Toyota	Prius	2000-2003
Volvo	V50	2004-	Toyota	Yaris	2001-
Volvo	XC90	2002-	VW	Golf	1998-2004
VW	Touareg	2003-	VW	Passat	1997-2000
VW	Passat	2005-	VW	Passat	2001-2004
			VW	Polo	2002-

PROCEDURE TO ASSESS SUBMARINING IN FRONTAL IMPACT

Stéphane Couturier
Jacques Faure
RENAULT SAS
France
Ricardo Satué
Joaquim Huguet
Applus+ IDIADA
Spain
Julien Hordonneau
IDESTYLE
France

Paper Number 07-0481

ABSTRACT

This study addresses the submarining issue left in frontal impacts today in the passenger cars, and proposes a methodology to assess it. The first part briefly describes the submarining phenomenon that consists of a sliding of the lap belt above iliac spine due to either bad safety belt geometry or poor coupling of the occupant to the car. This mechanism results in severe abdominal injuries (mesanterin laceration, severe hemoperitoneum, perforation,…). Some recent accident data coming from LAB (Laboratoire d'Accidentologie et de Biomécanique) are also presented in order to highlight the increasing importance of this phenomenon as the compartment intrusion is reduced, the knee support area is eliminated in order to avoid other injuries and the use of the seat belt is generalized in passenger car rear seats. The second part explains the reasons why, despite of evidence review, this phenomenon is not taken into account today, neither by the regulations nor by the ratings. The HIII dummy, widely used for safety assessment, integrates a very stiff lumbar spine. This feature prevents the pelvis rotation and consequently submarining. Therefore, other widely used dummies currently available are considered in this study in order to identify a more biofidelic behavior enabling the pelvis rotation and therefore detection of submarining phenomenon. In the third part, a full procedure based on a sled test and involving these suitable dummies is proposed. Associated criteria that could be used to assess the performance of a given restraint system are also described. The procedure is applied to vehicles with or without submarining countermeasures and the results are validated using the feedback on real accident data from the LAB. The results confirm the efficiency of the countermeasures and validate the assessment procedure.

INTRODUCTION

European official data from the European Road Safety Observatory (ERSO, www.erso.com) shows that Road traffic accidents in 2004 in the Member States of the European Union lead to about 47.000 fatalities and more than 1.8 million people injured. Coming back to the data in France provided by ONISR (Observatoire National Interministériel de la Sécurité Routière) in 2004, 5232 fatalities and 17435 seriously injured people have been observed. 3186 persons died in passenger cars. Frontal impacts represent 47% of killed and 69% of seriously injured people in passenger cars. The distribution is 1290 fatalities in front seats and 143 fatalities in rear seats. Recent progress in passive safety, coming from both regulation enforcement and consumers ratings allowed to solve most of the lethal issues in frontal impact which were :

-intrusion (steering wheel, firewall, footwell,…), decreased with well-designed absorbing structure

-head contact with steering wheel, avoided with frontal airbags

-chest injuries, reduced with belt load limiters

The aim of this paper is to highlight that abdominal injuries frequently occur in frontal crash today, either in front seat but especially in rear seats. Studies regarding abdominal injuries in the U.S. are already available in the literature. [1, 2, 3]. The first part includes a review of real accident data provided by the accident database of LAB, Laboratoire d'Accidentologie et de Biomécanique. The distribution of lethal injuries is shown in order to compare the well-known head and chest injuries with the abdominal ones. In the second part, an explanation is given on the fact that it is highly unlikely to detect submarining issue with the current procedures, either in regulations or in existing ratings, due to the use of the HIII dummy. An alternative test setup is proposed, allowing to observe the submarining phenomenon in a laboratory test. Several dummies and restraint systems are studied, to finally to propose a complete procedure to assess the performance of a given restraint system. This part is also showing that efficient countermeasures exist in recent vehicles. Finally, the third part is a review of real accident data provided by the LAB on recent Renault cars fitted with suitable countermeasures. Injury data have been collected on these vehicles and they are compared with the data presented in the first part, in order to estimate the effectiveness of the countermeasures and to show that it is possible to solve this issue.

WHAT IS SUBMARING?

The submarining phenomenon consists in the sliding of the lap belt above iliac spine due and loading the soft abdominal tissues.

Submarining happens when the restraining forces acting on the pelvis are not in equilibrium during the deceleration of the vehicle and induce its rotation. These forces come from the seat belt, the seat and the dashboard. The seat belt may produce submarining when its positioning due to the anchorage geometry tends the belt to displace upwards on the abdomen. The lack of restraint of force from the seat generates submarining as it is unable to compensate the rotation induced by the seat belt restraint above the pelvis centre of gravity.

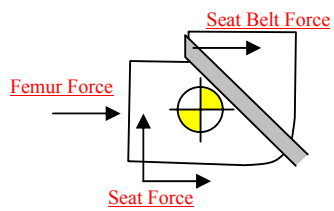

ACCIDENT DATA

To act all the developments carried out by Renault in term of safety, the LAB, Laboratoire d'Accidentologie et de Biomécanique, is in charge of performing for Renault in-depth analysis of real accidents occurring on French roads. In-depth crash investigations have been carrying out at LAB since 1970. There are actually two kinds of investigations. The first one concerns secondary safety. The goal is to understand the injury mechanisms in real-world crashes in order to improve occupant safety in cars by the means of protection devices or car structure. Almost all car manufacturers all over the world and even public research institutes have been carrying out that kind of study for decades. Specially trained accidentologists collect relevant information about types and violence of impacts, car deformations and occupant injuries and feed it into a corresponding database. They don't need to go on the scene of the crash. Information is collected by accidentologists a few days or a few weeks after the crash at hospitals and at wreck garages. This methodology leads to a wide range of researches estimating risk curves or evaluating the effectiveness of on-board protection devices.

The second one deals with primary safety. French car manufacturers started this activity in the early nineties, when it appeared that secondary safety would necessarily have limits and that there was a need for crash avoidance as well as a need for occupant protection. The challenge in this field is to understand the crash process, purpose new functions for active safety systems, and eventually to evaluate the effectiveness of new safety devices or avoidance systems on any kind of motorized vehicles.

In any case, agreements are signed with the French ministry of Justice to allow that kind of technical work on crashes apart from judicial process involving drivers at fault. Investigations are exclusively technical and are carried out for research purposes only.

In France, three institutes are presently carrying out that kind of in depth investigations with regards to primary safety concerns: the National Research Institute for Transport and Safety (INRETS) and The European Center for Safety Studies and Risk Analysis (CEESAR) with LAB (Laboratoire d'Accidentologie, de Biomécanique et d'étude du comportement humain).

As for secondary safety oriented investigations, LAB has identified two study designs. The first design aims at getting a representative sample of impacts and impact violence of cars involved in a road crash in France. For this purpose, all crashes involving a passenger car with at least one occupant injured are investigated in a restricted sample area in the West of Paris. About 200 cars and their occupant injuries are examined in-depth every year. The sample rate is relatively small as about 90 000 passenger cars are involved in injury crashes every year in France.

The second design aims at evaluating the effectiveness of protection systems supplied in newer cars. 150 cars involved in (mostly) severe crashes are chased all over the country each year. The only selection criterion is that the car must be a newer one, mostly Renault and PSA cars, equipped with the most recent safety devices.

The collection of the information about crashed cars takes about one and a half hour in the garage. Complementary collection is made afterwards at the hospital with the authorization of the medical doctors and the patients. Most of the data is then coded and filled in a special database. Information that cannot be coded is conserved in original dockets along with photos and sketches.

The two teams at CEESAR and LAB have investigated about 14 000 passenger cars, i.e. 25 000 occupants and 65 000 injuries since 1970, which makes this database one of the most important one in Europe.

This database allows not only to detect the remaining issues left in the real world like abdominal injuries we detail below, but also to check the real efficiency of the countermeasures fitted in the modern vehicles [4], once enough accidents involving these new cars have been studied. LAB investigation method has already been described in details in previous paper [5].

To highlight the submarining issue in frontal impacts, a first sample S1 of the following

accidents coming from the LAB database have been considered :

- vehicles from LAB database with a first registration year between 1990 and 2000
- frontal impact (+/- 30°), with a dashboard intrusion limited to 250mm. Indeed, above this value, fatalities are resulting from intrusion problems – these case usually match with old vehicles and cannot be solved thanks to restraint systems
- EES above or equal to 40km/h
- age above 9 years old, since below this, children must be sitting in Child Restraint System
- front passengers on one hand, and rear passengers on the other hand
- injuries on head, chest and abdomen are investigated, in the AIS3+ severity range. If the injury features on head and chest are well-known, abdominal ones can be found on peritoneum, mesentery, large bowels, abdominal big vessels… Injuries can be of different severity, from bruise to laceration and perforation.

Front seats occupants

The sample obtained from the request involves 1260 occupants, among which 74 fatalities and 380 AIS3+ injured occupants. Fatality and AIS3+ risk (ρ_i) can be calculated as follows :

$$\rho_1 = Fatality - risk = \frac{number - of - fatalities}{n}$$

$$\rho_2 = AIS3 + risk = \frac{number - of - AIS3 + occupants}{n}$$

where n is the number of involved occupants

confidence interval is [ρ-2σ ; ρ+2σ], where σ is the standard deviation :

$$\sigma = \sqrt{\frac{\rho(1-\rho)}{n}}$$

Table 1 presents, for front seats occupants, fatality and ASI3+ risk of the considered sample, as well as the confidence interval for each risk

Involved occupants	1260	Risk	Confidence interval
Fatalities	74	6%	$[5\% - 7\%]_{95\%}$
AIS3+ injured occupants	380	30%	$[28\% - 33\%]_{95\%}$

Table 1 : Fatality and AIS3+ risks for front seats occupants of sample S1

It is now important to understand from where these injuries come from. We can go deeper by analyzing in this same sample what are the injuries on head, chest and abdomen, which are the current lethal body areas. Concerning fatalities, most of these cases are not followed by an autopsy that could help precisely to find the origin of the death. Nevertheless, an autopsy has been performed on one third of fatalities, providing the distribution of injuries between head, chest and abdomen. We assume that the remaining cases without autopsy have the same injury distribution. For injured occupants, injury distribution is known from the hospital report recorded by LAB.

Table 2 presents the AIS3+ severity risk per lethal body region and their respective confidence interval

Body region	Head	Chest	Abdomen
Severity risk AIS3+ in a given body region	4%	16%	7%
Confidence interval	$[3\% - 5\%]_{95\%}$	$[14\% - 18\%]_{95\%}$	$[6\% - 9\%]_{95\%}$

Table 2 : Distribution in body regions of AIS3+ risks for front seats occupants of sample S2

Comments for front passengers :

- the main risk is the chest, typically ribs & sternum fracture due to the seat belt load. This kind of injury is well known and the effective solution is to fit the belts with load limiters allowing direct load reduction on chest.
- abdominal injuries are identified as the second risk coming after the chest, as a lethal issue
- if we consider the occupants with at least one AIS3+ injury (380 occupants), we observe that 90 occupants have suffered from at least one abdominal injury, eg 24% of seriously injured occupants have an abdominal injury..
- to illustrate this, we have detailed examples of real accidents studied by the LAB. The picture 1 and 2 illustrate one example where the driver has suffered an AIS4 to the abdomen, the precise injury being a severe hemoperitoneum and a mesenterin laceration. Due to a bad coupling of the pelvis with the seat, the seatbelt has passed over the iliac bones and entered the soft abdominal tissues, losing the pelvis load path. This is a typical injury pattern that can be observed when either lap belt anchorages are too high, or the seat and seat belt do not provide enough pelvis coupling

Figure 1 : seat after accident

Figure 2 : collapse of the seatbase structure

Rear seats occupants

The sample obtained from the request involves 146 occupants, among which 21 fatalities and 55 AIS3+ injured occupants. Fatality and AIS3+ risk (ρ_i), and their respective confidence are presented in table 3.

Involved occupants	146	Risk	Confidence interval
Fatalities	21	14%	$[9\% - 20\%]_{95\%}$
AIS3+ injured occupants	55	38%	$[30\% - 46\%]_{95\%}$

Table 3 : Fatality and AIS3+ risks for rear seats occupants of sample S1

Body region	Head	Chest	Abdomen
Severity risk AIS3+ in a given body region	2%	14%	23%
Confidence interval	$[0\% - 4\%]_{95\%}$	$[9\% - 20\%]_{95\%}$	$[16\% - 30\%]_{95\%}$

Table 4 : Distribution in body regions of AIS3+ risks for rear seats occupants of sample S1

Comments for rear occupants :

- the most important risk for rear occupants is on the abdomen
- the fatality risk for rear occupants is 2.5 times more important than the front occupants one (6% to 14%)
- Abdomen AIS3+ severity risk is much more important than chest one
- if we consider the occupants with at least one AIS3+ injury (55 occupants), we observe that 33 occupants have suffered from at least one abdominal injury, eg 60% of seriously injured occupants have an abdominal injury.

PROCEDURE TO ASSESS THE RESTRAINT SYSTEM PERFORMANCE FOR SUBMARINING ISSUE

Why the issue is not highlighted today ?

The anthropometric device currently used in crashworthiness is the HIII dummy. One particular feature is its very stiff lumbar spine that does not allow high pelvis rotation. It is assumed that it is that pelvis rotation which is at the origin of the upward movement of the lapbelt in the abdominal tissues.

To show that current test protocol cannot highlight this issue, we have conducted some tests involving restraint systems of cars where submarining issue has been observed in accident data. The test setup consists of a sled test simulating a full lap impact of the considered car at 56km/h, with only the seat and the belts system, including buckle pretensionner. The figure 3 details the test setup, where the driver airbag is not fitted, and to reduce the chest forward movement, the 4kN load limiter usually fitted on Renault cars is replaced by a 6kN one. The first test is performed with the current HIII dummy. In addition to its current instrumentation, a sensor is located in the pelvis to measure the rotation around the y axis and the lab belt is equipped with a force sensor.

Figure 3 : Test setup

Figure 4 shows the dummy position at 78ms, matching with the maximum forward pelvis movement. The lap belt is still stuck onto the pelvis and it never tried to escape from the pelvis, continuously maintaining the occupant without any aggression to the abdomen. This fact is also visible on the lap belt trace (figure 5), where no collapse is visible on the curve. It is assumed that if the lap belt enters the soft HIII abdomen, the load would decrease heavily.

Figure 4 : Test 1 – HIII dummy position when maximum pelvis forward movement is reached

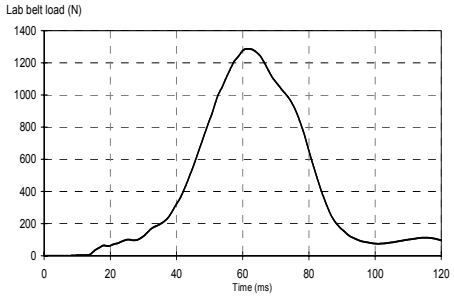

Figure 5 : Test 1 – HIII dummy lab belt force

This laboratory test, involving a given restraint system fitted in current cars, does not represent what happened in real accident data. The submarining phenomenon, supposed to be a movement of the lab belt towards the abdomen is not reproduced in this first test. We have already stressed that the lumbar spine stiffness could be at the origin of this biofidelity problem. We propose to repeat this test with the HII dummy, which was used before the HIII appeared. The HII lumbar spine is much softer than that of the HIII, and then more in line with human being anatomy. Both are compared on figure 6

Figure 6 : HIII (left) and HII (right) lumbar spine

Keeping exactly the same test setup, a second test is performed with a HII dummy. Figure 7-a presents the test at 58ms, where the lap belt is still on the pelvis, and figure 7-b shows the situation 15ms later where the lap belt has clearly left the pelvis to move into the abdomen. Figure 8 present the sequence between 50 and 75ms. This phenomenon is also visible on the figure 9 comparing the lap belt force from the two tests. A strong force breakdown begins at 58 ms, matching with the event seen on the film.

Figure 7-a : Test 2 – HII dummy position at 58ms – lab belt still on the pelvis

Figure 7-b : Test 2 – HII dummy position at 73ms – lab belt in the abdomen

Figure 8 : Test 2 – HII dummy submarining sequence (from 50 to 75 ms)

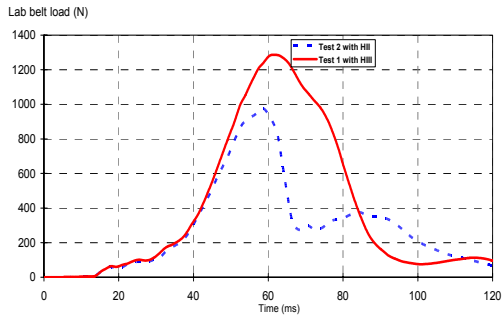

Figure 9 : Test 1&2 - lap belt forces comparison

The pictures comparison of the two tests shows that the pelvis rotation is much higher for the HII dummy, as we assumed from dummy features. This fact is checked after integration of the rotation sensors traces provided during the 2 tests, figure 10. The pelvis rotation obtained with HII raises much quicker and is almost twice more than with HIII, enabling to reproduce submarining.

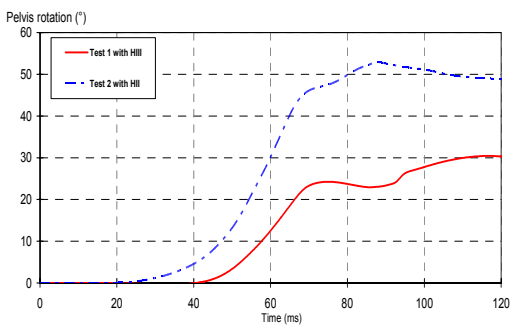

Figure 10 : Test 1&2 – pelvis rotation comparison

Keeping the same setup, the use of HII dummy instead of HIII dummy allows to reproduce the submarining phenomenon observed in real accident data.

Can submarining phenomenon be observed with another dummy than HII ?

HII dummy is barely used today since it was replaced by HIII, now used in all regulations because it is supposed to provide more information on risk in frontal impact. For example, the HII is not fitted with chest deflection sensor that is widely used today to assess risk on thorax. Going further in dummy investigation, on opportunity is to focus on the dummy used in aeronautic field, named HIII-FAA; Actually, this dummy is based on the HIII, the only differences being the lumbar spine, lumbar spine support on pelvis, upper-femur and chest flesh which are those of HII. Indeed, since HII and HIII have the same pelvis, it is easy to switch the lumbar spine. Then, a current HIII dummy, provided the FAA kit, is easily changeable towards a HIII-FAA dummy. The drawback is that current HIII chest sensor must be removed due to HII chest flesh that wraps the lower rib. Nevertheless, it is possible to replace the current sensor by a wire sensor whose data will be studied farther in this study. Figure 11 gives the wire sensor setup.

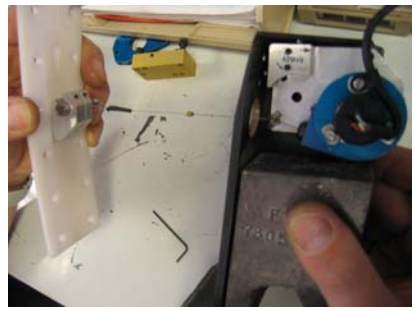

Figure 11 : detailed view of the wire sensor to replace chest deflection rod sensor

The test 3, similar to those performed before with HIII and HII dummy, is carried out with this new HIII-FAA dummy, the conditions being exactly the same. The behaviour of this new dummy is similar to the HII one, where the pelvis rotation is enabled. Figure 12 shows the dummy at around 73ms, where the lap belt is clearly in the abdomen, matching with high pelvis rotation, then reproducing the behaviour observed and expected on the HII. Figure 13 gathers the lap belt loads of the 3 tests, where traces of HII and HIII-FAA are similar, especially with the occurrence of a breakdown in force which is not present in the test involving the HIII. Figure 14 compares the pelvis rotation of the 3 tests. The magnitude of the rotation is similar for HII and HIII-FAA, and much smaller in the HIII case.

Figure 12 : Test 3 – HIII-FAA dummy position at 73ms – lab belt in the abdomen

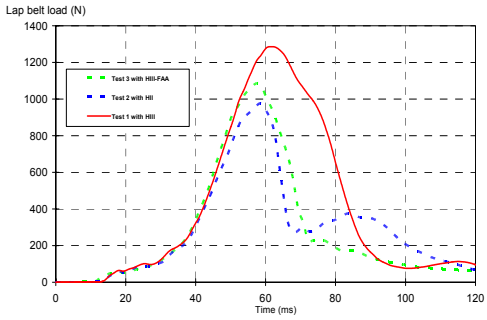

Figure 13 : Test 1, 2&3 - lap belt forces comparison

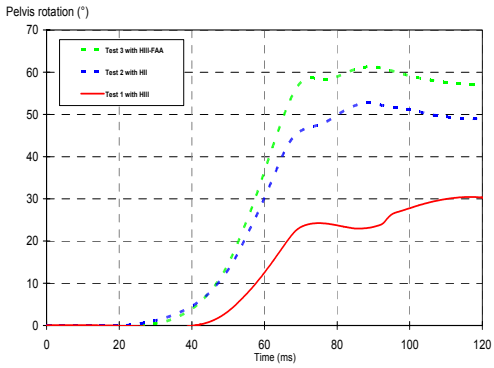

Figure 14 : Test 1, 2&3 – pelvis rotation comparison

A summary of the 3 previous tests is proposed in the table 6. 3 criteria are indicated :

- Did a lap belt load breakdown occurs during the test ?
- Is submarining visible on the film ?
- What is the maximum pelvis rotation ? Note that we considered the maximum pelvis rotation during the time the pelvis is still moving forward. Indeed, the rotation can continue to increase during the dummy rebound, when the pelvis begins to move rearward. But, after that, there is no more risk of submarining. Then the maximum pelvis rotation must be considered during the pelvis forward movement time range.

	Test #	Dummy involved	Lab belt load breakdown	Submarining on the film	Pelvis rotation (°)
Restraint system #1	1	HIII	NO	NO	30
	2	HII	YES	YES	53
	3	HIII-FAA	YES	YES	60

Table 6 : Summary of the first 3 tests with a given restraint system #1

It is now proven that the current HIII-50th is not able to detect submarining phenomenon, whereas HII and HIII-FAA does it. Especially, the most important thing is to enable the pelvis rotation which is the good indicator of the submarining risk. The lab belt load breakdown and the visual signal on the film are only consequences.

ASSESSMENT OF DIFFERENT RESTRAINT SYSTEMS WITH THE PROPOSED PROCEDURE

We now proposed to involve 2 other restraint systems, in order to highlight that this procedure can assess the performance of submarining countermeasures. Restraint system #2 is composed of a single pretension system (belt retractor), like restraint system #1 (with pyrotechnic buckle), but with a more recent seat, stiffer and including an anti-submarining steel ramp on the seat base. Restraint system #3 is the same as #2 but with a double pretension (belt retractor and pelvis pretensioner). Better results are expected with these 2 restraint systems compared to #1. Table 7 present the results for the 3 restraint systems, involving the 3 dummies. Table 8 presents the same results, but showing for each dummy, the results for every restraint system

	Test #	Dummy involved	Lab belt load breakdown	Submarining on the film	Pelvis rotation (°)
Restraint system #1	1	HIII	NO	NO	30
	2	HII	YES	YES	53
	3	HIII-FAA	YES	YES	60
Restraint system #2	4	HIII	NO	NO	17
	5	HII	NO	NO	31
	6	HIII-FAA	NO	NO	35
Restraint system #3	7	HIII	NO	NO	12
	8	HII	NO	NO	25
	9	HIII-FAA	NO	NO	30

Table 7 : Summary of the 9 tests with results relative to restraint systems

	Test #	Restraint system #	Lab belt load breakdown	Submarining on the film	Pelvis rotation (°)
HIII	1	1	NO	NO	30
	4	2	NO	NO	17
	7	3	NO	NO	12
HII	2	1	YES	YES	53
	5	2	NO	NO	31
	8	3	NO	NO	25
HIII-FAA	3	1	YES	YES	60
	6	2	NO	NO	35
	9	3	NO	NO	30

Table 8 : Summary of the 9 tests with results relative to dummies

From this new set of tests, we can deduce that HIII dummy never highlight submarining phenomenon in term of visual and lap belt load signals. We can observe that even if the pelvis rotation is less important than that got with HII and HIII-FAA, the magnitude of this rotation obtained for the 3 different restraint systems is different and vary from 12 to 30°. It would mean that the only way to assess submarining risk with this dummy is through pelvis rotation.

Regarding HII and HIII-FAA results, they are very close, especially in term of visual signal on the film and lap belt load breakdown. One difference appears: the pelvis rotation for HII seems always lower than that of HIII-FAA. We assumed that the reason comes from abdomen flesh : HIII-FAA is equipped with the current HIII abdomen, which is smaller than that of HII. Then, the bigger HII abdomen tends to prevent the pelvis

rotation more than the HIII one. Anyway, the lumbar spine stiffness is overwhelming in this pelvis rotation.

Figure 15 presents a graph with the pelvis rotation obtained for the 9 tests

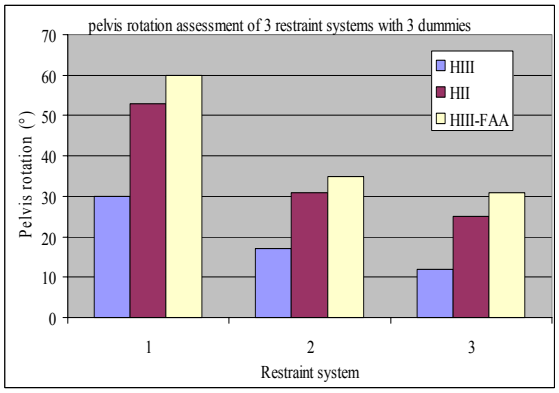

Figure 15 : pelvis rotation comparison for the 9 tests

For restraint system #1, the proposed procedure makes the link between what has been observed in real accident data and what can be highlighted in the laboratory. The laboratory test can now confirmed that this restraint system present a submarining risk in real life.
Concerning restraint system #2 and #3, no lap belt breakdown occurs and there is no visual signal on the film. The only difference is on pelvis rotation, which is 5° more important for restraint system #2 whatever the considered dummy is. One can assume that the submarining risk is higher for restraint system #2 in real life. The last part of this document will study the effectiveness of restraint system #3 since this system is really fitted in vehicles. Nevertheless, restraint system #2 matches actually with system #3 where the second pretension has been removed, and it is not fitted on real vehicles. Then its effectiveness in real world cannot be calculated.

As a partial conclusion, when a given restraint system is submitted to the previous procedure and presents the following results :

- Visible overpassing of the lap belt above the pelvis, through the film
- Lap belt load breakdown during the test
- Pelvis rotation above [55°] with HII dummy and above [60°] with HIII-FAA dummy

  → We can state that submarining risk in real life is high

- No visible overpassing of the lap belt above the pelvis, through the film
- No lap belt load breakdown during the test
- Pelvis rotation below [25°] with HII dummy and below [30°] with HIII-FAA dummy

  → We can state that submarining risk in real life is low

This last assertion needs to be confirmed with the third part of this document, where effectiveness of restraint systems #3 is studied.

Is this procedure repeatable?

All the tests already performed have been repeated and we provide those concerning restraint systems #2 as an example (tests 10 to 12). Table 9 presents the results, where no difference can be observed on neither pelvis rotation values nor lab belt load breakdown & visual signal on films.

	Test #	Dummy involved	Lab belt load breakdown	Submarining on the film	Pelvis rotation (°)
Restraint system #2	4	HIII	NO	NO	17
	10	HIII	NO	NO	18
	5	HII	NO	NO	31
	11	HII	NO	NO	30
	6	HIII-FAA	NO	NO	35
	12	HIII-FAA	NO	NO	35

Table 9 : Tests repeatability

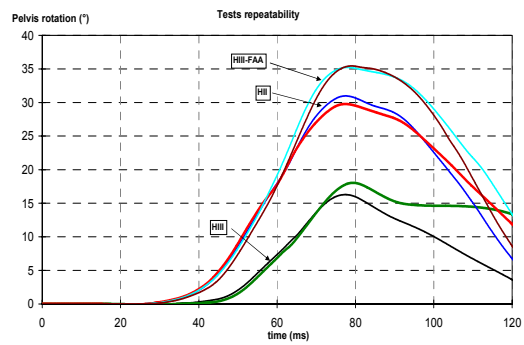

Figure 16 : Test repeatability for all dummies with restraint system #2

The previous tests are a good indication to show that the procedure is repeatable

Chest deflection

It has been mentioned that the current chest deflection sensor used in HIII dummy should be removed when using HIII-FAA, and that a wire sensor has been added in this dummy. It is now interesting to check if the data provided by the wire sensor in the HIII-FAA give similar results to those obtained with the normalized rod pot in the HIII. Table 10 presents the different values obtained regarding restraint system #3. Moreover, test #7 (involving HII) and test #9 (involving HIII-FAA) have been repeated (test #13 and #14). Figure 17 shows the chest deflection curves for the 4 tests.

	Test #	Dummy involved	Chest deflection (mm)
Restraint system #3	7	HIII	32
	13	HIII	30,3
	9	HIII-FAA	31
	14	HIII-FAA	32,4

Table 10 : Chest deflection obtained with HIII&current rod pot sensor and with HIII-FAA&wire sensor

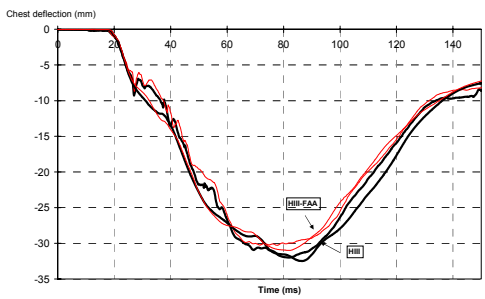

Figure 17 : Chest deflection curves got with HIII and HIII-FAA for restraint systems #3

The values are very similar and present low variation. It shows the ability of the replacing wire sensor to assess the chest risk at the same level as the current chest deflection sensor.

ACCIDENT DATA : FEEDBACK ON RECENT CARS

As submarining issue seems to be an important issue in real world accidents, especially for rear seats occupants but also for front ones, countermeasures have been developed on Renault recent cars, thanks to the procedure detailed before. A second sample S2 is considered from LAB database. It takes into account the same request as in sample S1 except that only the recent Renault cars are considered, e.g. vehicles equipped with submarining countermeasures, including antisubmarining ramp, suitable belt anchorages geometry and double pretension (for front seats) or single pretension (for rear seats). This advanced restraint system has been fitted in Laguna II for the first time in 2001 and then on most of the vehicles range. The sample obtained from the request leads to 157 front occupants (including 3 fatalities and 25 AIS3+ injured occupants) and 11 rear occupants (no fatality and 1 AIS3+ injured occupant). Fatality risk, AIS3+ risk and AIS3+ per body region risk (ρ_i), and their respective confidence interval are calculated and compared with those of sample 1 in table 11&12 (front seats occupants), and 13&14 (rear occupants).

SAMPLE 1 :

Involved occupants	1260	Risk	Confidence interval
Fatalities	74	6%	$[5\% - 7\%]_{95\%}$
AIS3+ injured occupants	380	30%	$[28\% - 33\%]_{95\%}$

SAMPLE 2 :

Involved occupants	157	Risk	Confidence interval
Fatalities	3	2%	$[0\% - 4\%]_{95\%}$
AIS3+ injured occupants	25	16%	$[10\% - 22\%]_{95\%}$

Table 11 : Fatality and AIS3+ risks for front seats occupants of sample S2 compared with S1

SAMPLE 1 :

Body region	Head	Chest	Abdomen
Severity risk AIS3+ in a given body region	4%	16%	7%
Confidence interval	$[3\% - 5\%]_{95\%}$	$[14\% - 18\%]_{95\%}$	$[6\% - 9\%]_{95\%}$

SAMPLE 2 :

Body region	Head	Chest	Abdomen
Severity risk AIS3+ in a given body region	3%	9%	3%
Confidence interval	$[0\% - 6\%]_{95\%}$	$[4\% - 13\%]_{95\%}$	$[0\% - 5\%]_{95\%}$

Table 12 : Distribution in body regions of AIS3+ risks for front seats occupants of sample S2, compared with S1

SAMPLE 1 :

Involved occupants	146	Risk	Confidence interval
Fatalities	21	14%	$[9\% - 20\%]_{95\%}$
AIS3+ injured occupants	55	38%	$[30\% - 46\%]_{95\%}$

SAMPLE 2 :

Involved occupants	11	Risk
Fatalities	0	0%
AIS3+ injured occupants	1	9%

Table 13 : Fatality and AIS3+ risks for rear seats occupants of second sample S2 compared with S1

SAMPLE 1 :

Body region	Head	Chest	Abdomen
Severity risk AIS3+ in a given body region	2%	14%	23%
Confidence interval	$[0\% - 4\%]_{95\%}$	$[9\% - 20\%]_{95\%}$	$[16\% - 30\%]_{95\%}$

SAMPLE 2 :

Body region	Head	Chest	Abdomen
Severity risk AIS3+ in a given body region	0%	9%	9%

Table 14 : Distribution in body regions of AIS3+ risks for rear seats occupants of sample S2, compared with S1

Comments on this cars fitted with submarining countermeasures :

- Front seats : the global fatality and AIS3+ risks are decreased respective to the first set. The main differences are on chest and especially abdomen injuries which are lower in this second set of cars. This reveals the efficiency on one hand of 4kN load limiter that allows to decrease chest load and then chest injury which confirms previous studies [6, 7] and on the other hand of submarining countermeasures fitted in these vehicles. Figure 18 shows the antisubmarining ramp in a seat after

a real accident. The double pretension fitted in this car has produced a good coupling of the pelvis that was caught and restrained by the deformable ramp.

Figure 18 : front seat after real accident – pelvis impact on anti-submarining ramp

- Rear seats : The sample is too small to draw some conclusions, but the trend seems good, since no fatality has been observed yet, and the AIS3+ risk has been observed on only 1 occupant among 11. More data will be obtained in the future to validate this conclusion. Figure 19 presents a rear seat steel ramp after a real impact. The steel part is deformed highlighting that the pelvis was restrained, the pretension having taken the belt gap and stuck the occupant pelvis on the seat.

Figure 19 : rear seat after real accident – pelvis impact on anti-submarining ramp

DISCUSSION

- Accident data presented in the first part for cars with a first registration between 1990 and 2000 reveal that submarining phenomenon is at the origin of many fatalities and serious injuries in frontal impact, not only for front seats but also and especially for rear seats. The problem is due to a low performance of restraint systems in coupling the occupant pelvis, the consequence being an escape of the lap belt from the pelvis bones, and a loading of this lap belt in the abdominal soft tissues, causing rapidly serious injuries or fatalities.
- The importance of this issue comes from the difficulty to observe the problem with the current dummy used in frontal impact on one hand, and from the fact that no regulation or rating (except NCAP made by China by CATARC) is dealing with rear occupant seats on the other hand.
- For front seats, the main risk is still coming from chest, the second one being abdominal injuries.
- For rear seat, submarining phenomenon is the overwhelming priority and abdominal injuries are much more frequent than chest injuries. Only considering frontal impact fatalities, the AIS3+ risk is higher when belted than unbelted. It has been stressed already in other publications (Lamielle – AAAM 2006). The trend in recent vehicle is to decrease the passenger compartment intrusion. If the consequences are extremely positive in reducing head&chest contact to steering wheel, in lowering legs injuries due to intrusion,…it also leads to have stiffer cars and then stronger deceleration pulse. For rear seats, if one considers that the restraint device is not changed, a more severe pulse will lead to a higher abdominal risk for rear occupants. Then, if nothing is done in this area, it is expected that this phenomenon will be more and more observed in the real world.
- Coming back to the laboratory, we have explained why this issue cannot be observed today with the current HIII dummy and we propose an alternative with either the former HII dummy or HIII-FAA dummy, whose the main feature is to have a softer lumbar spine with a behaviour more in line with that of human being. These 2 ATD's show the submarining phenomenon observed in real accident data, especially through the pelvis rotation and the lap belt load breakdown. The procedure has been applied to different restraint systems whose the performance are checked in the real world. A good correlation is obtained since a poor (or good) restraint system in the real world is also assessed poor (or good) by the proposed procedure.
- The countermeasures fitted in recent Renault vehicles seem very effective. For front and rear seats, the need for load limiter is confirmed to avoid chest injuries. Load limiters are fitted in the analyzed cars, on front (4kN) and rear (6kN) seats. Data indicate a risk decreasing respective to vehicles of the 90's which were not systematically fitted with this device.
- For front and rear seats, abdominal risk is also decreased showing that the countermeasures fitted in the set of recent cars are effective, even if more data on rear seats are needed to draw conclusions . It also shows that the proposed procedure provides a good assessment of the risk.

REFERENCES

[1] Huelke D., Mackay G. & Morris A. Intrabdominal injuries associated with lap shoulder belt usage. Proc., S.A.E. Conf., S.A.E. Paper 930639; 1993.

[2] Elhagediab A. & Rouhana S. Patterns of abdominal injury in frontal automotive crashes. 16th ESV Conference, Windsor Canada, 98-Sl-W-26; 1998.

[3] Yoganandan N., Pintar F., Generalli A. & al. Patterns of abdominal injuries in frontal and side impacts. 44th Annual Proceedings Association for the Advancement of Automotive Medicine, Chicago, Illinois, 44:17-36; 2000.

[4] Huere J.F., Forêt-Bruno J.Y., Faverjon, G., Le Coz J.Y., Airbag efficiency in frontal real world accidents, 18 th ESV Conference, Amsterdam, June 2001, Paper number: 2001-S1-O-193

[5] Faverjon G. Méthodologie des enquêtes sur les accidents réels. Le concours médical 107-30, pp2834-2839; 1985.

[6] Foret-Bruno JY., Trosseille X., Page Y. & al. Comparison of thoracic injury risk in frontal car crashes for occupant retrained without belt load limiters and those restrained with 6kN and 4kN belt load limiters. Proc.45th Stapp, p375; 2001.

[7] Forêt-Bruno J.Y., Trosseille X., Le Coz J.Y., Bendjellal F., Steyer C., Phalempin T., Villeforceix D., Dandres P., Got C., Thoracic injury risk in frontal car crashes with occupant restrained with belt load limiter, SAE paper 98S-4, 1998.

ACKNOWLEDGEMENTS

Many thanks to Y. Page at LAB for the review of this paper, and to M. Labrousse at LAB, for his help on accident data. Many thanks also to CTAG-IDIADA reverse acceleration sled test facility (Vigo, Spain) team for their motivation, dedication and effectiveness in the execution of the tests carried out for this research.

THE BENEFITS OF DOUBLE PRETENSION IN DECREASING KNEES & LOWER LEGS INJURIES IN FRONTAL IMPACTS

Jacques Faure
Stéphane Couturier
RENAULT SAS - France
Yves Page
Maxime Labrousse
Laboratoire d'Accidentologie, de Biomécanique et d'étude du comportement humain (LAB) - France

Paper Number 07-0491

INTRODUCTION

European official data from the European Road Safety Observatory (ERSO, www.erso.com) shows that Road traffic accidents in 2004 in the Member States of the European Union lead to about 47.000 fatalities and more than 1.8 million people injured. Coming back to the data in France provided by ONISR (Observatoire National Interministériel de la Sécurité Routière) in 2004, 5232 fatalities and 17435 seriously injured people have been observed. 3186 persons died in passenger cars. Frontal impacts represent 47% of killed and 69% of seriously injured people in passenger cars. The distribution is 1290 fatalities in front seats and 143 fatalities in rear seats. Recent progress in passive safety, coming from both regulation enforcement and consumers ratings allowed to solve most of the lethal issues in frontal impact which were :

- Intrusion (steering wheel, firewall, footwell,…), which decreased with well-designed absorbing structure
- Head contact with steering wheel, avoided with frontal airbags
- Chest injuries, reduced with seat belt load limiters.

The aim of this paper is to review the evolution of lower legs injuries throughout the last vehicles generations to find out the benefits of advanced restraints systems such like double pretension.

The first part of this paper is dedicated to an explanation of the Renault double pretension system, adopted on most of the line-up. Test data using Renault's current procedure will show the effectiveness of that technical solution compared to a single pretension restraint system. The effectiveness will be shown not only for current 50th percentile occupant usually used in regulation and ratings, but also 5th and 95th percentile occupants.

The second part is a review of real accident data provided by the LAB. Injury data have been collected on vehicles fitted with a double pretension and compared with those of the rest of the fleet, in order to estimate the effectiveness of double pretension.

1° DOUBLE PRETENSION RESTAINT SYSTEM

1-1°) Description of the different restraint systems

The main purpose of pretensionning is to optimize the occupant coupling with the seat, and to reduce his relative speed with that of the structure. Buckle or retractor pretensioners are already well-known to yield a good occupant chest coupling with the seat. Firing the pretensioner once the impact is detected leads to a retractor pull-in or a downward movement of the buckle, allowing to remove all the gaps in the belt as well as to maintain the occupant chest and pelvis as close as possible to the seat.

In addition to that single pretension, a second pretensioner can be fitted to increase the occupant pelvis coupling with the seat and then limit the pelvis forward displacement. Figures 1&2 show an example of pelvis pretensioner before and after deployment.

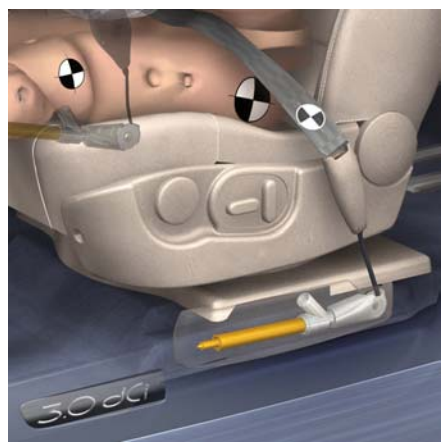

Figure 1 : pelvis pretensioner before test

Figure 2 : pelvis pretensioner deployed

Some specific car designs prevent from being able to fit a second pretensioner on the outer side of the front seat. It is the case, for example, with 3 door or convertible cars, for which the front seats need to be moved forward to allow rear passengers to ingress. In that case, there is generally a sliding outer seat belt anchorage, and no pretensionner can be fitted. To reach the same performance level, a deployable cushion, named Pelvis Restraint Cushion, can be fitted in the front seat base. It consists of an inflatable metal box located just below the occupant thighs. The deployment of such a device reduces the pelvis forward movement in the same manner as the pelvis pretensioner. Figures 3 & 4 show a seat base cushion before and after deployment. Picture 5 shows the deformation of the seat base deployable cushion after its interaction with the occupant's pelvis.

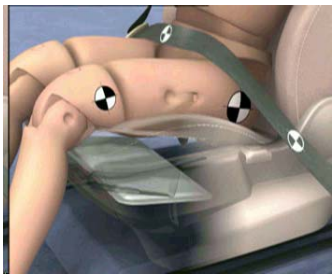

Figure 3 : Pelvis Restraint Cushion at rest

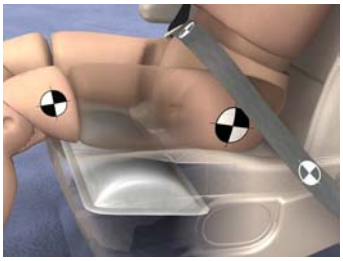

Figure 4 : Pelvis Restraint Cushion deployed, before interaction with occupant

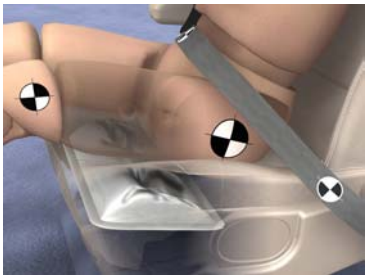

Figure 5 : Pelvis Restraint Cushion deployed, after interaction with occupant

1-2°) Assessment of the performance through a full lap frontal impact

1-2-1°) Test setup

The performance of a restraint system can be assessed through the following test configuration :

Full lap test on a rigid wall. The test features are given below :

- Velocity : 56km/h
- Offset : 100%
- No deformable barrier to really assess the restraint system performance
- Instrumented HIII dummy

This test configuration can be performed either through a full scale test or a sled test. The following test campaign has been performed using a High-G sled test where the input pulse is that of the car obtained when tested against a rigid wall at 56km/h. The setup contains seats and belt systems with the actual geometry. The belt is equipped with a pyrotechnic retractor for the single pretension configuration and a pyrotechnic retractor + lap belt pretensioner in case of double pretension configuration. Since the purpose is to assess lower leg performance, the airbag is not present and to reduce the chest forward movement without airbag, a 6kN load limiter is fitted instead of the 4kN usually present in the Renault cars.

The table below summarizes the different tests presented in this paper :

Configuration / Setup	Restraint system	Dummy size		
Full lap test 56km/h	Single pretension	5th percentile	50th percentile	95th percentile
	Double pretension	5th percentile	50th percentile	95th percentile

The figures 6&7&8 present the setup of configuration 2 with the 3 dummy sizes

Figure 6 : setup with 5th

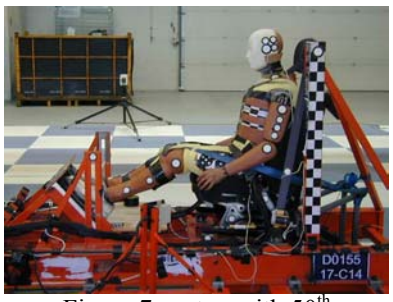

Figure 7 : setup with 50th

Figure 8 : setup with 95th

1-2-2°) Performance assessment method

If we assume that hard contact of lower legs with the dashboard is at the origin of the injuries, one possibility to assess the performances of a restraint system for this body region is to calculate the knee forward movement during the test. We make the assumption that the knee displacement is the same as the pelvis displacement. We consider that in full scale test, when the knee is loaded by the dashboard, the pelvis can continue its forward displacement more than that of the knee by rotating around the tibia. It means that the knee forward displacement is lower than that of the pelvis. We can then assume that, with a given seat, the smaller the pelvis forward displacement is, the lower is the risk for the occupant's leg to be injured. This displacement can be calculated by 2 methods: a double integration of the pelvis acceleration and a wire sensor fixed on the rear part of the pelvis and attached to the sled. To do so, the dummies used for this test campaign were instrumented in the pelvis region as below:

- accelerometers in X & Z directions (with the pelvis SAE-J211 reference), providing $\ddot{X}_{pelvis}(t)$ and $\ddot{Z}_{pelvis}(t)$
- angular velocity sensor providing Ω(t), the integration of which gives the pelvis rotation angle θ (t) due to the relative torso/leg movement
- wire sensor between the sled (behind the seat) and the pelvis
- accelerometer in X direction on the sled
-

The figure 9 describes the different measurements and axis involved in the tests.

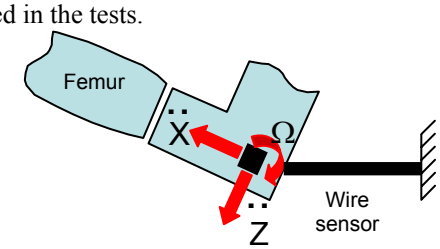

figure 9 : description of the sensors involved in the tests and their axis.

The pelvis forward movement relative to the sled can be calculated using the following formula:

$$Pelvis - Displacement = \iint_t (\ddot{X}_{pelvis}(t)\cos\theta(t) + \ddot{Z}_{pelvis}(t)\sin\theta(t))dt^2 - \iint_t \ddot{X}_{Sled}(t)dt^2$$

If the accuracy of this formula can be discussed in full scale test, depending on the structure behavior, it gives reliable results when using a sled.

1-2-2°) Tests results

Graph 1 compares the pelvis forward displacement obtained by double integration of pelvis traces for a 50th percentile with double or single pretension during a full lap test. The pelvis displacement decreases from 255mm in the single pretension test to 180mm in the dual pretension test. It appears that the performance is much better thanks to the double pretension for the 50th occupant size

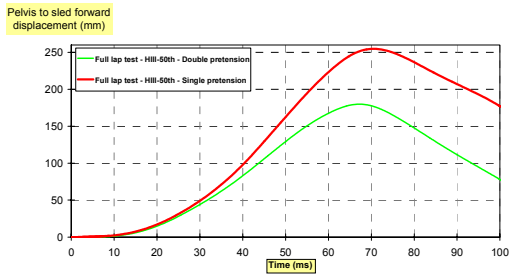

Graph 1 : pelvis forward displacement of 50th percentile during 56km/h full lap test

Graph 2 compares the pelvis forward displacement obtained by double integration of pelvis traces for a 95th percentile with double or single pretension during a full lap test. Here again, the pelvis displacement is reduced, decreasing from 325mm in the single pretension test to 233mm in the dual pretension test. For the 95th occupant size also, it seems that the performance is much better thanks to the double pretension.

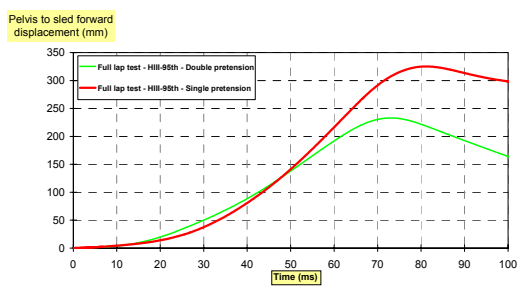

Graph 2 : pelvis forward displacement of 95th percentile during 56km/h full lap test

The graph 3 compares the pelvis forward displacement obtained by double integration of pelvis traces for a 50th percentile with double or single pretension during a full lap test. Here again, the pelvis displacement is reduced, decreasing from 172mm in the single pretension test to 153mm in the dual pretension test. For the 5th occupant size also, it seems that the performance is much better thanks to the double pretension.

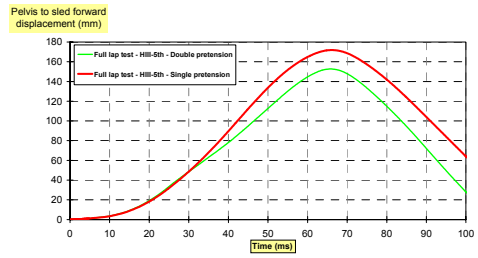

Graph 3 : pelvis forward displacement of 5th percentile during 56km/h full lap test

For the 6 previous tests, the pelvis maximum forward displacements are summarized below:

Pelvis maximum forward displacement from accelerometers (mm)			
Configuration / Occupant size	5th percentile	50th percentile	95th percentile
Double pretension	153	180	233
Single pretension	172	255	325
Reduction	**11,0%**	**29,4%**	**28,3%**

The reduction of pelvis displacement reaches around 29% for both 50th and 95th percentile occupants and 11% for 5th occupants. This is supposed to reduce significantly the knee and tibia contacts in the IP, and also reduce the knee and lower legs injuries.

The same approach is made with the wire sensor traces, whose the maximum for each test is summarized below:

Pelvis maximum forward displacement from wire sensor (mm)			
Configuration / Occupant size	5th percentile	50th percentile	95th percentile
Double pretension	128	176	199
Single pretension	164	255	277
Reduction	**22,0%**	**31,0%**	**28,2%**

The trend is the same as in the previous results, since the displacement reached with a double pretension system is, for both 50th and 95th percentile occupants, reduced of around 29% respective to a single pretension system. We also notice that for 5th occupants, the results lead to a 22% reduction in pelvis displacement between both configurations.

We can stress that the results between the 2 measurements methods, accelerometers and wire sensor, give exactly the same results for the 50th dummy size whereas it presents some discrepancies for 5th and 95th dummies. In these 2 cases, it seems that the wire sensor results is lower than those obtained with accelerometers,

but the ratio between single and double pretension pelvis displacement is pretty the same with the 2 methods for these 2 occupant sizes.

Thanks to this set of results, we can assume that the double pretension system should significantly reduce the knee contact with the IP, and we expect from this a reduction of lower injuries in real accident data for the vehicles equipped with such advanced restraint systems.

2°) EFFICIENCY OF DOUBLE PRETENSION IN REAL WORLD

To confirm all the developments carried out by Renault in term of safety, the LAB, Laboratoire d'Accidentologie et de Biomécanique, is in charge of performing for Renault in-depth analysis of real accidents occurring on French roads. In-depth crash investigations have been carrying out at LAB since 1970. There are actually two kinds of investigations. The first one concerns secondary safety. The goal is to understand the injury mechanisms in real-world crashes in order to improve occupant safety in cars by the means of protection devices or car structure. Almost all car manufacturers all over the world and even public research institutes have been carrying out that kind of study for decades. Specially trained accidentologists collect relevant information about types and violence of impacts, car deformations and occupant injuries and feed it into a corresponding database. They don't need to go on the scene of the crash. Information is collected by accidentologists a few days or a few weeks after the crash at hospitals and at wreck garages. This methodology leads to a wide range of researches estimating risk curves or evaluating the effectiveness of on-board protection devices.

The second one deals with primary safety. French car manufacturers started this activity in the early nineties, when it appeared that secondary safety would necessarily have limits and that there was a need for crash avoidance as well as a need for occupant protection. The challenge in this field is to understand the crash process, purpose new functions for active safety systems, and eventually to evaluate the effectiveness of new safety devices or avoidance systems on any kind of motorized vehicles.

In any case, agreements are signed with the French ministry of Justice to allow that kind of technical work on crashes apart from judicial process involving drivers at fault. Investigations are exclusively technical and are carried out for research purposes only.

In France, three institutes are presently carrying out that kind of in depth investigations with regards to primary safety concerns: the National Research Institute for Transport and Safety (INRETS) and The European Center for Safety Studies and Risk Analysis (CEESAR) with LAB (Laboratoire d'Accidentologie, de Biomécanique et d'étude du comportement humain).

As for secondary safety oriented investigations, LAB has identified two study designs. The first design aims at getting a representative sample of impacts and impact violence of cars involved in a road crash in France. For this purpose, all crashes involving a passenger car with at least one occupant injured are investigated in a restricted sample area in the West of Paris. About 200 cars and their occupant injuries are examined in-depth every year. The sample rate is relatively small as about 90 000 passenger cars are involved in injury crashes every year in France.

The second design aims at evaluating the effectiveness of protection systems supplied in newer cars. 150 cars involved in (mostly) severe crashes are chased all over the country each year. The only selection criterion is that the car must be a newer one, mostly Renault and PSA cars, equipped with the most recent safety devices.

The collection of the information about crashed cars takes about one and a half hour in the garage. Complementary collection is made afterwards at the hospital with the authorization of the medical doctors and the patients. Most of the data is then coded and filled in a special database. Information that cannot be coded is conserved in original dockets along with photos and sketches.

The two teams at CEESAR and LAB have investigated about 14 000 passenger cars, i.e. 25 000 occupants and 65 000 injuries since 1970, which makes this database one of the most important one in Europe.

Therefore, we can measure the real efficiency of advanced restraint systems fitted in new cars, once enough accidents involving these new cars have been studied. Now that the Renault range is composed of 8 models fitted with double pretension, some of them existing since 2001, it is now possible to have a reliable feedback from the real accident data that can provide LAB. From this database, we have considered the following accidents in 2 samples :

- Frontal impact from 11 to 1 O'Clock
- Belted occupants, drivers only, since they are supposed to be more exposed to hazards through steering wheel
- The body region that is studied includes all the limbs from hip to tibia and all AIS2+ injuries are considered.
- 3 ranges of EES (Energy Equivalent Speed) are considered to highlight the difference in performance according to the accident severity : [40-49km/h], [50-59 km/h] and [60-80km/h]
- A first sample S1 with other cars from LAB database, limited to the cars with a first launch from 1990

(conception year), which are not supposed to be equipped with double pretension. In this sample, all the vehicles from the second set detailed below are removed.

A second sample S2 with vehicles equipped with a double pretension (Laguna, Vel Satis, Espace IV, Mégane II, Scenic II, Mégane II Convertible, Modus, Clio III). We also looked at depth of intrusion in the two samples since it is admitted that intrusion can cause lower legs injuries and that intrusion is expected to be more predominant in old vehicles than in newer ones. The calculation of the effectiveness of double pretension then takes into consideration the intrusion parameter.

The sample obtained from the above requests are composed of:

- In sample S1 : 993 involved drivers, among which 196 are injured on the considered limbs, with a AIS2+ severity
- In sample S2 : 114 involved drivers, among which 5 are injured on the considered limbs, with a AIS2+ severity. In this sample, we must stress that the double pretension system is mainly composed of lap belt pretensioners. Due to a smaller distribution in production cars, the Pelvis Restraint Cushion is not yet sufficiently represented to draw any conclusion on that specific device.

AIS2+ risk (ρ_i) in each EES range can be calculated as follows :

$$\rho_i = AIS2 + risk = \frac{number - of - AIS2 + drivers}{n_i}$$

where n_i is the number of involved drivers in the EES range, and confidence interval is [ρ-2σ ; ρ+2σ], where σ is the standard deviation defined below :

$$\sigma = \sqrt{\frac{\rho(1-\rho)}{n_i}}$$

Table 1 and 2 present, in the 3 EES ranges and for the 2 samples of cases, the distribution of involved and injured people, the AIS2+ risk (ρ) and the confidence interval :

	Sample S1			
	Total	EES range (km/h)		
		EES 40-49	EES 50-59	EES 60-80
Involved drivers	993	295	375	323
AIS2+ injured drivers	196	14	65	117
AIS2+ risk (ρ)		5%	17%	36%
Confidence interval		$[3\%-7\%]_{95\%}$	$[13\%-21\%]_{95\%}$	$[13\%-41\%]_{95\%}$

Table 1 : data for sample S1 (vehicles with single or no pretension)

	Sample S2			
	Total	EES range (km/h)		
		EES 40-49	EES 50-59	EES 60-80
Involved drivers	114	43	30	41
AIS2+ injured drivers	5	0	0	5
AIS2+ risk (ρ)		0%	0%	12%
Confidence interval		$[0\%-0\%]_{95\%}$	$[0\%-0\%]_{95\%}$	$[2\%-22\%]_{95\%}$

Table 2 : data for sample S2 (double pretension vehicles)

The efficiency E_i of the restraint systems fitted in vehicles of sample S2 can be calculated for each EES range from the AIS2+ risks in EES range i of sample S1 (ρ_{i1}) and sample S2 (ρ_{i2}), as follows:

$$E_i = 1 - \frac{\rho_{i1}}{\rho_{i2}}$$

An overall efficiency can also be calculated by weighting the risks of injuries in the two samples by EES values and intrusion values. Actually, the severity distribution of accidents in the LAB database does not match the real distribution since this database contains comprehensive studies in a given area and in-depth studies on specific vehicles. We have therefore associated the above data with an assumed, distribution of the severity:

EES Values (km/h)	
40-49	60%
50-59	30%
60-80	10%

The overall effectiveness can then be deduced by:

$$e = 1 - \left(\frac{\sum_i wi * Ri}{\sum_j wj * Rj} \right),$$

with i, index for cars with double pretensioners, j index for cars without double pretensioners, and w the weighting factors for EES and intrusion values.

The overall effectiveness is then 88 %, with a confidence interval at 95 % of [56% ; 97 %]

3°) DISCUSSION

The two aims of this paper were :

- to evaluate the performance of the double pretension as an advanced restraint systems through laboratory tests, involving several occupant sizes
- to check the efficiency in decreasing the lower legs injuries in real accidents.

The performance has been assessed with a sled test campaign. The setup included seat and full seat belt systems taking into account on one hand a dual pretension system, and on the other hand, a single pretension system. The test configuration chosen for these tests is a full lap test 56km/h, which is supposed suitable to assess any restraint performance. The performance is assessed in term of pelvis forward displacement, since this displacement is assumed to be linked with injuries. It is expected that, for a given vehicle, a smaller pelvis displacement will reduce the lower legs injuries. 3 adult dummy sizes were involved, all equipped with accelerometers and angular velocity sensor in the pelvis, and also a wire sensor measuring directly the pelvis displacement.
Whatever the occupant size considered, it clearly appears that the double pretension reduce the pelvis displacement compared to a single pretension, up to 30% for 50th and 95th occupant sizes, and between 11 and 22 % for the 5th occupant size, depending on the measurement methods.
The two measurements methods lead to the same tendency between the different restraint systems type, though the values are different, especially for 5th and 95th percentile. This could be explained by the fact that the initial tension is not under control, and that pelvis could begin to move forward without pulling out the wire. Moreover, the wire is fixed behind the pelvis on the top part, inducing differences due to the pelvis rotation.
Anyway, both methods indicate that the dual pretension restraint system reduces the pelvis displacement with respect to a single pretension one.

The accident database from LAB has been used to check the efficiency of the dual pretension restraint systems compared to the rest of the fleet. The investigation has been carried out by selecting the drivers in frontal impact, in vehicles for which the first registration is after 1990 only. This sample has then been split in cars equipped with a dual pretension system and cars without. Each sample described above has been split in three severity ranges, starting from 40km/h. The injuries taken into account are all those related to lower legs, including hip, and the studied gravity is AIS2+.

The AIS2+ risk in each severity range has been determined for the 2 samples of vehicles. It allows calculating the global efficiency of a dual pretension restraint system, which reaches 93%. The efficiency found through the accident data clearly shows that lower legs injuries are strongly reduced in these vehicles compared to previous vehicles generations. This efficiency result could seem quite high especially if we assume that it is only based on the pelvis displacement comparison. Actually, the first set of cars taken from the LAB database includes quite old cars that are not fitted even with a single pretension. We can then assume that the pelvis displacement in those cars are higher and produce more severe lower legs injuries. That is why the 30% reduction in pelvis displacement observed in the test campaign, between single and dual pretension, is not in line with the efficiency found through accident data. This reduction would much higher than 30% if we compare dual pretension with no pretension, and this would be more in line with the global efficiency of 93% found through accident data.
One can also stress that it is possible that the decreasing of lower legs injuries is associated with structure intrusion reduction and not only the outcome of advanced restraint systems. We agree that such advanced restraint systems fitted in a car presenting a lot of intrusion (footwell and dashboard) won't be of some use since a dashboard contact will occur. Nevertheless, one additional case has been studied from the LAB database : a recent car without intrusion (eg no structural modifier in the EuroNCAP frontal impact) but equipped with a single pretension. The sample is too small and the values non significant enough to be presented here, but the first trend is to have AIS2+ injuries from 50km/h EES, whereas with a dual pretension system, these injuries appear above 60km/h. A small structural intrusion could then considered as a first step towards a strong reduction of lower legs injuries but is not enough for very severe accidents.
Due to the statistic sample size, it is not possible yet to observe differences in term of efficiency between pelvis pretensioner and Pelvis Restraint Cushion but we expect that it will be possible in the future. Nevertheless, the first feedback from the Pelvis Restraint Cushion behaviour is positive. The figure 10 presents a picture of the Pelvis Restraint Cushion after interaction with the driver in a real accident. The deformation shows clearly the impacts of left and right part of the pelvis. This pattern is exactly the same as that observed in tests with dummies. We can then expect a decrease of the lower legs injuries thanks to this device.

Figure 10 : Pelvis Restraint Cushion after interaction with the driver in a real accident

ACCURACY OF VEHICLE FRONTAL STIFFNESS ESTIMATES FOR CRASH RECONSTRUCTION

Qian Wang
Hampton C. Gabler
Virginia Tech
United States

Paper Number 07-0513

ABSTRACT

The National Highway Traffic Safety Administration (NHTSA) estimates delta-V from detailed measurements of vehicle deformation using the WinSMASH crash reconstruction code. Previous research has shown that WinSMASH delta-V estimates underpredict true delta-V by 25% on average. One possible explanation for this error is inaccuracies in the stiffness values used in the delta-V reconstruction calculation. The accuracy of codes, such as WinSMASH, is dependent upon vehicle stiffness values computed from post-impact crush measurements in crash tests. Any error in these crush measurements will be reflected as inaccuracies in the stiffness coefficients, and ultimately as errors in WinSMASH delta-V estimates. This paper investigates the accuracy of post-impact crush measurements in 93 frontal New Car Assessment Program (NCAP) tests of model year 2005-2007 vehicles.

INTRODUCTION AND BACKGROUND

Estimating the total change in velocity or delta-V of a vehicle during a crash is a way to evaluate the severity of a motor vehicle accident. The calculated delta-V can be used as an important parameter to study the occupant injuries resulting from the crash. Therefore, the fidelity of these studies will be affected by the accuracy of the delta-V estimations.

NHTSA uses WinSMASH, a derivative of CRASH3 to estimate the delta-Vs of real-world crashes through post-crash reconstruction [1]. The algorithm of CRASH3 [2] was based on the work done by Campbell in which a linear relationship was observed between static crush and impact speed into a fixed rigid barrier [7]. The delta-V calculation is based on the estimation of the absorbed crush energy by the vehicle from the post-crash measurements of the vehicle deformation. The damage algorithm in WinSMASH uses the post-crash measurements of the vehicle to estimate the energy absorbed by the vehicle in the approach phase of the crash, which is then used to estimate the delta-V by applying the Newton's second law of motion and conservation of linear momentum.

Previous research has shown that WinSMASH delta-V estimates underpredict true delta-V by 25% on average [3, 1, 4, 5]. One possible explanation for this error is inaccuracies in the stiffness values used in the delta-V reconstruction calculation. The accuracy of codes, such as WinSMASH, is dependent upon vehicle stiffness values computed from post-impact crush measurements in crash tests. Any error in these crush measurements will be reflected as inaccuracies in the stiffness coefficients, and ultimately as errors in WinSMASH delta-V estimates.

Calculation of Delta-V

Equation 1 and Equation 2 are used by WinSMASH to calculate delta-V for one of the simplest collision configurations, a central collision, which is defined as a collision where the line of action of the collision forces passes through the centers of mass of the two vehicles. For the frontal vehicle crash with a rigid barrier, Equation 1 and Equation 2 can be simplified to Equation 3.

$$\Delta V_1 = \sqrt{\frac{2E_a m_2}{m_1(m_1+m_2)}} \qquad (1)$$

$$\Delta V_2 = \sqrt{\frac{2E_a m_1}{m_2(m_1+m_2)}} \qquad (2)$$

$$\Delta V = \sqrt{\frac{2E_a}{m}} \qquad (3)$$

Where ΔV_1 is the change in velocity of vehicle 1 during the approach period, ΔV_2 is the change in velocity of vehicle 2 during the approach period, E_a is the total energy absorbed during the approach period, m_1 is the mass of vehicle 1, and m_2 is the mass of vehicle 2.

The model discussed in this paper only considers the total change in velocity during the approach period, which is from the time of the initial impact to the

time when the velocity of the vehicle reaches zero before it begins to rebound.

The damage algorithm, which incorporates the suggestions proposed by Prasad [2] in 1990, provides a way to describe the vehicle stiffness curve and to calculate the absorbed energy. The vehicle crush behavior, which is described by the linear relationship between $\sqrt{2E_a/w}$ and residual crush, is determined by two parameters, d_0 (the intercept of the $\sqrt{2E_a/w}$ vs. crush curve), and d_1 (the slope of the $\sqrt{2E_a/w}$ vs. crush curve.), and is shown in Figure 1. The dissipated energy is calculated by integrating this linear relationship over the crush profile of the case vehicle. Equation 5 is used for the calculation of the absorbed energy.

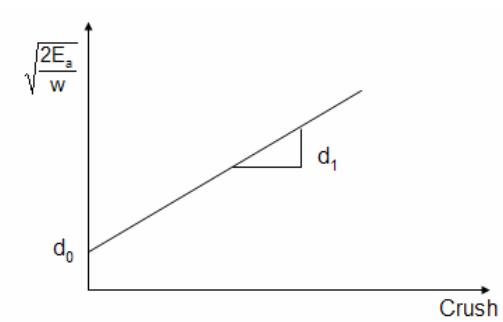

Figure 1. Linear relationship between $\sqrt{2E_a/w}$ and residual crush.

$$\sqrt{\frac{2E_a}{w}} = d_0 + d_1 c \qquad (4)$$

$$\text{Or, } E_a = \frac{w}{2}(d_0 + d_1 c)^2 \qquad (4')$$

Integrating (4'), we get

$$E_a = \int_0^w 0.5(d_0 + d_1 c)^2 \, dw \qquad (5)$$

Where E_a is total energy absorbed during approach period, m is the mass of the vehicle, w is the total length of indentation (the length of the total contact damage incurred by the vehicle), d_0, d_1 are vehicle stiffness values, and c is the post-crash crush measurements.

Calculation of Vehicle Stiffness Values d_0 and d_1

The NHTSA vehicle crash test database [8] is used to generate vehicle-specific stiffness coefficients d_0 and d_1 for accident reconstruction. The database contains the results of over 5000 crash tests conducted by NHTSA since 1979. Each test entry contains a complete description of each test which includes vehicle weight, length, center of gravity, static crush measurements, and instrumentation time histories.

With the assumption of the linear relationship between $\sqrt{2E_a/w}$ and residual crush, at least two data points are required to determine the intercept d_0 and the slope d_1. The high speed data point is obtained from a rigid full frontal barrier crash test usually conducted at 56 km/h (35mph) as part of the NHTSA NCAP program. The low speed data point is obtained by assuming that 12.07 km/h (7.5 mph) is the highest full frontal barrier impact speed which will not result in any permanent vehicle deformation. The stiffness coefficients d_0 and d_1 are obtained from a linear curve fit of the two data points. Equation 6, 7, and 8 are used to calculate the vehicle stiffness values. For frontal impact tests with a rigid fixed barrier, an average of the crush measurements can be used in Equation 6 if six values of crush measurements at equally spaced intervals are available. Equation 9 is used to calculate the average crush.

$$d_1 = \frac{\sqrt{\frac{2E_2}{w_2}} - \sqrt{\frac{2E_1}{w_1}}}{C_2 - C_1} \qquad (6)$$

$$d_0 = \sqrt{\frac{2E_2}{w_2}} - d_1 C_2 \qquad (7)$$

$$E_1 = \frac{1}{2} m v_1^2, E_2 = \frac{1}{2} m v_2^2 \qquad (8)$$

$$C = \frac{1}{5}\left(\frac{c_1}{2} + c_2 + c_3 + c_4 + c_5 + \frac{c_6}{2}\right) \qquad (9)$$

Where $\sqrt{\frac{2E}{w}}$ is the energy dissipated per unit width of the crush, v_1 is the low speed (assumed to be 12.07 km/h (7.5 mph)), v_2 is the vehicle test speed, w_1 is the vehicle width, w_2 is the total length of indentation, C_1 is the zero crush intercept, and C_2 is the average of post-test crush measurements.

Sensitivity of Stiffness Coefficients to Errors in Crash Test Crush Measurements

The objective of this section is to describe the sensitivity of the WinSMASH stiffness coefficient d_1 to errors in measurement of the average crush in the high speed crash test. The coefficient d_0 is not a function of C_2 and hence is insensitive to errors in the crush measurement C_2.

By definition, C_1, the crush at the low speed impact speed, V_1, equals zero. Using Equation 6:

$$d_1 = \frac{\sqrt{\frac{2E_2}{w_2}} - \sqrt{\frac{2E_1}{w_1}}}{C_2} \qquad (10)$$

Taking the derivative of this expression with respect to C_2 and approximating the infinitesimal derivatives by the finite differentials δd_1 and δC_2:

$$\delta d_1 = -\left(\frac{\sqrt{\frac{2E_2}{w_2}} - \sqrt{\frac{2E_1}{w_1}}}{C_2} \right) \frac{\delta C_2}{C_2} = -d_1 \frac{\delta C_2}{C_2} \quad (11)$$

Rewriting the expression to normalize δd_1 by d_1 and δC_2 by C_2:

$$\frac{\delta d_1}{d_1} = -\frac{\delta C_2}{C_2} \qquad (12)$$

So we see that a 10% overestimate in the average crash test crush C_2 will result in a 10% underestimate of the stiffness coefficient d_1.

Sensitivity of Delta-V Estimate to Errors in Crash Test Crush Measurements

To determine the effect of errors in crash test crush measurements on delta-V calculations in the field, we consider the simple case of a real world full frontal perpendicular crash into a rigid barrier. From the preceding equations, it can be shown that

$$\Delta V = \Delta V_1 + \left(\frac{\Delta V_2 - \Delta V_1}{C_2} \right) C \qquad (13)$$

Where ΔV = change of velocity of the case vehicle to be estimated and C=crush of the case vehicle. In the development of the stiffness coefficients, ΔV_1 is the change of velocity at the lowest velocity which does not result in any permanent deformation (assumed to be 7.5 mph). ΔV_2 is the change of the velocity in the high speed crash test, and C_2 is the resulting average static crush.

For mathematical convenience, we define an offset delta-V equal to $\Delta V - \Delta V_1$.

$$(\Delta V - \Delta V_1) = -(\Delta V_2 - \Delta V_1) \frac{C}{C_2} \qquad (14)$$

To compute the effect of errors in C_2, we take the derivative of the expression with respect to C_2, and approximate the derivatives by finite differentials:

$$\delta(\Delta V - \Delta V_1) = -\left(\frac{\Delta V_2 - \Delta V_1}{C_2} \right) C \frac{\delta C_2}{C_2} \quad (15)$$

Rewriting the expression to normalize $\delta(\Delta V - \Delta V_1)$ by $(\Delta V - \Delta V_1)$ and δC_2 by C_2:

$$\frac{\delta(\Delta V - \Delta V_1)}{(\Delta V - \Delta V_1)} = -\frac{\delta C_2}{C_2} \qquad (16)$$

Therefore, for the case of a real world full frontal perpendicular crash into a rigid barrier, a 10% overestimate in the crash test average crush C_2 will result in a 10% underestimate in the offset delta-V quantity $\Delta V - \Delta V_1$. The effect of crush measurement errors for other configurations can be computed using the relationship derived earlier showing the influence of measurement errors in C_2 on the stiffness coefficient d_1.

OBJECTIVE

The objective of this study is to determine the accuracy of post-crash test crush measurements, and their influence upon frontal stiffness coefficients used for crash reconstruction.

APPROACH

The mathematical methods for calculating delta-V suggest that the success of vehicle delta-V estimation will greatly rely on the accuracy of vehicle-specific stiffness coefficients which are obtained from the vehicle tests using crush measurements. This study presents the accuracy of post-test crush measurements in NCAP tests conducted from 2005-2007 using (1) double integration of accelerometers in the occupant compartment, (2) comparison of pre- and post-test vehicle length measurements, and (3) analysis of high speed videos. The paper will present

and compare WinSMASH stiffness coefficients computed using each of these measurement techniques.

Double Integration of Accelerometers

The test vehicles investigated in this project were fully instrumented to measure the acceleration of the vehicles during the tests. The quality of the acceleration time history was examined before the analysis to ensure that the responses truly represent the test vehicle. The accelerometers mounted in the crush zone were not considered in this study.

The maximum static crush was calculated using the accelerometers mounted in the occupant compartment. Two accelerometers were used for each test vehicle to represent the kinematics of the occupant compartment of the vehicle. The mounting locations for the accelerometers were generally the left and right sills, the left and right floorpans, or the left and right rear seats. Any bias errors, which were caused by the accelerometers not being perfectly zeroed out before the test, were corrected before the integration. The displacement of the vehicle occupant compartment as a function of time was obtained by integrating the acceleration curve twice. The maximum static crush was achieved when the vehicle rebounded and separated from the barrier. The time of separation was defined for this study to be that time when the total force of load cells mounted on the rigid barrier reached zero.

Comparison of Pre- and Post-test Vehicle Lengths

Physically measuring the vehicle damage profile is the method currently being used by NHTSA for accident reconstruction. The techniques for field vehicle damage data collection and the detailed instructions regarding the use of these measurements are stated in the NHTSA test reference guide [6].

The NHTSA protocol estimates static crush using three methods which measure the lengths of the vehicle before and after each test. In each of the methods described below, our study uses the maximum value of the differences between pre- and post-test measurements as the maximum static crush of the vehicle.

The first method is to use six points DPD1-DPD6 (Damage Profile Distances) to determine the dimensions of the crush. The six DPD points are equally spaced along the length of the crush profile. Four points are used if the length of the damage is 400mm or less. The length of the damaged area L and the distance from the midpoint of L to the vehicle center of gravity are also calculated, and will be used in the reconstruction program. The depths of crush are measured from the original outline of the vehicle before the test to the final crushed position. For frontal damage, the DPD measurements are taken from the vehicle's left (the driver side of the vehicle) to the vehicle's right (Figure 2).

The second method is to use pre- (BX1 through BX21) and post-test (AX1 through AX21) Vehicle Measurement Data to calculate the change in length of the vehicle and distances between different vehicle components. The data BX1 through BX21 and AX1 through AX21 represent a range of vehicle measurements required for determining the extent of damage to the vehicle. The measurement most relevant to this study is the change in Total Length of Vehicle at Centerline (BX1 – AX1) (Figure 2).

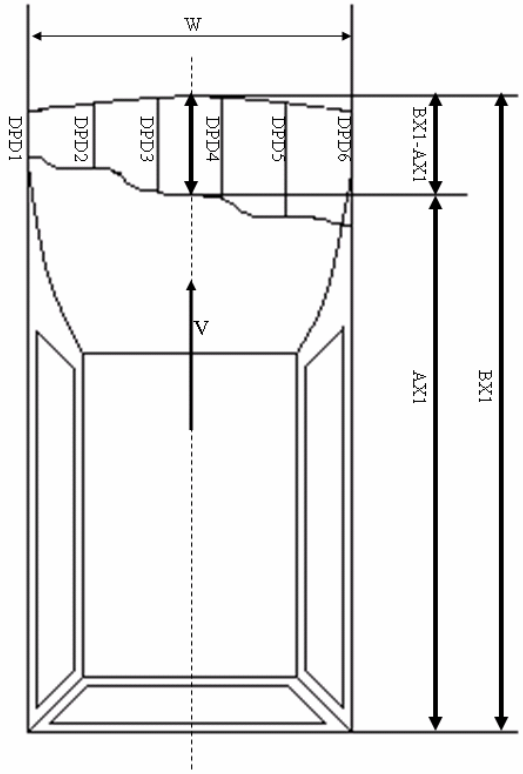

Figure 2. DPD and BX-AX crush measurements.

Finally, the maximum crush distance is recorded as CRHDST, which indicates the maximum static crush distance (damage penetration), regardless of its location. In 54 of the 93 NHTSA NCAP tests, CRHDST equaled the BX1-AX1.

Static Crush Patterns

Different post-test crush profiles were observed from the tests we investigated. Normally, a perpendicular full frontal barrier test will result in a flat post-test profile. However, during rebound from the barrier, different portions of the front structure may unload by differing amounts leading to an irregular static crush profile (Figure 3 and Figure 4). This phenomenon indicates that simply measuring static crush at the centerline of the vehicle, using for example the quantity BX1-AX1, may overestimate the average static crush.

Figure 3. Post-test right front 3/4 view of the vehicle (Test 5615).

Figure 4. Post-test front underbody of the vehicle (Test 5615).

Normally, all structural restitution ceases once barrier forces upon the vehicle drop to zero at time of separation. In unusual cases, the bumper has been observed to springback after separation. Bumper springback after separation occurs will have no effect on delta-V. Hence basing stiffness calculation on physical measurement to the bumper in these cases will introduce a bias in delta-V. These cases can be difficult to detect. Video cameras are not always in the right position to photograph structural unloading after the vehicle rebounds from the rigid wall. Because the bumper is not instrumented, this phenomenon cannot be detected with accelerometers.

Two examples of irregular post-test crush profile are NHTSA NCAP test 5615 and 5818. The pre-test and post-test frontal profile of the vehicle for test 5615 is shown in Figure 5. The detailed post-test crush patterns for 12 NHTSA NCAP tests of model year 2007 are shown in Table 1 (See Appendix).

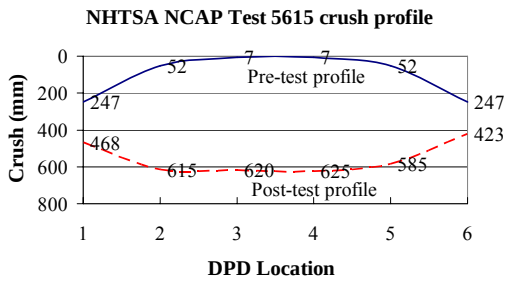

Figure 5. Pre-test and post-test frontal profile of the vehicle for NHTSA NCAP test 5615

Analysis of High-speed Videos

Real-time and high-speed cameras are used in NHTSA NCAP tests to document the frontal barrier impact events. Therefore, analysis of high speed videos provides another way to calculate the maximum dynamic crush of the vehicle in addition to the double integration of accelerometers. Maximum dynamic crush is the amount a vehicle deforms from initial impact to the point of maximum deformation. Due to the position and angle of the cameras in the tests, the maximum static crush, which is the amount a vehicle deforms from initial impact to the point of separation from the barrier, is generally difficult to obtain from the test videos.

Motion analysis software was used to identify a marker on the door of the vehicle and track its position one frame at a time throughout the image sequence. The positions of the marker at the time when the vehicle starts contacting the rigid barrier and when the vehicle fully stops were recorded and used to calculate the maximum dynamic crush.

Case Example

NHTSA NCAP test 5720 was chosen as an example to examine the accuracy of crush measurements using different methods. NHTSA Test 5720 was conducted at a speed of 56.65 km/h (35.2 mph). The test vehicle was a 2007 Mazda CX-7 having a test weight of 1968

kg. Two accelerometers were mounted on the left and right rear seat of the test vehicle. As shown in Figure 6, the time of separation was determined to be 139 ms based on the time when the total barrier forces reached zero. The maximum static crush at the time of separation was calculated as 563 mm (Figure 7) and 483 mm for the left and right rear seat of the vehicle respectively by double integration of the acceleration curves. DPDs measured from the vehicle were 127 mm, 394 mm, 559 mm, 547 mm, 350 mm, and 39 mm for DPD1 to DPD6. The values were 575 mm, 407 mm, and 454 mm for BX1-AX1, BX19-AX19, and BX20-AX20 respectively. The CRHDST recorded in the test report was 575 mm for the maximum static crush.

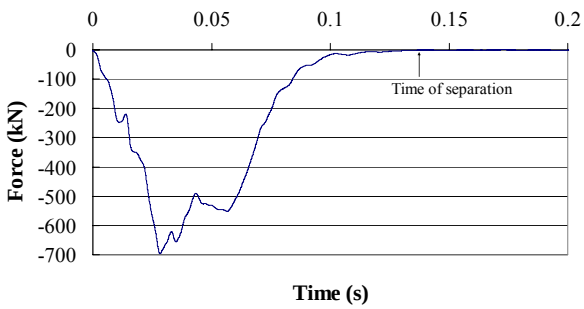

Figure 6. Total barrier forces as a function of time for NCAP Test 5720.

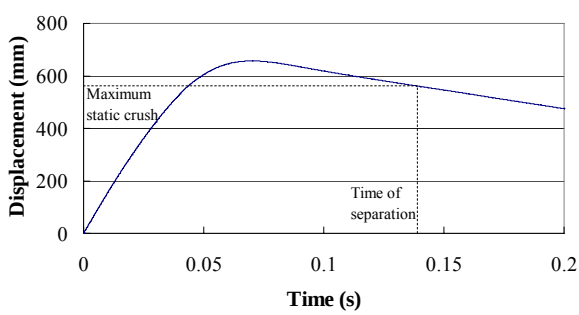

Figure 7. Displacement of the left rear seat as a function of time for NCAP Test 5720.

In the analysis of full frontal barrier tests, it is generally assumed that the left and right of the vehicle crush uniformly. In this test however, the left and right crush patterns of the front structure were not symmetrical as shown both by integration of the acceleration curves and physical measurements. Film analysis was conducted to investigate the reason for this variation. High speed videos taken from left and right side of the vehicle were analyzed to obtain the maximum dynamic crush, and results were compared to the data calculated from the accelerometers. The time of the maximum dynamic crush was 77 ms, which was determined by double integration of the accelerations. The maximum dynamic crush calculated by left and right rear seat accelerometers was 656 mm and 636 mm respectively. The maximum dynamic crushes obtained from high speed video analysis were 729 mm and 711 mm for left and right view of the videos.

Two conclusions can be drawn from the test. First, the accelerometers do not always provide an exact measurement of dynamic crush. In this test, the dynamic crush computed from accelerometers was in error by 10%. Second, even in a perpendicular full frontal barrier test, the left and right side crush may not be the same. Although the crush values obtained by film analysis were higher than accelerometer data, it was observed that the left side of the vehicle had more crush than the right side, which was consistent with the maximum static crushes.

RESULTS AND DISCUSSIONS

Maximum Static Crush by Different Methods

Ninety-three NCAP frontal barrier impact tests were investigated on the accuracy of post-test crush measurements in this project. In these tests, a vehicle impacts a rigid barrier with full frontal structure engagement with an initial velocity of around 56 km/h. The maximum static crush was calculated by double integration of the accelerometers as described above. The results were compared with the pre- and post-test measurements DPDs, BX1-AX1, and CRHDST.

Results of the maximum static crush obtained from the accelerometers and physical measurements are shown in Figure 8 to Figure 13. In each graph, the maximum static crush computed from the accelerometers is plotted on the horizontal axis. The dotted 45 degree diagonal lines indicated the perfect agreement between the horizontal and vertical axis values. Trendlines were created to compare the physical measurements to the accelerometers. R^2 is a measure of goodness of fit surrounding the trendlines. It was observed from Figure 8 to Figure 13 that the physical measurements of the maximum static crush were on average 6 % less than the values calculated using the accelerometers. The values of the goodness of fit (R^2) for each comparison showed considerable scattering. The maximum static crush based on the maximum DPDs had a slightly better fit to the values calculated using the accelerometers than the other measurements. No significant difference was noticed between the left and right accelerometers

comparing with the same physical measurements, as similar values of the goodness of fit were obtained.

Direct comparison was also completed between the accelerometer data obtained from the left and right side of the occupant compartment, and the results are plotted in Figure 14. It was found that the acceleration data obtained from both sides of the vehicle occupant compartment were very consistent with each other, which was indicated by the goodness of fit value (R^2) of 0.82.

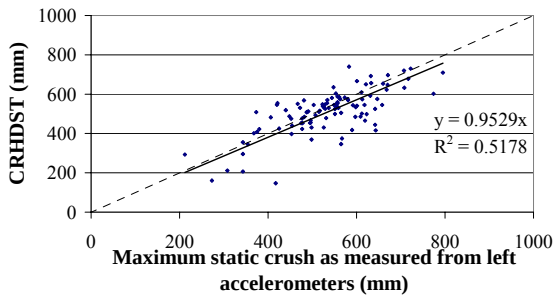

Figure 8. Comparisons of the maximum static crush computed from CRHDST and left accelerometers.

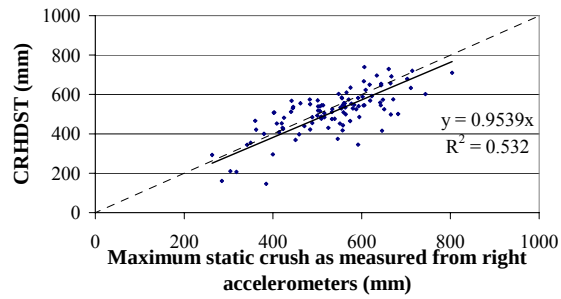

Figure 9. Comparisons of the maximum static crush computed from CRHDST and right accelerometers.

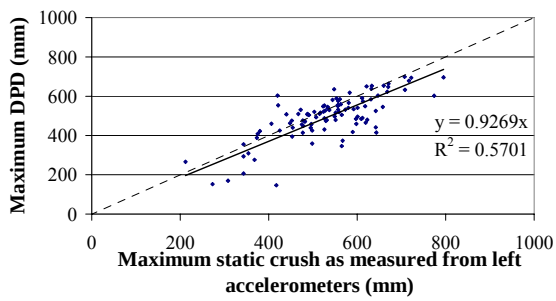

Figure 10. Comparisons of the maximum static crush computed from maximum DPDs and left accelerometers.

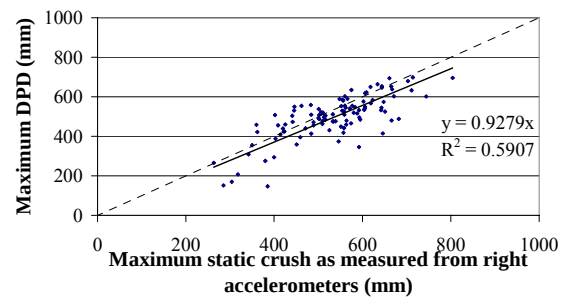

Figure 11. Comparisons of the maximum static crush computed from maximum DPDs and right accelerometers.

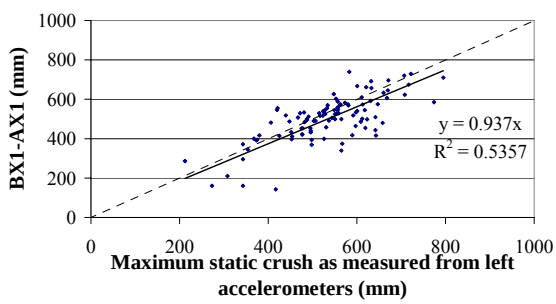

Figure 12. Comparisons of the maximum static crush computed from BX1-AX1 and left accelerometers.

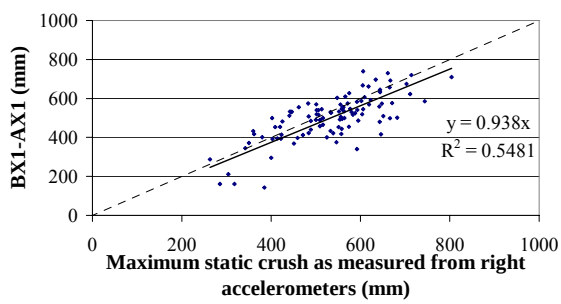

Figure 13. Comparisons of the maximum static crush computed from BX1-AX1 and right accelerometers

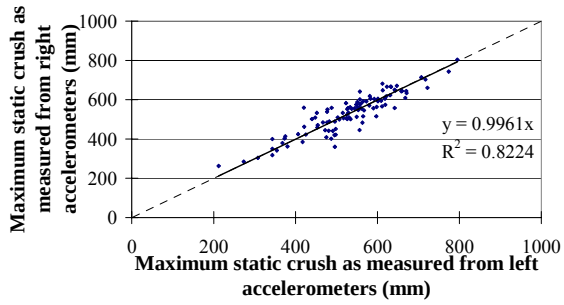

Figure 14. Comparisons of the maximum static crush computed from left and right side accelerometers.

Results of High-speed Video Analysis

In addition, video analysis was completed for 13 NHTSA NCAP tests of model year 2007. Test videos were not available for Test 5818, a 2007 Nissan Versa. The results were compared to the maximum dynamic crush calculated by accelerometers and illustrated in Figure 15 and Figure 16. These figures show that the maximum dynamic crush obtained from the acceleration curves were on average 3% less than the value estimated by the analysis of high-speed videos. The goodness of fit values suggest that the left side accelerometers had a better correlation with the videos ($R^2 = 0.82$) than the right side accelerometers ($R^2 = 0.65$). It was concluded from the figures that when video analysis was unavailable, utilizing accelerometers was a good alternate method to estimate the vehicle maximum dynamic crush accurately.

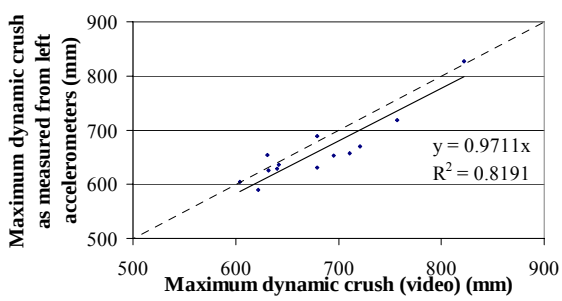

Figure 15. Comparisons of the maximum dynamic crush between video analysis and left side accelerometers in 13 model year 2007 vehicles.

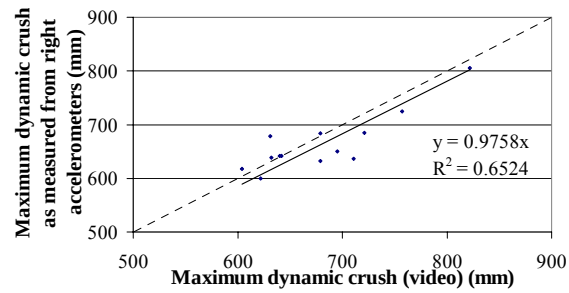

Figure 16. Comparisons of the maximum dynamic crush between video analysis and right side accelerometers in 13 model year 2007 vehicles.

Study of Vehicle Stiffness Coefficients and Delta-V Estimations Using Different Measurements

Accurate crush measurements are the basis for WinSMASH reconstruction of delta-V in real world crashes. Errors in static crush measurements will be reflected as inaccuracies in the stiffness coefficients, and ultimately as errors in WinSMASH delta-V estimates. The effects of vehicle crush measurements using different methods on vehicle stiffness coefficients and delta-V estimations will be discussed in the following section.

The investigation was conducted on 14 NHTSA NCAP tests of model year 2007 vehicles. Estimates of average crush obtained by different post-test crush measurements (DPDs, BX1-AX1, and the accelerometers) were used to calculate the vehicle stiffness coefficients. The comparisons of different crush measurements were completed in two steps. First, the average crush calculated using different crush measurements was compared, and the results are illustrated in Figure 18. Second, vehicle stiffness coefficients were calculated using the average crushes. The comparison between different methods was shown in Figure 19.

Equation 9 was used to calculate the average crush. Value c1 to c6 were the crush measurements along the damage profile. The average crush was calculated in three different methods. For the first method (denoted as DPDs in figures), original DPD measurements were used in the equation. For the second method, it was noticed that the post-test damage profile of the vehicle was nonuniform along the vehicle width. Large variations were also observed in different test vehicles. Our concern was that the post-test measurements may not really represent the true deformation of the vehicle during the test. Therefore, for the second method (denoted as

DPDs' in figures), it was assumed that the vehicle had a uniform post-test damage profile. The average of DPD3 and DPD4 was used as the maximum static crush, and was subtracted from the original profile (six equally spaced points along the vehicle) of the vehicle to calculate the average crush. For the third method, the change in Total Length of Vehicle at Centerline (BX1 – AX1) was subtracted from the pre-test profile of the vehicle, and then used in Equation 9. As an example, the average crush computed using these three methods is plotted in Figure 17 for NHTSA NCAP test 5615. Along the same line, the average of maximum crushes by right and left accelerometers was used as the post-test profile, and was subtracted from the pre-test profile of the vehicle to calculate the average crush.

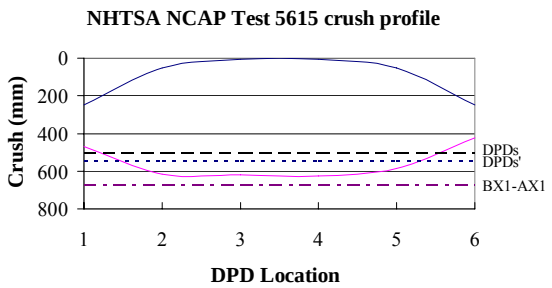

Figure 17. The average crush computed using three methods for NHTSA NCAP test 5615.

For 13 NHTSA NCAP tests of model year 2007, accelerometers were corrected to agree with the video dynamic crush. The accelerometer static crush was recomputed, and is shown in Table 2. Vehicle stiffness coefficients calculated using the corrected accelerometer static crush are also tabulated in Table 2.

It was observed from Figure 18 that the average crush calculated by physical measurements was generally 5% less than the value predicted by the accelerometers. The reason for this difference could be the continued expansion of the vehicle after its separation from the barrier or errors in measurement. Also from the figure, no significant difference was noticed between the average crush calculated by the first two methods mentioned above (DPDs and DPDs') despite the concern we had before the analysis.

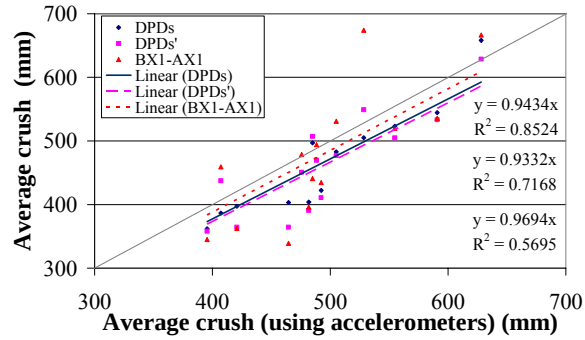

Figure 18. Comparisons of the average crush computed from physical measurements and accelerometers.

When the average crush was used to compute the vehicle stiffness coefficients (as shown in Figure 19), vehicle stiffness coefficient d_1 (the slope of the stiffness curve) calculated using physical measurements was approximately 7% greater than the value calculated using accelerometers. This discrepancy in stiffness coefficients indicated that the physical measurements estimated the test vehicle had a stiffer structure than predicted by the accelerometers.

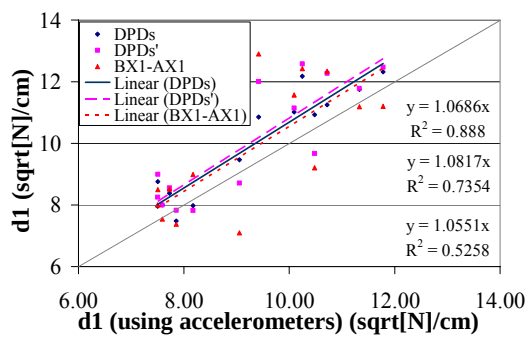

Figure 19. Comparisons of the vehicle stiffness coefficient computed from physical measurements and accelerometers.

Implications of the Results

Accelerometers can be used as an upper bound on crush. We originally thought that accelerometers might provide a true measure of crush. This was based heavily on the belief that all restitution of the front structure ended after the vehicle separated from the wall. Examination of high speed videos however shows that the bumper can spring back somewhat after separation from the wall. Despite the fact that bumper springback has no effect on delta-V, post-test measurements of frontal deformation use this final bumper position to compute static crush.

From the comparisons of the maximum static crush computed from physical measurements and accelerometers, 27 cases in the 93 case data set appeared to show physical measurements in error. These would be cases in which physical measurements of static crush exceeded the static crush computed using the accelerometers. This situation is not possible in a rigid full frontal barrier test. For the 27 cases, the maximum static crush from DPD measurements exceeded the static crush computed from the accelerometers by 9% on average, with a range from 0.2% to 25%. As shown in the derivation in the previous section, a 9% overestimate in crush will lead to a 9% underestimate in d_1 and also a 9% underestimate in ΔV- 7.5 mph in full frontal rigid barrier crashes.

Therefore, our recommendations for the post-test measurements are that: (1) all physical measurements should be checked against accelerometers; (2) all accelerometers should be checked against high speed videos and corrected if necessary. It should be noted that this does not guarantee that the physical measurements which have lower crush than accelerometers are correct, but this procedure does catch some measurement problems.

LIMITATIONS

Several limitations were found for the three different methods to obtain the maximum crush. Although the data calculated by left and right side accelerometers were generally very close, relatively large discrepancies were observed in some test cases. The differences could be the result of failure and errors by the accelerometers or the variation of the vehicle impact angle during the test. The limitation for video analysis was that the marker tracked in the videos was on the door of the vehicle instead of the floor of the occupant compartment, and it could only be used to calculate maximum dynamic crush to help examine the accuracy of accelerometers since the time of separation was difficult to determine in videos.

CONCLUSIONS

This paper has presented the accuracy of vehicle crush measurements in 93 NCAP frontal impact tests conducted from 2005-2007 and the WinSMASH stiffness coefficients as well as the delta-V estimates computed using different measurement techniques.

- The results from comparing the maximum static crush by different methods showed that the physical measurements of the maximum static crush were on average 6 % less than the values calculated using the accelerometers.

- The comparison of the accelerometer data obtained from the left and right side of the occupant compartment demonstrated that acceleration data obtained from both sides were very consistent with each other.

- Results of high-speed video analysis indicated that utilizing accelerometers to estimate the vehicle maximum dynamic crush was a good alternate method in addition to the video analysis. The maximum dynamic crush obtained from the acceleration curves were on average 3% less than the value estimated by analysis of high-speed videos.

- Study of vehicle stiffness coefficients and delta-V estimations using different measurements showed that the average crush calculated by physical measurements was 5% less than the value computed by the accelerometers. As a result, vehicle stiffness coefficient d1 calculated using physical measurements was mostly 7% greater than the value calculated using accelerometers.

- The comparisons of the maximum static crush computed from physical measurements and accelerometers showed that in 27 cases of the 93 case data set DPD measurements exceeded accelerometers by 9% on average. A 9% overestimate in crush will lead to a 9% underestimate in d_1 and also a 9% underestimate in ΔV- 7.5 mph in full frontal rigid barrier crashes.

- Physical measurements of static crush in crash tests should be checked against high speed videos and accelerometers prior to computation of vehicle stiffness coefficients. When physical measurements are found to be in error and cannot be repeated, the maximum static crush computed from accelerometers in the occupant compartment or measured from high speed videos can be used as an upper bound on static crush.

REFERENCES

[1] Sharma, D., Stern, S., and Brophy, J. 2007. “An Overview of NHTSA’s Crash Reconstruction Software WinSMASH.” In Proceedings of the Twentieth International Conference on Enhanced Safety of Vehicles, Paper No. 07-0211, Lyon, France.

[2] Prasad, A.K. 1990. "CRASH3 Damage Algorithm Reformulation for Front and Rear Collisions." SAE 900098.

[3] Niehoff, P., and Gabler, H.C. 2006. "The Accuracy of WinSMASH Delta-V Estimates: The Influence of Vehicle Type, Stiffness, and Impact Mode." In the 50th Annual Proceedings of the Association for the Advancement of Automotive Medicine. Chicago, IL.

[4] Stucki, S.L. and Fessahaie, O. 1998. "Comparison of Measured Velocity Change in Frontal Crash Tests to NASS Computed Velocity Change." SAE 980649, Society of Automotive Engineers.

[5] Nolan, J.M., Preuss, C.A., Jones, S.L., and O'Neill, B. 1998. "An Update on Relationships between Computed Delta-Vs and Impact Speeds for Offset Crashes." In the Proceedings of the Sixteenth International Technical Conference on the Enhanced Safety of Vehicles (Windsor, Canada, June 1998), Paper No. 98-S6-O-07.

[6] "NHTSA Test Reference Guide." 2006. Version 5, Volume I : Vehicle Tests, Revision.

[7] Campbell, K. 1974. "Energy Basis for Collision Severity." SAE 740565.

[8] NHTSA Vehicle Crash Test Database, 2007, http://www-nrd.nhtsa.dot.gov/database/nrd-11/veh_db.html

APPENDIX

Table 1.
Crush patterns of 12 NHTSA NCAP tests of model year 2007
(solid lines represent pre-test profiles, dash lines represent post-test profiles)

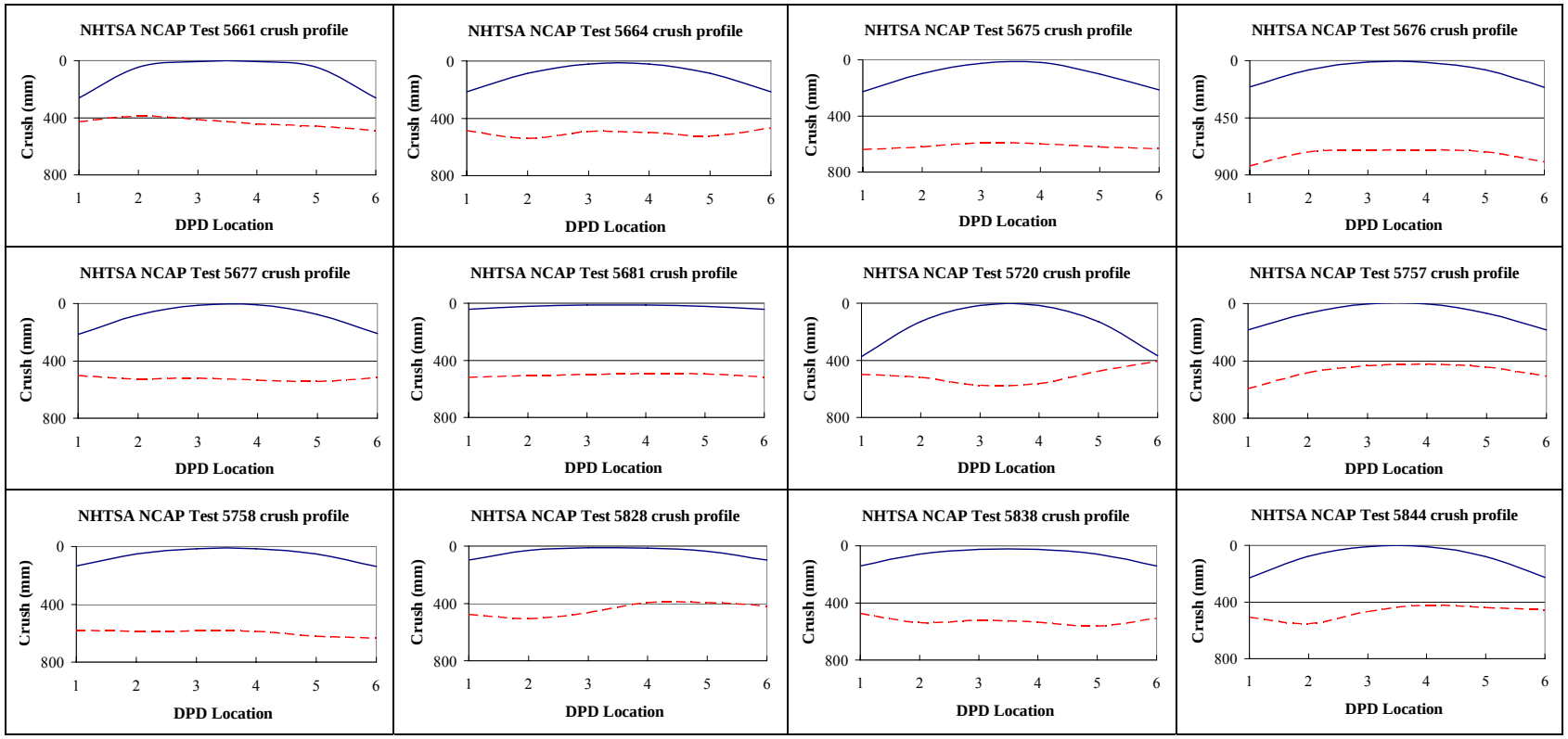

Table 2.
Summary of the data presented in Figure 18 and Figure 19

Test	Make	Model	Year	Average static crush (mm)		Stiffness coefficient d0 ($\sqrt{N}$)	Stiffness coefficient d1 ($\sqrt{N}/cm$)				
				Accelerometer (uncorrected)	Accelerometer (corrected)		Accelerometer (uncorrected)	Accelerometer (corrected)	DPDs	DPDs'	BX1-AX1
5615	CHEVROLET	TAHOE	2007	528.5	557.5	123.25	9.06	8.58	9.47	8.71	7.10
5661	DODGE	CALIBER	2007	395.5	416.5	101.10	10.10	9.58	11.02	11.15	11.57
5664	HONDA	FIT	2007	492.3	497.8	95.41	7.51	7.43	8.76	9.00	8.50
5675	TOYOTA	CAMRY	2007	554.8	548.8	102.08	7.51	7.59	7.96	8.25	8.01
5676	CHEVROLET	SUBURBAN	2007	628.1	633.1	128.23	7.86	7.79	7.48	7.83	7.38
5677	TOYOTA	YARIS	2007	475.7	478.7	91.81	7.59	7.54	8.00	8.00	7.54
5681	TOYOTA	FJ CRUISER	2007	505.0	539.5	115.88	11.78	11.03	12.32	12.47	11.20
5720	MAZDA	CX-7	2007	407.2	461.2	109.71	10.48	9.21	10.93	9.67	9.21
5757	LEXUS	ES 350	2007	464.6	507.1	107.39	9.42	8.63	10.85	12.01	12.90
5758	FORD	RANGER	2007	590.9	557.4	111.23	7.73	8.19	8.38	8.55	8.52
5818	NISSAN	VERSA	2007	485.0	485.0	96.94	8.18	8.18	7.98	7.82	8.99
5828	JEEP	COMPASS	2007	481.8	476.3	105.75	10.25	10.35	12.18	12.58	12.42
5838	HYUNDAI	SANTA FE	2007	488.4	485.9	118.40	11.33	11.39	11.75	11.78	11.19
5844	SATURN	AURA	2007	420.8	452.8	107.32	10.72	9.94	11.25	12.27	12.34